Dissertations, Master's Theses and Master's Reports - Open

Dissertations, Master's Theses and Master's Reports

2005

Testing Wisconsin asphalt mixtures for the 2002 AASHTO mechanistic design procedure

Christopher J. Robinette
Michigan Technological University

Recommended Citation

Robinette, Christopher J., "Testing Wisconsin asphalt mixtures for the 2002 AASHTO mechanistic design procedure ", Master's Thesis, Michigan Technological University, 2005.
https://digitalcommons.mtu.edu/etds/264

TESTING WISCONSIN ASPHALT MIXTURES FOR THE
2002 AASHTO MECHANISTIC DESIGN PROCEDURE

By

CHRISTOPHER J. ROBINETTE

A THESIS

Submitted in partial fulfillment of the

Requirements for the degree of

MASTER OF SCIENCE IN CIVIL ENGINEERING

MICHIGAN TECHNOLOGICAL UNIVERSITY

This thesis, "Testing Wisconsin Asphalt Mixtures for the 2002 AASHTO Mechanistic Design Procedure" is hereby approved in partial fulfillment of the requirements for the degree of MASTER OF SCIENCE IN CIVIL ENGINEERING.

DEPARTMENT: Civil and Environmental Engineering

Thesis Advisor: R. Christopher Williams

Department Chair: C. Robert Baillod

Date:_____

ABSTRACT

There has been a continuous evolutionary process in asphalt pavement design. In the beginning it was crude and based on past experience. Through research, empirical methods were developed based on materials response to specific loading at the AASHO Road Test. Today, pavement design has progressed to a mechanistic-empirical method. This methodology takes into account the mechanical properties of the individual layers and uses empirical relationships to relate them to performance. The mechanical tests that are used as part of this methodology include dynamic modulus and flow number, which have been shown to correlate with field pavement performance.

This thesis was based on a portion of a research project being conducted at Michigan Technological University (MTU) for the Wisconsin Department of Transportation (WisDOT). The global scope of this project dealt with the development of a library of values as they pertain to the mechanical properties of the asphalt pavement mixtures paved in Wisconsin. Additionally, a comparison with the current associated pavement design to that of the new AASHTO Design Guide was conducted. This thesis describes the development of the current pavement design methodology as well as the associated tests as part of a literature review. This report also details the materials that were sampled from field operations around the state of Wisconsin and their testing preparation and procedures. Testing was conducted on available round robin and three Wisconsin mixtures and the main results of the research were:

- The test history of the Superpave SPT (fatigue and permanent deformation dynamic modulus) does not affect the mean response for both dynamic modulus and flow number, but does increase the variability in the test results of the flow number.
- The method of specimen preparation, compacting to test geometry versus sawing/coring to test geometry, does not statistically appear to affect the intermediate and high temperature dynamic modulus and flow number test results.
- The 2002 AASHTO Design Guide simulations support the findings of the statistical analyses that the method of specimen preparation did not impact the

performance of the HMA as a structural layer as predicted by the Design Guide software.

- The methodologies for determining the temperature-viscosity relationship as stipulated by Witczak are sensitive to the viscosity test temperatures employed.

- The increase in asphalt binder content by 0.3% was found to actually increase the dynamic modulus at the intermediate and high test temperature as well as flow number. This result was based the testing that was conducted and was contradictory to previous research and the hypothesis that was put forth for this thesis. This result should be used with caution and requires further review.

- Based on the limited results presented herein, the asphalt binder grade appears to have a greater impact on performance in the Superpave SPT than aggregate angularity.

- Dynamic modulus and flow number was shown to increase with traffic level (requiring an increase in aggregate angularity) and with a decrease in air voids and confirm the hypotheses regarding these two factors.

- Accumulated micro-strain at flow number as opposed to the use of flow number appeared to be a promising measure for comparing the quality of specimens within a specific mixture.

- At the current time the Design Guide and its associate software needs to be further improved prior to implementation by owner/agencies.

List of Contents

List of Figures

List of Tables

Acronyms and Symbols

2D	A Heavy single unit truck with two axles and 6 tires
3SU	A heavy single unit truck with three axles
2S-1	A heavy tractor-semitrailer truck with three axles
2S-2	A heavy tractor-semitrailer with four axles
3S-2	A heavy tractor-semitrailer with five or more axles
2-S1-2	A heavy tractor-semitrailer-trailer combination with five or more axles
A	Witczak Predictive Equation Regression Intercept
AADT	Average Annual Daily Traffic
AADTT	Average Annual Daily Truck Traffic
AASHO	American Association of State Highway Officials
AASHTO	American Association of State and Highway Transportation Officials
ALF	Accelerated Loading Facility
ASTM	American Society for Testing and Materials
BSG (G_{mb})	Bulk Specific Gravity
COV	Coefficient of Variation
D60	Grain size that corresponds to 60 percent passing
E* and $\lvert E^*\rvert$	Complex Modulus and Dynamic Modulus, respectively
E' and E''	Elastic and Viscous Modulus, respectively
ESAL	Equivalent Single Axle Load
FHWA	Federal Highway Administration
F_N	Flow Number
F/P_b	Fines to Asphalt Binder Ratio
G_b	Asphalt Specific Gravity
G_{sb}	Aggregate Bulk Specific Gravity
G_{se}	Aggregate Effective Specific Gravity
HMA	Hot Mix Asphalt
IDT	Indirect Tension Test
IRI	International Ride Index
JMF	Job Mix Formula
JTFP	Joint Task Force for Pavements
LTPP	Long Term Pavement Performance
LVDT	Linear Variable Differential Transducer
M-E	Mechanistic-Empirical
MTSG (G_{mm})	Maximum Theoretical Specific Gravity
MTU	Michigan Technological University
NCAT	National Center for Asphalt Technology
NCHRP	National Cooperative Highway Research Program
N_{design}	Design number of gyrations for a Superpave Mix Design
NMAS	Nominal Maximum Aggregate Size
P_b	Asphalt Binder Content
P_{eff}	Effective Asphalt Binder Content
PI	Plasticity Index
PTF	Pavement Testing Facility

QC/QA	Quality Control/Quality Assurance
R^2	Coefficient of Determination
RAP	Recycled Asphalt Pavement
RTFO	Rolling Thin Film Oven
SGC	Superpave Gyratory Compactor
SHRP	Strategic Highway Research Program
SMA	Stone Matrix Asphalt
SSD	Saturate Surface Dry
SPS	Special Pavement Study
SPT	Simple Performance Test
SST	Superpave Shear Tester
TAI	The Asphalt Institute
TOC	Technical Oversight Committee
UTM	Universal Testing Machine
V	Witczak Predictive Equation Regression Slope
VFA	Voids Filled with Asphalt
VMA	Voids in the Mineral Aggregate
WHRP	Wisconsin Highway Research Program
WisDOT	Wisconsin Department of Transportation
WSDOT	Washington Department of Transportation
ε_o	Strain
ϕ	Phase Angle
σ_o	Stress

Ryan Jennaro – Laboratory Technician
Monarch Paving
       Perry Atterhold – Manager
       Don Murphy – Plant Technician
       Barry Larsen – Plant Operator
       Nancy Whitecell – Laboratory Technician
D.L. Gasser
       Mike Burns – Vice President
       Stephanie Brandt - Laboratory Technician
       Matt Platt – Plant Operator
Northeast Asphalt
       Jay Rosemeier – Area Manager
       Chris – Laboratory Technician
       Brent – Plant Operator (Antigo)
       Dan Feldner – Area Manager
       Jim – Plant Operator (Plymouth)
B.R. Amon & Sons
       Tom Amon – Owner
       Adam Blanchard – Laboratory Technician
       Jack Noltze – Plant Operator
       Joe Kyle – Manager
Wisconsin Department of Transportation
       Judi Ryan – Engineering Specialist (Asphalt Mix Design)
       Tom Brokaw
       Steve Noel
       Phillip Wilson
       Jeff Olsen
       Brad Byom

CHAPTER 1: INTRODUCTION

1.1 Pavement Design Development

  The American Association of State Highway Officials (AASHO) Road Test in the

late 1950's formed the basic principles for flexible pavement design in the United States.

The AASHO Road Test was meant to identify relationships between the loading

magnitude and arrangement as well as pavement thickness to performance. Based on the

results of the Road Test, empirical relationships were developed, that made the pavement

design process relatively simplistic. Some of the basic inputs include a soil support

value, loading, and a regional factor, used to develop a structural number for a layer and

ultimately a layer thickness (WSDOT Manual, 1995). This procedure is outlined in the

1972 American Association of State Highway and Transportation Officials (AASHTO)

Interim Guide for Design of Pavement Structures. There have been continual revisions to

this design guide and the AASHTO Guide for Design of New and Rehabilitated

Pavement Structures (Design Guide) is the culmination of research and field experience.

The Design Guide is based on a Mechanistic-Empirical (M-E) design approach and has

been put together under the auspices of the National Cooperative Highway Research

Program (NCHRP) as projects 1-37, 1-37A, 1-40A & B, 9-19, and 9-29 (Guide for

Mechanistic-Empirical Design of New and Rehabilitated Pavement Structures, 2004).

1.2 Project Objectives

The Wisconsin Department of Transportation (WisDOT) currently uses the AASHTO 1972 Interim Guide for the Design of Pavement Structures for hot mix asphalt. This pavement design procedure is a strictly empirical pavement design approach, however with the latest research and available computer capabilities, mechanistic pavement design procedures have become more feasible. The Design Guide and its associated software has been built on the mechanical properties of the pavement layers while still using functions to predict pavement life, thus making it a mechanistic-empirical pavement design approach. This pavement design procedure also allows for default values of the mechanical properties to be used, which are based on previous measurements of these properties.

The intent of this project was to examine typical hot mix asphalt (HMA) pavements that are constructed in the State of Wisconsin. The analysis compares the suggested pavement structures based on the current (1972) pavement design guide and that of the current Design Guide. In order to develop the pavement structure as outlined by the Design Guide the mechanical properties of the HMA layers were measured. These properties include dynamic modulus and flow number, which have been found to be significant predictors of rutting and fatigue by Witczak et. al. (2002). Properties of the other layers in the system have been obtained from the WisDOT pavement design inputs. The objective was to account for typical construction variability that occurs and determine their impact upon both mechanical tests. Further, an examination of these mechanical test results on pavement design and determine if the performance tests and Design Guide as they currently exist are ready for implementation by owner/agencies.

2

1.3 Overall Project Experimental Plan

The first step in developing the experimental plan was to identify HMA designs that have realistic construction parameters. The pavements should be representative of HMA designs used in practice by owner/agencies. Predominate factors that have been identified in the mix design process are the level of anticipated traffic, the nominal maximum aggregate size (NMAS), and mix type (dense- or open-graded).

In this research plan, the level of traffic had been initially segmented into three categories by equivalent single axle loads (ESAL), which corresponds to an 18,000-lb axle load. Low volume traffic levels was considered to have less than or equal to 1×10^6 ESALs. Medium volume traffic levels was greater than 1×10^6 ESALs up to 3×10^6 ESALs. Finally, high volume traffic levels was greater than 3×10^6 ESALs. The reason for this segmentation is that the level of anticipated traffic is a critical variable in the pavement design process that ultimately results in aggregate angularity and thickness recommendations. Changes in pavement thickness can significantly affect the amount of rutting that occurs in the pavement structure and consequently has been noted as one of the variables important in the experimental matrix.

The second factor that was considered was the nominal maximum aggregate size (NMAS). The sizes that were considered are as follows: 25.0-mm, 19.0-mm, and 12.5-mm. As noted by Akhter and Witczak (1985) the size of the aggregate plays a significant role in permanent deformation.

The type of mix was also analyzed in terms of dense- and open-graded and are a function of the gradation. A Stone Matrix Asphalt (SMA) will be considered an open-graded mix for this project. An SMA promotes stone-on-stone contact by having highly

crushed material, with a higher fines content and added fibers. SMAs have been utilized

in Europe for many years and were introduced to the United States in 1991 (Brown,

1997). As part of Brown's study it was observed that 31 SMA projects had been paved in

the US between 1991 and 1993. This is not to say that SMA projects have not been

paved after this time frame; they have, but it points to the increased utilization of this

type of mix design. As a result of this higher utilization, the SMA mix type has been

included in this study for the high traffic level pavements, where it is intended to mitigate

permanent deformation. It should be noted that owner/agencies predominately pave

dense-graded mixes, with open-graded mixes used only on high volume roads, and thus

have been factored into the experimental matrix found in Table 1.1.

Table 1.1 Preliminary Experimental Matrix for Field Sampling

Nominal Maximum Aggregate Size	Mix Type	Traffic Level		
		Low	Medium	High
25.0mm	Dense		X	XXX
	Open			
19.0mm	Dense	X	XXX	X
	Open			X
12.5mm	Dense	XXX	XXX	XXX
	Open			X

[1] An X denotes a single mix.

This plan directly emphasizes low and medium volume roads because these represent the

majority of the roadway miles an owner/agency maintains, and hence the greatest number

of mix designs performed annually. However, the high volume roadways have the

greatest vehicle-miles traveled in the state, making them more prone to failure by

permanent deformation, and thus these mixes have been included too.

1.4 Individual Job Experimental Plan

Each job has a replicate experimental plan that has been developed which examines the effects of changes in air voids and asphalt binder content considered in Table 3.1. The reason for this portion of the research project was to understand variations that typically occur during field production. Depending on the ease of compaction and the temperature of the mat, the in-situ air voids after initial construction can vary significantly. This variability can significantly affect pavement performance. Contractors will typically seek 92.0% G_{mm} or 8.0% air voids so that they can receive full pay for a job in Wisconsin, however this may not always be achievable and thus higher air void contents were examined (Wisconsin Construction Specification, 2004).

In terms of the asphalt content, the contractors are allowed to deviate ±0.3% from that of the asphalt content stipulated in the accepted job mix formula (JMF), which was stated in Section 460.2.8.2.1.5 of the Wisconsin Constructions Specifications (2004) and is typical of most owner/agencies. It should be noted that since mixes were being sampled from field produced mixes being placed on roadways, testing at a lower asphalt binder content than that produced was not possible. This portion of the experimental plan can be found in Table 1.2.

Table 1.2 Experimental Plan for Volumetric Changes

		Asphalt Binder Content	
		Sampled (Assumed Optimum)	Sampled + 0.3%
Air Voids (compaction effort)	Low	X[1]	N/T[2]
	Target	X	X
	High	X	N/T

[1] An X denotes six specimens for each project.

[2] N/T denotes not tested.

Changes in air voids were obtained through changing the weight of mix in the specimen and compacting to a given height of 170.0-mm. Low, target, and high refer to 4.0, 7.0, and 10.0% air voids, respectively. Testing was also carried out with specimens in which the asphalt binder content was increased 0.3% by weight of the mix. This material necessitated further mixing. The extra asphalt binder was sampled from the plant where the mixture was produced. The procedures for sample procurement and preparation for testing are outlined in Chapter 3.

1.5 Hypotheses for Testing Results

Based upon past testing and research from the literature review, hypotheses were developed regarding the factors considered in the experimental plan. The statistical analyses of these hypotheses are presented in Chapter 7. These hypotheses are outlined in the following sections for dynamic modulus, flow number, and pavement design.

1.5.1 Dynamic Modulus

These are the following relationships that are expected to be observed from dynamic modulus testing and developed prior to the use of Superpave Simple Performance Test (SPT).

- As temperature increases, dynamic modulus will decrease and phase angle will increase.

- As air voids increase and likewise compaction effort decreases, dynamic modulus will decrease.

- As the asphalt cement content increases, dynamic modulus will decrease.

- As the aggregate angularity (corresponding with traffic volume) increases, dynamic modulus will increase.

1.5.2 Flow Number

These are the following relationships that are expected to be observed from flow number testing and developed prior to the use of Superpave SPT.

- As air voids increases, the flow number will decrease.

- As the asphalt cement content increases, the flow number will decrease.

- As the aggregate angularity (corresponding with traffic volume) increases, the flow number will increase.

1.5.3 Pavement Structure

It is expected that the mechanistic-empirical pavement design would yield a slightly thinner HMA layer than compared to that of the solely empirical pavement design procedure. The reason being is that the empirical pavement design has a greater factor of safety built into the model than mechanistic-empirical pavement design. Minimal distresses would be indicative of thinner layer thicknesses. The current Design Guide software is more of a design check as opposed to a design guide. The analysis approach was to input varying thicknesses for the layer in question with the pavement structure remaining constant and the level of distress through simulations conducted with the Design Guide software.

1.6 Contents of this Document

Chapter 2 of this document discusses past research and studies that have been conducted that pertain directly to the Superpave SPT. Included is a brief description of the research conducted along with the major findings of the studies that directly apply to this project. Chapter 3 explains the procedures that were undertaken to sample, prepare, and test the specimens for this project. Chapter 4 discusses the mixes that were sampled and some of the difficulties with the original experimental plan. Chapter 5 reviews the specimen preparation, in terms of the volumetric properties. Chapter 6 presents the preliminary test results of the Superpave SPTs. Chapter 7 presents the results of the SPT testing of the three mixtures from the State of Wisconsin and analyzes the results in terms

of the hypotheses that were developed. Chapter 8 summarizes the conclusions that were

reached. Chapter 9 outlines the recommendations for future work based on the findings

of this project.

CHAPTER 2: LITERATURE REVIEW

2.1 Mechanistic and Mechanistic Empirical Design Approach

In 1885, Joseph Boussinesq developed a method for determining induced stresses and strains in an infinite elastic half-space based on a point load (Coduto, 1999). These equations were based on a linear elastic material and have been applied to asphalt pavements. Asphalt pavement mixtures have been around since 1874 (Roberts, 2002), with informal pavement design procedures starting in 1920 (Vesic, 1964). These early pavement design procedures were based primarily on "rules of thumb" as well as past experience. Burmister (1943) appears to be the first researcher to apply a mechanistic analysis to a multi-layer system for the purposes of a pavement design. A considerable amount of work has been conducted since Burmister, which has ultimately led to the development of the current AASHTO Design Guide for New and Rehabilitated Pavements, henceforth referred to as the Design Guide.

A mechanistic pavement design utilizes mechanical modeling to determine the stress, strain, and displacement under a load (Timm, 1998) and more importantly, a wheel load. With knowledge of the various layer properties (which depends on the method of analysis) of the pavement structure, these reactions can be determined and incorporated into empirical transfer functions to determine the number of load applications to failure. Numerous transfer functions have been developed and center on the distresses of rutting and fatigue. Current pavement design procedures are based on empirical relationships that were derived from testing conducted at the AASHO Road Test in the late 1950's.

However, these procedures have become outdated due to changes in load configurations and the general magnitude of the loads. The AASHO Road Test was conducted over a relatively short period of time and did not capture the effects of aging. In addition, being a test track, the applicability of the results to other regions is limited due to the lack of variability in climate and materials with which the structure was built. Other issues are addressed in Section 2.3. With a mechanistic pavement design procedure, these issues can be addressed, where the mechanical properties of the HMA can be determined under varied climatic conditions and materials specific to the pavement. Mechanistic models can easily adapt to changes in the vehicle configuration and load spectra. It should be noted that the mechanistic pavement design procedure does not drastically change the pavement cross-section from that of empirically based designs; however, it provides the ability to analyze changes in traffic and materials and employ them in the design (Newcomb, 2001).

In order to conduct an analysis of a flexible pavement system (Figure 2.1) using a multi-layered theory, several assumptions must be made (Huang, 2003):

- Each layer is homogeneous, isotropic, and linearly elastic and has an elastic modulus, E, and Poisson's ratio, v, which is representative of that particular layer.

- The layer itself does not induce a load on the supporting layers due to its presence and the layer is infinite in the horizontal directions.

- Each layer has a specific layer thickness and the lowest layer is considered to be infinite in thickness.

- The load that is applied to the surface layer is uniform over a circular area with radius a and is applied as a pressure q.

- The final assumption is that the interface of the layers are in constant contact with one another and act together, thus the normal and shearing stresses and the horizontal and vertical displacements present at the interface are equal for each layer.
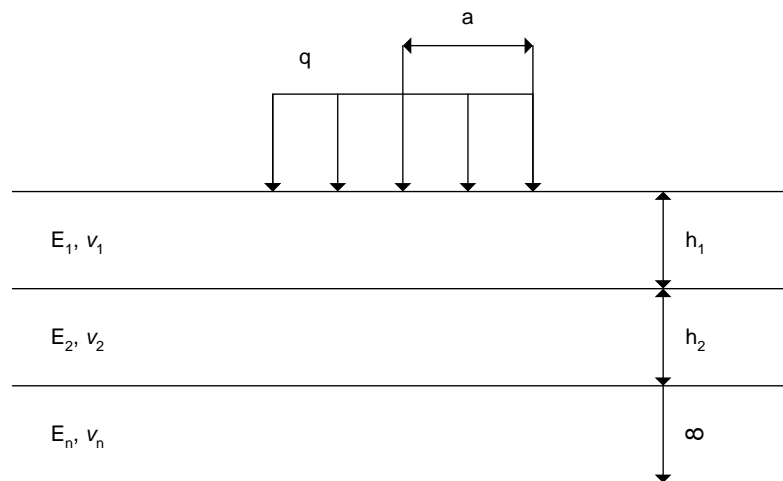
Figure 2.1 n-Layered System (Huang, 2003)

2.2 Mechanistic and Mechanistic-Empirical Pavement Design Development

Donald Burmister was the first researcher to apply elastic layer theories developed by Love and Timeshenko to determine stress and displacement of a pavement structure (1943). Burmister realized that most pavements were multi-layer systems and that the theories that were developed by Boussinesq (infinite elastic half-space) and Boit and later Pickett (infinitely elastic second layer) were not applicable to such systems. Burmister deemed that settlement was the most important aspect to consider in pavement design. Burmister used the basic Boussinesq equations to develop his own set of

equations for a two-layered system. A correction coefficient was employed and compared to that of the Boussinesq results, to verify the solutions. The correction coefficient was a function of the radius of the load to the thickness of the first layer and the ratio of the elastic modulus of the second layer to that of the first layer. Burmister demonstrated through example pavements how the graphical representation of the correction coefficient could be used in various material and loading conditions for the determination of layer thicknesses. In addition, an approach for a three-layer system was presented. In the discussion of the paper by Burmister (1943), T.A. Middlebrook, U.S. Engineer Department, War Department cited that there was no field knowledge of the true stress-strain characteristics to warrant the use of the developed method by Burmister. It was also noted that pavement failures are not by deflections but rather the stresses and strains that are developed under loading (Huang, 2003).

Inan effort to better understand the mechanisms of pavement failure, the critical location where the failure originates needed to be identified. There are two major modes of failure for flexible pavement: permanent deformation and fatigue cracking. Kerkhoven and Dormon determined that the critical location where rutting was believed to occur could be readily attributed to compressive strains at the surface of the subgrade (1953). The interface of the other pavement layers should also be examined to ensure that higher compressive strains do not persist. The mode of fatigue cracking was found to be the horizontal strains at the bottom of the asphalt layer (Saal and Pell, 1960).

Foster and Ahlvin developed charts to determine the vertical, radial, tangential, and shear stresses as well as deflections due to a circular load (1954). A designer could use these charts for specific depths and distances from the load in the pavement structure.

The charts were based on a single layer with a specific modulus and a Poisson's ratio of 0.50. From the charts of the stresses, the strains could be determined.

Jones (1962) conducted a study to measure the vertical and horizontal stresses and strains in a three-layer system at the bottom of the asphalt layer and at the surface of the subgrade. Jones considered the ratio of the modulus of adjacent layers, the ratio of the thickness of adjacent layers, and the radius of the load to that of the thickness of the second layer to determine the stress. Utilizing these inputs, stress and strain factors were calculated and applied for a given load. It should be noted that a Poisson's ratio of 0.50 was also used in the study and that in practice not all materials adhere to this value. Huang cites that the Poisson's ratio has only a small impact on pavement response and thus differences with the actual ratio are negligible (2003). In working with Jones, Peattie developed graphical representations of the stresses and strains within the various layers of the system (1962). The drawback to this system is that interpolation between the values is both arbitrary and difficult.

In an effort to validate the mechanistic functions of Boussinesq and Burmister, an analysis of the AASHO Road Tests was conducted by Vesic and Domaschuk (1964). The true stress-strain characteristics of a pavement under a variety of loading and environmental conditions were readily available from this field study. It was determined that the stress distribution and the deflection basins closely approximated the Boussinesq results. This does not discount Burmister's findings but demonstrates that there is a need to better understand the mechanics of flexible pavement, because field results inherently have greater variability and uncontrollable environmental conditions. Areas where

additional study was suggested were the effects of pavement temperature, the presence of moisture, and the rate of load application.

Molenaar and Van Gurp (1982) presented a mechanistic-empirical model for the design of flexible pavements. This study examined 93 in-service pavement structures and used the program BISAR to relate layer equivalent thicknesses to that of maximum radial strain in the asphalt layer and vertical strain in the surface of subgrade. BISAR is a computer program that was developed by Shell; it considers both vertical and horizontal stresses and is based on Burmister's layered theory (Huang, 2003). By using the elastic modulus values of the pavement at a reference temperature that was representative of Dutch conditions, an equivalent layer thickness could be determined. Equation 2.1 shows the definition of equivalent layer thickness.

$$h_e = \sum_{i=1}^{2} 0.9 h_i \sqrt[3]{\frac{E_i}{E_3}}$$
(2.1)

where:
        h_e = equivalent layer thickness (m),
        h_i = thickness of layer i (m),
        E_i = elastic modulus of layer i (N/m^2), and
        E_3 = elastic modulus of the subgrade (N/m^2).

The equivalent layer thickness could also be used to determine the number of loads until failure occurred due to a 100-kN axle load. In addition, probability-of-survival curves were developed that showed as the equivalent layer thickness increased, the number of loads until failure likewise increased.

To better understand flexible pavements response to loading an explanation of the models used to describe the interaction of loading and the response of flexible pavements was identified by Lytton et al (1993). Lytton et al presents in detail, the different models that are used to describe the elastic, plastic, viscoelastic, and viscoelastoplastic models as

they apply to the different distresses and temperatures that a pavement endures

throughout its life. At low temperatures a linear elastic or viscoelastic model is

appropriate, with Maxwell, Kelvin-Voigt, and Burger components in series or in parallel

as illustrated in Figure 2.2. The Burger model with Kelvin model elements in series can

capture the viscoelastoplastic behavior of a flexible pavement at the higher temperatures.

The reason that a series of Kelvin models are required is that a single Kelvin model is not

adequate to capture the retarded strain that takes place over time.

(a) **(b)** **(c)**
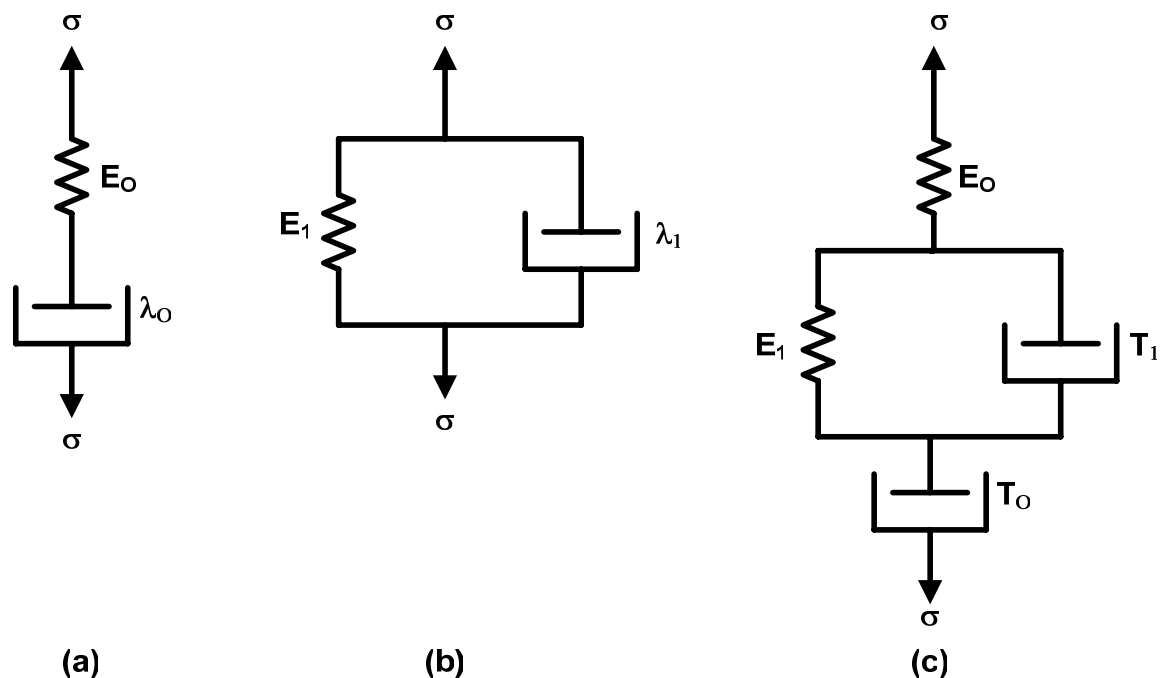
Figure 2.2 Mechanical Models: (a) Maxwell, (b) Kelvin-Voigt, and (c) Burger

The equations for these particular models can be found in Huang (2003) pp. 78-80. For

higher temperatures, flexible pavements response is said to best be described by a

viscoelastoplastic model. A viscoelastoplastic model (Figure 2.3) is representative of a

repeated load, where a load is placed on a pavement and there is instantaneous

deformation followed by some creep; and with the unloading of the pavement, there is an

16

instantaneous elastic rebound followed by creep recovery. Figure 2.3 displays a single loading cycle and the materials response due to the loading.
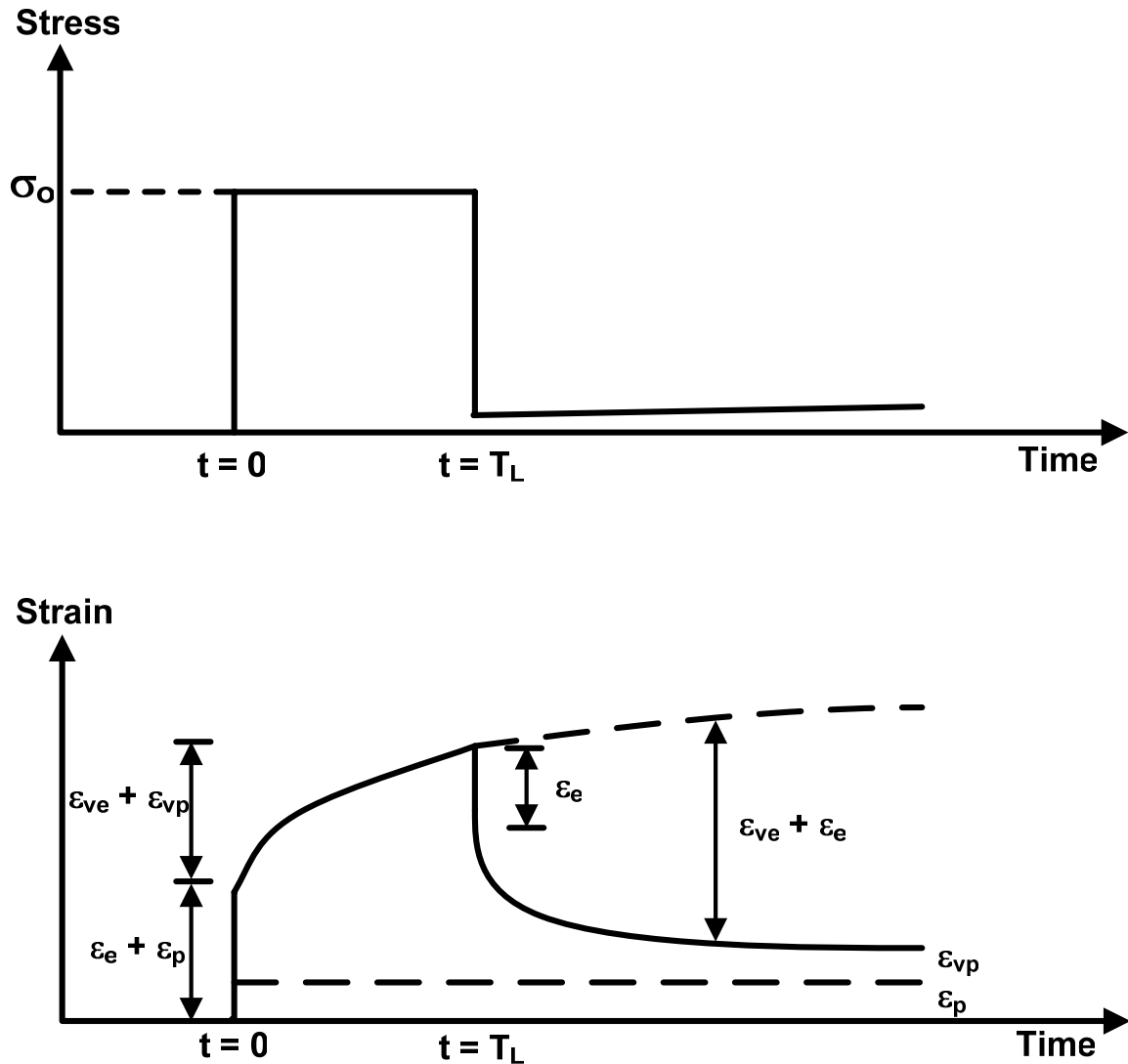
Figure 2.3 Viscoelastoplastic Component Model (Lytton et al, 1993)

In Figure 2.3, ε_e is the elastic strain - recoverable and time independent, ε_p is the plastic strain - irrecoverable and time independent, ε_{ve} is the viscoelastic strain - recoverable and time dependent, and ε_{vp} is the viscoplastic strain - irrecoverable and time dependent (Uzan et al, 1985).

Lytton et al (1993) went on to develop a 2D finite element analysis program which was similar to that developed by Owen and Hinton (1980), with only minor modifications based on a viscoelastoplastic model. The model that Owen and Hinton uses is a four parameter model with a spring and dashpot in series and a second spring and dashpot in parallel to the first series. Additionally, one of the dashpots is modeled with a friction slider to account for the initial viscoelastic response prior to initial yielding followed by viscoplastic response. The model for fatigue used by Lytton et al was similar to that used by VESYS. The VESYS cracking model follows equation 2.2

$$N_q = k_1 \varepsilon^{-k_2} \tag{2.2}$$

N_q represents the number of loads until failure, k_1 and k_2 are model constants, and ε is maximum tensile strain. Miner's law was also incorporated to determine the fatigue ratio. The models used by Lytton et al were then calibrated to field observations for both distresses.

Van Cauwelaert et al (1988) developed a linear-elastic program that could be utilized on a standard personal computer; the name of the program was WESLEA. This was in contrast to other programs like BISAR which required a mainframe. WESLEA can analyze up to five-layers with a semi-infinite base layer and 20 loads. The deflection of the pavement was based on a Newton-Coates integration formula and requires a minimum of six steps. The steps of the integration are based on the modulus ratio (the ratio of the elastic modulus of upper layer to that of the lower layer). By optimizing the number of steps required to perform the deflection calculation, the analysis period could be minimized. In addition, WESLEA has a component that accounts for friction at the interface of the layers. The interface friction component was developed based upon

composite beams. Van Cauwalaert et al went on to show that there no significant difference between the deflections determined by BISAR and that the time of computation was significantly less. The comparison included varying wheel loads, distance from the loaded area, pavement structures, and wheel configurations, all showing similar solutions. Additionally, a subroutine of BISDEF was added to WESLEA to create WESDEF to backcalculate pavement modulus through nondestructive testing (NDT). WESDEF utilized WESLEA's optimization routine to determine the individual pavement layer modulus values. BISDEF and WESDEF showed a good correlation between the modulus values of the individual layers.

Collop et al (2003) have developed a finite element program named CAPA-3D which uses the viscoelastoplastic model to determine the stresses throughout an element due to loading. This program uses the Burger model for material characterization as it was mainly concerned with permanent deformation. The program allows for the development of the pavement structure where each layer is characterized by its Young's Modulus, Poisson's ratio, and thickness. Collop et al ran a simulation with a load of 700kPa at 20°C to show the stress, accumulated strain and damage, and equivalent viscosities throughout the element, due to a single load application. The simulations illustrated that the location of the maximum strain was reliant on the stress-dependence of the flexible pavement. Stress-dependent pavements showed the greatest stress at approximately one-half the thickness of the asphalt layer, whereas non-stress-dependent pavements showed more of an even distribution of vertical strain.

Uzan (2004) presented a mechanistic-empirical pavement design method that considered the ratio of the resilient to plastic strain as a function of traffic composition,

temperature changes throughout the day, environmental conditions, and changes in material response with depth. This method allows the surface and the underlying layers to be broken down into sublayers so that permanent strains can be more effectively determined as opposed to the overall deformation of the entire layer. Uzan used the program JULEA to conduct the pavement analysis and numerous points within the pavement structure were examined in response to the loading (not just directly under the load). This research yielded two important findings: 1) a design load can be used to reduce the number of axle configurations, and 2) the stiffness of the pavement can be improved by increasing the thickness of the asphalt pavement layer, which reduces permanent deformation.

2.3 Development and Design of the Current Mechanistic-Empirical Design Approach

The foundation for the 1972 AASHO Design Guide and later iterations of the Design Guide are based on conditions existing at the AASHO Road Test and are thus solely empirical in nature. Many of the conditions used during the test have changed considerably and are not readily applicable to the later iterations of the Design Guide. Some of the major conditions that have spurred the need for changes in the Design Guides are as follows (McGhee, 1999):

1. Pavement rehabilitation design procedures were not originally considered.
2. The AASHO Road Test was carried out in a single geographic location, making it difficult to readily address differences in climatic conditions.

3. There was only one type of underlying material used for the subgrade and an unstabilized dense-graded subbase, which once again makes it difficult to address differences in materials.

4. Vehicles have drastically changed and as a result the vehicles used during the AASHO Road Test are not representative of today's vehicles.

5. Drainage of the underlying layers was not addressed.

6. The level of loading was also considerably less than those experienced by some of the arterials of the U.S. Highway system today.

7. The length of the test was only 2 years and most pavements are expected to perform for 20 to 50 years.

Considerable steps have been made to resolve many of the aforementioned issues through research and field performance testing. One of the methods employed is the use of test tracks like WesTrack and the National Center for Asphalt Technology's (NCATs) test track. These testing facilities focused mainly on flexible pavement performance, but utilized a better cross-section of materials that are used in practice through repeated load applications with typical vehicle configurations. These testing facilities produced recommendations for better selection of pavement structures and material characteristics sought in flexible pavement designs. Both test tracks also consider the rehabilitation of a pavement structure. These rehabilitations included crack repair, mill and fill, as well as full-depth reconstruction depending on the level of distress and goals of the test track (Epps et al, 1999).

While test tracks are one solution to determining pavement performance, actual road performance (e.g., highways, freeways, etc.) is just as beneficial. In 1987 the Long

Term Pavement Performance (LTPP) program was started under the Strategic Highway Research Program (SHRP) and continues today. The main goal of this program is to collect meaningful data pertinent to field pavement performance. Numerous test sections have been studied all over the continental US and parts of Canada. Data that are collected from these test sections include climatic conditions, traffic (load spectra and configuration), material properties, and pavement structure with numerous pavement performance measures being employed. An extensive data analysis is being performed and tailored so that the information can be used in the calibration and development of later AASHTO Design Guides.

With this abundance of information from both field data and test tracks, different testing procedures have been applied to find a "golden test," which predicts pavement performance based on the measured mechanical properties of test specimens. M.W. Witczak of Arizona State University has done considerable work in this area by developing a testing procedure that correlates the mechanical properties of asphalt pavement to test track performance under NCHRP 9-19 (Witczak et al, 2002). Several tests have shown promising results which include dynamic modulus, flow time, and flow number. Considerable work has been done to incorporate these tests into a pavement design procedure as part of the current AASHTO Design Guide under an M-E design approach.

2.3.1 Previous Barriers to Mechanistic-Empirical Design Implementation

The 1986 Design Guide recognized that future designs would have to be based upon M-E principles. However, the process is calculation intensive and the computers of

the time were not capable of analyzing these advanced pavement design procedures. The

main reason for the lack of computational capability is that differential equations and

finite element analysis were utilized in the different analysis methods (McGhee, 1999).

Today's computers now make these design processes possible and a move has been made

to put them into practice. The intent of the current Design Guide and its associated

software was to fully characterize the fundamental engineering properties of the materials

used in pavement structure for an M-E design.

The 1986 Design Guide identified additional benefits of an M-E design procedure

with particular emphasis to flexible pavements are as follows:

1. Design traffic loading is simply an estimate in the design phase, however

   pavement loading conditions are dynamic throughout the pavements life.

   These changes can be easily factored into the rehabilitation and

   maintenance schedule as necessary, under an M-E pavement design.

2. Procedures can easily be developed to analyze in-situ pavement

   performance. These procedures can be used to determine factors that

   contribute pavement performance that exceeds or does not meet

   expectations.

3. A hot mix asphalt (HMA) pavement oxidizes with time. With the

   oxidation process, the binder stiffens, and this phenomenon can be

   factored into the design through the use of mechanistic procedures.

4. Mountainous regions and northern portions of the US experience seasonal

   fluctuations; particularly freeze-thaw cycles which leads to the weakening

   of the pavement and can be considered.

However, the most prominent reason not identified by the 1986 Design Guide is the ability to more accurately determine when failure would occur in a pavement through performance based testing of materials that make up the structure. Having a better understanding of a pavements' structural performance can lead to economic benefits. The rehabilitation schedule can be more efficiently developed, because the variability in pavement performance can be reduced and the life of the pavement extended through a better assessment of the climate, materials, vehicle loadings, and the variation of performance in the design life. As a result of being able to better identify when rehabilitations need to be scheduled, McGhee cited that an annual savings of $1.14 billion per year over the next 50 years could be realized (1999).

A purely mechanistic pavement design can not currently be used as a standalone procedure from that of necessary empirical relationships. Simply knowing the locations of the greatest stress and strain within the pavement does not reflect its ability to withstand loading. Hence, empirical relationships are then used to predict the life of the pavement in terms of the number of load cycles to failure. This is why the procedure is referred to as an M-E design. The 1993 AASHTO Design Guide cites that the primary benefits from the proper use of a mechanistic design are: first an improved reliability of design in terms of the longevity of the pavement; second, the ability to predict specific types of distress in terms of rutting and fatigue, thus rehabilitation and maintenance schedules can be developed accordingly; finally, a mechanistic design procedure will have the ability to extrapolate from limited field and laboratory results.

2.3.2 The Current Design Guide

The AASHTO Joint Task Force for Pavements (JTFP) is in charge of the development and implementation of pavement design processes. This responsibility has led to the development of past Design Guides (1972, 1986, and 1993). The newest Design Guide was the 2002 edition released in 2004. The recognition for the necessity for re-evaluation of the pavement design process came from the JTFP. In an effort to better understand what experts from federal and state highway agencies, contractors, and academics sought in an improved Design Guide, a workshop was put together by the JTFP on March 24-26, 1996. The areas that were determined of particular interest were as follows: traffic loading, foundations, material characterization, pavement performance, and environment (McGhee, 1999). The ultimate goal of the Design Guide was identified as primarily utilizing a mechanistic design approach. This would involve determining an ideal test that could be used to determine the fundamental engineering properties of the individual layers of the pavement structure.

The current Design Guide uses two different software packages to determine the stresses, strains, and deflections in the pavement structure due to loading. The first is JULEA, which is a multi-layer elastic theory program (AASHTO Design Guide, 2004). The Design Guide states that "JULEA provides an excellent combination of analysis features, theoretical rigor, and computational speed for linear pavement analysis." However, some unbound materials (predominately subbase and subgrade materials) exhibit non-linear response to loading in that they exhibit stress-dependent stiffness, which can vary with thickness. To account for non-linear responses, the program DSC2D has been incorporated into the analysis package (AASHTO Design Guide, 2004).

Both JULEA and DSC2D use specific coordinates to perform their analyses of four axle types (single, dual, tandem, and tridem). Both programs determine the location of the maximum damage based upon the given conditions and is used to determine the pavements performance. One reservation for using the program DSC2D is that it has not been calibrated based on field experience, unlike JULEA, for use in the current Design Guide.

The design procedure outlined in the current Design Guide is mechanistic-empirical in nature due to the fact that calibration factors must be used to relate the properties that predict permanent deformation, fatigue cracking, and the International Roughness Index (IRI). IRI measures the longitudinal profile of a pavement by means of a profilometer and is relevant to comfort of the motorists utilizing the facility. Models to relate field performance to the laboratory-measured parameters have been developed. These models are as follows (AASHTO Design Guide, 2004):

$$\text{Permanent deformation in the AC layer: } \frac{\varepsilon_p}{\varepsilon_r} = 10^{-3.1552} \cdot \beta_{r1} T^{1.734 \cdot \beta_{r2}} N^{0.39937 \cdot \beta_{r3}}$$

(2.3)

where:
      β_{r1}, β_{r2}, β_{r3} = calibration factors,
      ε_p = permanent strain,
      ε_r = resilient strain,
      T = AC temperature, and
      N = number of load repetitions.

$$\text{Fatigue Cracking: } N_f = C \cdot k_1 \left(\frac{1}{\varepsilon_t}\right)^{k_2} \left(\frac{1}{E}\right)^{k_3} \qquad (2.4)$$

where:
      C = lab to field adjustment factor,
      k_1, k_2, k_3 = laboratory developed constants,
      ε_t = tensile strain at the bottom of the asphalt layer, and
      E = elastic modulus of the asphalt layer.

The permanent deformation model has been derived from the work of Leahy, Ayers, and Kaloush as part of NCHRP 9-19 (Appendix GG-1, AASHTO Design Guide, 2004). The fatigue model is the general form of the model and the models most commonly used were developed by Shell and the Asphalt Insititute (Appendix II-1, AASHTO Design Guide, 2004). Calibration factors for these models have been developed for a national, state, and local basis. These calibration factors come from the Long Term Pavement Performance Program, MnRoad, and the AASHO Road Test for new construction, rehabilitation, and overlays.

2.4 Superpave Simple Performance Test (SPT)

The initial development of the Superpave^{TM} mixture design procedure included steps for aggregate and binder characterization, aggregate blending, and volumetric testing of Superpave Gyratory Compactor (SGC) prepared specimens. Two performance tests were also developed: 1) the Superpave Shear Tester (SST), and 2) the Indirect Tensile Tester (IDT) (The Asphalt Institute, 1996). However, these tests are typically not conducted as part of the mix design process.

Various projects such as WesTrack, NCAT, and MnRoad have been conducted to measure the field performance of the newer Superpave mixture design method. Out of these projects and NCHRP Project 9-7, the volumetric testing as a stand-alone procedure has been put into question. As part of the current Design Guide, mixture performance characteristics are used as inputs into the design.

In 1996, the Federal Highway Administration (FHWA) developed a request for bids on a research project to develop a simple performance test to be used in conjunction

with a new Design Guide. This test would measure the performance of HMA to be used

in a particular pavement layer based upon fundamental engineering properties in

conjunction with the established volumetric testing procedures. Various tests were

employed, analyzed, and correlated with performance data from test track facilities that

could be used as the Superpave Simple Performance Test (SPT).   As previously

mentioned, Witczak et al, 2002, found that dynamic modulus, flow time, and flow

number have been shown to have promising correlations with field performance.

The fundamental engineering properties for the hot mix asphalt (HMA) layer are

obtained from what has been termed the Superpave SPT. Witczak et al (2002) defined

the SPT as "A test method(s) that accurately and reliably measures a mixture response

characteristic or parameter that is highly correlated to the occurrence of pavement distress

(e.g., cracking and rutting) over a diverse range of traffic and climatic conditions." These

tests include dynamic modulus $|E*|$, flow time (F_T), and flow number (F_N), which are

conducted at elevated temperatures to determine the mixtures' stiffness analogous to

permanent deformation. Dynamic modulus $|E*|$ alone is run at other stipulated

temperatures so that it can be applied to field conditions and to correlate stiffness to crack

development at the intermediate end of the temperature spectrum. Correlations to field

performance, along with the advantages and disadvantages of these tests from both

Brown et al (2001) and Witczak et al (2002b), can be found in Table 2.1.

Table 2.1 SPT Advantages and Disadvantages (NCHRP Report 465, 2002 and NCAT Report 01-05)

Test	Parameter	Test Condition	Model	R^2	Se/Sy	Advantages	Disadvantages
Dynamic Modulus	E*/sinϕ	Sinusoidal Linear 130°F 5 Hz	Power	0.91	0.310	• Direct input for 2002 Pavement Design Guide • Not forced to use master curves • Easily linked to established regression equations • Non destructive tests	• Coring and sawing • Arrangement of LVDTs • Confined testing gave poor results • Need further study of reliability of confined open graded specimens • Equipment is more complex • Difficult to obtain 1.5:1height-to-diameter ratio specimens in lab
Repeated Loading (Flow Number)	F_N	Unconfined 130°F Various Frequencies	Power	0.88	0.401	• Better simulates traffic conditions	• Equipment is more complex • Restricted test temperature and load levels does not simulate field conditions • Difficult to obtain 1.5:1height-to-diameter ratio specimens in lab

Past research on the performance tests that have been incorporated into the current Design Guide are discussed herein.

2.4.1 Dynamic Modulus Test Setup

Dynamic modulus is one of the oldest tests to be used to measure the fundamental properties of hot mix asphalt (HMA). Dynamic modulus testing has been studied since the early 1960's by Papazian and became a standard test in 1979 by the American Society for Testing and Materials (ASTM) under D3497 "Standard Test Method for Dynamic Modulus of Asphalt Concrete Mixtures." Under the testing procedure for dynamic modulus, a sinusoidal (haversine) compressive stress is applied to the axial ends of a test specimen. The testing procedure includes various frequencies and temperatures to capture the visco-elastic properties of the HMA. This testing scheme is intended to account for various loading and temperature conditions observed in the field. Figure 2.4

shows the typical load application along with a specimens' response to the loading.
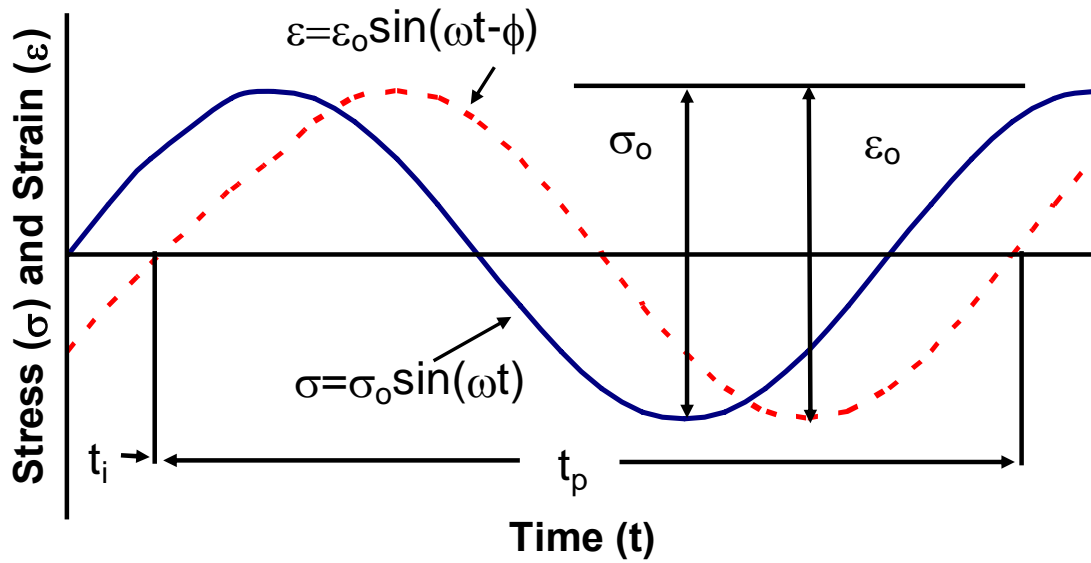
Figure 2.4 Dynamic Modulus Loading

Under the established testing protocol ASTM D3497-79, the stress is applied to the

specimen (solid line) and the axial strain (dashed line) as a result of the stress is measured

during the course of the test. The complex modulus (E*) is mathematically defined as the

maximum (e.g., peak) dynamic stress (σ_o) divided by the peak recoverable axial strain

(ε_o) (Witczak et al, 2002). The complex modulus is sometimes referred to as the dynamic

modulus $|E*|$ and is just the absolute value of the complex modulus. Equation 2.5 shows

the mathematical equation for dynamic modulus.

$$|E| = \frac{\sigma_o}{\varepsilon_o} \qquad (2.5)$$

In order to determine the materials susceptibility to changes in environmental

conditions with particular interest to temperatures, the phase angle (ϕ) is measured. This

is mathematically defined as the time lag between a cycle of stress and strain divided by

the duration of the stress cycle. Mixtures that have a phase angle of 0° ($\phi = 0°$) during

the test exhibit purely elastic behavior, whereas those that have a phase angle of 90° ($\phi =$

90°) exhibit purely viscous behavior. In practice the phase angle ranges from roughly 10

to 45 degrees, but this is mainly temperature dependent and this will be discussed later in

the literature review. Equation 2.6 shows the mathematical definition of phase angle.

$$\phi = \frac{t_i}{t_p} \times 360 \qquad\qquad (2.6)$$

where:
  t_i = time lag between a cycle of stress and strain (s),
  t_p = time for a stress cycle (s), and
  i = imaginary number.

The complex modulus can be related to the phase angle through the elastic and

viscous moduli (E' and E", respectively). The elastic (eq. 2.7) and viscous moduli (eq.

2.8) are determined by the following:

$$E' = \frac{\sigma \cos(\phi)}{\varepsilon_o} \qquad\qquad (2.7)$$

$$E'' = \frac{\sigma \sin(\phi)}{\varepsilon_o} \qquad\qquad (2.8)$$

Dynamic modulus is a measure of the relative stiffness of a mix. Mixes that tend to have

good rut resistance at high temperatures likewise have a high stiffness. Although the

tradeoff is at intermediate temperatures, stiffer mixes tend to be more prone to cracking

for thicker pavements (Shenoy and Romero, 2002). For this reason, dynamic modulus

testing is run at both an intermediate and high temperatures to measure HMA's resistance

to these two distresses for the current Design Guide.

2.4.2 Dynamic Modulus Literature Review

Dynamic modulus has been one of the most studied tests in terms of determining the mechanical properties of asphalt pavement. As previously mentioned Papazian (1962) was the first to develop the test procedure for dynamic modulus. Papazian took into account that HMA is a viscoelastic material and that by applying a sinusoidal stress at a given frequency that the measured strain would follow the same frequency however lagged by the stress by an angle ϕ. The stress is therefore related to the strain by a complex number which is a function of the frequency.

Coffman et al (1964) conducted dynamic modulus tests with a simulated mix from the AASHO Road Test; the only aggregate characterization that was performed was that of a gradation. Some of the basic relationships that are inherent in dynamic modulus testing were realized from this research study. These relationships include: 1) as temperature increases, dynamic modulus decreases, and 2) phase angle increases with an increase in temperature.

Shook and Kallas (1969) conducted a study that identified factors that directly influence the measurement of dynamic modulus. A matrix of specimen variables were developed, which included varying asphalt content, air voids, asphalt viscosity, and compaction effort. Four-inch diameter by eight-inch high cylindrical specimens were prepared for testing. A sinusoidal uniaxial stress was applied to the specimen and the axial strain was measured by strain gauges affixed to the sides of the test specimens. The specimens were tested under varying temperatures and frequencies to accurately measure the effects the variables had on the measured value of the dynamic modulus. With

everything else being held constant several relationships were recognized: 1) with an increase in air voids, dynamic modulus decreases, 2) as asphalt viscosity decreases, so does dynamic modulus, 3) as asphalt content decreases, dynamic modulus increases, and 4) decreasing the compaction effort decreases dynamic modulus.

Numerous models have been developed to predict dynamic modulus values of HMA by using measurable variables like aggregate and asphalt characteristics as well as the loading regimen. An extensive study was undertaken by Akhter and Witczak (1985) in an effort to identify variables that were relevant to a dynamic modulus predictive equation. These variables apply to the mix design process because they have a direct influence on the stiffness of the pavement layer. Over 130 mix designs were evaluated under this study with data contributions being made by The Asphalt Institute (TAI). From an analysis of the mix designs, it was determined that the mixture temperature was the most significant variable in a dynamic modulus predictive equation. This was in addition to the already identified variables that were controllable in terms of material properties, which include the amount and type of asphalt (asphalt content and viscosity) and the gradation of the aggregate (percent retained on the 3/4in, 3/8in, and #4 sieves and percent passing the #200), and air voids in the mix. The frequency of loading also played a significant role in a dynamic modulus predictive equation. Equation 2.9 shows the latest dynamic modulus equation developed by Witczak (2002b).

$$\log|E^*| = -1.249937 + 0.029232(\rho_{200}) - 0.001767(\rho_{200})^2 - 0.002841(\rho_4) - 0.058097(V_a)$$
$$-\frac{0.802208(V_{beff})}{V_{beff} + V_a} + \frac{3.871977 - 0.0021(\rho_4) + 0.003958(\rho_{3/8}) - 0.000017(\rho_{3/8})^2 + 0.005470(\rho_{3/4})}{1 + e^{(-0.603313 - 0.313351 \times \log(f) - 0.393532 \times \log(\eta))}}$$

(2.9)

where:
   E^* = dynamic modulus (10^5psi),
   η = bitumen viscosity (10^6psi),

f = loading frequency (Hz),
V_a = air void content (%),
V_{beff} = effective bitumen content (% by volume),
$\rho_{3/4}$ = cumulative percent retained on 19mm sieve,
$\rho_{3/8}$ = cumulative percent retained on 9.5mm sieve,
ρ_4 = cumulative percent retained on 4.75mm sieve, and
ρ_{200} = percent passing 0.075mm sieve.

The main result of the study concluded that coarse aggregate mixes (mixes containing ¾-in material and greater) provided a higher modulus value and would result in a longer performance life. In addition, mixes that were gap-graded, or had very little material retained on the No. 4 sieve tended to yield higher modulus values.

Witczak et al found that dynamic modulus testing has a strong relationship with field performance data from WesTrack, the FHWA's Accelerated Loading Facility (ALF), and MnRoad for permanent deformation (2002b). Four-inch diameter by six-inch high cylindrical specimens were procured from materials from the individual test sites and tested under confined and unconfined loads. Various frequencies and temperatures were tested and the strains induced by a dynamic load were recorded. Different models for measuring dynamic modulus values were employed and statistically analyzed for goodness-of-fit. The strongest relationship that was shown was with E*/sinϕ, where the specimen is tested unconfined and modeled linearly. Tests that were conducted with a confining stress, exhibited a poor relationship when compared to field measured rutting. Table 2.1, shown previously, lists some of the major advantages and disadvantages of dynamic modulus for permanent deformation as found by this study.

In addition to testing dynamic modulus to correlate rut performance, dynamic modulus was run at low and intermediate temperatures by Witczak et al, (2002b) to determine its relationship with that of thermal and fatigue cracking from materials

procured from the ALF, MnROAD, and WesTrack test sites. The testing was once again conducted on confined and unconfined specimens and various parameters relating to dynamic modulus related to field performance. None of the testing showed strong correlation with field performance, but because of the compatibility with dynamic modulus testing for use in a fatigue model for the current Design Guide; it was recommended for further development. Witczak et al found that results from testing were highly correlated with field distresses when the test results were analyzed by E*max (sinϕ) and run unconfined.

Further field validation of dynamic modulus as a predictor of pavement performance was conducted by Zhou and Scullion (2003). Zhou and Scullion were able to use field performance as a benchmark for determining the rutting susceptibility of a mix, using the SHRP Special Pavement Studies (SPS-1) sections on US-281. There were a total of 20 test sections all of which underwent varying degrees of permanent deformation, but had the same traffic levels. Rut depths were measured via a trenching operation and information available from DATAPAVE (2004) were used in the analysis. DATAPAVE is software provided by LTPP and consists of an online database of all the test sections for the SHRP program. DATAPAVE also uses models to estimate temperature in flexible pavement at varying depths with varying levels of reliability. Samples were taken from between the wheelpaths and specimens remolded to yield the necessary dimensions as stipulated by ASTM D-3497. The specimens were run unconfined at 40°C with an axial stress level of 138kPa. A frequency sweep was also conducted as part of the testing. Zhou and Scullion found that as the frequency increased there was an increase in the measured E*. In addition, the poor performing mixes could

be discerned from those of the good performing mixes, regardless of frequency. The general relationship that was recognized was that as the E* increased, the amount of rutting measured decreased. It was also found that E* and E*/sinϕ were highly correlated and both could be used for comparison purposes of whether or not a mix is more or less rut susceptible.

Clyne et al (2003) performed an analysis of materials from four sections of the MnROAD test site. The testing that was performed focused around the dynamic modulus test setup as stipulated by NCHRP 9-29.   Testing was conducted over five frequencies (0.01, 0.1, 1, 10, and 25Hz) and six test temperatures (-20, -10, 4, 20, 40, 54°C). For sawed/cored specimens it was found that coefficients of variation (COV) of 30-50% were not uncommon. Four relationships were realized from this testing, the first being that holding frequency constant, the dynamic modulus decreases with an increase in temperature. Second, that as temperature increases from -20 to 20°C the phase angle increases, but from 40 to 50°C it decreases as aggregate interlock becomes the controlling factor. Third, under constant temperature, as the frequency increases, so does the measured dynamic modulus. Finally, the dynamic modulus data provides a smooth data set when plotted over the testing temperature and frequencies, but the phase angle is more significantly scattered, meaning that it is difficult to obtain consistent data.

Mohammad et al performed extensive dynamic modulus testing on both field and laboratory prepared specimens from a 25.0-mm dense-graded mixture paved in Louisiana (2005). The study examined the effects of changes in asphalt content, sampled materials over several days of production, and multi-laboratory variability. Mohammad et al showed that by decreasing the asphalt binder content of laboratory prepared mixtures

increases dynamic modulus and decreases the phase angle. Also shown was that the phase angle trends with frequency change with temperature. At 25°C, the phase angle decreases with an increase in frequency and at 45 and 54°C the phase angle increases with frequency up to about 10Hz and begins to decrease. The analysis of test results from multiple days of production found that there was no statistical difference. In terms of the multi-laboratory variability, at 25°C, there was no statistical difference between the results found by FHWA and the Louisiana Transportation Research Center (LTRC). At the high test temperature of 54°C, there was a statistical difference, in that the dynamic modulus results as found by the FHWA testing facility were lower than that of the LTRC.

2.4.3 Tertiary Flow

Tertiary flow, defined in Section 1.5.2, has been identified as a measure of the fundamental engineering properties of HMA. Tertiary flow was first identified by Hills (1973) in a study that pertained to the creep of asphalt mixtures. It was found that the rate of deformation decreased until a critical strain was reached and then the strain rate began to increase. Hills also observed during the course of the test that the volume of the specimen increased, which meant that the individual aggregate particles were moving past each other in order for additional deformation to occur in the specimen. It was noted that no field-rutted pavement had been observed as undergoing this dilation (an increase in air voids and change in the specimen volume). Subsequent research has identified dilation of asphalt pavement (Mallick, 1995).

Tertiary flow, along with dynamic modulus, can then be linked to distress prediction models (Witczak et al, 2002a). Extensive testing has been conducted in terms

of correlating tertiary flow to pavement performance by Witczak et al (2002b) as part of

NCHRP Projects 9-19 and 9-29. This testing parameter is anticipated to be one of the

inputs used in later revisions of the current Design Guide.

2.4.4 Repeated Load Test (Flow Number) Test Setup

The test for flow number is based on a repeated loading and unloading of an

HMA specimen where the permanent deformation of the specimen is recorded as a

function of the number load cycles. The loading is for 0.1-sec followed by a 0.9-sec

dwell (or unloading) of the specimen. There are three phases of flow that occur during

this type of test, primary, secondary, and tertiary. Under primary flow, there is a decrease

in the strain rate with time. With continuous repeated load application the next phase is

secondary flow, which is characterized by a relatively constant strain rate. Finally the

material enters tertiary flow, where the strain rate begins to increase as the test

progresses. Tertiary flow signifies that the specimen is beginning to deform significantly

and the individual aggregate that makes up the skeleton of the mix is moving past each

other. Flow number is based upon the initiation of tertiary flow (or the minimum strain

rate recorded during the course of the test). The sample loading and strain measurements

can be found in Figure 2.5.
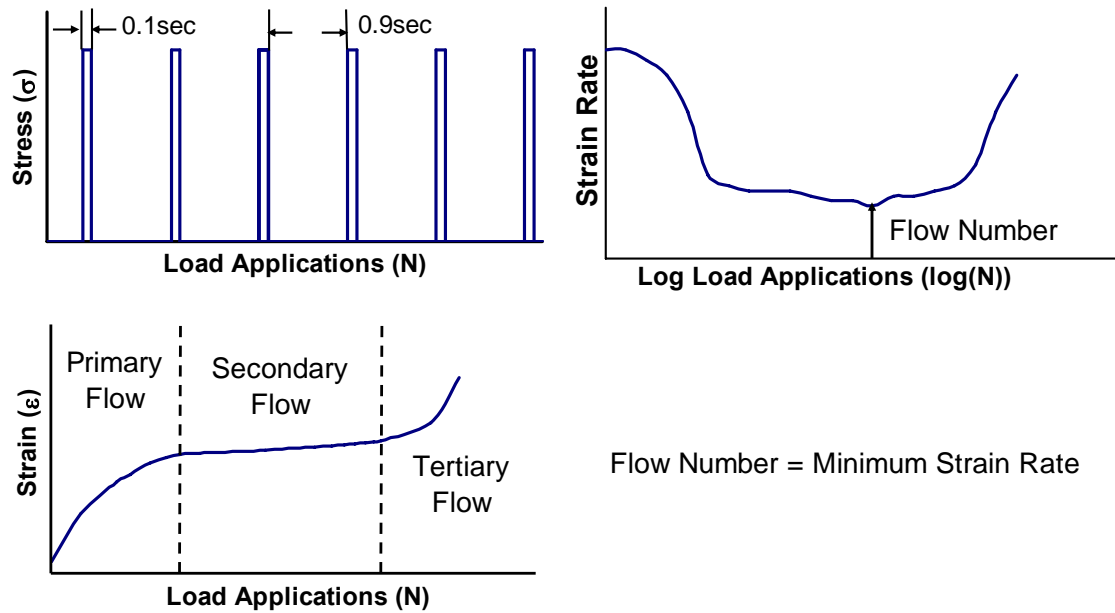
Figure 2.5 Flow Number Loading

Flow number is more analogous to field conditions because loading of the pavement is not continuous; there is a dwell period between loadings. This allows the pavement a period to recover some of the strain induced by the loading. According to Don Christensen, Ray Bonaquist, and Leslie Ann Myers, flow number has currently been selected as a test to be used to complement dynamic modulus in the current Design Guide, whereas flow time is not being used in practice (personal conversation, 2004).

2.4.5 Repeated Load Test (Flow Number) Literature Review

Brown and Snaith (1974) conducted a multiple variable investigation and their effects on the number of load applications to failure. With all other variables remaining constant, only one variable was tested at a time. Failure was defined by a marked increase in the deformation rate and the number of cycles that had occurred to what was considered the failure point (similar to that of tertiary flow). The most noteworthy results

39

of the testing were: 1) as temperature increased, strain increased substantially, 2) as the applied stress was increased the strain increased, 3) as confining stress was increased, the strain decreased, 4) the rate of strain was time dependent upon frequencies above 1Hz, and 5) a binder content of 4% by mass of the mix yielded the highest stiffness at lower temperatures (10 to 30°C or 50 to 86°F) and 3% by mass of the mix at higher temperatures (40°C or 104°F). One of the variables that showed an insignificant effect on strain was that of the rest period between load applications. It should be noted that some of the specimens that were tested under unconfined conditions developed cracks within the specimen; these cracks led to dilation of specimens.

Brown and Cooper (1984) tested cored specimens from a roller compacted slab. These specimens were tested under a repeated triaxial load with different aggregate gradations, confining stresses, and binder based upon penetration grading (AASHTO T 49 and ASTM D). One of the conclusions found in the study was that, for the formulated mixtures, there was little influence of the penetration grade on the development of permanent shear strain in the specimen, with all other variables held constant. Further testing showed that major changes in gradation, particularly with gap-graded mixes, developed higher shear strain under fewer load cycles. Additional testing went on to discount the Marshall flow and stability testing, which showed a negative correlation with the results of repeated triaxial loading test.

A study was conducted by Mallick et al (1995) in three phases to determine the effects of air voids on dynamic creep testing (repeated loading), correlating field rutting with the measured strain from dynamic creep testing of field samples, and finally crushed aggregate performance. Testing was conducted in accordance with ASTM D4123-82.

All of the dynamic creep tests were conducted at 60°C (140°F), which is representative of average high pavement temperatures throughout the US. Varying deviator and confining stresses were applied to the specimens depending on the phases of the study, but were typical of field conditions. During the first and second phase of the study a 826.8kPa (120psi) normal pressure and 137.8kPa (20psi) confining pressure was used. For the third phase the normal pressure was 1653.6kPa (240psi) and a confining pressure of 275.6kPa (40psi) was used, which were analogous to common applied airfield stresses. From the first phase of the study a rather clear logarithmic relationship was found between air voids and permanent strain. It was noted that at a level of 3.0% air voids and less, was a defining point in which permanent strain began to increase rapidly. Also analyzed during this phase of the study was the change in air voids of the specimens after testing. It was found that specimens with 3.0% or less initial air voids underwent dilation, while specimens with greater than 3.0% initial air voids underwent consolidation. This was consistent with observed field behavior, where pavements with low initial air voids tended to shove, creating more air voids and under compacted pavements experience densification through traffic loading. The second phase used field procured samples with known loading levels to analyze the permanent deformation that occurred in the field to that of the permanent strain from repeated loading. This phase showed a very strong correlation with permanent strain and rutting rate (defined as millimeters of rutting / square root of million of ESALs). This means that dynamic confined creep testing could potentially be used to identify rutting potential of a mix. The last phase of testing was with varying angular materials; with the dynamic creep

testing, inferior mixes were identified by the higher measured permanent strain. These inferior mixes contained little or no angular material.

Brown and Gibb (1996) studied the effects of varied gradation and asphalt type as well as asphalt content, on permanent deformation and uniaxially loaded specimens. A small-scale Pavement Testing Facility (PTF) was setup and four pavement sections were cored for repeated load testing. Pavements that showed high levels of rutting in the wheel track testing also showed a good correlation with the specimen going to failure when tested at the same temperature in uniaxial compression. Testing performed at different temperatures from that of the PTF tended to misrepresent the performance of the pavement. With this realization, an effort was placed on understanding the roles of the binder and the aggregate. Through estimates of the binder stiffness, the strain rate decreases on a log-log scale, which means as binder stiffness decreases, the aggregate structure must carry the load to resist permanent deformation. One of the major conclusions of the study was that repeated loading in terms of uniaxial compression was better at measuring permanent deformation because permanent strains were analogous to field loading conditions. In the field there is an accumulation of strain in the pavement with each additional loading, but there is a dwell period before the next load application, and a repeated loading configuration best simulates this condition.

Flow number is defined as the number of load applications when shear deformation begins (Witczak et al, 2002b). Flow number attempts to identify a mixtures resistance to permanent deformation by measuring the shear deformation that occurs due to a haversine loading. The testing regimen calls for repeated cyclical loads to be applied for 0.1 sec followed by 0.9 sec dwell (or rest). The point at which shear

deformation (tertiary flow) begins is where the flow number is recorded. A power model was used in data analysis. Unconfined testing showed a higher correlation with permanent deformation data from MnRoad, ALF, and WesTrack. The volumetric data from some of the test sections at WesTrack may have been inaccurately reported and as a result the correlation could actually be higher in testing conducted. Table 2.1, shown previously, lists some of the major advantages and disadvantages of flow number as found by Brown et al (2001) and Witczak et al (2002b).

Kaloush and Witczak (2002) found that repeated loading simulated field loading and test parameters could be used for several applications. However, the disadvantages to such a test are the complexity with developing design guidelines and that the specimens may need to be confined. In this particular study it was found that confined testing correlated best with field results and that either axial or radial strains could be used for flow time measurement.

In addition to evaluating dynamic modulus as a means of comparing poor and good performing mixes, Zhou and Scullion (2003) also ran their specimens through a repeated loading test. In the analysis, models that were developed (and later presented in Zhou et al, 2004) were employed to so that each of the stages of permanent deformation (primary, secondary, and tertiary creep) could be characterized. Once again, Zhou and Scullion found that there was good correlation between field performance and the flow number. They concluded that the flow number test could be used as a means of comparing mixes for rut susceptibility.

Mohammad et al also examined the effects of binder content flow number. The asphalt binder content changes consisted of ±0.5% from that of optimum. Through a

statistical analysis, flow number was found to not be as sensitive to changes in asphalt content as dynamic modulus. The analysis did show that the specimens with the low asphalt binder content had the highest flow number.

2.5 Specimen Geometry

Witczak et al (2000) examined the effects of specimen geometry on dynamic modulus, flow time, and flow number test results. Three different Superpave mixes were developed with a single PG 64-22 binder. Over 200 specimens were prepared using a Superpave Gyratory Compactor (SGC); these specimens were then cut down to fill a matrix of heights and diameters to be tested for the uniaxial compression tests. It was generally recognized that smaller specimens in terms of the diameter were observed to have lower air void contents. One of the major findings was that the lower the height to diameter ratio (H/D), the higher the recorded dynamic modulus, and is likely due to the proximity of the Linear Variable Differential Transformers (LVDTs) to the load platens. For the determination of phase angle, the effects of H/D are exceptionally notable in that stiffness decreases with an increasing diameter. This is especially important because at 40°C (140°F), there was more than ten degree difference in the phase angle between 70 and 150mm diameter specimens. It was believed that the relationship between the specimen diameter and the measured phase angle was attributable to the radial changes in the structure of the gyratory specimen. The flow number was also observed to decrease as the H/D ratio increased. It was stated that this result was rational because with "short specimens, end friction restricts large lateral expansion that accompanies tertiary flow in uniaxial specimens" (Witczak, 2000). An effort was made to standardize an exact

specimen for dynamic modulus testing, flow time, flow number based on the information in Table 2.2. It was recommended that a height to diameter ratio of 1.5 would be sufficient; the diameter of the test specimens was selected to be 100-mm (4.0-in) with a height of 150-mm (6.0-in).

Table 2.2 Uniaxial Data Analysis (Witczak et al, 2000)

| Parameter | H/D Ratio | | | |
| | Graphical[1] | Analysis of Variance | | |
	Effect for Increasing H/D	Significant	Multiple Comparisons	Limit
$\lvert E^* \rvert$ 4C	Decreases	No	1=1.5=2=3	1.5
Diameter 4C	None	No	1=1.5=2=3	1.0
$\lvert E^* \rvert$ 40C	None	No	1=1.5=2=3	1.0
Diameter 40C	None	No	1=1.5=2=3	1.0
$\varepsilon_{\pi 2000}$	None	No	1=1.5=2=3	1.0
Flow	Decreases	Yes	1>1.5=2=3	1.5
Parameter	Diameter			
	Graphical	Analysis of Variance		
	Effect for Increasing D	Significant	Multiple Comparisons	Limit
$\lvert E^* \rvert$ 4C	None	No	70=100=150	70
Diameter 4C	Decreases	Yes	70>100>150	None
$\lvert E^* \rvert$ 40C	None	No	70=100=150	70
Diameter 40C	Decreases	Yes	70>100>150	None
$\varepsilon_{\pi 2000}$	Decreases	Yes	70>100=150	100
Flow	Increases	Yes	70<100=150	100

[1]References the graphical change in the test parameter with a change in the H/D ratio.

In addition to performing an analysis on Mn/ROAD material for dynamic modulus, Clyne et al (2003) also performed a comparison on specimen preparation. Testing included specimens that were saw/cored to the diameter of 100mm and a height of 150mm and specimens compacted to the same diameter and height.   Clyne et al found that the specimens compacted to the test specimen geometries had lower coefficients of

variation (COVs), but higher E* values as compared to the cored specimens by 40-50%. It was also noted that the sawed/cored group had higher phase angle values by 10 to 20%.

Birgisson et al (2005) found that there was as little difference as 0.6 to 1.9 percent difference between the two specimen preparation procedures used by Clyne et al (2003) for the measured dynamic modulus values at 40°C. It was further noted by Birgisson et al that there was only a difference of 0.2-0.3 percent air voids between the center of and the outer edges of the specimen, thus further validating the legitimacy of using a 100mm diameter by 150mm high gyratory compacted specimen as opposed to a specimen sawed and cored to those dimensions.

2.6 Specimen Variability

Hills (1973) experimented with various compaction methods and their effects on creep. A gyratory compactor, impact hammer (Marshall Method), static, and rolling loads were used to compact the specimens, with the varying levels of compactive effort employed for the gyratory and Marshall methods. It was observed that the rolling compaction method yielded the lowest mix stiffness of all the compaction methods, with the gyratory compactor showing the highest mix stiffness for both compactive efforts. The compactive effort significantly affected the voids in the mix, but there seemed to be no direct correlation between voids and mix stiffness.

As previously mentioned (Mallick, Akter and Witczak, and Shook and Kallas), the volumetric properties can significantly affect the parameter that is being tested. In a round robin study by the University of Connecticut (Mahoney and Stephens, 2003), trends were noticed in the type of SGC that was employed. Differences that are a result

of the selection of the compactor can significantly affect the volumetric properties. This study found that a Pine AFG1A consistently yielded the lowest air void contents, and that a Troxler 4140 SGC, generated the highest air void contents of SGC's included in the round robin study. The sample size for this study was relatively limited, but showed that there is variation among the SGCs in use. Although this article did not directly pertain to Superpave SPT, it does illustrate that the type of SGC used can have an influence on air voids, which plays a significant role in mix stiffness.

Azari et al (2004) analyzed the affects of specimen homogeneity on the measurement of dynamic modulus and flow number. Eight specimens were procured that were homogeneous in composition and verified through x-ray computed tomography. Another eight specimens were procured that were inhomogeneous, where the bottom of the specimen was coarse graded and the top was fine graded. The specimens were tested at 21 and 45°C with 10Hz frequency for the dynamic modulus test. It was found that there were no statistical differences between the means of the two groups at both temperatures. The listed rejection probabilities for the t-values as 17 and 90% for 21 and 45°C, respectively, thus showing there was not a significant statistical difference between the two groups. The inhomogeneous specimens were noted as having a higher degree of variability at both temperatures, but were not analyzed statistically. Azari et al found that there was no difference between the flow number results of the two groups and the t-value corresponded to a 55% rejection probability.

Birgisson et al (2005) examined the effects of specimen preparation on dynamic modulus results. Specimens were compacted in a 102mm diameter mold and compacted to the test height. Another set of specimens were 102mm diameter specimen which was

cored out from a 150mm gyratory compacted specimen (it could not be determined whether the specimen was cut down to the testing height). Testing was conducted at 0.1, 1, 10, and 25Hz at 40°C. Birgisson et al found that differences in the two sample preparation methods ranged from 0.6 to 1.9percent. It was also noted that when the data was plotted that the lines between the frequencies crossed, which implied that there was not a bias in the sample preparation method.

2.7 Test Variability

In addition to studying specimen geometry, Witczak et al (2000), studied the repeatability of the testing through LVDT configuration and the number of specimens needed for testing. Based on dynamic modulus, phase angle, permanent deformation regression constants, and flow number testing, the recommendation that three replicate specimens with four LVDTs be used per test; however, the configuration of the LVDTs was not given. It was found that with this testing system that the standard error associated with the tests could be reduced to 10.0% for mixes with nominal maximum aggregate sizes (NMAS) of 25.0-mm or less.

2.8 Volumetric Sensitivity

A quarter fractional factorial experimental design was carried out by Anderson et al, (1998) to explore the effects of key mixture components on both volumetric and mechanical properties of mixes. The key mix components that were varied during testing included: asphalt content, fine gradation, coarse gradation, intermediate gradation, and

the natural to crushed stone ratio. A baseline mixture was developed and the aforementioned mix components were varied based on typical production tolerances. In terms of the volumetric testing, asphalt content and fine gradation were identified as the prominent factors, along with several lower order interactions. As a result of the experimental design being a quarter fractional factorial, the lower order interactions could not be eliminated from the analysis and a single variable identified as being a major contributor to the changes in volumetric properties of the mix. This was found to hold true for the mechanical testing that was performed. The mechanical tests that were employed included the Repeated Shear Test – Constant Height and, Simple Shear, at various frequencies.   The mechanical testing resulted in assorted interactions, but the asphalt content was the most prominent factor in the mix performance.

In a study of the data from WesTrack (Epps and Hand, 2001), it was determined that changes in asphalt content and the percent passing the #200 sieve significantly affected the volumetric properties and the rut performance of the mix. Coarse-graded mixes indicated a higher sensitivity to decreases in asphalt content as measured by rutting at WesTrack than compared to that of fine-graded mixes. Mixes that had higher than optimum asphalt content experienced significantly greater rutting, as expected. Finer mixes were found to be more sensitive to changes in the material passing the #200 sieve. With the typical standard deviations for asphalt content and percent passing the #200 stated as being 0.3 and 0.9 percent, respectively, there is considerable variation that can occur in material that is plant produced. Having identified these sensitivities and taking into account the aforementioned variations, it was recommended that performance based

tests supplement the existing Superpave volumetric mix design system. It was suggested that these tests could be used to measure the potential variability of field produced mixes.

CHAPTER 3: PROCEDURES

3.1 Materials Collection

As part of the current Design Guide, three replicate specimens are required for two tests that are conducted as part of the Superpave SPT. Three specimens should reduce the amount of error that is inherent in each test. Since flow number tests are destructive, a minimum of 12 specimens are needed to be procured per mix. However, a total of 24 specimens were initially compacted for each mix design under the assumption that flow time would be stipulated as a Superpave SPT. As a result the determination of the amount of material needed went as follows: each specimen weighs roughly 7000g, 24 specimens' times a factor of safety of roughly two yields 327kg (720lb) of mix from each project sampled. This extra material could then be used for additional and supplemental testing as needed. K.L. Hoffman (2002) found that there were considerable differences between sampling from the truck and behind the paver. This study only showed that there were differences, which were highly correlated to the NMAS of the mix, but it does not point to one as being a better choice over the other. Truck sampling was noted as being more convenient, while from behind the paver, materials would be more representative of the in-situ pavement. For ease and time, materials were sampled directly from the back of the truck in accordance with ASTM Standard D979 and D3665. In addition to the mix, the asphalt binder was also sampled so that the sensitivity of the binder in the Superpave SPT could be evaluated by adding asphalt binder to the sampled

field mix. Five gallons of the liquid binder was found to be more than sufficient in procuring samples with additional asphalt binder for the testing required.

In addition to the collection of materials pertinent to each job, the job mix formula (JMF), a load ticket, and the pavement design for each job were obtained. This information would be required for the analysis in later portions of this research project and aid in the identification of key variables in the designs that resist the two prominent distresses of permanent deformation and fatigue.

3.2 Specimen Preparation and Testing

Outlined below are the specimen preparation methods that were used to procure gyratory compacted specimens for testing. This includes splitting samples, maximum theoretical gravity determination, specimen compaction, specimen sawing/coring, bulk specific gravity determination, and performance testing.

3.2.1 Splitting

Loose mix that was sampled from each of the 20 jobs was heated up to 143 or 160°C for approximately 2hrs depending on the level of traffic (>10million ESALs or ≤10million ESALs, respectively). Buckets contained roughly 27kg (60lbs) of mix and required splitting. Splitting was conducted in accordance with ASTM C702. Sample sizes include two-1250g samples for maximum theoretical specific gravity (G_{mm}) testing for optimum and bumped binder contents as well as 24 samples of approximately 7000-g samples for the two Superpave SPTs with different air voids and binder contents. The

two G_{mm} samples were taken from separate buckets in order to obtain a representative sample of the mix being tested.

Special care was taken so as to ensure that a representative sample was prepared for each specimen. Krutz and Sebaaly (1993) noted that particularly coarse mixes tended to yield higher coefficient of variation when repeated and static triaxial tests were performed. The high coefficient of variation was attributed mainly to the segregation in the mix, therefore great care was taken when splitting coarser mixes to minimize segregation.

3.2.2 Maximum Theoretical Specific Gravity (G_{mm})

Maximum theoretical specific gravity (G_{mm}) was conducted in accordance with AASHTO T209/ASTM D2041 for two 1250g split samples for each job. The G_{mm} was used to determine the volumetric properties of the original gyratory compacted sample as well as after it had been sawed/cored for performance testing.

3.2.3 Specimen Compaction

Specimens were compacted in a Pine AFGC125X SGC that can procure specimens in the dimensions of roughly 150-mm in diameter by 170-mm in height. Specimens were compacted to 4.0, 7.0, 10.0 percent air voids to fulfill the matrix previously presented. To obtain specimens at 4.0, 7.0, and 10.0 percent air voids, a correction factor was used to determine the weight needed to produce a specimen that had a height of 170-mm and was at the target percent air voids. WisDOT stipulates that

specimens be compacted to N_{des}, and thus a correction factor was not readily available for each mix. As a result, a typical value of 1.020 was used for each mix, Section 6.3 comments further on correction factors.

3.2.4 Bulk Specific Gravity (G_{mb})

The bulk specific gravity was determined before and after the sawing/coring of the specimen. The testing was conducted in accordance with AASHTO T166/ASTM D2726. During the sawing/coring procedure, the specimen was exposed to a wet environment, as the saw blades and coring bit are water cooled. The procedure for determining bulk specific gravity for a wet specimen calls for it to be dried at 52°C for a 24hr period to ensure a constant dry weight. Unfortunately, at this temperature, the specimen could potentially undergo creep, thus changing the volumetrics and dimensions of the specimen and this was to be avoided. Lytton et al (1993) found that the weight of a specimen in which the bulk specific gravity had been determined could change up to 25grams over a 15day period. It appeared that after two days of drying, that the rate of weight change went asymptotical towards its true dry weight, this trend was also found during this research project as shown in Figure 3.1.
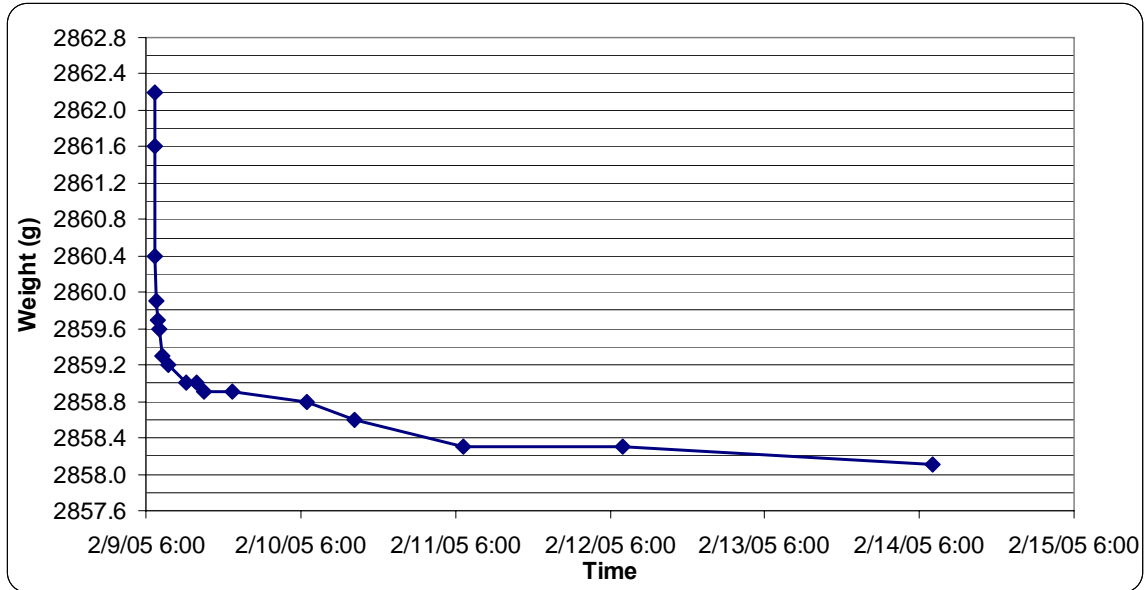
Figure 3.1 Changes in Weight of Specimen After G$_{mb}$ Determination

Figure 3.1 shows the change in weight of a specimen that was sawed/cored and the bulk specific gravity immediately determined and the change in weight monitored over the proceeding days. As a result the dry weights of the sawed/cored specimens were not determined until at least two days of drying had occurred. This precaution also mitigated the effects of water on test results particularly at the intermediate temperature for the dynamic modulus testing. The submerged and saturated surface dry (SSD) weight was determined immediately after sawing/coring. The Draft Test Protocol in NCHRP 9-29 calls for the specimens to only deviate by +/-0.5 percent from the target air void contents of 4.0, 7.0 and 10.0 percent; however, this was relaxed to +/-1.0 (2001). The reason for this change was that there was variability in the HMA due to it being a field sample as opposed to a laboratory batched specimen. It was also meant to account for the lack of availability of a correction factor for each mix.

3.2.5 Specimen Cutting and Coring

The two diametrical ends of the specimen were sawed off using a dual parallel diamond bladed saws that are water cooled to yield a specimen with a cut height of 150-mm, with less than two degrees from absolute parallelism for the ends. There was a twofold reason for why both ends were sawed off; the first is to remove high air void content areas from the specimen ends; second, it provides a smooth and parallel surface, which mitigates the necessity of caps, where caps add restraint to the specimen during testing (Bonaquist, 2001). The Draft Test Protocol from NCHRP 9-19 calls for a 100-mm diameter specimen after coring. A coring machine with a diamond tip was used to obtain the 100-mm diameter specimen from the 150-mm gyratory specimen. The sawing and coring was done all inclusive of a single piece of equipment.

3.3 Specimen Measurement

The specimen's diameters were measured at 0° and 90° of the third points and the mid-height, to constitute a total of six diameter measurements. The diameter measurements were averaged and the standard deviation determined. Per the NCHRP 9-29 Interim report, if the standard deviation of the diameter was greater than 2.5mm, it was discarded. Measurements are reported to the nearest 0.1mm. The height of the specimen was determined at 0°, 90°, 180°, and 270° and averaged. The only requirements on specimen height was that it should be between 148 and 152-mm.

3.4 Testing and Calculations

Outlined below are the testing procedures and calculations associated with the three Superpave SPTs. The three Superpave SPTs are dynamic modulus (at intermediate and high temperature) and flow number.

3.4.1 Dynamic Modulus

The testing procedure described herein is derived from NCHRP 9-29 Interim Report under the First Article Equipment Specification for the Flow Number Test Version 2.0 (September 26, 2001). This testing protocol has been referred to as Project 9-19 Draft Protocol A1: Dynamic Modulus of Asphalt Concrete Mixtures and Master Curves.

A 100-mm diameter by 150-mm high cylindrical specimen was tested under a repeated haversine compressive stress at two effective test temperatures unconfined. A Universal Testing Machine (UTM) 100 was used to conduct the testing with a temperature controlled testing chamber. The testing configurations for dynamic modulus are given in Table 3.1.

Table 3.1 Dynamic Modulus Testing Configurations

	SPT for Fatigue	SPT for Rutting
Temperature	$T_{eff\ fatigue}$	$T_{eff\ rutting}$
Dynamic Load	Induce 75-150μstrain	Induce 75-150μstrain
Loading Rates	0.1 to 25Hz	0.1 to 25Hz

The effective fatigue and rutting temperatures are discussed in Section 6.1.1. The dynamic load was determined based on the conditioning cycle which produced a

corresponding pavement strain of 75-150μstrain (Leslie Ann Myers, personal

conversation, 2004).

There were a total of four different frequencies run at each temperature. These

frequencies are stated in Table 3.2 along with the number of load cycles for each

frequency.

Table 3.2 Cycles for Test Sequence

Frequency, Hz	Number of Cycles
25	200
10	100
1	25
0.1	6

Testing was conducted from that of the high to lower frequencies to mitigate the amount

of deformation that is induced upon specimens during testing. The same specimen was

tested throughout the duration of the testing procedure.

Three axial Linear Variable Differential Transducers (LVDTs) were affixed

around the perimeter of the specimen to record the strain in the specimen over the length

of the test. Witczak et al found that as the number of LVDTs and replicate specimens

was increased, the standard error of the mean decreased (2002). It should be noted that

Witczak et al found that the amount of error, however was far more dependent upon the

NMAS of the mix (2002). The testing that was conducted as part of this study used only

three LVDTs because of the testing setup available from Shedworks and three replicate

specimens were used. The LVDTs were adjusted to the end of their linear range so as to

keep the entire range available during the course of the application of the compressive

stress.

The specimen was placed in the testing chamber until the effective test temperature was attained in the test specimen. This was found with the aid of a dummy specimen with a temperature sensor embedded in the center. After the effective test temperature was reached, the specimen was then centered under the loading platens so as to not place an eccentric load on the specimen. The test was conducted in accordance with the aforementioned parameters in Tables 3.1 and 3.2.

There are four main calculations that are performed by the associated software. The first is the loading stress, σ_o, that is applied to the specimen during the test (Equation 3.1).

$$\sigma_o = \frac{\overline{P}}{A}$$ (3.1)

where:

σ_o = stress,
$\overline{P}$ = average load amplitude, and
A = area of specimen.

The recoverable axial strain from the individual strain gauges, ε_o, is determined as follows:

$$\varepsilon_o = \frac{\overline{\Delta}}{GL}$$ (3.2)

where:

ε_o = strain,
$\overline{\Delta}$ = average deformation amplitude, and
GL = gauge length.

Dynamic modulus, $\left| E* \right|$ for each LVDT:

$$\left| E* \right| = \frac{\sigma_o}{\varepsilon_o}$$ (3.3)

The final equation is to determine the phase angle, for each LVDT:

$$\phi = \frac{t_i}{t_p}(360) \qquad\qquad (3.4)$$

where:

ϕ = phase angle,

t_i = average time lag between a cycle of stress and strain (sec), and

t_p = average time for a stress cycle (sec).

The software that was available for this project performed the above calculations. It reported the $\left| E^* \right|$ and the phase angle for all three LVDTs as well as the permanent and resilient micro-strain and the applied stress for each load cycle.

3.4.2 Flow Number

The testing procedure described herein was derived from NCHRP 9-29 Interim Report under the First Article Equipment Specification for the Flow Number Test Version 2.0 (September 26, 2001). This testing protocol has been referred to as Project 9-19 Draft Protocol W1: Simple Performance Test for Permanent Deformation Based Upon Repeated Load Test of Asphalt Concrete Mixtures.

A 100-mm diameter by 150-mm high cylindrical specimen was tested under a repeated haversine compressive stress at a single effective temperature unconfined. A UTM 100 and UTM5 machines were used to conduct the tests with a temperature controlled testing chamber. The two machines were used due to the fact that the flow number test was the most time intensive test. The load was applied for a duration of 0.1-sec and a dwell period of 0.9-sec. No design axial stress levels have been stipulated in the NCHRP 9-19 or 9-29 Protocols, but in discussions with Leslie Ann Myers a deviator stress of 600kPa (87psi) which is analogous to the load used in the Superpave gyratory compactor (2004). Since no confining pressure was used, the axial stress is the deviator

stress stated (600kPa). The effective test temperature was considered the temperature at which permanent deformation would occur equivalent to seasonal correction throughout the year. The methodology for determining the effective temperature is found in Section 6.1.1.

The strains for these tests were measured directly through the machines actuator as opposed to affixing axial LVDTs to the sides of the specimen. Additionally, the LVDTs that were available for the dynamic modulus tests would not work for this test because they only had a range of 1mm, whereas most specimens did not fail until at least 3-7mm of permanent deformation occurred, well beyond the 1mm range.

Specimens were placed in the testing chambers until the effective test temperature was obtained in the test specimens. This was found with the aid of dummy specimens with a temperature sensor embedded in the center. After the effective test temperature had been reached, the specimen was then centered under the loading platens so as to not place an eccentric load on the specimen. The test was conducted in accordance with the aforementioned parameters.

The loading regime was applied to the specimens for a total of 15,000 continuous cycles or until the specimen failed and results in excessive tertiary deformation, which ever occurred first. Excessive deformation was considered 30,000μstrain. The exact length of the test was variable as it was contingent on the test temperature and the properties of the material tested.

There was a three step process for flow time calculation. The procedure consisted of 1) numerical calculation of the strain rate 2) smoothing of the creep data; and 3)

identification of the minimum smoothed creep rate as this is where the flow number occurs. The following equation was used to determine the creep rate:

$$\frac{d(\varepsilon_p)_i}{dN} = \frac{(\varepsilon_p)_{i+\Delta N} - (\varepsilon_p)_{i-\Delta N}}{2\Delta N} \tag{3.5}$$

where:

$\dfrac{d(\varepsilon_p)_i}{dN}$ = rate of change of strain with respect to cycles or creep rate at i cycle (1/cycle),

$(\varepsilon_p)_{i+\Delta N}$ = strain at i+ΔN cycles,

$(\varepsilon_p)_{i-\Delta N}$ = strain at i-ΔN cycles, and

ΔN = number of cycles sampling points.

The next step required that the data be smoothed through a running average of five points. Two creep rates before and after and including the creep rate at that instant was used. Equation 3.6 was used to determine the smoothed creep rate:

$$\frac{d\varepsilon_i'}{dN} = \frac{1}{5}\left(\frac{d\varepsilon_{i-2\Delta N}}{dN} + \frac{d\varepsilon_{i-\Delta N}}{dN} + \frac{d\varepsilon_i}{dN} + \frac{d\varepsilon_{i+\Delta N}}{dN} + \frac{d\varepsilon_{i+2\Delta N}}{dN} \right) \tag{3.6}$$

where:

$\dfrac{d\varepsilon_i'}{dN}$ = smoothed creep rate at i sec (1/cycles),

$\dfrac{d\varepsilon_{i-2\Delta N}}{dN}$ = creep rate at i-2ΔN cycles (1/cycles),

$\dfrac{d\varepsilon_{i-\Delta N}}{dN}$ = creep rate at i-ΔN cycles (1/cycles),

$\dfrac{d\varepsilon_i}{dN}$ = creep rate at i cycles (1/cycles),

$\dfrac{d\varepsilon_{i+\Delta N}}{dN}$ = creep rate at i+ΔN cycles (1/cycles), and

$\dfrac{d\varepsilon_{i+2\Delta N}}{dN}$ = creep rate at i+2ΔN cycles (1/cycles).

The final step was to determine the cycle where the minimum creep rate occurs in the data set. If no minimum occurred during the test, then the flow number was reported as being greater than or equal to the number of loads applied during the course of the test.

When several minimum creep rates occurred in a data set, then the first minimum value was reported as the flow number.

3.4.3 Testing Durations

Table 4.3 shows the durations of each of the activities associated with the Superpave SPT Protocol. This table shows not only time requirements for the individual specimen testing, but also for one job and the entire Superpave SPT conducted for this research project. Several of these activities can be done in parallel with multiple samples.

Table 3.3 Durations for SSPT Preparation and Testing (NCHRP 465, 2002b)

Laboratory Activity		Estimated Time for One Prepared Specimen	Estimated Time for One Job[1]	Estimated Time for All Testing
Sample Preparation	Heating Up	2hrs	2hrs	40hrs
	Splitting	2min	2hrs	40hrs
	G_{mm} Testing	4hrs	4hrs	80hrs
	Aging	2hrs	2hrs	40hrs
	Compaction	5min	2hrs	40hrs
	Extraction	2.5min	1hr	20hrs
	Run G_{mb}	6min	2.4hrs	48hrs
	Sawing and Coring	30min	12hrs	240hrs
	Run G_{mb}	6min	2.4hrs	48hrs
	Measure Specimen	2min	40min	13.3hrs
	Total Setup Time	1.3hrs	30.5hrs	609.3hrs
Specimen Preparation	Glue Studs	2min	2hrs	40hrs
	Mount LVDT Brackets	2min	2hrs	40hrs
	Condition Specimens	6-8hrs	6-8hrs	120-160hrs
	Affix LVDTs	2min	2hr	40hrs
	Total Preparation Time	6-8hrs	12-13hrs	240-280hrs
SPT	Dynamic Modulus / One Temperature	20min	2hrs	40hrs
	Dynamic Modulus / All Temperatures	6hrs	10hrs	20days[2]
	Flow Number	30-180min	3-12hrs[3]	60-240hrs
	Total Testing Time	1-4.3hrs	13-22hrs	260-440hrs

[1]Based on a total of 24 specimens procured per job with only 3 test specimens per SSPT.

[2]Time is based on two different test temperatures being conducted.

[3]Assumes two testing machines.

CHAPTER 4: PROJECTS SAMPLED

4.1 Experimental Plan Changes

It was realized that some experimental cells could not easily be filled upon contacting and setting up jobs to sample that were applicable to the first iteration of the experimental plan for this project. The WisDOT does specify a 25.0-mm mix, but are reserved mainly for new construction as a base material. In working with both the state and contractors of Wisconsin, it was found that 25.0-mm mixes are rare regardless of the traffic volume; in fact to our knowledge only two were paved during the 2004 construction season. One 25.0-mm mix was completed before the research team was aware of the mix being placed and the other was an open-graded mix and did not fall into the experimental matrix. The other problem identified was finding open-graded mixes that fit the proposed experimental matrix. Only one open-graded mix (12.5-mm SMA) was found and sampled. It should also be noted that WisDOT only specifies gradation requirements for 9.5 and 12.5-mm SMA mixes. As a result, some modifications had to be made to the experimental matrix. Instead of deleting jobs that could not be found, they were reallocated to other portions of the matrix, thus maintaining the overall number of jobs for the research project as well as making the subsequent analysis more robust. The updated matrix can be found in Table 4.1.

Table 4.1 Revised Project Matrix

Nominal Maximum Aggregate Size	Mix Type	Traffic Level			
		E-0.3	E-1	E-3	>E-3
25.0mm	Dense				
	Open				
19.0mm	Dense	X	XX	XXX	XXX
	Open				
12.5mm	Dense	XX	XX	XXX	XXX
	Open				X

The "E" presented in Table 4.1 is for equivalent single axle loads (ESAL) and is the standard by which the load spectrum is normalized for highway design.

4.2 Sampled Projects

Projects were sampled throughout the State of Wisconsin during the summer 2004 construction season. Sampling materials from across the State represented a better cross-section of the materials that were used during the season. However, most high traffic volume projects were found in the southern regions of Wisconsin, whereas lower traffic volumes could be found all around the State. This was mainly due to the population distributions and the location of major trunklines throughout the State. Figure 4.1 illustrates the locations of mixes that were sampled for this particular project, whereas Appendix A: Project JMF's contains all of the material properties related to these jobs.
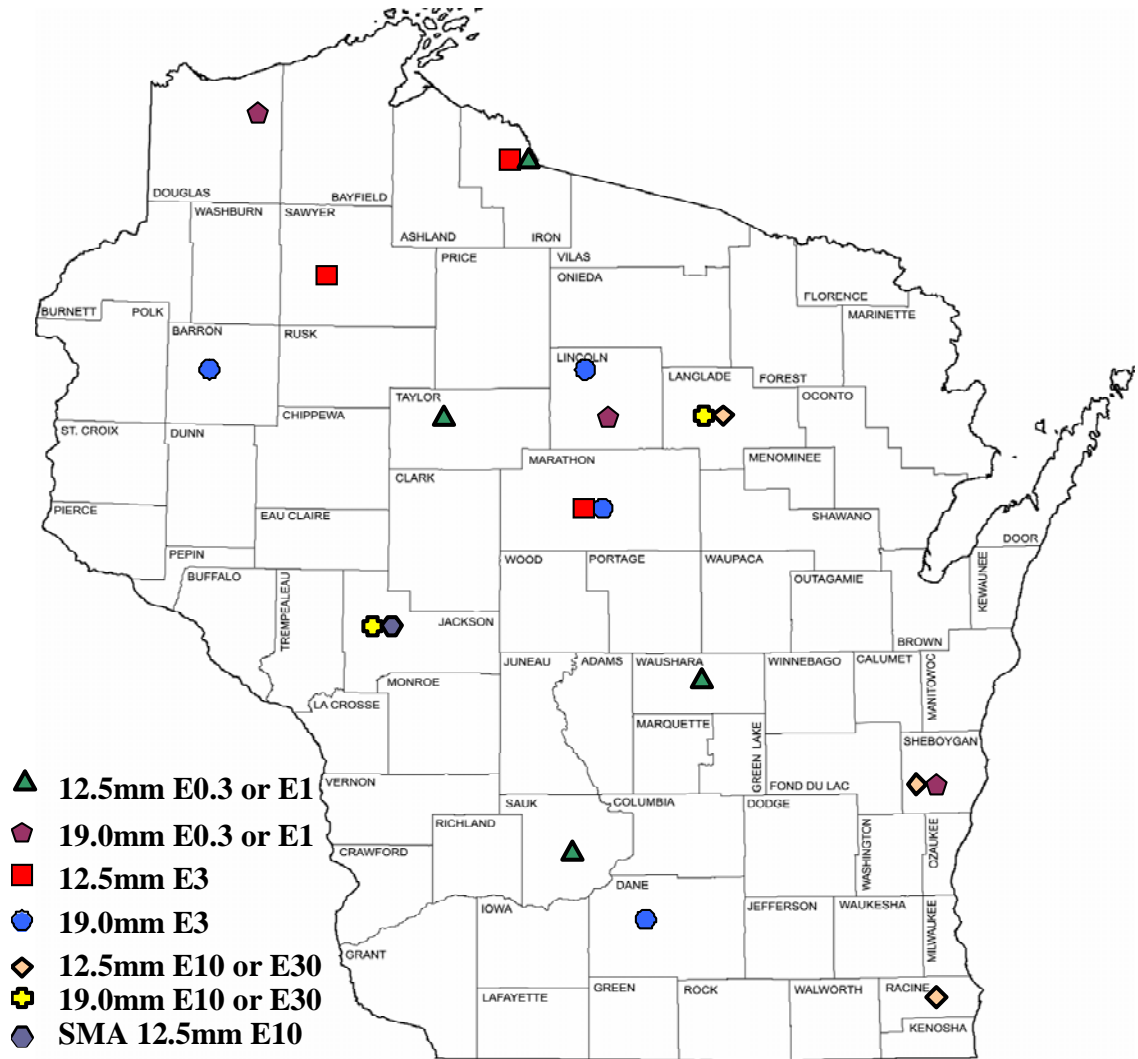
Figure 4.1 Project Locations (Prepared by Demographic Services Center, Wisconsin Department of Administration and the Wisconsin State Cartographer's Office)

At the time of this writing, 19 of the 20 proposed mixes have been sampled. A job was lined up to fill the last cell in the matrix, but due to mix changes and lack of an alternative project, this last mix has not been sampled. The one cell that was not filled was an E-10 19.0mm dense mixture. WisDOT has been made aware of this missing mix and efforts are being made to sample it during the early 2005 construction season.

There was an E-3 25.0-mm open-graded mixture that was sampled for this project, but did not fall into the revised project matrix. It was initially sampled because it

was believed that it would fall into the preliminary matrix for a dense-graded mixture, but upon review of the gradation it was realized that it was an open-graded mixture. Specimens have been prepared from this job, but have not been made a part of this research project.

It is worth observing that the sampling that was conducted as part of this project went smoothly for every job. The contractors, consultants, and the WisDOT officials were all extremely helpful during this sampling process. These people are recognized in the acknowledgements section at the beginning of this document.

4.3 Sampling

As previously mentioned, sampling was conducted at the plant site, just after trucks had been loaded out. Figure 4.2 shows a truck being loaded out.

Figure 4.2 Truck Being Loaded Out

The truck then pulls up to the sampling rack where it receives its load ticket and the materials can be sampled from the back of the truck. Figures 4.3 and 4.4 show examples of a sampling rack and the methodology used when sampling materials from the back of a truck, respectively.

Figure 4.3 Sampling Rack

Figure 4.4 HMA Sampling

All except one job was sampled from the back of the truck. The one exception was a job that was sampled by a method of creating a mini-stockpile from material run through the reject chute of the hot mix plant.

In total 12 5gallon pails of the HMA were obtained from each job. Samples procured from the back of the truck were taken from 12 different locations so as to obtain a representative sample of the mix being produced. The surface layer was scraped off in an effort to minimize the amount of segregated material being sampled. The reason being is that the coarser fraction of the HMA will tend to roll down the sides of the pile, leaving the finer fraction at the top of the pile (Dukatz, 1996). However, underneath the surface layer, is an ideal representation of the material. For the HMA sampled from the mini-stockpile, locations were selected from the base to the top of the pile and around its perimeter, while keeping in mind the different strata of the stockpile, in that, the bottom of pile comprises the greatest percentage of the material and hence the greatest percentage of the material was sampled from this location. Figure 4.5 illustrates the composition of a cone stockpile in terms of its percentages with height.
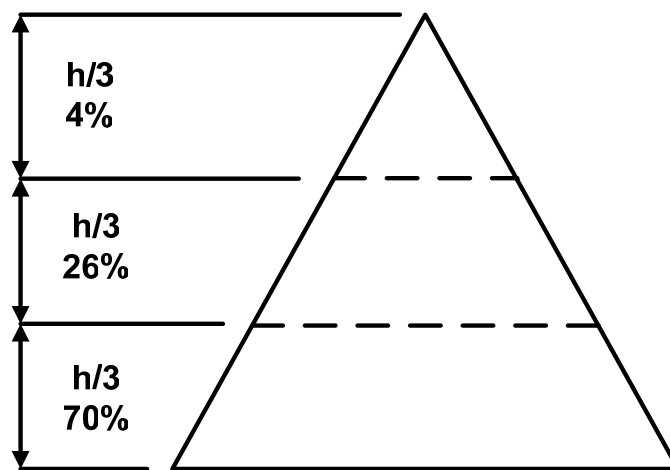
Figure 4.5 Stockpile Cone Proportions

Materials were brought back from the various plant sites and stored either in the Water Resources Building or in the basement of Dillman Hall at Michigan Technological University prior to sample preparation.

5.1 Sample Preparation Flowchart

Figure 5.1 depicts the sample preparation activities. The following sections discuss the procurement of quality samples that are representative of the mix that has been sampled and paved during the 2004 construction season.
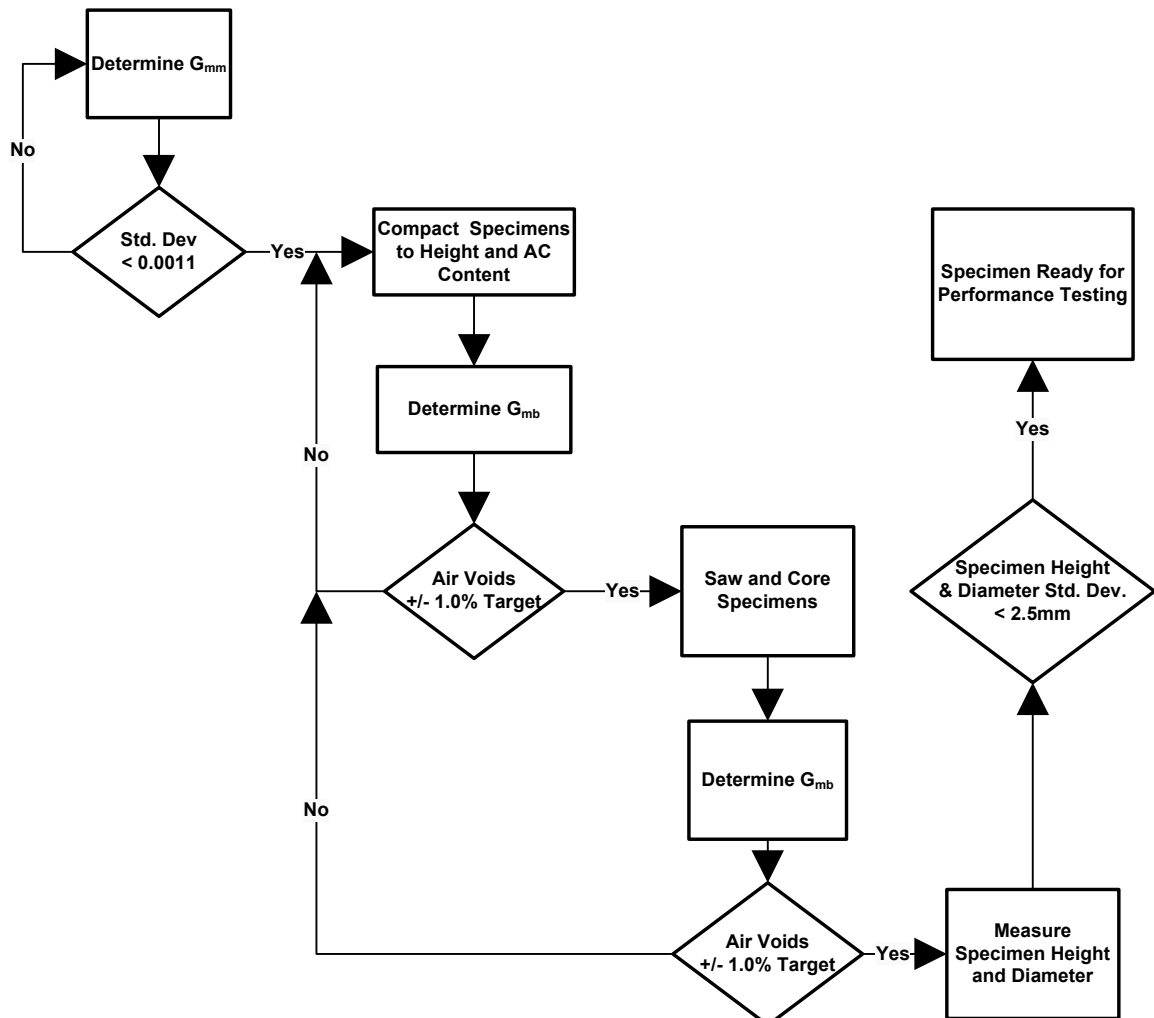
Figure 5.1 Sample Preparation Flow Chart

5.2 Maximum Theoretical Specific Gravity

The maximum theoretical specific gravity (G_{mm}) was determined by AASHTO T209/ASTM D2041. The precision outlined in the specification states that the single-operator is 0.0011 for two standard deviations, which represents "the difference between the results of two properly conducted tests." These guidelines are based upon laboratory prepared specimens, where the aggregate gradations are closely monitored. For this study, there was significantly less control over what was in the sample as it was a field mix. Every attempt was made to obtain a representative sample by means of quartering, thus mitigating the differences between samples. In reviewing the standard deviations of the two G_{mm} samples for each project, it was found that all except one mix fell within the single-operator precision. The standard deviation for this particular mix was 0.0158, but this was for the SMA which had a tendency to segregate, but it was felt that the difference was not significant enough to warrant further testing. Considering the nature of the samples (field mix), the results are acceptable for the work conducted in this study. Table 5.1 shows the mean and standard deviations for each of the projects.

Table 5.1 G_{mm} Mean and Standard Deviation for Each Project

Project	Optimum AC		Optimum +0.3% AC	
	Mean G_{mm}	Std. Dev.	Mean G_{mm}	Std. Dev.
Baraboo E-0.3 12.5mm	2.486	0.0052	2.474	0.0005
Medford E-1 12.5mm*	2.502	0.0032	2.489	0.0119
Wautoma E-1 12.5mm*	2.532	0.0086	2.521	0.0036
Hurley E-0.3 12.5mm*	2.498	0.0058	2.476	0.0100
Hayward E-3 12.5mm	2.543	0.0069	2.483	0.0082
Wausau E-3 12.5mm*	2.450	0.0009	2.436	0.0073
Hurley E-3 12.5mm*	2.484	0.0048	2.472	0.0050
Antigo E-10 12.5mm	2.551	0.0051	2.492	0.0038
Plymouth E-10 12.5mm	2.588	0.0005	2.581	0.0013
Racine E-10 12.5mm*	2.510	0.0086	2.486	0.0039
Northfield E-10 12.5mm SMA	2.517	0.0158	2.504	0.0035
Cascade E-1 19.0mm	2.578	0.0083	2.554	0.0056
Bloomville E-1 19.0mm	2.521	0.0015	2.505	0.0006
Brule E-0.3 19.0mm*	2.569	0.0086	2.553	0.0012
Waunakee E-3 19.0mm*	2.511	0.0025	2.495	0.0035
Mosinee E-3 19.0mm*	2.445	0.0043	2.438	0.0001
Cumberland E-3 19.0mm*	2.586	0.0069	2.572	0.0136
Antigo E-10 19.0mm	2.535	0.0031	2.521	0.0075
Northfield E-10 19.0mm	2.505	0.0015	2.493	0.0006
Tomahawk E-3 25.0mm*	2.560	0.0118	2.529	0.0111

* utilized RAP in the mix

Of the 20 mixes presented in Table 5.1, recycled asphalt pavement (RAP) constituted a

portion of the aggregate mixture in 11. RAP is inherently variable in nature, which

comes from the fact that one stockpile can constitute several sources and that each source

has a unique gradation, depth of milling, binder content, and age. These factors all

contribute to the variability in field samples and can additionally explain some of the

inconsistency in the G_{mm} samples and the comparisons that are made later in this section with that of the contractor's G_{mm} determination.

As expected, the G_{mm} decreased with an increase in asphalt content and is due to the fact that asphalt binder has a lower specific gravity (~1.020-1.030) than aggregate (~2.600-2.700 depending on the aggregate source). When additional asphalt binder was added to the mix, the percentage of the aggregate correspondingly decreases. The aggregate has a higher specific gravity and since there is a slightly smaller proportion, the specific gravity decreases.

The measured standard deviation appears to be insensitive to the NMAS, with the testing that was conducted. This indicates that the variability in the test results was not contingent on the NMAS of the mix.

A comparison was made between the MTU and the contractors G_{mm} supplied in the JMF for both the optimum and asphalt cement bump.   Figures 5.2 and 5.3 reflect both of the G_{mm}'s, respectively.
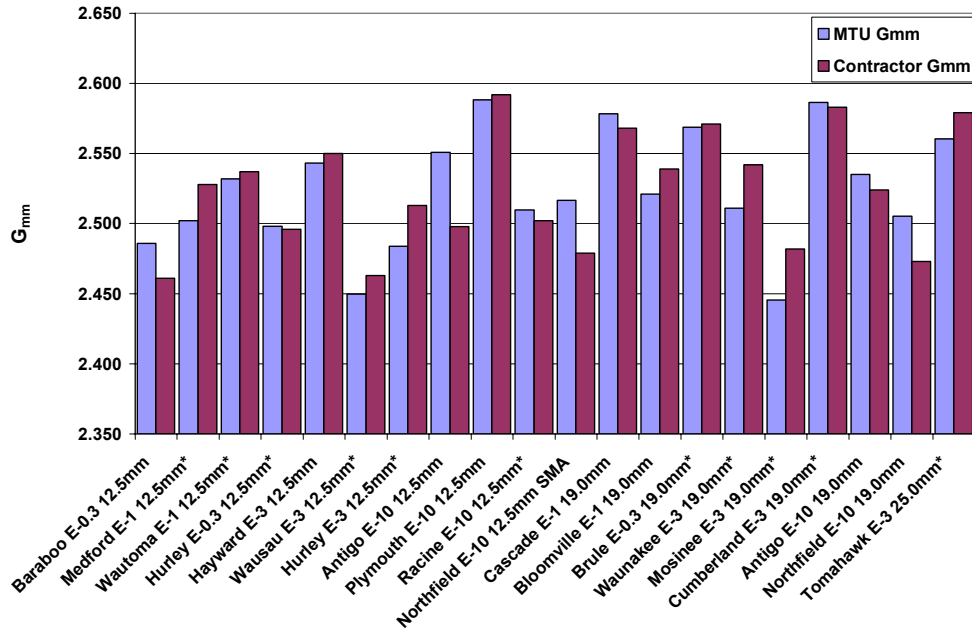
* utilized RAP in the mix

Figure 5.2 MTU and Contractor G_{mm} Optimum Asphalt Binder Content
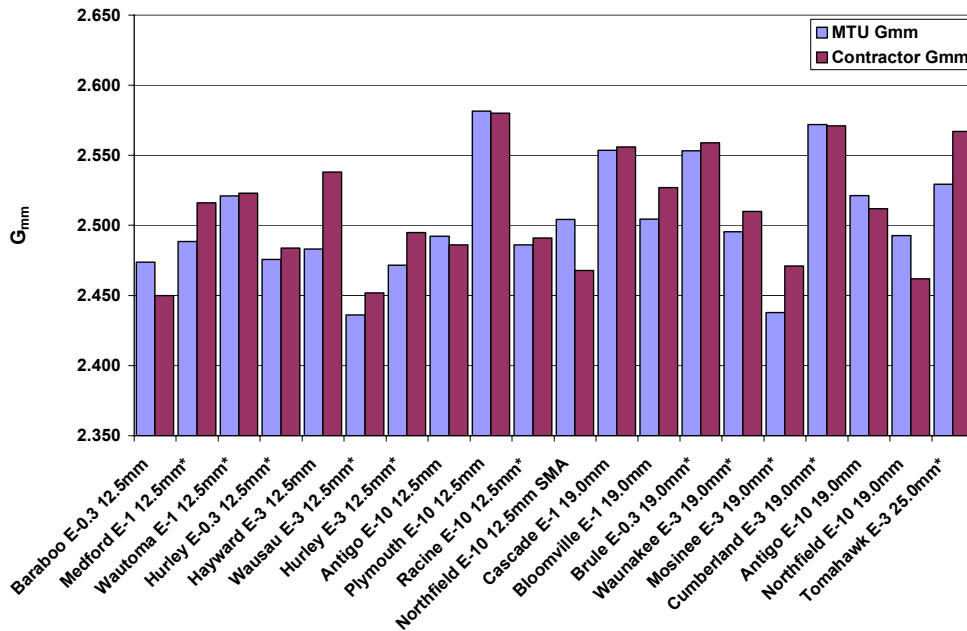
* utilized RAP in the mix

Figure 5.3 MTU and Contractor G_{mm} +0.3% Optimum Asphalt Binder Content

There were some differences between the MTU and contractor determined G_{mm} as seen in

Figures 5.2 and 5.3. Some, in fact, do not fall within the multilaboratory precision of

0.0190 as outlined in AASHTO T209. There are several possible explanations for these differences, in addition to the RAP component. One reason for the difference lies in the fact that the samples were from the field and there are numerous sources where both variability and segregation can occur. Every effort was made to obtain a representative sample from the back of the truck and during the sample reduction process, but the processes prior to these steps could not be controlled. A second possible reason is that there could have been changes in mix design that deviate from the JMF. These changes are made when issues arise during the lay down of the HMA. A third reason could be that the asphalt binder content in the sampled mix is higher than that of the binder content stated in the JMF; this will be commented on later in this section.

A regression analysis was conducted on the G_{mm} from MTU and that of the contractor for both optimum and asphalt binder content increase of 0.3%. A simple linear regression was developed between the two datasets and the p-values for the slopes and intercepts analyzed. If the two datasets were truly equal, the intercept equals zero and a one for the slope, indicating unity. For the optimum asphalt binder content the p-value for the intercept equal to zero was 0.24 and for the slope equal to one was 0.35 (coefficient of correlation = 0.83). For the asphalt binder content increase of 0.3%, the p-value for the intercept equal to zero was 0.34 and for the slope equal to one was 0.35 (coefficient of correlation = 0.84).   Thus it was reasonable to assume that the G_{mm} measurements were equal.

Earlier it was commented that the contractor may have increased the binder content, and this warrants comment as it may explain the differences between MTU's G_{mm} and that of the contractors. The asphalt binder constitutes the most expensive

component of the mix; as a result, most contractors would strive to decrease the amount of binder in the mix to make the mix more economical in a low bid situation. This is sound logic; however, the structure in which HMA paving projects are bid must be understood. The way that HMA items are bid in Wisconsin on State projects are by the mix itself and the amount of asphalt binder used, thus two separate bid items. This is unlike most owner/agencies where the HMA is bid on a single item basis (HMA and binder content combined). The JMF would stipulate optimum binder content and the quantity for the job thus determined and bid as such for the mix and asphalt. During production, changes can be made to the mix, but must fall within the constraints of ±0.3% asphalt binder content from the optimum listed in the JMF (WisDOT, 2002). Increasing the asphalt binder content during production would then have to be reflected in the bid item and thus increasing the cost of the item and increasing the contractor's payment. If the asphalt binder was increased from the JMF to production, the G_{mm} that was determined by MTU should be lower than that in the JMF. Figure 5.4 appears to support this finding as most of the data points are biased towards a lower G_{mm} measurement by MTU as compared to the JMF's.
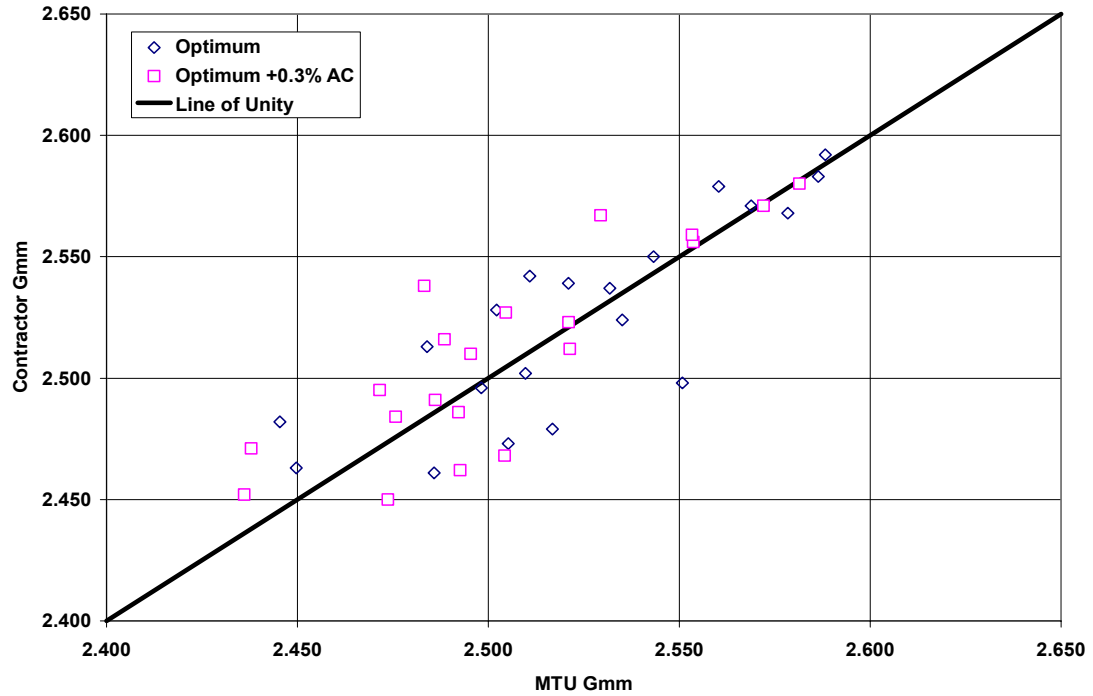
Figure 5.4 MTU G$_{mm}$ vs. Contractor G$_{mm}$

This may not be the true reason for the difference and in fact probably is a multitude of reasons, thus necessitating the measurement of the G$_{mm}$ as it is applicable to the materials that were sampled for this particular research project. One way to ascertain the actual cause of the difference would be to run an extraction; however, this was beyond the scope of the project. The measured G$_{mm}$ is important as it is critical input for the compaction process and thus must be representative of the material on hand, as a result the MTU G$_{mm}$ were used in the following analyses.

<u>5.3 Compaction</u>

In Wisconsin, HMA mix designs are based on compacting specimens to N_{des}, thus the air voids of the specimen can be directly measured via the AASTHO T166/ASTM D2726 method. This presents a problem because in order to compact the specimens to height, a correction factor is needed. The ratio of the estimated G_{mb} to that of the measured G_{mb} constitutes the correction factor, thus a specimen must either be compacted to N_{max} or a correction factor estimated for each mix. To save time on sample preparation a correction factor was estimated, drawing from previous knowledge with HMA, a typical range for correction factor is 1.01 to 1.03 and thus an estimate of 1.02 was used for the correction factor of each mix. In examination of the actual correction factors, there was a range of 1.011 to 1.022, so in some instances the estimate was slightly conservative, but did not significantly affect the measured air voids of the compacted specimens which will be shown in Section 5.4.

All specimens for this project were compacted using a Superpave Gyratory Compactor (SGC) model AFGC125X; this machine was selected because of its familiarity and higher production. This gyratory compactor was fully calibrated to ensure that the specimens were compacted at an angle of 1.25degrees with a pressure of 600kPa and that the height was being measured properly. The calibration was again verified half-way through specimen production to ensure that specimens were undergoing a similar compaction process.

The specimens were split according to the weights required to produce a specimen that was compacted to approximately 170.0mm at the targeted air voids. These weights

were determined from the G_{mm} test results and the guidance outlined TAI's SP-2 (1996). The optimum +0.3% asphalt binder content were the specimens split first so that they were up to the proper temperature for mixing. The other 18 samples were then split and placed back in the convection oven at the prescribed temperature. The six specimens were then mixed with the +0.3% asphalt binder content and placed in the convection oven. Specimens were then compacted in the order of 7.0, 4.0, and 10.0% air voids at the optimum binder content followed by the optimum +0.3% asphalt binder content specimens to 7.0% air voids.

Specimens were then left to cool until room temperature was reached, at that time they were labeled and prepared for G_{mb} testing. Figure 5.5 shows 360 of the 456 specimens that have been prepared for this study, the specimens are two deep.

Figure 5.5 Prepared Gyratory Specimens

The 12.5mm SMA mix from Northfield was not compacted as creep is a problem with these particular mixtures.

5.4 Bulk Specific Gravity of Gyratory

The G_{mb} of all the gyratory specimens were determined after they were allowed to cool to room temperature (25°C). There was a noticeable variability in the measured G_{mb} and ultimately the determined air voids for specimens from the same job and compacted to the same target air void content. This was likely attributable to the variability in the constituent properties of the mix either from the mixing, sampling, or splitting processes. In Section 3.2.5, an initial criterion of specimen acceptance for air voids, as stipulated by NCHRP 9-29, was ±0.5% air voids from the target for mix design purposes. This specification was relaxed for this study to account for the aforementioned sources of variability. The new specification was set at ±1.0% air voids from the target. This was based on the gyratory compacted specimen. It was anticipated that the air voids would not change significantly after sawing and coring, but these attributes are measured directly without cutting the sample. Hence, this specification only applied to the gyratory compacted specimens. All volumetric data for the specimens of this project can be found in Appendix B: Specimen Volumetrics.

The general trend that was realized during the bulk specific gravity testing of the gyratory specimen was that at 10.0% target air voids the specimens had a lower than desired air void content, at 7.0% the specimens tended to be on target, and at 4.0% the measured air voids were higher than desired. The number of gyrations for the 10.0% air voids tended to be in the range of 5-20 gyrations. After the gyratory compactor reached

the predetermined height based on sample weight and the G_{mm}, the gyratory still applied a load to square the specimen as a direct result the specimen underwent further compaction and has been typically found to be 1.5-mm. This further compaction decreases the air voids where if the specimen was compacted to the desired height the desired air voids may have been obtained. The 4.0% air void specimens tended to be undercompacted. The reason for the trend was not readily apparent, but a vast majority of the specimens fell within the constraints of the target air voids. Any specimens that did not fall within the range of ±1.0% air voids of target were not included in the experimental plan.

As previously mentioned, it was anticipated that the air voids would not change significantly in the specimens after they had been sawed/cored, except for the mixtures that were coarse-graded and had large surface voids on the compacted specimens. The only jobs that were believed to have significantly different air voids were the Northfield E-30 19.0mm and the Tomahawk E-3 25.0mm mixtures as they reported significantly less air voids than targeted and a large quantity of water drained out of the specimen when removed from the water tank during bulk specific gravity testing.

5.5 Volumetrics of Sawed/Cored Test Specimens

The volumetric properties of the sawed/cored test specimens can be found in Appendix C. Only three mixtures are reported as these were the three that were tested for this project. To comment on the volumetrics of the Northfield mix, it was extremely coarse and had significant surface and interconnected voids and it was felt that water was draining out during the SSD method of air void determination. It was believed that these voids led to the low air void determination as found by the SSD method. To address this issue it would have been beneficial to run the Corelok on the compacted gyratory

specimens, but the specimen did not fit in the Corelok's chamber. The Corelok

determines the bulk specific gravity of a specimen through the use of a vacuumed bag.

The sawed/cored specimens were however run through the Corelok machine as they fit in

the chamber and it was found that there was no difference in the air voids of the specimen

when compared to that of the saturated surface dry (SSD) method. The most probable

reason for this result was that the sawed/cored specimen did not have the same surface

irregularities as its compacted counterpart. In the later plots and analysis the air voids on

the Northfield job are lower than the target values of 4.0, 7.0, and 10.0, but it was felt that

the differences were negligible as the general trends in the data are present.

The air voids of the sawed/cored specimens were slightly lower than that of the

gyratory measured air voids. The decrease was typically by about 0.5 to 1.0% air voids.

These changes are not significant and if the test air voids were ever specified for the

testing phase instead of the gyratory air voids, the correction factor for the three mixes

are presented in the Appendix C: Specimen Volumetrics After Sawing/Coring.

CHAPTER 6: TESTING SETUP AND PRELIMINARY TESTING

6.1 Testing Parameters

The testing parameters of temperature, stress level, and confinement for this project needed to be determined before testing could commence. To address these issues past literature was consulted, engineering judgment exercised, contacts utilized, and specimen testing conducted.

6.1.1 Test Temperatures

The testing temperatures for intermediate and high temperature dynamic modulus and flow number testing are stipulated by an effective temperature (T_{eff}) in NCHRP Report 465. Effective temperature is defined as being "a single test temperature at which an amount of permanent deformation would occur equivalent to that measured by considering each season separately throughout the year." In conversations with the FHWA, the current means by which the effective temperatures are calculated as part of NCHRP 9-19 were given. The equation for effective pavement temperature for rutting (dynamic modulus and flow number) follows (FHWA, 2004):

$$T_{eff\,rutting} = 30.8 - 0.12\,z_{cr} + 0.92\,MAAT_{design} \qquad (6.1)$$

where:
    z_{cr} = critical depth down from pavement surface, mm, and
    $MAAT_{design}$ = mean annual air temperature, ºC.

$$MAATdesign = MAAT_{average} + K_{\alpha}\sigma_{MAAT} \qquad (6.2)$$

where:
    $MAAT_{average}$ = mean annual air temperature, ºC,
    K_{α} = appropriate reliability level of 95% (1.645), and

σ_{MAAT} = standard deviation of distribution of MAAT for site location.

The critical depth is to be considered 20-mm from the surface, regardless of the location of the lift in the pavement structure. The $MAAT_{average}$ was collected from the Wisconsin State Climatology Office from stations that were located in close proximity to where each job was paved (Wisconsin State Climatology Office, 1/7/2005). The σ_{MAAT} was found in LTPPBind v2.1 as the high air temperature standard deviation. LTPPBind is a software program that provides guidance on asphalt binder grade selection based on climatic information. The rutting effective test temperatures based on equation 6.1 are summarized in Table 6.1.

Table 6.1 Rutting Effective Test Temperatures (°C)

Project No.	County	$MAAT_{design}$ (°C)	σ_{MAAT} (°C)	$K_\alpha MAAT_{design}$ (°C)	T_{eff} (PD)
5300-03-77	Sauk	6.3	1.6	8.9	36.6
9225-05-70	Taylor	5.1	1.7	7.9	35.7
6300-03-60	Waushara	6.3	2.3	10.1	37.7
9311-13-60	Iron	4.3	2.2	7.9	35.7
8520-13-71	Sawyer	4.8	2.2	8.4	36.1
6675-00-70	Marathon	6.4	1.7	9.2	36.9
1185-02-70	Iron	4.3	2.2	7.9	35.7
1605-04-70	Langlade	4.8	1.6	7.4	35.2
4840-02-71	Sheboygan	7.4	1.6	10.0	37.6
3230-06-60	Racine	8.4	2.0	11.7	39.2
1023-04-12	Jackson	5.9	1.8	8.8	36.5
4540-14-71	Sheboygan	7.4	1.7	10.2	37.7
9030-08-70	Lincoln	5.0	2.4	9.0	36.6
8510-14-71	Douglas	4.4	2.0	7.7	35.5
5992-04-14	Dane	7.7	1.6	10.3	37.9
6370-00-60	Marathon	6.4	1.7	9.2	36.9
1550-17-71	Barron	5.4	1.7	8.2	36.0
1605-04-70	Langlade	4.8	1.6	7.4	35.2
1023-04-12	Jackson	5.9	1.8	8.8	36.5
9040-05-70	Oneida	4.9	1.8	7.9	35.6

The effective pavement temperature for fatigue was determined by using the SHRP equation supplied by the FHWA and is shown in the following equations.

$$T_{eff\ fatigue} = 0.8\ MAPT - 2.7 \tag{6.3}$$

where:

　　　　$MAPT$ = mean annual pavement temperature, ℃.

$$MAPT = T_{20mm} = T_{air} - 0.00618\ lat^2 + 0.2289\ lat + 42.2\ (0.9545) - 17.78 \tag{6.4}$$

where:

　　　　T_{20mm} = temperature at 20-mm depth from pavement surface, ℃,
　　　　T_{air} = mean annual air temperature, ℃, and
　　　　lat = latitude of location, degrees.

The $MAAT_{average}$ from equation 6.2 was used for T_{air} in equation 6.4. The latitude was determined by location of where the project was paved.

Based on the above methods the following effective test temperatures were used for each individual project listed in Table 6.2 for fatigue testing.

Table 6.2 Fatigue Effective Test Temperatures (°C)

Project No.	County	T_{air} (ºC)	Latitude (degrees)	MAPT (ºC)	$T_{eff\,fatigue}$
5300-03-77	Sauk	6.3	43.47	27.1	19.0
9225-05-70	Taylor	5.1	45.13	25.4	17.6
6300-03-60	Waushara	6.3	44.11	26.9	18.8
9311-13-60	Iron	4.3	46.46	24.1	16.6
8520-13-71	Sawyer	4.8	45.74	24.8	17.2
6675-00-70	Marathon	6.4	44.93	26.8	18.7
1185-02-70	Iron	4.3	46.46	24.1	16.6
1605-04-70	Langlade	4.8	45.16	25.0	17.3
4840-02-71	Sheboygan	7.4	43.74	28.0	19.7
3230-06-60	Racine	8.4	42.71	29.4	20.9
1023-04-12	Jackson	5.9	44.50	26.3	18.4
4540-14-71	Sheboygan	7.4	43.68	28.1	19.8
9030-08-70	Lincoln	5.0	45.12	25.3	17.5
8510-14-71	Douglas	4.4	46.72	24.1	16.6
5992-04-14	Dane	7.7	43.32	28.5	20.1
6370-00-60	Marathon	6.4	44.93	26.8	18.7
1550-17-71	Barron	5.4	45.60	25.5	17.7
1605-04-70	Langlade	4.8	45.16	25.0	17.3
1023-04-12	Jackson	5.9	44.50	26.3	18.4
9040-05-70	Oneida	4.9	45.46	25.0	17.3

6.1.2 Unconfined or Confined Testing

Due to the large volume of specimens that were tested for this project, all specimens were tested unconfined. In addition to the number of specimens, Witczak et al (2002b) found that both unconfined and confined testing for the two test configurations yielded high correlations with field recorded pavement deformation and there was no significant difference.

6.1.3 Stress Level

Finally the magnitude of the stress level had to be determined for each test setup. A review of the testing conducted as part of NCHRP Report 465 yielded no definitive stress level for each test setup (Witczak et al, 2002b). The stress levels used were more location and test specific. In discussions with the FHWA, it was found that the stress level for dynamic modulus was dependent on the materials response to the loading (2004). FHWA recommended that the permanent strain at the different frequencies should be between 75 to 125 micro-strain and the load should be adjusted accordingly. Thus through the conditioning cycles the stress levels were determined for the dynamic modulus test at the intermediate and high temperatures on an iterative basis.

The dynamic stress level that was used for flow number was 600kPa (87psi), which simulates the stress level of the gyratory compactor and the contact (static) stress was 30kPa (4.4psi).

6.2 Preliminary Testing

HMA from a previous Round Robin study conducted by MTU was available for performing initial testing under the SSPT parameters. This mix was a 12.5mm E-3 mix with a PG 64-22 binder and contained 15% RAP. The mixtures characteristics are presented in Table 6.3.

Table 6.3 Characteristics of HMA Tested

Gradation		Volumetrics	
3/4" (19.0mm)	100.0	G_{mm}	2.516
1/2" (12.5mm)	98.2	Asphalt Specific Gravity (G_b)	1.028
3/8" (9.5mm)	86.0	Aggregate Effective Specific Gravity (G_{se})	2.749
No. 4 (4.75mm)	51.0	Aggregate Bulk Specific Gravity (G_{sb})	2.671
No. 8 (2.36mm)	28.1	Fines to Asphalt Binder Ratio (F/P_b)	1.07
No. 16 (1.18mm)	23.4	Voids in the Mineral Aggregate (VMA)	14.5
No. 30 (600µm)	16.9	Voids Filled with Asphalt (VFA)	73.2
No. 50 (300µm)	11.2	Asphalt Binder Content (P_b)	5.0
No. 100 (150 m)	7.0	Effective Asphalt Binder Content (P_{eff})	3.96
No. 200 (75µm)	4.9		
1 Crushed Face	97.2		

There were two main groups of specimens that were compacted to 7.0% air voids for this testing: 1) specimens measuring 150-mm in diameter and 170-mm in height and, 2) specimens measuring 100-mm in diameter and 150-mm in height at similar air voids. The 150-mm diameter specimens were then cut down using a saw/coring rig to 100-mm in diameter by 150-mm in height. These specimens served to not only verify the operation of the saw/coring rig, but were used to determine if the intermediate and high temperature dynamic modulus tests actually induced a significant enough permanent strain and/or damage in specimens to affect the results of the flow number test. These test specimens also served to examine the method of preparation in terms of the specimens being compacted to the test diameter and height to that of those sawed/cored to the test diameter and height.

In the manner that both the effective fatigue and rutting temperatures were determined, the Round Robin material was tested for the area for which it was produced (Clarkston, Michigan). The temperatures that were determined were 21.3°C and 39.2°C

for the fatigue and rutting temperatures, respectively. The respective deviator stresses were determined to be 207kPa (30psi) and 69kPa (10psi) for fatigue and rutting tests.

6.2.1 Round One Preliminary Testing

Testing was first conducted with the 100-mm in diameter by 150-mm in height compacted specimens. The first step in testing was to determine if there truly was any damage imparted on specimens due to testing and to ensure that the same set of specimens may be used for the two test configurations. Five specimens were separated into two groups, three in an experimental group and two in a control group. Flow number was the only test performed on the control group. The experimental group was run at the intermediate and high test temperatures for the dynamic modulus test and then flow number.

During this initial testing phase, some of the shortcomings in the flow number testing procedure came to light. The testing procedure that was stipulated by NCHRP 9-29 dictated that the test setup be terminated at 10,000 load cycles or when excessive deformation occurred. The test software allows for an axial strain termination and a load cycle termination; however, since there were no LVDTs attached to the sides of the specimen, the axial strain was not a controlling termination setting. Secondly, the software shows tendencies to identify a local minimum strain rate as the flow number, even though the strain rate continues to decrease. This shows that the global minimum strain rate (the point at which tertiary flow occurs) was not being reached, thus the actual flow number for the specimen would be significantly higher. Figure 6.1 illustrates a local

minimum was found at 5104 load cycles, but in viewing the plot of the accumulated

strain rate, there was a definitive decreasing strain rate.
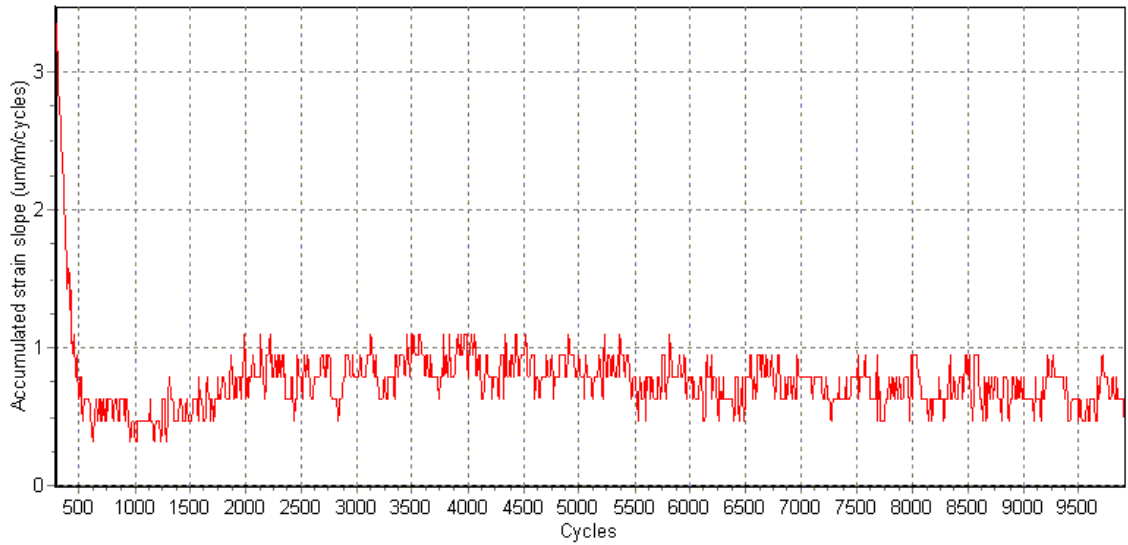
Figure 6.1 Accumulated Strain Rate: Global Flow Number Not Reached

It should be noted that some of the specimens during this initial testing phase did exhibit

a global minimum strain rate and was preceded by a significant increase in the strain rate

(Figure 6.2).
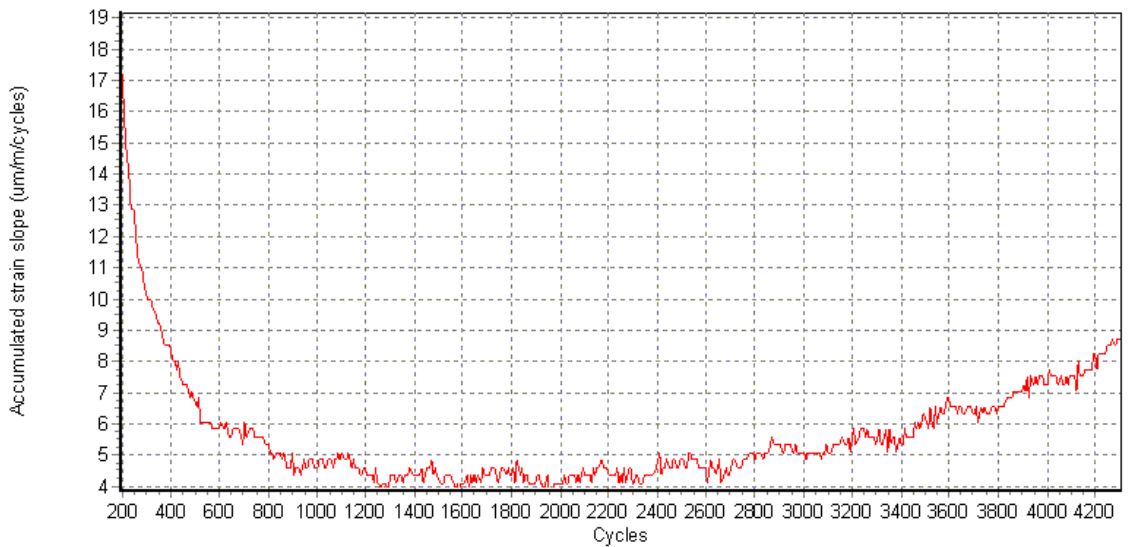
Figure 6.2 Accumulated Strain Rate: Global Flow Number Reached

92

To ensure that the global flow number was reached a second round of testing was conducted with 24 specimens where the termination cycle was 15,000.

The dynamic modulus testing that was conducted during this round of preliminary testing showed that the first hypothesis that was put forth in Section 3.4.1, which stated as temperature increased, the dynamic modulus value decreased and the phase angle increased, was confirmed. Since the dynamic modulus test was run on three specimens, the variability associated with the test was evaluated. Figure 6.3 shows the dynamic modulus mean and the error bars represent one standard deviation from the mean.
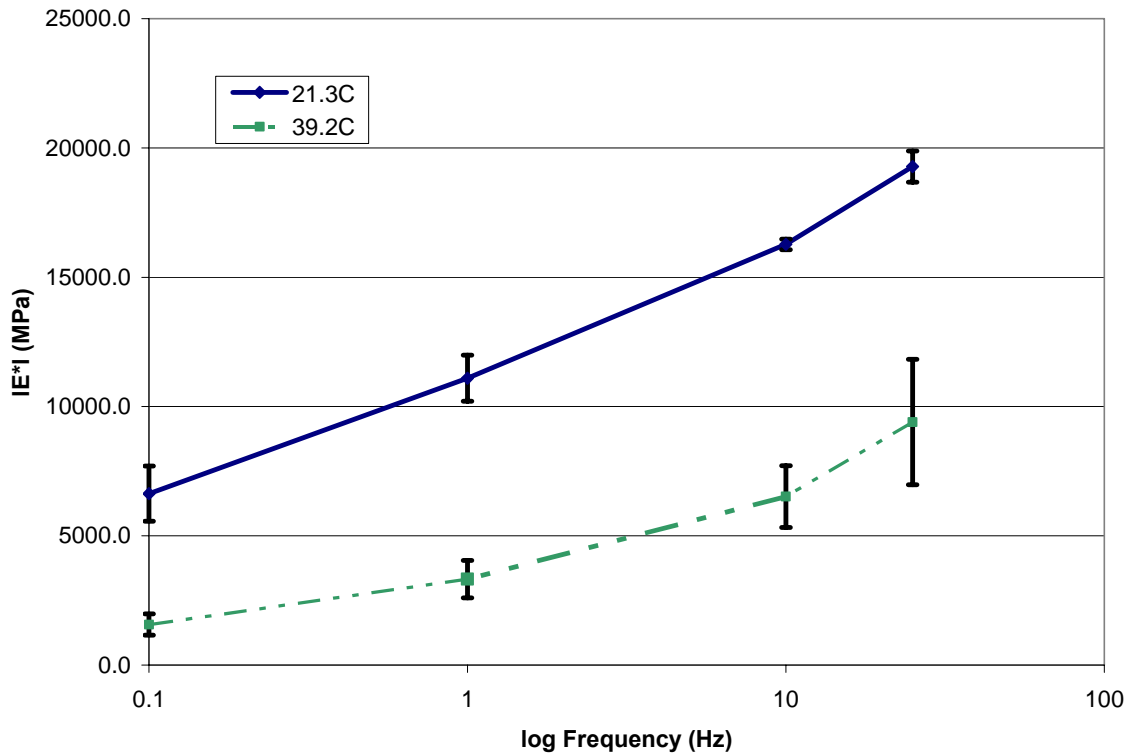
Figure 6.3 Round One Preliminary Testing Dynamic Modulus vs Frequency

Figure 6.3 illustrates that there is a general trend for the variability in the test to decrease with a decrease in the load frequency.

During the analysis of the dynamic modulus data, there appeared to be an abnormality in the phase angle at the high test temperature (39.2°C) and the frequency of 25Hz, it was highly variable and lower than the corresponding phase angle at the intermediate temperature (21.3°C). One explanation for this occurrence was machine compliance issues. At this particular frequency, the UTM 100 applies 25 load cycles per second and the machine lacks the ability to properly measure the lag in strain at this temperature. In review of the work done by Myers (2005), it was found that this occurrence did not take place. Figure 6.4 shows the relationship between phase angle and frequency.
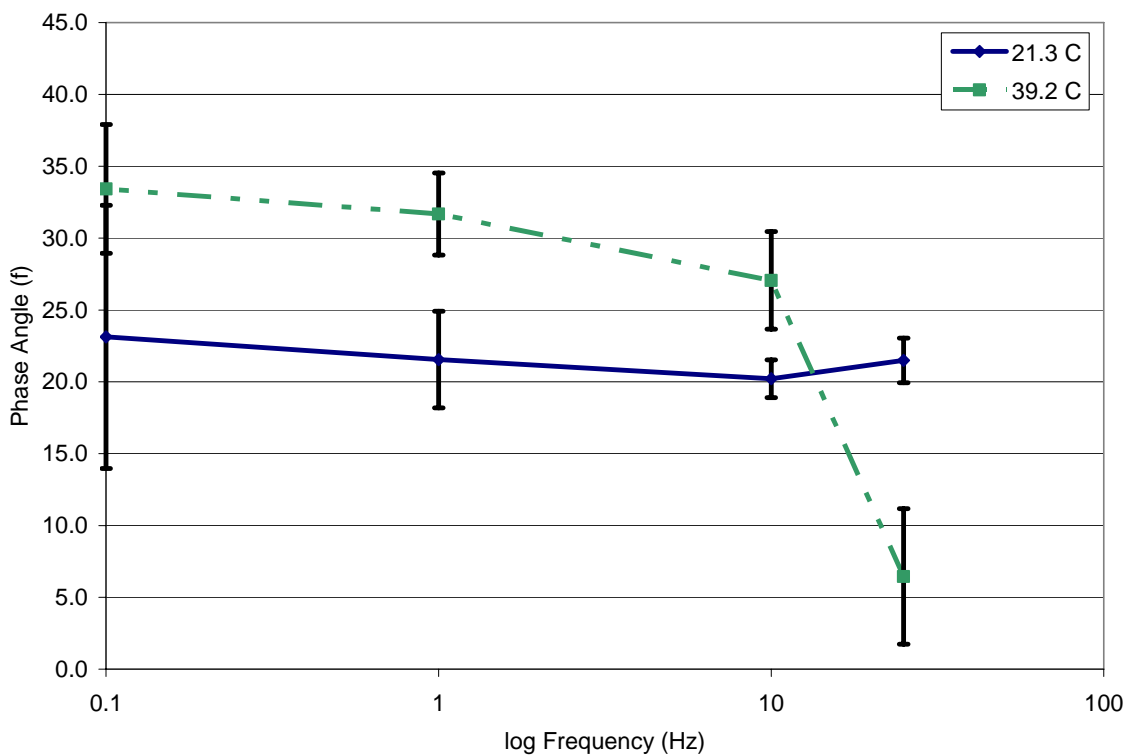
Figure 6.4 Round One Preliminary Testing Phase Angle vs Frequency

6.2.2 Round Two Preliminary Testing

During the second round of testing, the Round Robin material was once again used to prepare 24 specimens compacted to approximately 7.0% air voids. The increase in the number of specimens was meant to make the analysis more robust. Eight specimens were allocated to each of three groups henceforth referred to as 1st, 2nd, and 3rd experimental groups. Only flow number was run on the 1st experimental group. The intermediate and high temperature dynamic modulus and flow number tests were run in this order on the 2nd experimental group. Finally, the high temperature dynamic modulus and flow number tests were conducted in this order on the 3rd experimental group. This testing scheme was meant to help identify any portions of the testing regime that imparted any damage to the test specimens, which would indicate whether or not the dynamic modulus test is a truly non-destructive test. A visual representation of the testing scheme can be found in Table 6.4.

Table 6.4 Round Two Testing Scheme

	Group	Int. Temp. lE*l	High Temp. lE*l	Flow Number	Number of Specimens
Compacted to Geometries	1st Exp.			X	8
	2nd Exp.	X	X	X	8
	3rd Exp.		X	X	8

The same testing parameters as used in Round One of the preliminary testing were used. It should be noted that the specimens from this round of preliminary testing

had a shelf life of only 2-4days depending on when they were tested, the specimens for Round One had a shelf life of approximately two months.

The effects of the individual testing stages needed to be determined and the most logical approach was to use the flow number test data as the benchmark. The objective was to determine if a specimen with a testing history (intermediate and high temperature lE*l) could be used for flow number testing. In stepwise fashion, comparisons were made with the flow number test data from the 1st experimental group. The 3rd experimental group was first compared to that of the 1st experimental group as it would isolate the effects of the high temperature dynamic modulus test. The flow number test data for the specimens that were compacted to the test geometries can be found in Table 6.5.

Table 6.5 Round Two Preliminary Testing Flow Number Results

Statistic	1st Exp. Group Flow Number	2nd Exp. Group Flow Number	3rd Exp. Group Flow Number
Average	1631.5	1547.5	1901.9
Std. Dev.	426.3	810.7	898.0
COV (%)	26.13	52.39	47.22

Using the program *SAS*, the ANOVA procedure and Levene's test were used to determine if the averages and the variances for both groups were equal, respectively. The ANOVA procedure is a statistical method used to compare two or more populations or treatments (Ayyub and McCuen, 2003). The Levene's test were used to test for equal variances among the 1st and 3rd experimental groups. The Levene's test is used to determine if the samples of two or more groups have equal variances and is referred to as homogeneity of

variance (Levene, 1960). The ANOVA procedure yielded an F_{stat} of 0.59 (p-value =

0.45) while the Levene's test an F_{stat} of 0.88 (p-value = 0.36). What this indicates was

that the high temperature dynamic modulus test temperature does not have a significant

impact on the flow number test results in terms of the mean and variance. It should be

noted that the Levene's test was used in place of the Barlett's test as the Bartlett's test is

sensitive to the assumption of normality and the 3rd experimental group exhibit

nonlinearity when the normal probability plot was developed (Ayyub and McCuen,

2003).

The second portion of the statistical analysis was to compare the flow number

results between the 1st experimental group and the 2nd experimental group, as it was

found that the high temperature dynamic modulus testing did not affect the flow number

results. The ANOVA procedure and Levene's test was used to determine if the averages

and the variances for both groups were equal, respectively. The ANOVA yielded an F_{stat}

of 0.07 and a p-value of 0.80. This showed that there was no statistical difference

between the means of the two data sets.   Figure 6.5 shows an instance where the normal

probability plot has some nonlinearity and where the Levene's test would be applicable.
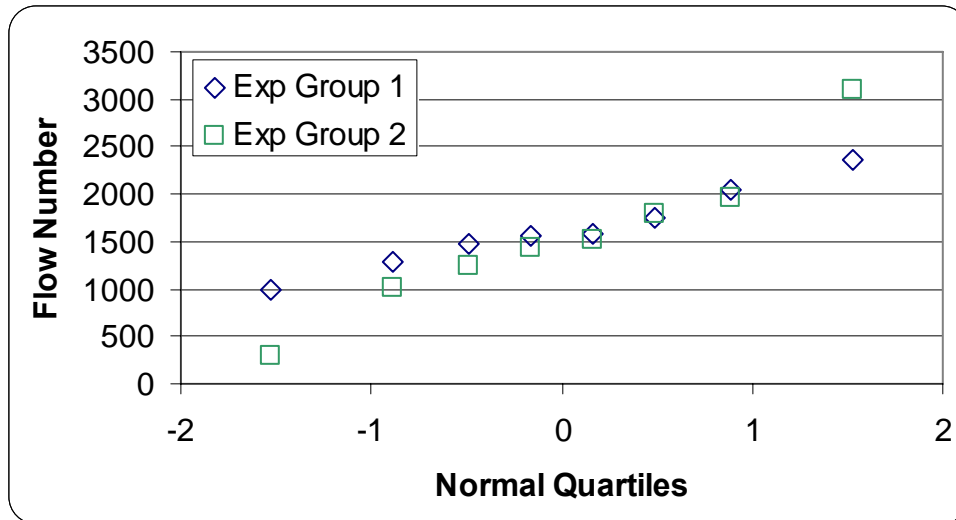
Figure 6.5 Normal Probability Plots of Testing Groups

Based upon these plots the assumption of normality was determined to be invalid based on the tails of the second experimental group. Conducting the Levene's test it was found that there was no statistical significant difference in the variances of the two data sets (F_{stat} = 1.60 and a p-value = 0.23). It was concluded from these results that the two data sets were of the same population, but it should be cautioned that running specimens through all three test procedures did result in a higher degree of variability for the flow number test values than just testing for flow number. This may necessitate a larger sample size for the flow number test than the three specimens recommended by Witczak et al (2002b).

Referencing the ages of the specimens in the two tests, it appeared as though shelf life may have resulted in some aging effects on the flow number test results. During this round of testing, the measured flow number was significantly lower than during Round One testing and was less than 3,200 load cycles as opposed to an excess of 10,000.

The next portion of the analysis of the Round Two testing was to determine if there was any difference between the measured dynamic modulus values at the high temperature as measured by the 2nd and 3rd experimental groups. Again, the 3rd experimental group consisted of specimens run at only the high temperature for dynamic modulus. The same analysis procedure that was presented previously was used for this portion of the analysis. The statistics for the two data sets are presented in Table 6.6 with all data in MPa.

Table 6.6 Round Two Preliminary Testing Dynamic Modulus Results

	Frequency (Hz)			
2nd Exp. Group	0.1	1.0	10.0	25.0
Average	925.3	2137.7	5103.7	9518.6
Std. Dev.	321.1	849.2	1751.4	3872.4
COV (%)	34.71	39.73	34.32	40.68
3rd Exp. Group				
Average	1050.0	2266.8	5408.2	10332.7
Std. Dev.	317.5	451.8	974.3	2690.2
COV (%)	30.24	19.93	18.01	26.04

The analysis for this portion of testing showed that there was no statistical difference between the averages of the two experimental test groups at each frequency. The ANOVA procedure and Bonferroni test were run at both 0.05 and 0.10 levels of significance. The Bonferroni method is used to make pairwise comparisons between a set of treatments (Ayyub and McCuen, 2003). It was found that the variances for the 1.0 and 10.0Hz frequencies were statistically different using the Levene's test at the 0.10 level of significance (p-value = 0.03 and 0.09, respectively). One specimen was omitted from the 2nd experimental group as it was found to be an outlier; furthermore the dynamic modulus of one of the specimens was also determined to be an outlier at 25Hz. The reason for these specimens being removed from the analysis was that UTM 100 was not

applying a high enough load during the course of the test and as a result the determined dynamic modulus was significantly higher than the running average. This cause was not realized until later on during the course of testing. It should be noted that even though the statistical tests showed that there was no difference in the variances of the two data sets, there appeared to be an increase in the variability associated with the 2nd experimental group. Appendix D contains the statistical output for this analysis and the dynamic modulus values are listed in MPa.

Similar results were found during Round Two of testing for the phase angle with frequency. There was a general decrease in the phase angle with an increase in frequency marked by a significant drop in the measured phase angle at the high temperatures at 25Hz. The general relationship can be seen in Figure 6.6.
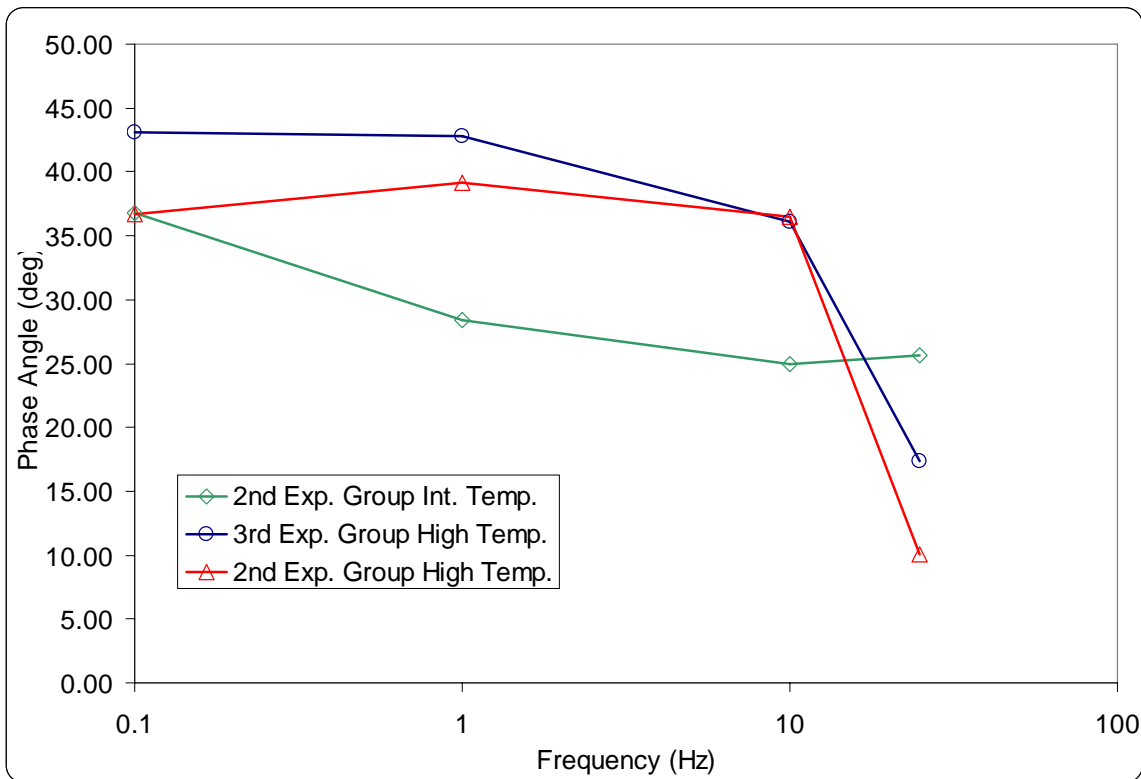
Figure 6.6 Round Two Preliminary Testing Phase Angle vs Frequency

6.2.3 Round Three Preliminary Testing

During this round of testing the 150mm in diameter by 170mm in height specimens were cut down to 100mm in diameter by 150mm in height using a saw/coring apparatus manufactured by Shedworks. Also considered were 150mm in diameter by 170mm in height specimens that were compacted several months earlier so that aging of cut down specimens could be examined. Again, the Round Robin mix was used during testing to eliminate the effects of changes in material properties. Three groups of specimens were formed; a 4th and 5th experimental group and an aged group. The 4th experimental group consisted of eight specimens with only flow number considered. The 5th experimental group consisted of eight specimens that were tested at the intermediate and high temperature dynamic modulus and then flow number. Round One of testing showed that the high temperature dynamic modulus did not impact the flow number results. It was expected that similar results would be yielded during this portion of analysis so only the complete test history of intermediate and high test temperature dynamic modulus were considered. The aged group was the specimens cut down from the 150-mm in diameter by 170-mm in height specimens that were compacted several months earlier. The effects of the three testing procedures were examined on the flow number testing results. Additionally, this testing round was meant to determine if there was any statistical difference with cut and cored specimens and specimens compacted to the testing geometries from Round Two of the preliminary testing. Appendix D shows the full results of this analysis with all data in MPa. Table 6.7 displays a visual representation of this portion of the testing.

Table 6.7 Round Two Testing Scheme

	Group	Int. Temp. lE*l	High Temp. lE*l	Flow Number	Number of Specimens
Cut Down to Geometries	4th Cont.			X	8
	5th Exp.	X	X	X	8

The results of the comparison between 4th experimental group, the 5th experimental, and aged group are shown in Table 6.8.

Table 6.8 Round Three Preliminary Testing Flow Number Results

	4th Exp. Group	5th Exp. Group	Aged Group
Statistic	Flow Number	Flow Number	Flow Number
Average	2174.5	2049	4483
Std. Dev.	262.5	637	1830.7
COV (%)	12.07	31.09	40.84

The Bonferroni test showed that there was no statistical difference between the means of the 4th and 5th experimental groups at 0.05 and 0.10 levels of significance. The two data sets appear to be normally distributed and thus the Bartlett's test was valid for the testing for equal variances. The Bartlett's test is used to verify the assumption of equal variances used in the ANOVA procedure (Ayyub and McCuen, 2003). Conducting the Bartlett's test it was found that there was a statistical significant difference in the variances of the two datasets (χ^2_{stat} = 4.58 and a p-value = 0.03). This means that specimens that have been sawed and cored and tested at the intermediate and high dynamic modulus test temperatures induced a higher degree of variability in the flow number test results as compared to specimens just tested under flow number. This was similar to the results found with the specimens that were compacted to the test geometries in Round Two.

Additionally, the age of the specimen adds to the increased variability of the flow number.

An analysis was also conducted to compare the flow number results from Rounds Two and Three of the preliminary testing. The effects of flow number were first examined for only flow number (1st vs. 4th experimental groups). The ANOVA procedure found that the two groups were statistically different (F_{stat} = 7.59 and a p-value = 0.02), whereas the variances for the two groups were equal (Bartlett's test χ^2_{stat} = 1.27 and a p-value = 0.29). Further analysis showed that the mean response of the specimens that were sawed/cored to the test geometries yielded a higher flow number. This suggests that the method of specimen preparation has a significant impact on the mean response of flow number.

The testing history was also considered to determine its effects on flow number between the methods of specimen preparation (2nd vs. 5th experimental group). It was anticipated that a similar result would be found, that there was a statistical difference between the mean responses, but this was not the case. The ANOVA procedure showed that the two groups were in fact statistically similar (F_{stat} = 1.89 and a p-value = 0.19). The variance was also shown to be equal with the use of the Bartlett's test (χ^2_{stat} = 0.38 and a p-value = 0.54). This presents an interesting result, as it indicates that having a test history would bring the mean response into alignment between the two methods of specimen preparation. This is interesting because it has been shown that in none of the statistical tests that having a testing history has an impact on the mean response of flow number.

The effects of the dynamic modulus values on the different specimen preparation methods were also examined over the four frequencies considered. The 2nd and 5th experimental groups were used to conduct this analysis. Tables 6.9 and 6.10 present the relevant statistical information from both experimental groups for the intermediate and high dynamic modulus test temperatures. A total of eight specimens were considered during this portion of the analysis.

Table 6.9 Dynamic Modulus Results at Int. Temperature

	Frequency (Hz)			
2nd Exp. Group	0.1	1.0	10.0	25.0
Average	3450.7	7352.2	13465.0	16924.3
Std. Dev.	1165.9	2278.7	4467.3	5089.1
COV (%)	33.79	30.99	33.18	30.07
5th Exp. Group				
Average	3345.9	7154.2	12686.5	15972.6
Std. Dev.	838.5	1641.3	2553.2	2851.0
COV (%)	25.06	22.94	20.13	17.85

Table 6.10 Dynamic Modulus Results at High Temperature

	Frequency (Hz)			
2nd Exp. Group	0.1	1.0	10.0	25.0
Average	925.3	2137.7	5103.7	9518.6
Std. Dev.	321.1	849.2	1751.4	3872.4
COV (%)	34.71	39.73	34.32	40.68
5th Exp. Group				
Average	1082.1	2215.2	4952.3	8439.8
Std. Dev.	308.4	578.2	1020.2	3087.3
COV (%)	28.50	26.10	20.60	36.58

It was determined using the ANOVA procedure that at all of the temperature and frequency combinations, there was no statistical difference between the two specimen preparation methods. There was however two variances that were found to not be equal at $\alpha=0.10$ level of significance. These two suspect variances were for 39.2°C at 1.0 and

10.0 Hz, where the critical p-values occurred at 0.09 and 0.07. For the other temperature and frequency combinations, the critical p-values were between 0.46 and 0.94.

It is interesting to note that although there were statistical differences in flow number in the aged specimens with that of the experimental groups, there were no apparent differences with the dynamic modulus results of the aforementioned groups. This result indicates that dynamic modulus is insensitive to the age of the tested specimen, but flow number would be a good candidate test to use when determining the materials response to aging.

The phase angle results from this round of testing were similar to that of the previous rounds. Figure 6.7 shows the phase angles versus frequency measurements for Rounds Two and Three of the preliminary testing.
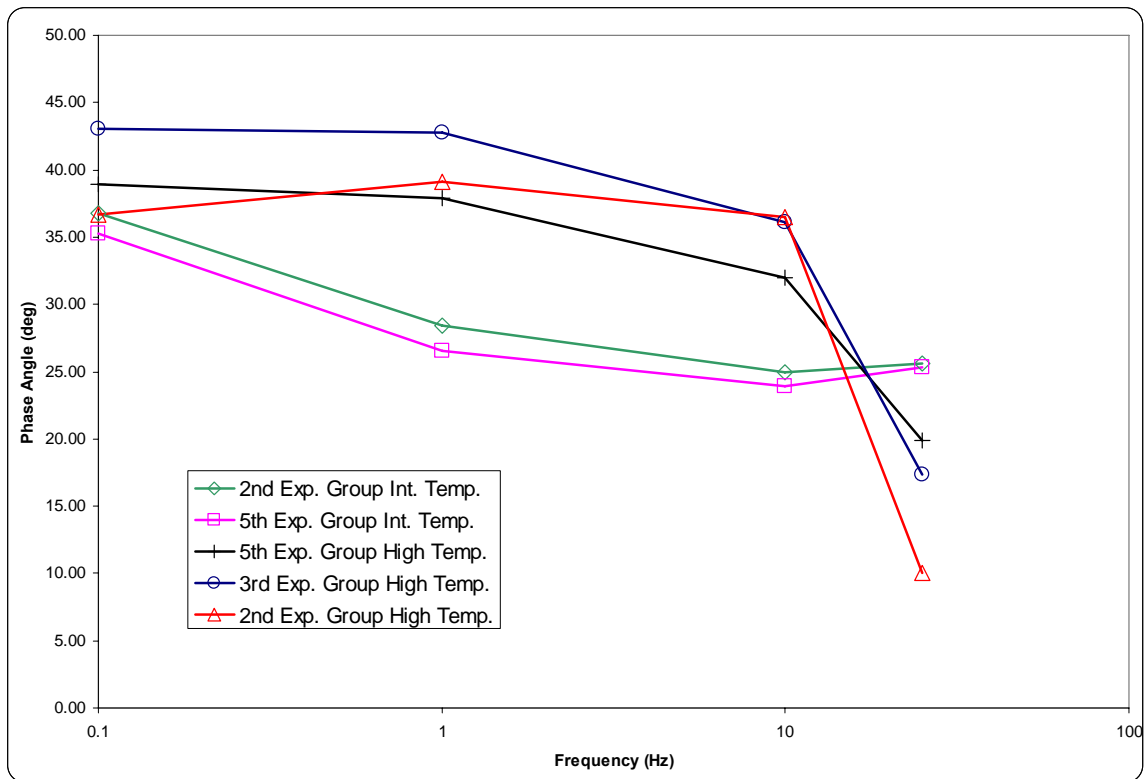
Figure 6.7 Rounds Two and Three Preliminary Testing Phase Angle vs Frequency

As can be seen in Figure 6.7, there was no difference between the different specimen preparation methods as to the affects of the phase angle. The basic trends in the phase angle as realized by the preliminary testing include: 1) as the temperature increases, the phase angle likewise increases and acts more as a viscous material, and 2) as the frequency increases, there is a decrease in the phase angle which means that the material is behaving elastically.

6.2.4 Preliminary Testing of Design Guide Software

An analysis was conducted using the software from the Design Guide to determine the effects on the dynamic modulus results from the 2nd and 5th experimental groups. The intent was to determine if there were any differences in the distresses that were yielded from the software when considering the different preparation methods. Again the specimens from the 2nd experimental group were compacted to the test geometries of by 100-mm in diameter by 150-mm in height with the specimens from the 5th experimental group being cut down to the test geometries from a 150-mm in diameter by 170-mm in height gyratory specimen. The statistical means and standard deviations were determined for each frequency and each temperature were determined. Then confidence intervals at 60, 75, 90, and 95% were determined for the aforementioned populations. The confidence intervals for 75, 90, and 95% can be found in Appendix C for the respective frequency and temperature.

A hypothetical pavement structure was developed to examine the effects of the different specimen preparation methods for the confidence intervals. The developed pavement design had six layers, an asphalt surface course 3-in thick, two asphalt base

courses at 5-in thick apiece, 12-in of crushed stone, 6-in of A-3 soil, and an A-5

subgrade. The A-3 and A-5 soil classification refers to a fine sand and a silty soil,

respectively, and are based on the AASHTO soil classification system. The surface

course served as the experimental layer where the dynamic modulus values were directly

inputted for a Level One design, all of the other layer properties were held constant

during the analysis. As the Design Guides software has numerous inputs for each of

these layers, the properties are presented in Appendix E. Default values were used for

the traffic characteristics and an AADTT of 1500 used.

The Design Guide software requires that the dynamic modulus test be run at a

minimum of three test temperatures; however, there was only two temperatures available

from the preliminary testing. As a quick means of conducting the analysis, the dynamic

modulus values were linearly interpolated between the intermediate and high test

temperatures at each of the frequencies. From previous knowledge linear interpolation

was appropriate at 0.1 and 1.0Hz whereas at 10.0 and 25.0Hz a polynomial function

would be more appropriate.

The Design Guide software was run using the dynamic modulus values at the

intermediate and high temperature as well as the interpolated value for each of the

aforementioned confidence intervals. From the outputs, the changes in the predicted

distresses were recorded over the different confidence intervals. Of immediate interest

from the analysis it was found that the Design Guide software could not correctly process

the upper ends of the confidence intervals (e.g., 60, 75, 90, and 95th percentiles). The

software yielded almost 3-in of instantaneous rutting in the surface layer which does not

occur at the lower percentiles, which leads to the conclusion that the software has a

limiting function for the layer modulus values. If this is indeed the case, significant difficulties could be encountered by other users when it comes to materials that undergo little strain due to loading. Predicted distresses were determined for the 5, 10, 25, 40, and 50th percentiles (correspond to the 95th, 90th, 75th, and 60th confidence intervals) for permanent deformation of the entire pavement, permanent deformation in the AC layer, IRI, surface down cracking, and bottom up cracking. Figure 6.8 shows the results of permanent deformation in the AC layer for the two methods of specimen preparation.
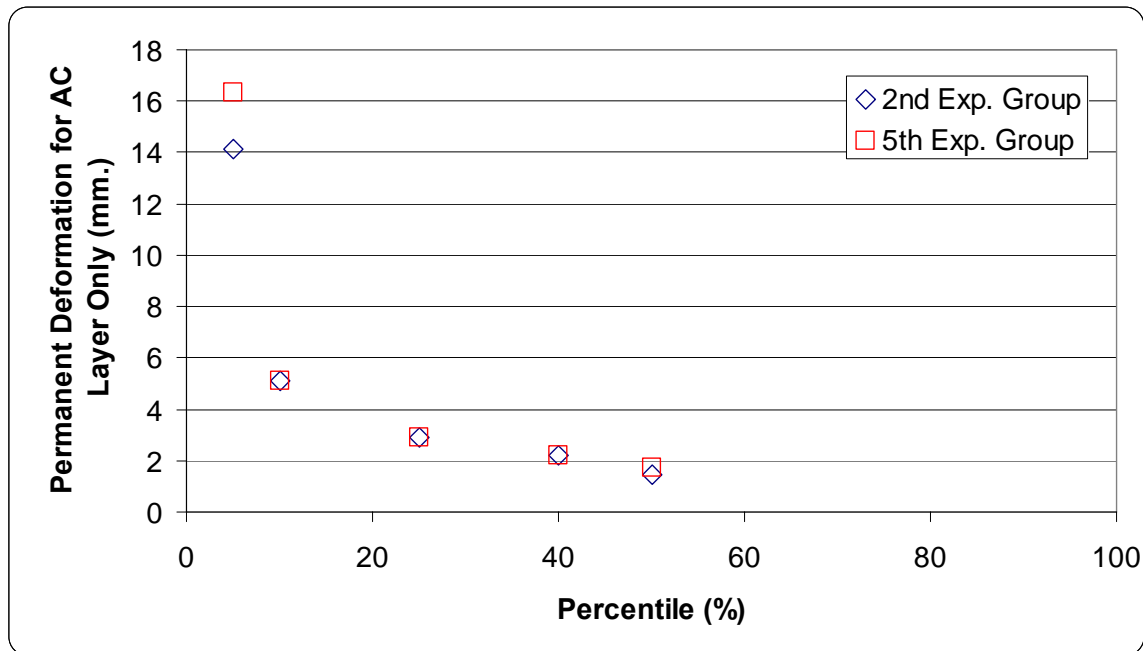
Figure 6.8 Permanent Deformation vs. Confidence Percentile

Figure 6.8 shows that the permanent deformation in the AC layer for both of the experimental groups were closely related. Similar results were found for the total permanent deformation of the pavement, surface down cracking, bottom up cracking, and IRI. What the results indicate from the limited dataset, is that the method of specimen preparation does not affect the outcome of the pavement design and thus either method may be used to procure specimens for this type of analysis. Future work should consider

both the nominal maximum aggregate size and open-graded mixtures as these factors are additionally relevant.

6.2.5 Preliminary Testing Results Summary

The comparisons that are made above are summarized here.

Specimens compacted to test geometries:

1. Does high temperature dynamic modulus affect the statistical response of flow number?

   Mean: No

   Variance: No

2. Does intermediate and high temperature dynamic modulus affect the statistical response of flow number?

   Mean: No

   Variance: No

3. Does intermediate temperature dynamic modulus affect the statistical response of the high temperature dynamic modulus?

   Mean: No

   Variance: Yes

Specimens sawed/cored to test geometries

4. Does intermediate and high temperature dynamic modulus affect the statistical response of the high temperature flow number?

   Mean: No

   Variance: Yes

Method of preparation

5. Does the method of specimen preparation affect the statistical response of flow

    number?

        Mean: Yes

        Variance: No

6. Does the method of specimen preparation affect the statistical response of flow

    number when the test specimens have a test history?

        Mean: No

        Variance: No

7. Does the method of specimen preparation affect the statistical response of

    intermediate and high temperature dynamic modulus?

        Mean: No

        Variance: Yes

8. Does the method of specimen preparation affect the 2002 Design Guide software

    analysis?

        Rutting AC Layer: No

        Rutting Total Pavement: No

        IRI: No

        Alligator Cracking: No

        Longitudinal Cracking: No

The conclusions reached from this research indicate that the same test specimen

may be used throughout a testing scheme as it will not affect the mean response if there is

a testing history. There are however tendencies for there to be an increased variability.

Additionally, the specimens compacted to testing geometries can be used in lieu of specimens cut and cored from gyratory compacted specimens 150-mm in diameter by 170-mm in height.

Three concerns have arisen from this portion of testing. First, the age of the specimens do appear to significantly affect flow number results. Efforts should be made to minimize the aging of the specimen prior to testing. Second, the air voids were noted to decrease by 1.0-1.5% from the 150-mm by 170-mm specimens to that of the specimens cut down to the testing geometries. To address this issue, the crucial air void content must be determined, whether it be from the compacted specimen or the cut down specimen. The compacted air voids would be the easiest to measure and manage during an analysis. The cut down specimen would need to employ a correction factor so that the desired air voids could be obtained. Third, mixes that exhibit low strain measurements due to loading and resulting high dynamic modulus values may present problems for the Design Guide software.

One final caution needs to be stated. When using dynamic modulus and flow number test results in a quality control situation, the same testing history should be used (e.g. flow number test results in QC/QA cannot be compared to flow number test results done during mix design if dynamic modulus testing was done on the same set of specimens). In this manner, a similar amount of micro-strain will have been induced upon the specimen through testing. Likewise, trends have shown that there was an increase in variability in the mean response with specimens that had a testing history.

6.3 Predictive Dynamic Modulus

The predictive dynamic modulus equation developed by Witczak et al (2002b) was employed (previously explained in Section 4.5) to validate the data from this study. The inputs for this equation include bitumen viscosity, loading frequency, air void content, effective bitumen content, and material retained and passing on certain sieves. The gradations and effective binder content were determined from the JMF supplied by the contractor. The loading frequencies have been predetermined and are stated in Table 4.2. The air void content for each tested specimen was determined from G_{mb} testing. The bitumen viscosity was the only property left to determine.

The bitumen viscosity was determined by three different methods. The first was the viscosity of the original binder, a mix/laydown condition as stipulated by Mirza and Witczak (1995), and finally rolling thin film oven (RTFO) aged binder viscosity. The RTFO simulates the aging of the asphalt binder during production and placement. The Design Guide stipulates temperatures at which the bitumen viscosities are to be conducted as shown in Table 6.11.

Table 6.11 Conventional Binder Tests

Test	Temperature, °C (°F)
Penetration	15 (59)
Penetration	25 (77)
Rotational Viscosity	80 (176)
Rotational Viscosity	100 (212)
Rotational Viscosity	121 (250)
Rotational Viscosity	135 (275)
Rotational Viscosity	176 (349)

The original binder was tested under all of the shown conditions except 80°C, it was quickly realized that the temperature specification of 176°C was unreasonable as no

contractor would produce a mixture at this temperature due to environmental issues. The RTFO aged material was tested at 80, 100, 121, and 135ºC.

Penetration testing was conducted in accordance with ASTM D5. Penetration testing measures the consistency of asphalt binder by applying a weighted needle to the sample over a given period of time. The penetration results had to first be converted to an equivalent viscosity (cP) in order to determine the temperature susceptibility of the binder, the conversion equation follows (Guide for Mechanistic-Empirical Design of New and Rehabilitated Pavement Structures, 2004).

$$\log \eta = 10.5012 - 2.2601 \log(\text{Pen}) + 0.00389 \log(\text{Pen})^2 \qquad (6.5)$$

where:
η = viscosity, Poise, and
Pen = penetration, mm/10.

Rotational viscosity testing was conducted in accordance with ASTM D4402. Viscosity testing measures the flow characteristics of the asphalt binder. A vessel is filled with a 10.5gram sample and a standard spindle is submerged in the binder. The viscometer is typically set to 20rpms and three measurements are made at the outlined temperatures. Every asphalt binder for this project was tested in the outlined manner and temperatures.

The Mirza and Witczak (1995) equation (Equation 6.6) was developed to convert the original binder viscosities to mix/laydown conditions (similar to RTFO aged material).

$$\log \log \eta_{t=0} = a_0 + a_1 \log \log(\eta_{orig}) \qquad (6.6)$$
$$a_0 = (0.054405 + 0.004082 \text{ code})$$
$$a_1 = (0.972035 + 0.010886 \text{ code})$$

where:
$\eta_{t=0}$ = mix/laydown viscosity (cp) at temperature T_R (Rankine),
η_{orig} = original viscosity (cp) at temperature T_R (Rankine), and

113

Code = hardening resistance (code = 0 for average).

The value of zero was used for the code value. Birgisson et al (2005) found that

rotational viscosity testing on RTFO aged material and the derived mix/laydown equation

above yielded similar results.

The temperature susceptibility of each asphalt binder was determined by

regressing the logarithm of the logarithm of the mix/laydown bitumen viscosity against

the logarithm of the test temperature in Rankine. The regression equation follows.

$$\log \log \eta_{t=0} = A + VTS \log T_R \tag{6.7}$$

where:
        A = regression intercept,
        VTS = regression slope of the viscosity temperature susceptibility, and
        T_R = temperature, Rankine.

Each binder has a unique intercept and slope. An equivalent bitumen viscosity was

determined using the effective test temperatures at each location. This bitumen viscosity

was then used in the dynamic modulus predictive equation. Results for the penetration

and viscosity testing can be found in Appendix F: Bitumen Temperature Susceptibility.

6.3.1 A and VTS Comparisons

In the Design Guide (2004) a library of values have been developed for the

viscosity-temperature susceptibility logarithm constants in Equation 6.7 for Superpave,

viscosity, and penetration graded binders.   Comparisons were then made between these

values and the values determined from viscosity testing of the individual project binders.

There are differences in the A and VTS values that were calculated, but they did not

appear to be significant. However, when the equivalent viscosities were determined for

the effective test temperatures, illogical results were found on several projects. In some

cases the determined equivalent viscosities actually decreased when aged in a RTFO as compared to the original binder equivalent viscosities. This decrease in viscosity is not reasonable due to the fact that the RTFO is meant to simulate aging because of construction and mix/laydown, and in essence makes the binder stiffer, thus resulting in an increased viscosity. In review of the actual viscosity test results at similar temperatures it was found that the RTFO aged binders are higher than that of the corresponding original binder. The only source for the discrepancy was the methodology for determining the equivalent viscosities as presented by Witczak et al (2002b). Evaluating the methodology for determining the A and VTS values, Equation 6.7 attempts to force the data array to be linear when plotted as log log viscosity (cP) versus log temperature (Rankine), however the viscosity at 15 and 176ºC (2.715 and 2.908 are the analogous log temperatures, respectively) does not appear linear with the other test results. This tendency can be seen in Figure 6.9, it also shows the reason behind the elevated equivalent viscosities at the lower temperatures. It should also be pointed out that the regression equations that are presented on each plot represent the A and VTS values, the A being the intercept and VTS being the slope.
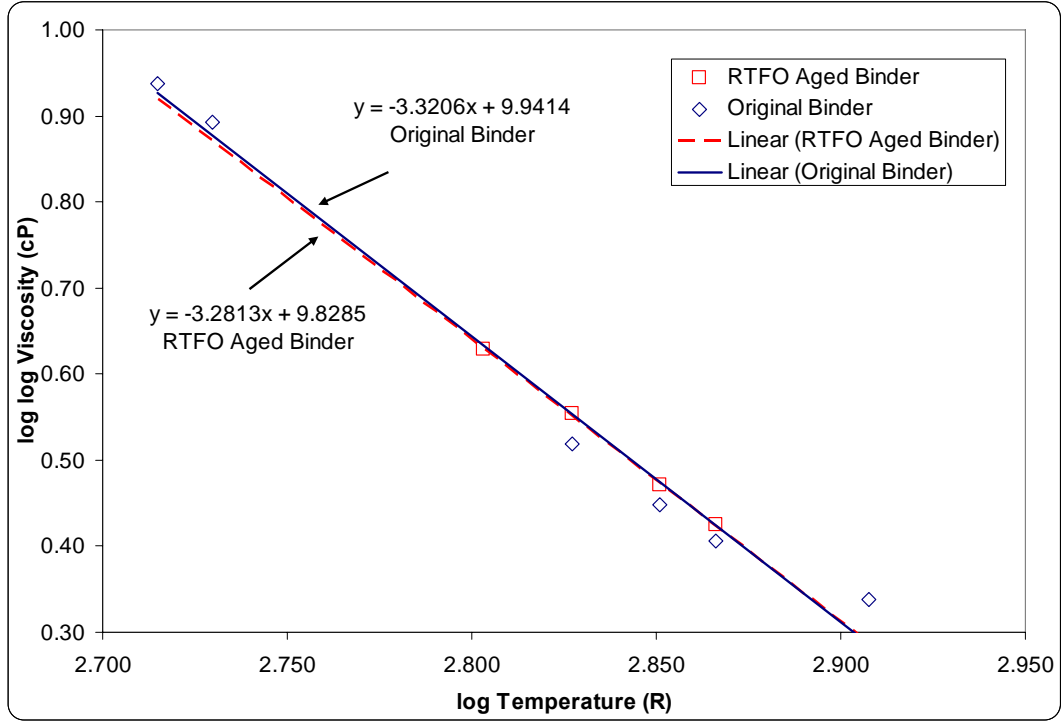
Figure 6.9 Original vs RTFO Aged Binder Viscosities
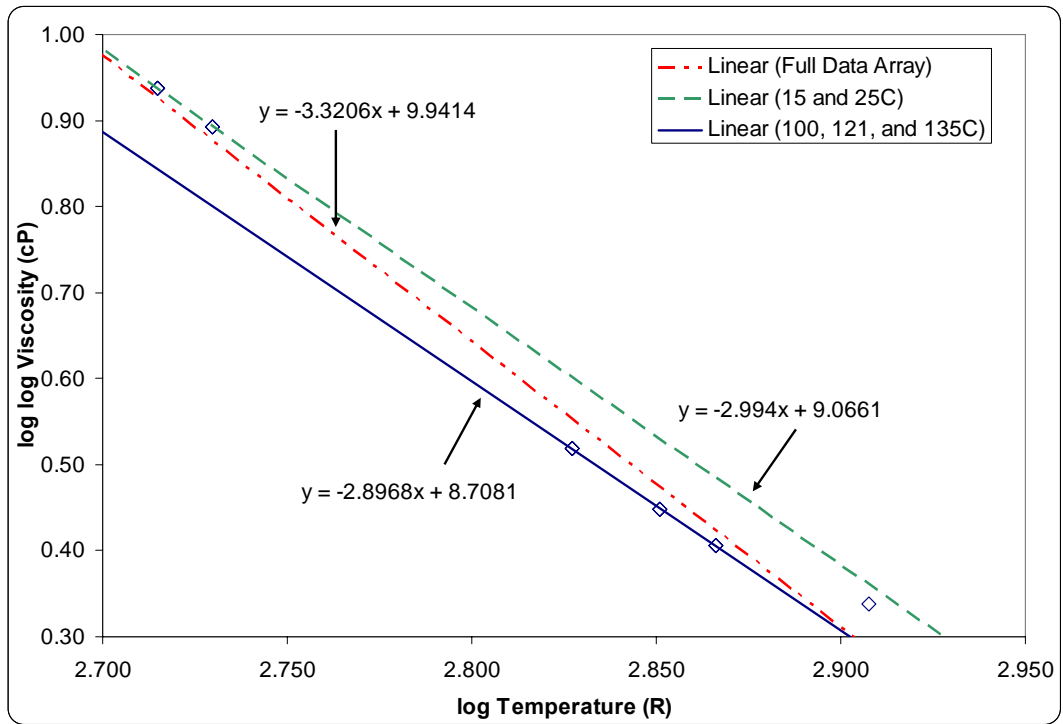
Figure 6.10 Viscosity-Temperature Susceptibility

116

Figure 6.10 shows data from the original binder test results from the Baraboo project. The semi-dashed line was from all the regressed test temperatures-viscosities that were suggested for this testing regime. The solid line shows the regression of only the temperature-viscosity relationships at 100, 121, and 135ºC. The dashed line was the regression of the 15 and 25ºC temperature-viscosity relationships. Figure 6.10 further illustrates that the procedure outlined by the Design Guide does not present a truly linear relationship and that temperature selection of the viscosity tests has a significant impact on viscosity temperature susceptibility. Due to this non-linearity, the viscosity at 15, 25, and 176ºC governs the A and VTS values, thus presenting illogical results as previously enumerated. It should be emphasized that the results at 15 and 25ºC were measured by performing penetration tests and converting the results to an analogous viscosity and as a result significant errors may have occurred due to the inherent reliability of the equation. These stipulated test temperatures and the procedure should be further reviewed for legitimacy as it currently does not appear to yield results that are reasonable. For the time being it appears as though the temperatures between 80 and 135ºC present the most logical selection for viscosity test temperatures, at these temperatures no equations are needed to determine equivalent viscosities and can reasonably be run with the rotational viscometer.

To comment on these differing viscosities from the four sources, the one selected in design has a significant impact on the thickness of the layers of the system. Selecting a viscosity higher than what it really was at that temperature could result in premature failure due to rutting. Likewise, if the actual viscosity was higher than estimated, it would result in an over designed pavement structure, resulting in higher construction

costs. This further emphasizes the need to analyze the affects of the test temperature selection as it has significant economical impacts on pavement construction and future rehabilitations.

6.4 Round Robin Mix

The JMF for the Round Robin mix was available and thus an analysis of the Witczak predictive equation to the measured dynamic modulus was possible. The only information that was not available was the temperature-viscosity relationship of the binder, but it was known to be a PG64-22, so the Design Guide stipulated A and VTS constants were used to determine the binder viscosity at the aforementioned test temperatures (10.890 and -3.680, respectively). Table 6.11 shows the relevant information for the Witczak (2002b) predictive equation.

Table 6.11 Round Robin Material Attributes

Variable	Value
Viscosity @ 21.3°C (10^6 Poise)	1,019
Viscosity @ 39.2°C (10^6 Poise)	17.768
Air Voids	Variable
Effective Binder Content (%)	9.68
Retained on 19.0mm Sieve (%)	0.0
Retained on 9.5mm Sieve (%)	14.0
Retained on 4.75mm Sieve (%)	49.0
Passing on 0.075mm Sieve (%)	4.9

Figure 6.11 presents the measured and predictive dynamic modulus for the Round Robin mix as it pertains to the measured values from Rounds One and Two of the preliminary testing. It was comprised of 142 data points from the two different temperatures and four frequencies.

118
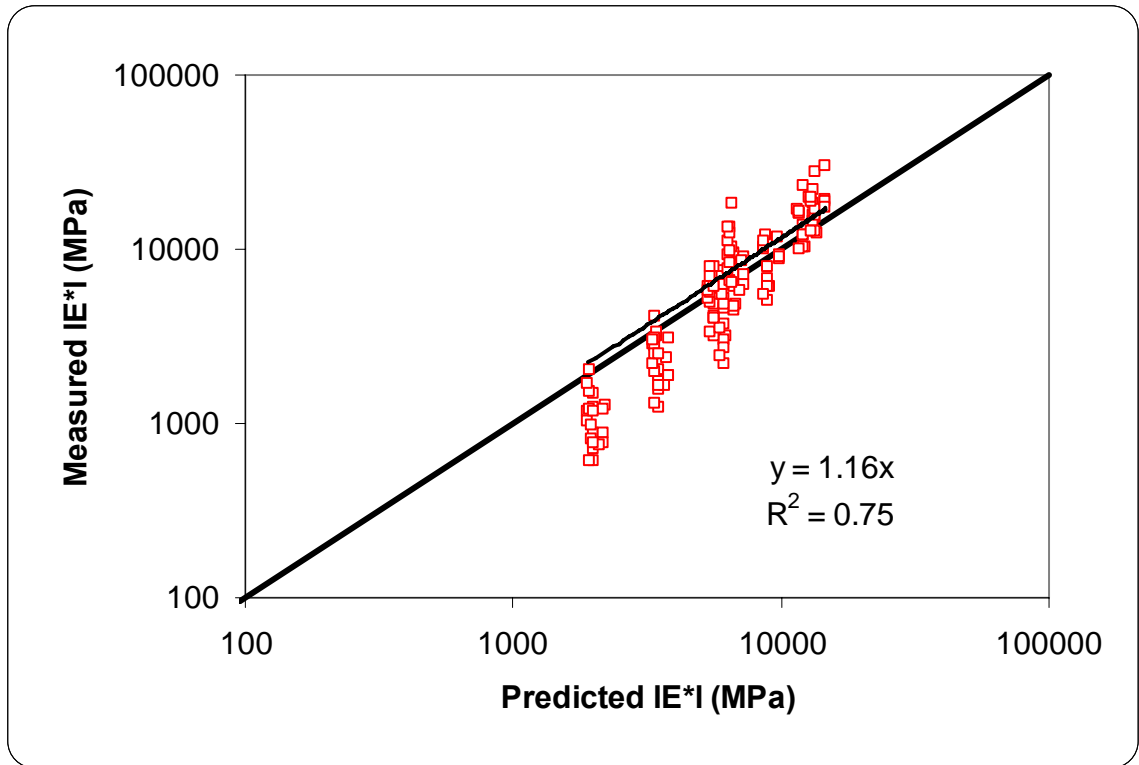
Figure 6.11 Relationship between Predicted and Measured lE*l for Specimens Compacted to Size

The predictive equation developed by Witczak et al (2002b) was limited in scope as to the materials that were tested for its development; however Birgisson et al (2005) have presented a method to calibrate the equation to the local conditions where the material is placed. The predictive and measured dynamic modulus values were regressed, Birgisson et al (2005) set the intercept of the regression equation through zero, this modeling is reasonable as a negative dynamic modulus value may be estimated with a simple linear regression equation. Multiplying Witczak et al equation by 1.16 will shift the Round Robin mix to the actual measured dynamic modulus values.

Figure 6.12 presents the measured and predictive dynamic modulus for the Round Robin mix of the specimens that were cut down to the test geometries. It was comprised

of 96 data points from the two different temperatures and four frequencies. The shift

factor for the sawed/cored specimens would be 0.84 to increase the reliability of the

predictive equation. An alternative would be to recalibrate the coefficients of the

Witczak predictive equation.
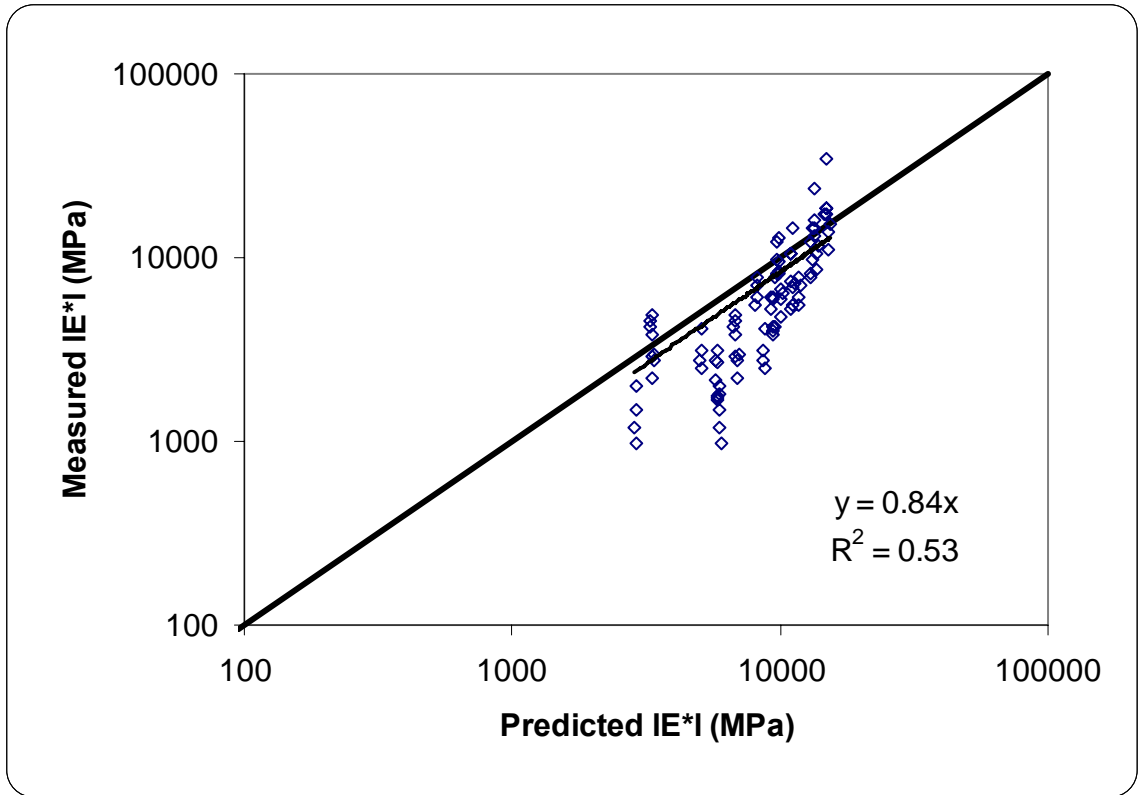
Figure 6.12 Relationship between Predicted and Measured lE*l for Specimens Sawed and Cored

CHAPTER 7: WISCONSIN MIX TESTING

7.1 Jobs Tested

An abbreviated testing schedule was developed for this thesis. The projects that were tested include:

- Northfield E-30 19.0mm Dense Graded,
- Mosinee E-3 19.0mm Dense Graded, and
- Bloomville E-1 19.0mm Dense Graded.

The tests were conducted per the outlined parameters in Chapter 6.

The test results for the intermediate and high temperature dynamic modulus and flow number can be found in Appendix G. Before proceeding, the phase angle variations in the test data warrant comment. The phase angle on the 10.0 and 25.0Hz frequencies at the high test temperatures exhibited the highest coefficient of variation (COV) in the data sets; this was once again believed to be caused by the compliance issues with the testing machine and its inability to properly apply the desired stress level. During testing, the phase angle was not of the greatest interest as the dynamic modulus was the direct input into the Design Guide software. Contained herein are the results from the dynamic modulus and flow number testing as well as an analysis of the Design Guide software as it pertains to the tested mixtures.

7.2 Dynamic Modulus Loading Stress

All of the testing parameters have been discussed in Section 6.1 except for the

axial stress that was applied to the specimen. The reason being was that the axial stress

that yielded 75-125μm strain needed to be determined for both the intermediate and high

test temperatures through iterative testing. Table 7.1 shows the axial stress used for each

mix and test temperature.

Table 7.1 Mixture Applied Axial Stress

Mixture	Int. Temperature Axial Stress (kPa)	High Temperature Axial Stress (kPa)
Bloomville E-1 19.0mm	103	35
Mosinee E-3 19.0mm	69	35
Northfield E-30 19.0mm	173	35

The same stress was used for each of the frequencies except at the high temperature for

25.0Hz; an axial stress of 69kPa was actually used. This was due to the capacity of the

machine, at the higher frequencies, the testing machine was not able to apply the

programmed load, and it would frequently apply approximately a zero load and provide

obviously erroneous results. To overcome this obstacle, the axial load for only this

frequency was increased. This frequency was carefully monitored to ensure that the

excessive permanent axial micro-strain was not imparted during testing. This deficiency

in the axial stress was probably another cause for why the phase angle was not at times

properly measured at the high temperature.

7.3 Dynamic Modulus Test of Hypotheses

Contained in this are the results of the dynamic modulus testing as it pertains to the hypotheses put forth in Section 1.5.1. The effects of temperature, air voids, asphalt binder content, and traffic level will be discussed further in the ensuing subsections.

7.3.1 Temperature

The test hypothesis for temperature was that as it increased, the dynamic modulus should decrease. The dynamic modulus results were plotted at the different temperatures, however to reduce the amount of information that is disseminated, only the dynamic modulus data from the 7.0% air voids at the optimum asphalt binder content were compared (Figures 7.1 through 7.3).
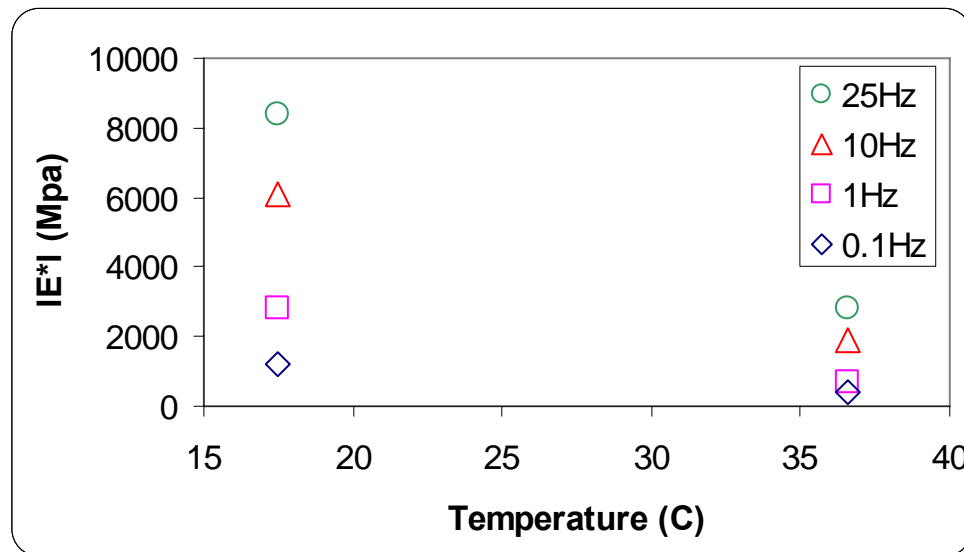
Figure 7.1 Bloomville E-1 19.0-mm $|E^*|$ Temperature Comparison
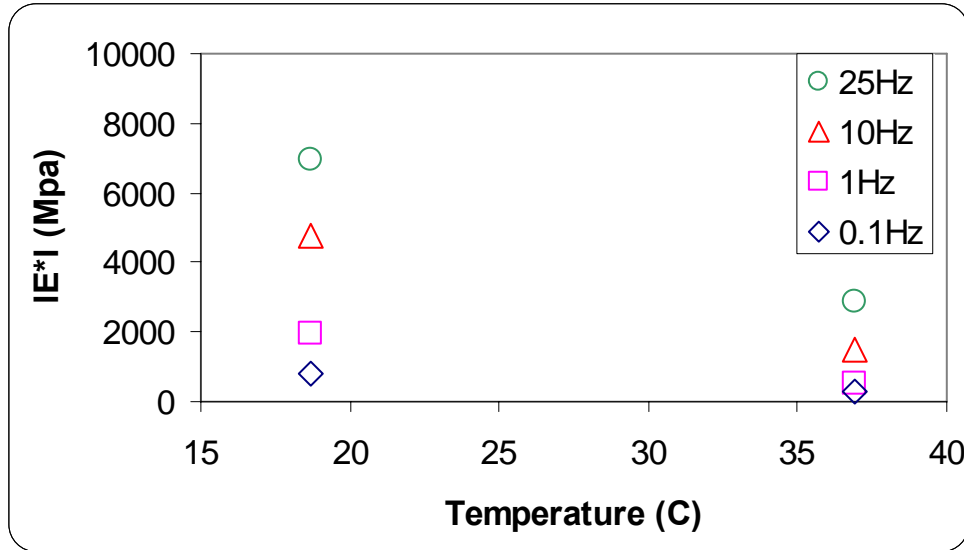
Figure 7.2 Mosinee E-3 19.0-mm $\left|E*\right|$ Temperature Comparison
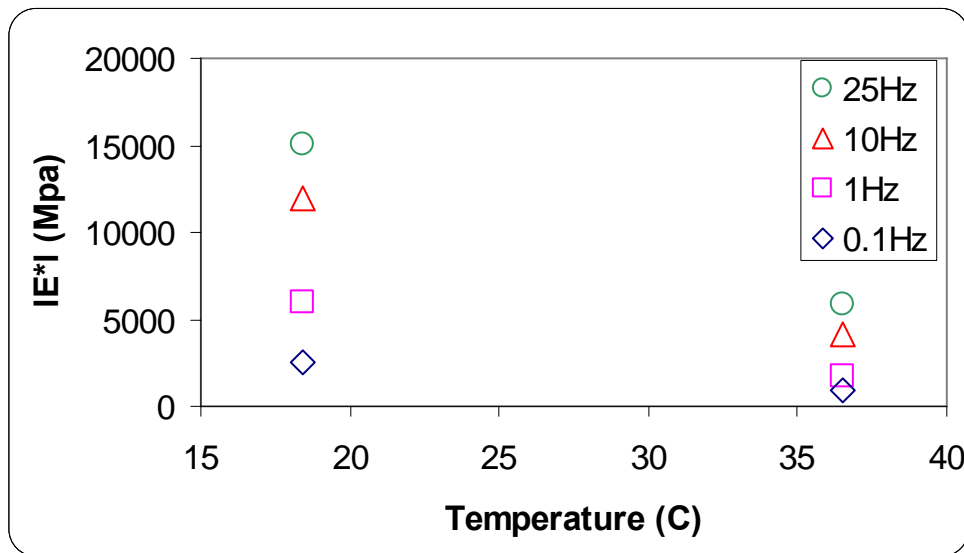
Figure 7.3 Northfield E-30 19.0-mm $\left|E*\right|$ Temperature Comparison

As can be seen in the above figures, the dynamic modulus does in fact decrease with temperature for the same mixture, regardless of frequency and traffic level. The same general trends were found with the other project matrix combinations. On average, the

high test temperatures dynamic modulus was 33% of the intermediate test temperature dynamic modulus.

7.3.2 Air Voids

The hypothesis that was put forth in regards to air voids was that as they increase the dynamic modulus should decrease. Figures 7.4 through 7.9 also present the basic trends in the data in terms of changes in air voids as they affect dynamic modulus. The figures show that for all three mixtures that as the air voids increase there was a decrease in the dynamic modulus, which confirms the hypothesis that was put forth prior to testing.
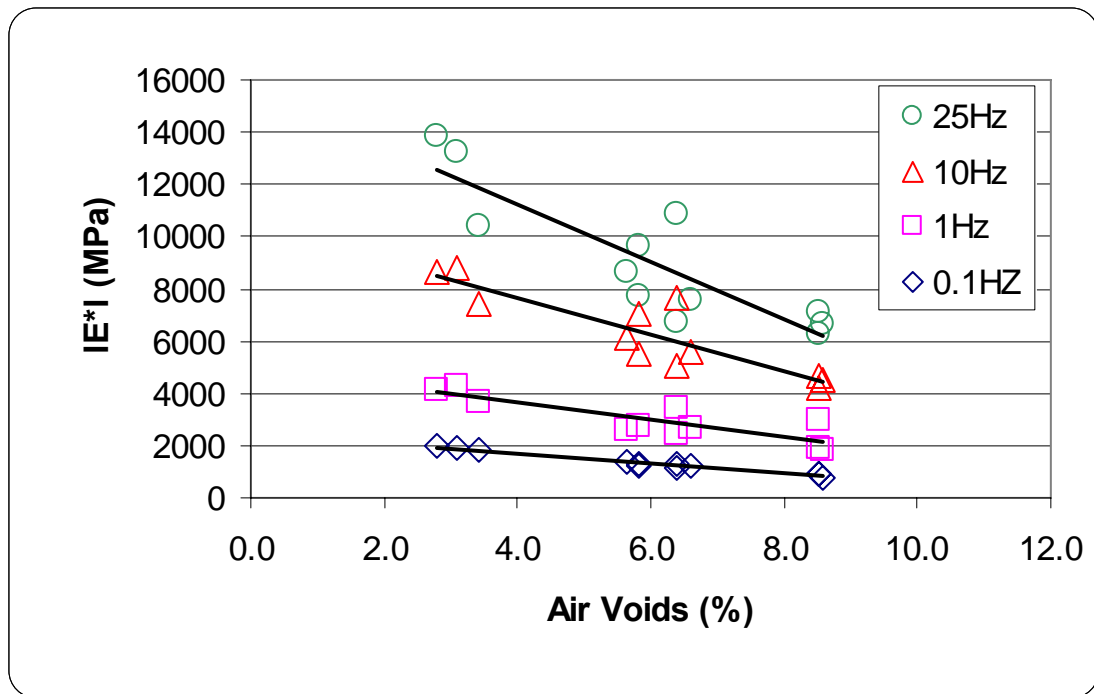
Figure 7.4 Bloomville E-1 19.0mm Int. Temperature
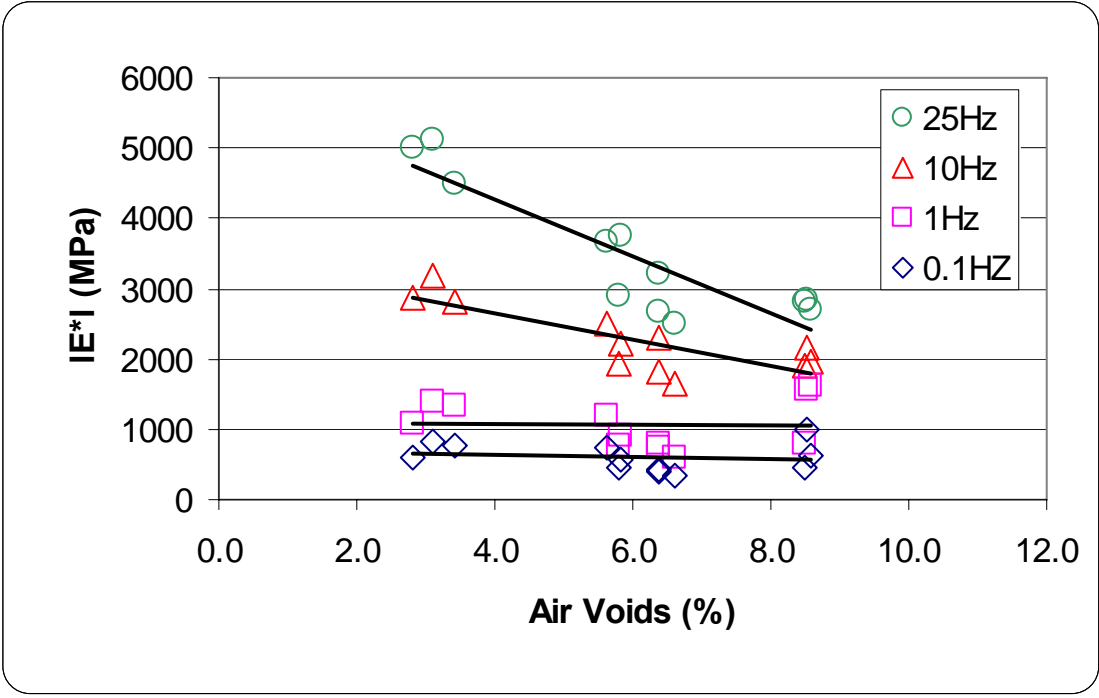
Figure 7.5 Bloomville E-1 19.0mm High Temperature
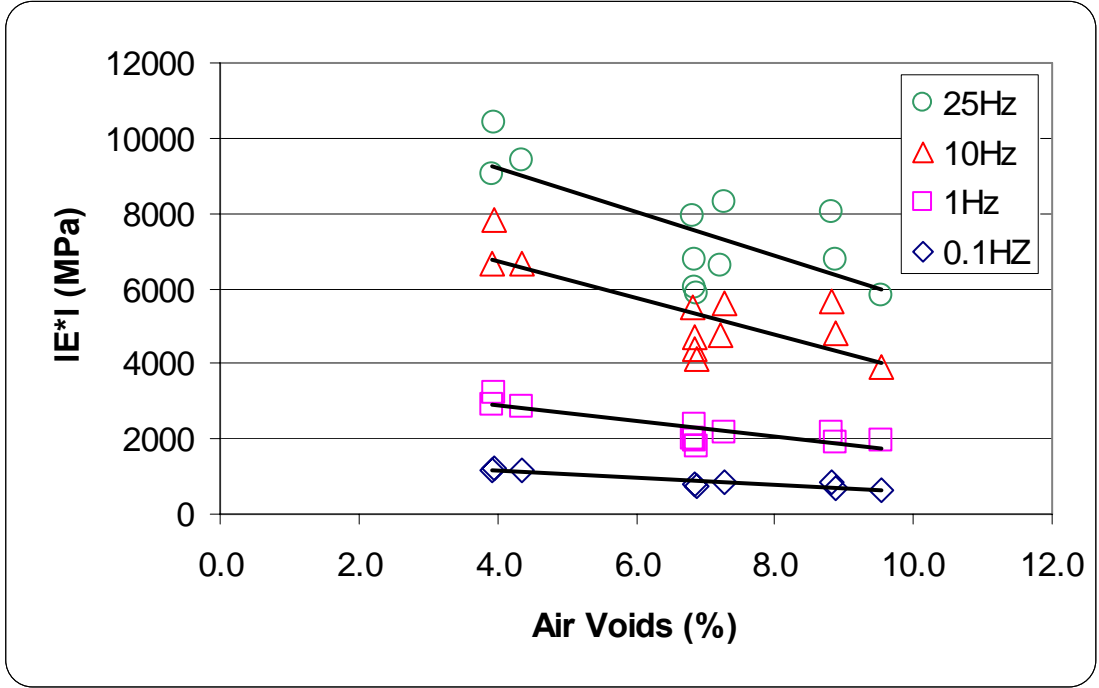
Figure 7.6 Mosinee E-3 19.0mm Int. Temperature

126
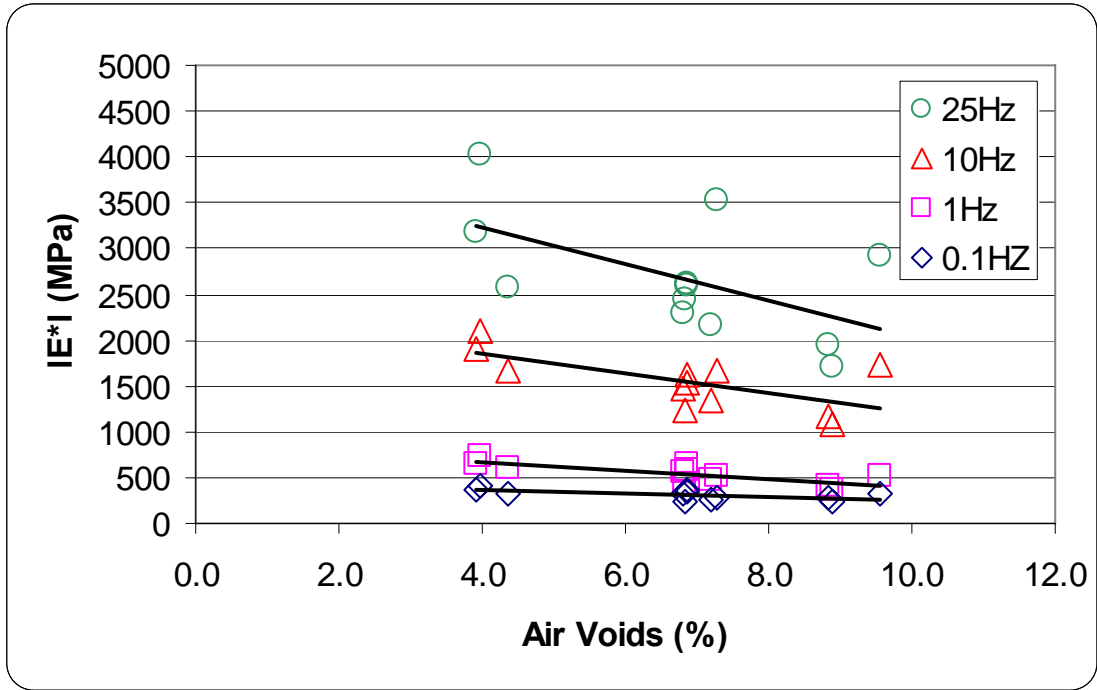
Figure 7.7 Mosinee E-3 19.0mm High Temperature
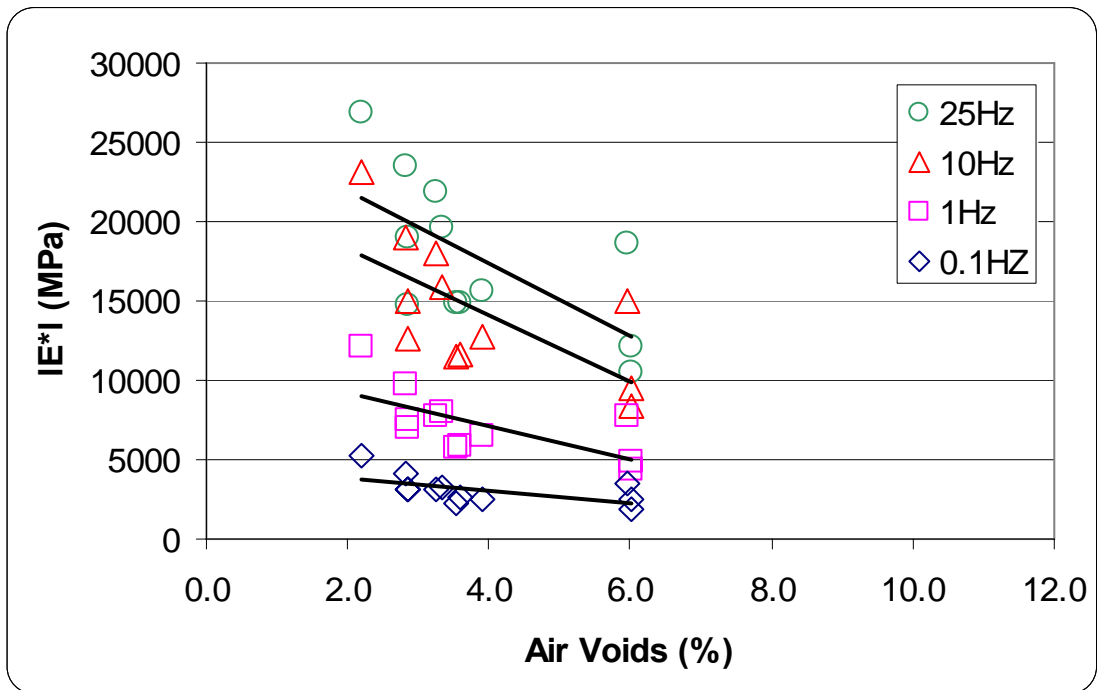
Figure 7.8 Northfield E-30 19.0mm Int. Temperature

127
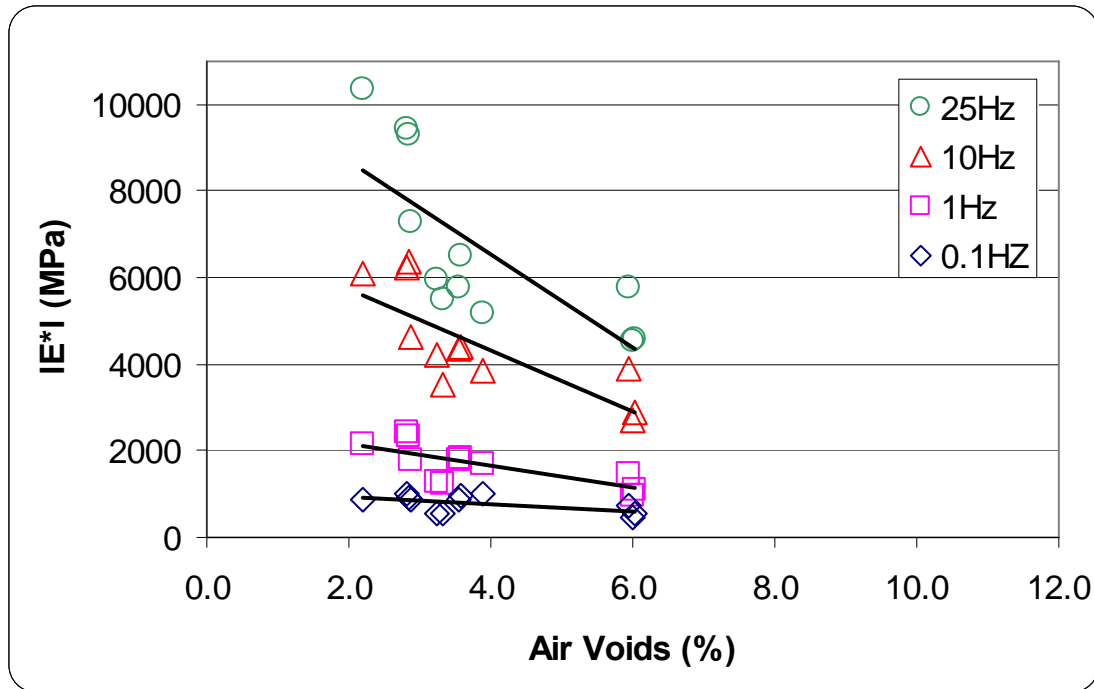
Figure 7.9 Northfield E-30 19.0mm High Temperature

To further illustrate the point that has been made, the Bonferroni grouping to perform multiple comparisons, in this instance, according to air void content, using the program *SAS*. The way that the Bonferroni grouping works is that the datasets are ranked from the highest to the lowest group mean response. Means with a common letter are statistically similar. This manner of grouping is performed until all datasets fall within a group. A 0.10 level of significance was chosen for this portion of the analysis. Tables 7.2 through 7.4 show the Bonferroni groupings in terms of the various air voids tested for each mixture. A separate analysis was conducted for each frequency and temperature and thus comparisons should only be made within a column of a particular frequency between the three different air void levels.

Table 7.2 Bloomville E-1 $|E^*|$ Bonferroni Groupings for Air Voids

Target Air Voids (%)	17.5°C Frequency (Hz)				36.6°C Frequency (Hz)			
	0.1	1.0	10.0	25.0	0.1	1.0	10.0	25.0
4.0	$A_{0.1}$	$A_{1.0}$	$A_{10.0}$	$A_{25.0}$	$A_{0.1}$	$A_{1.0}$	$A_{10.0}$	$A_{25.0}$
7.0	$B_{0.1}$	$B_{1.0}$	$B_{10.0}$	$B_{25.0}$	$A_{0.1}$	$A_{1.0}$	$B_{10.0}$	$B_{25.0}$
10.0	$C_{0.1}$	$C_{1.0}$	$B_{10.0}$	$B_{25.0}$	$A_{0.1}$	$A_{1.0}$	$B_{10.0}$	$B_{25.0}$

Table 7.3 Mosinee E-3 $|E^*|$ Bonferroni Groupings for Air Voids

Target Air Voids (%)	18.7°C Frequency (Hz)				36.9°C Frequency (Hz)			
	0.1	1.0	10.0	25.0	0.1	1.0	10.0	25.0
4.0	$A_{0.1}$	$A_{1.0}$	$A_{10.0}$	$A_{25.0}$	$A_{0.1}$	$A_{1.0}$	$A_{10.0}$	$A_{25.0}$
7.0	$B_{0.1}$	$B_{1.0}$	$B_{10.0}$	$B_{25.0}$	$A_{0.1}$	$A/B_{1.0}$	$A_{10.0}$	$A_{25.0}$
10.0	$B_{0.1}$	$B_{1.0}$	$B_{10.0}$	$B_{25.0}$	$A_{0.1}$	$B_{1.0}$	$A_{10.0}$	$A_{25.0}$

Table 7.4 Northfield E-30 $|E^*|$ Bonferroni Groupings for Air Voids

Target Air Voids (%)	18.4°C Frequency (Hz)				36.5°C Frequency (Hz)			
	0.1	1.0	10.0	25.0	0.1	1.0	10.0	25.0
4.0	$A_{0.1}$	$A_{1.0}$	$A_{10.0}$	$A_{25.0}$	$A_{0.1}$	$A_{1.0}$	$A_{10.0}$	$A_{25.0}$
7.0	$A_{0.1}$	$A/B_{1.0}$	$B_{10.0}$	$B_{25.0}$	$A_{0.1}$	$B_{1.0}$	$B_{10.0}$	$B_{25.0}$
10.0	$A_{0.1}$	$B_{1.0}$	$B_{10.0}$	$B_{25.0}$	$B_{0.1}$	$C_{1.0}$	$C_{10.0}$	$B_{25.0}$

The Bonferroni groupings show that 4.0% target air voids yields the highest dynamic

modulus measurement followed by 7.0 and 10.0% air voids and again confirms the

hypothesis that mixes with lower air voids have higher dynamic modulus values than

ones with higher air voids.

7.3.3 Asphalt Content

The hypothesis that was put forth the asphalt content was that as it was increased,

there should be a decrease in the dynamic modulus. To perform this analysis, only the

7.0% air void specimens were considered. The data then needed to be further filtered

into frequencies and test temperatures so that valid comparisons were made; this results

in 24 pairwise comparisons.

The statistics from the dataset do not support the hypothesis that was initially put

forth. Of the 24 comparisons made, only six showed tendencies for the optimum asphalt

binder content to have a higher dynamic modulus value.

Further review of the data showed that of the 24 comparisons, five were shown to

be statistically different and are listed in Table 7.5 with the relevant statistics.

Table 7.5 Statistical Differences between Asphalt Binder Contents

Mixture	Frequency (Hz)	Temp	Opt. AC Mean lE*l (MPa)	+0.3% Opt. Mean lE*l (MPa)	p-value
Bloomville	0.1	High	397.0	582.8	0.095
Northfield	0.1	Int.	2481.1	3127.8	0.003
Northfield	1.0	Int.	6006.7	7606.1	0.012
Northfield	10.0	Int.	11964.0	15474.9	0.093
Northfield	0.1	High	947.7	672.2	0.072

In review of the cells in Table 7.5 where the five statistical differences occurred, the variations in the test data only appeared to be a significant factor for two as the COV was 26.71% and 23.93% (Bloomville 0.1Hz high temperature +0.3% optimum binder content and Northfield 0.1Hz high temperature +0.3% optimum binder content, respectively) were found for one of the datasets. This indicates that a difference of only 0.3% asphalt binder content was not enough to show any differences in the materials' response. It was beyond the scope of this project to test additional asphalt binder contents but could be done to either further refute or support the hypothesis put forth here.

Tables 7.6 through 7.8 show the Bonferroni groupings as they pertain to changes in the asphalt binder content. A separate analysis was conducted for each frequency and temperature and thus comparisons should only be made within a column of a particular frequency between the two different asphalt binder contents.

Table 7.6 Bloomville E-1 $|E^*|$ Bonferroni Groupings for Asphalt Binder Content

Asphalt Binder Content	17.5°C				36.6°C			
	Frequency (Hz)				Frequency (Hz)			
	0.1	1.0	10.0	25.0	0.1	1.0	10.0	25.0
Opt.	$A_{0.1}$	$A_{1.0}$	$A_{10.0}$	$A_{25.0}$	$B_{0.1}$	$A_{1.0}$	$A_{10.0}$	$A_{25.0}$
+0.3% Opt.	$A_{0.1}$	$A_{1.0}$	$A_{10.0}$	$A_{25.0}$	$A_{0.1}$	$A_{1.0}$	$A_{10.0}$	$A_{25.0}$

Table 7.7 Mosinee E-3 $|E^*|$ Bonferroni Groupings for Asphalt Binder Content

Asphalt Binder Content	18.7°C				36.9°C			
	Frequency (Hz)				Frequency (Hz)			
	0.1	1.0	10.0	25.0	0.1	1.0	10.0	25.0
Opt.	$A_{0.1}$	$A_{1.0}$	$A_{10.0}$	$A_{25.0}$	$A_{0.1}$	$A_{1.0}$	$A_{10.0}$	$A_{25.0}$
+0.3% Opt.	$A_{0.1}$	$A_{1.0}$	$A_{10.0}$	$A_{25.0}$	$A_{0.1}$	A	$A_{10.0}$	$A_{25.0}$

Table 7.8 Northfield E-30 $|E*|$ Bonferroni Groupings for Asphalt Binder Content

Asphalt Binder Content	18.4°C				36.5°C			
	Frequency (Hz)				Frequency (Hz)			
	0.1	1.0	10.0	25.0	0.1	1.0	10.0	25.0
Opt.	$B_{0.1}$	$B_{1.0}$	$B_{10.0}$	$A_{25.0}$	$B_{0.1}$	$A_{1.0}$	$A_{10.0}$	$A_{25.0}$
+0.3% Opt.	$A_{0.1}$	$A_{1.0}$	$A_{10.0}$	$A_{25.0}$	$A_{0.1}$	$A_{1.0}$	$A_{10.0}$	$A_{25.0}$

The Bonferroni groupings only show three of the five statistical differences that were found with the ANOVA procedure. The four statistical differences can be identified by the "B" in Table 7.8. This analysis procedure reinforces the finding that there was no statistical difference between the two different asphalt contents that were examined for this project with the three mixtures that were tested. It should be noted that the Bonferroni groupings do not lend themselves to identifying tendencies with the +0.3% optimum asphalt binder content having a slightly higher dynamic modulus value than that of the optimum asphalt binder content specimens. These tendencies are most evident with the Northfield E-30 mix.

7.3.4 Traffic Level

The hypothesis for the effects of traffic level was that as it increased, dynamic modulus increased. Each mix was designed to a specific level of traffic and has been stated in terms of ESAL's. As the traffic level increases, so does the aggregate angularity of the mixtures required in design, thus presumably giving a higher resistance to flow due to loading. Table 7.9 displays the aggregate angularity of the mixtures that were tested.

Table 7.9 Aggregate Angularity of the Tested Mixtures

Mixture	One Crushed Face	Two Crushed Face	FAA[1]
Bloomville E-1	71.0	69.4	42.2
Mosinee E-3	97.1	97.0	43.3
Northfield E-30	100.0	93.3	45.1

[1]FAA is fine aggregate angularity

Table 7.9 shows that based solely on aggregate angularity the Northfield E-30 mix would be expected to have the highest dynamic modulus while the Bloomville E-1 mix would have the lowest dynamic modulus. In examining the test results from testing, this was not the case, the Northfield E-30 mix has the highest dynamic modulus followed by Bloomville E-1 then Mosinee E-3.

Again the Bonferroni groupings were employed and are shown in Tables 7.10 through 7.12 by the different air void contents. A separate analysis was conducted for each frequency and temperature and thus comparisons should only be made within a column of a particular frequency between the three different traffic levels.

Table 7.10 $|E^*|$ Bonferroni Groupings for 4.0% Air Voids

Traffic Level (ESAL)	Intermediate Temperature				High Temperature			
	Frequency (Hz)				Frequency (Hz)			
	0.1	1.0	10.0	25.0	0.1	1.0	10.0	25.0
1.0	$B_{0.1}$	$B_{1.0}$	$B_{10.0}$	$B_{25.0}$	$B_{0.1}$	$B_{1.0}$	$B_{10.0}$	$B_{25.0}$
3.0	$B_{0.1}$	$B_{1.0}$	$B_{10.0}$	$B_{25.0}$	$C_{0.1}$	$C_{1.0}$	$C_{10.0}$	$C_{25.0}$
30.0	$A_{0.1}$	$A_{1.0}$	$A_{10.0}$	$A_{25.0}$	$A_{0.1}$	$A_{1.0}$	$A_{10.0}$	$A_{25.0}$

Table 7.11 $|E^*|$ Bonferroni Groupings for 7.0% Air Voids

Traffic Level (ESAL)	Intermediate Temperature Frequency (Hz)				High Temperature Frequency (Hz)			
	0.1	1.0	10.0	25.0	0.1	1.0	10.0	25.0
1.0	$B_{0.1}$	$B_{1.0}$	$B_{10.0}$	$B_{25.0}$	$B_{0.1}$	$B_{1.0}$	$B_{10.0}$	$B_{25.0}$
3.0	$C_{0.1}$	$C_{1.0}$	$B_{10.0}$	$B_{25.0}$	$B_{0.1}$	$C_{1.0}$	$B_{10.0}$	$B_{25.0}$
30.0	$A_{0.1}$	$A_{1.0}$	$A_{10.0}$	$A_{25.0}$	$A_{0.1}$	$A_{1.0}$	$A_{10.0}$	$A_{25.0}$

Table 7.12 $|E^*|$ Bonferroni Groupings for 10.0% Air Voids

Traffic Level (ESAL)	Intermediate Temperature Frequency (Hz)				High Temperature Frequency (Hz)			
	0.1	1.0	10.0	25.0	0.1	1.0	10.0	25.0
1.0	$B_{0.1}$	$B_{1.0}$	$B_{10.0}$	$B_{25.0}$	$A_{0.1}$	$A_{1.0}$	$B_{10.0}$	$B_{25.0}$
3.0	$B_{0.1}$	$B_{1.0}$	$B_{10.0}$	$B_{25.0}$	$A_{0.1}$	$B_{1.0}$	$B_{10.0}$	$B_{25.0}$
30.0	$A_{0.1}$	$A_{1.0}$	$A_{10.0}$	$A_{25.0}$	$A_{0.1}$	$A_{1.0}$	$A_{10.0}$	$A_{25.0}$

The Bonferroni groupings illustrate that in all instances the Northfield E-30 mixture had the highest dynamic modulus measurements. The Bloomville E-1 mixture was either found to have a greater than or statistically equal dynamic modulus mean to that of the Mosinee E-3 at all of the frequency and air void content combinations. These results are unexpected as the aggregate angularity should have created a higher internal friction and thus undergo a smaller resilient deformation due to loading.

One explanation for this observation was that the asphalt binder for the Bloomville E-1 mixture was a PG 58-34 as compared to that of the PG 58-28 used in the Mosinee E-3 mixture. The measured viscosity for the Bloomville E-1 mixture was more

than double that of the Mosinee E-3 mixture at 80°C (38,450cP versus 18,367cP, respectively), thus making the mixture stiffer. It would be beneficial to compare the effects of the binder grade on a single mix and this would help to confirm this explanation, but again this was beyond the scope of the study.

7.4 Phase Angle Hypothesis

The phase angle measures the viscoelastic response of HMA due to loading. Figures 7.10 through 7.12 show the phase angle measurements for each job; the mean of three samples.
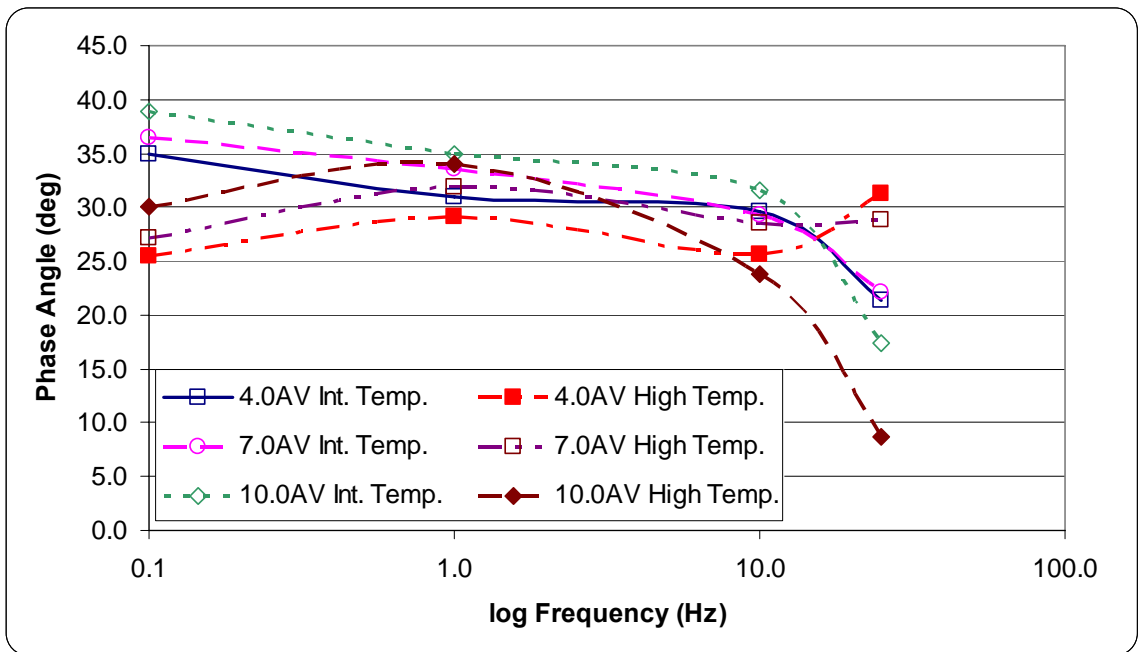
Figure 7.10 Bloomville E-1 Phase Angle Measurements
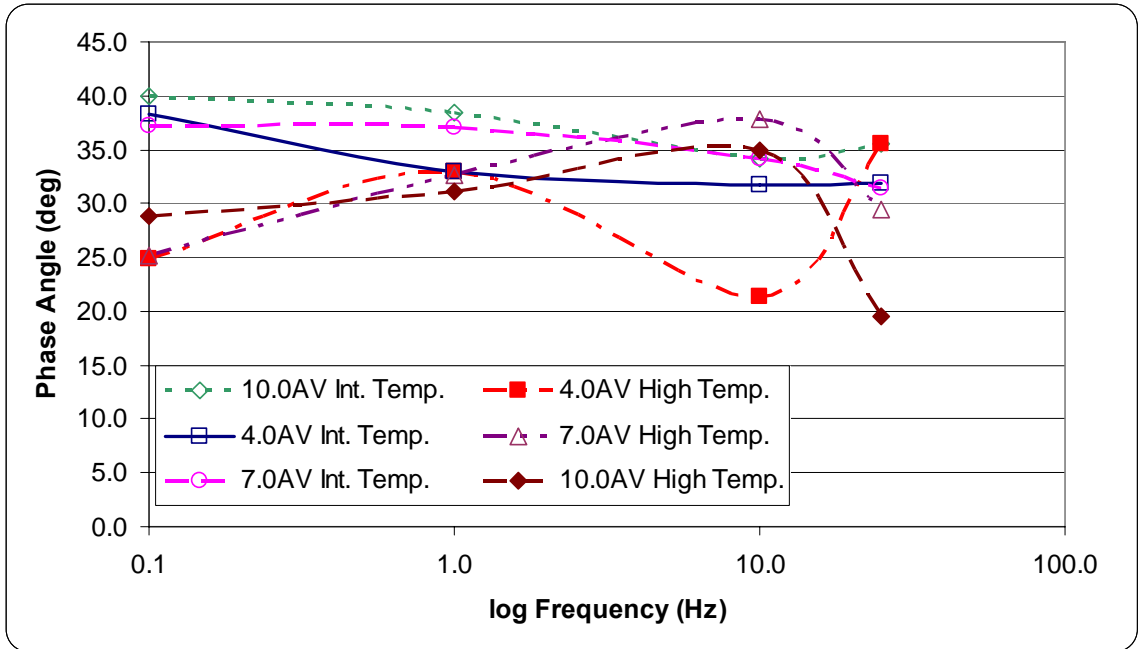
Figure 7.11 Mosinee E-3 Phase Angle Measurements
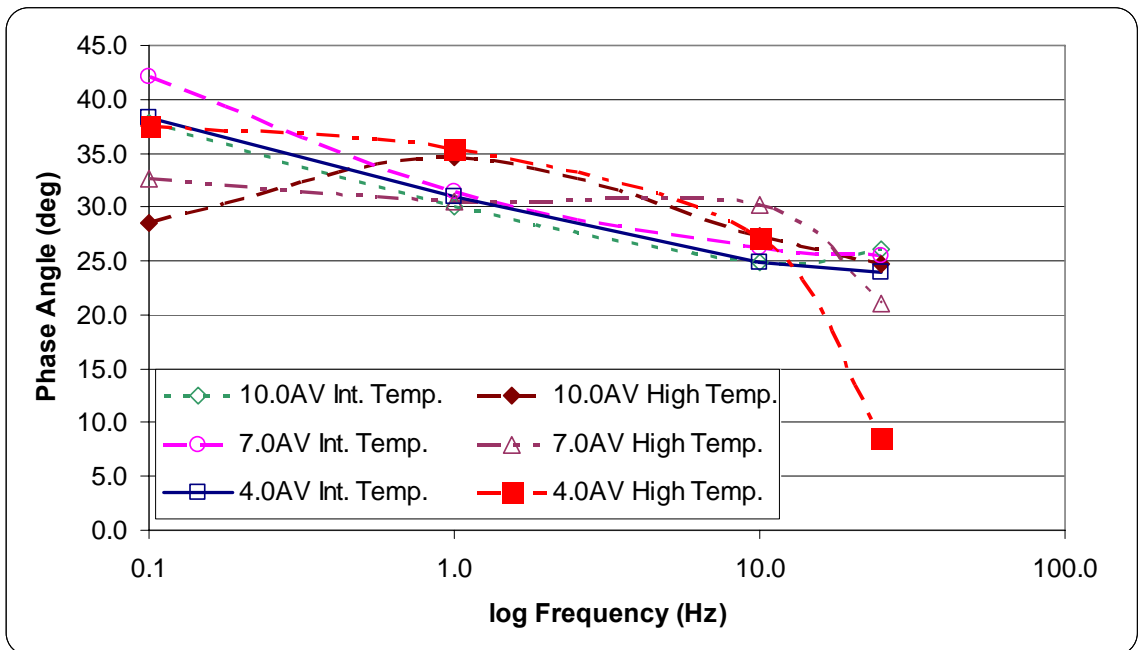
Figure 7.12 Northfield E-30 Phase Angle Measurements

The general trend for the phase angle at both temperatures was as the frequency

increased, the phase angle decreased. This means that at low frequencies, the specimens

were behaving more as a viscous material, and would be more affected by the aggregate properties. As no definitive patterns exist in the plots, it is difficult to test the hypothesis that was developed which states that as temperature increases; the phase angle should also increase. However, at the low frequency (0.1Hz), there is a definite trend present where the intermediate test temperature had a higher phase angle than the high test temperature. Over the frequencies of 1.0 and 10.0Hz, the high test temperature appeared to have a higher phase angle, than the lower one. Then another reversal occurs where the intermediate test temperature tends to have a higher phase angle at 25.0Hz. Mohammad et al (2005) showed that the phase angle would actually decrease with an increasing frequency at an intermediate temperature, while at a high test temperature the phase angle would increase from 0.1 to 10.0Hz and then decrease at 25.0Hz. In review of Mohammad's data plots, it would be difficult to determine a definitive answer to the hypothesis for this project as the answer to the aforementioned hypothesis would change with the test frequency.

7.5 Flow Number Test of Hypotheses

The hypotheses for the flow number tests were it decreased with an increase in asphalt content, air voids, and a decrease in traffic level analogous to aggregate angularity (Section 1.5.2). The following sections discuss these changes per the flow number testing of the three mixes for this project.

The air voids were once again varied by 4.0, 7.0, and 10.0%. Figure 7.13 shows a plot of the change in flow number with a change in air voids.
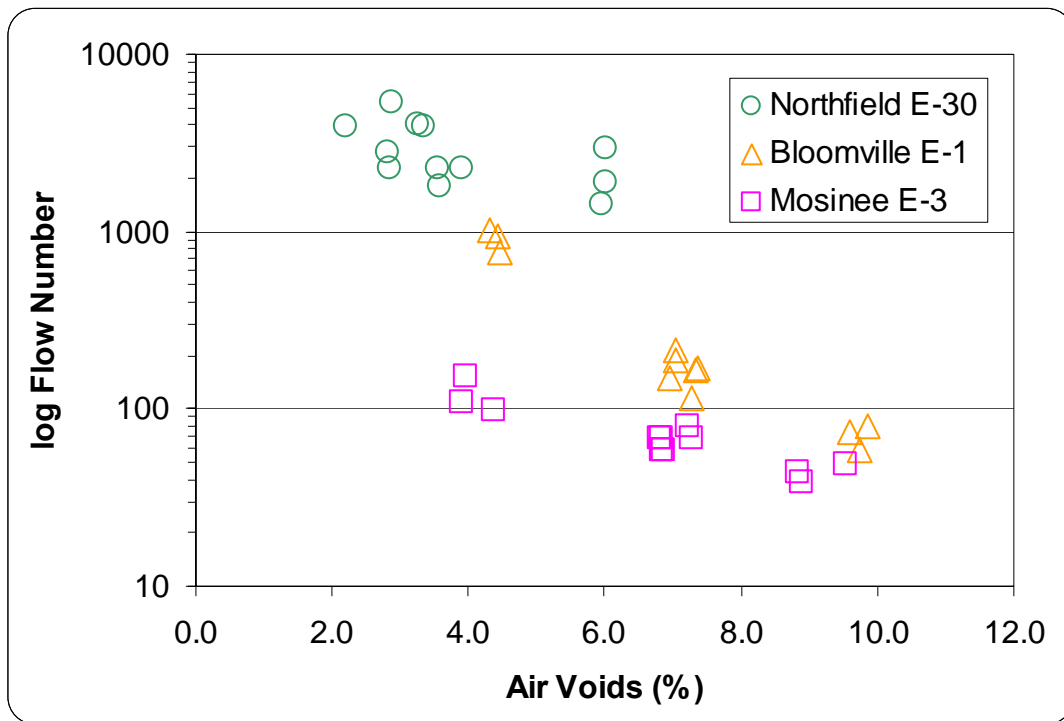
Figure 7.13 Effects of Air Voids on Flow Number

Figure 7.13 shows that as the air voids decrease, the flow number increases and confirms the hypothesis that was put forth for this variable. It would have been beneficial to examine the Northfield E-30 mixture at a higher air void content but the same general trend would likely exist.

Table 7.13 summarizes the Bonferroni groupings for changes in air voids and is depicted by the traffic levels considered in this project. A separate analysis was conducted for each traffic level and thus comparisons should only be made within a column of a particular traffic level between the three different air void levels.

Table 7.13 Flow Number Bonferroni Groupings for Air Voids

Target Air Voids (%)	Traffic Level (ESAL)		
	1.0	3.0	10.0
4.0	$A_{1.0}$	$A_{3.0}$	$A_{10.0}$
7.0	$B_{1.0}$	$B_{3.0}$	$A_{10.0}$
10.0	$B_{1.0}$	$B_{3.0}$	$A_{10.0}$

Table 7.13 verifies statistically at 0.10 level of significance that the 4.0% air voids yields the highest flow number followed by 7.0% and 10.0% air voids. The Northfield E-30 mix showed that the results were statistically similar, but the ordering of the data was such that the ordering went from the lowest to highest air voids.

7.5.2 Asphalt Content

The effects of a 0.3% asphalt binder content increase was considered for the flow number testing phase. Figure 7.14 shows a plot of the log-flow number versus the binder content; a 0 represents the optimum binder content whereas a 1 represents the 0.3% asphalt binder content increase above the optimum.
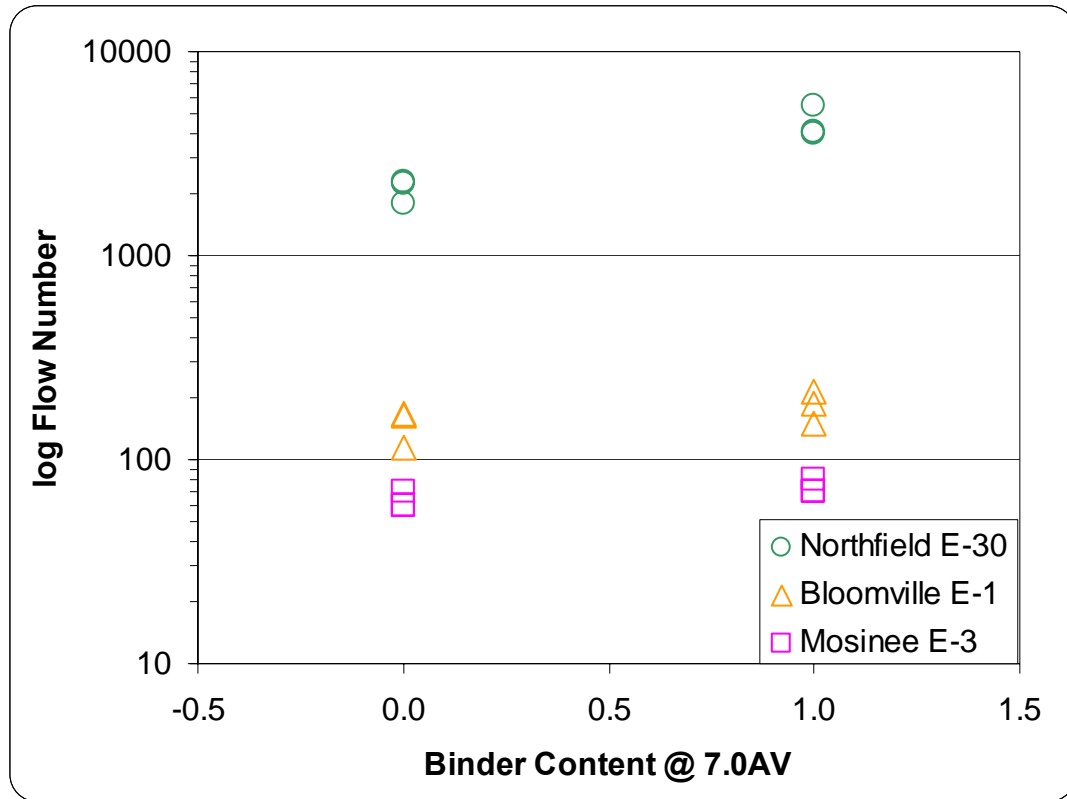
Figure 7.14 Effect of Binder Content on Flow Number

Figure 7.14 shows that there is a tendency that as the asphalt content increases there is a corresponding increase in the flow number. Table 7.14 shows the relevant statistics from the analysis.

Table 7.14 Statistical Analysis of Binder Content on Flow Number

	Binder	Mean	Std. Dev.	F-test	Levene's	$F_{crit\ 0.05}$	$F_{crit\ 0.10}$
Bloomville E-1	Opt	149	30.41	1.84	0.04		
	+0.3%	184	32.79				
Mosinee E-3	Opt	62	5.77	4.50	0.00	7.71	4.54
	+0.3%	72	5.77				
Northfield E-30	Opt	2112	283.36	21.71	3.08		
	+0.3%	4468	828.41				

The F-test was taken from the ANOVA procedure to test for equal means and the

Levene's test was used to test for equal variance. Table 7.14 shows that the two datasets

140

for each mix were equal in terms of mean and variance except for the Northfield E-30 mix. The asphalt binder should have a lower viscosity than that of the mixture at the high temperature and thus should govern the induced strain per load cycle.   By increasing the asphalt binder content, the mixture viscosity should further decrease therefore decreasing the flow number.

The specimens that were tested for the Northfield E-30 mixture were tested at two different times due to a breakdown in the test equipment. As a result, the two specimens sets were probably not conditioned the same length of time, but a dummy specimen was used to ensure that the core temperature reached the effective test temperature in both. The differences in time in which the specimens were tested may account for the significant difference in the flow number test results as aging of the specimens have already been shown to have an impact on mean flow number response.

7.5.3 Traffic Level

The three traffic levels were analyzed to determine the affects on flow number. Similar results were yielded as found with dynamic modulus testing, in that the Northfield E-30 mixture had the highest flow number followed by that of the Bloomville E-1, then the Mosinee E-3 mixtures. The general results can be seen in Figure 7.13. The aforementioned results were verified statistically using Bonferroni groupings and summarized in Table 7.15. A separate analysis was conducted for each air void content and thus comparisons should only be made between vertical cells of a particular frequency.

Table 7.15 Flow Number Bonferroni Groupings for Traffic Level

Traffic Level (ESAL)	Target Air Voids (%)		
	4.0	7.0	10.0
1.0	$B_{4.0}$	$B_{7.0}$	$B_{10.0}$
3.0	$B_{4.0}$	$B_{7.0}$	$B_{10.0}$
30.0	$A_{4.0}$	$A_{7.0}$	$A_{10.0}$

The statistical analysis shows that the Northfield E-30 mixture yields the highest flow number over the three target air void contents considered, while the Bloomville E-1 and Mosinee E-3 mixtures were found to be statistically equal at a 0.10 level of significance. Again, the Bonferroni grouping does not show tendencies only the statistical ordering and at the level of significance chosen, was not able to show that the flow number results from the Mosinee E-3 mixture as being lower than that of the Bloomville E-1.

7.6 Accumulated Micro-Strain at Flow Number

Mohammad et al (2005) suggest that the failure strain may be a critical value in the analysis of flow number as opposed to the load cycle. The accumulated micro-strain at the flow number was obtained and presented in Figures 7.15 through 7.17. Each flow number bar and accumulated micro-strain data point constitutes an average of three test points.
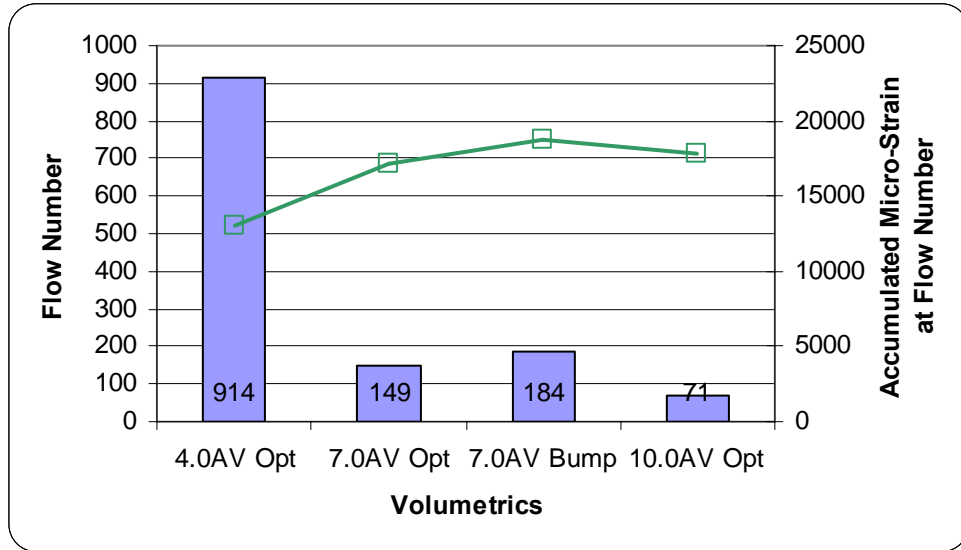
Figure 7.15 Bloomville E-1 Flow Number Analysis
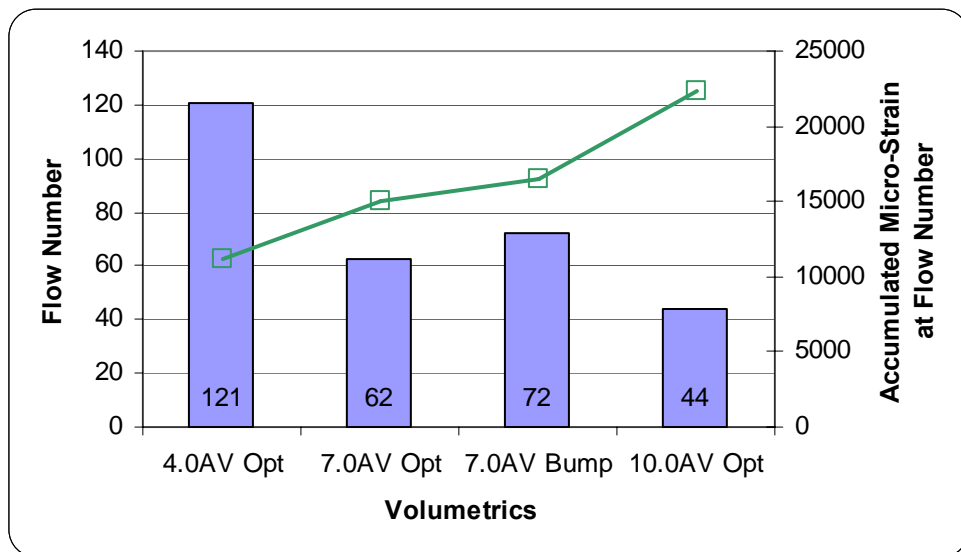
Figure 7.16 Mosinee E-3 Flow Number Analysis
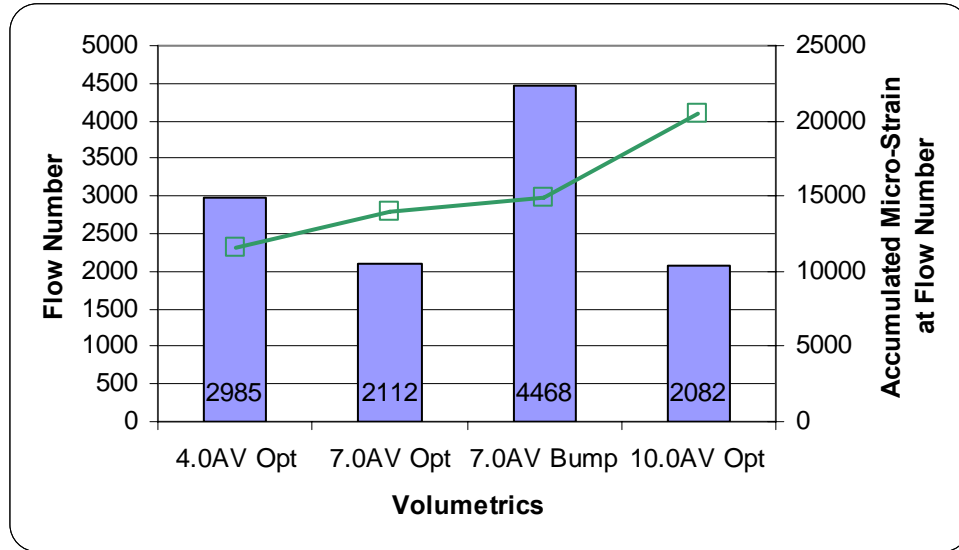
Figure 7.17 Northfield E-30 Flow Number Analysis

The above figures show that flow number generally decreases with an increase in air voids except for the Northfield 7.0% air voids with the +0.3% asphalt binder content. Figures 7.15 through 7.17 tend to indicate that the accumulated micro-strain at flow number may be a better measure to use for comparing the changes in asphalt binder content. The higher asphalt binder content has a higher accumulated micro-strain at flow number than the optimum asphalt binder content and the same trend was present when air voids are considered. The plots suggest that poorer quality specimens for a particular mixture increase the accumulated micro-strain at flow number, making it a better measure for comparing the quality of the specimens in a mixture. On the other hand, flow number appears to be a better measure for comparing different mixtures as can be seen in the above figures, the flow number tends to increase with an increase in traffic volume (this trend has been verified in Section 7.5.3). Further testing should be conducted to validate these observations.

7.7 Predictive Equation

The Design Guide software currently used the Witczak predictive equation for Level 2 and 3 designs. To reiterate, the Witczak predictive equation is limited in scope to that of the mixes that were used in the development of the model and does not directly apply to the three mixes that have been tested for this project.

7.7.1 Witczak Predictive Equation

The JMFs that were provided by the contractors were used to extract the necessary information for the Witczak predictive equation in addition to the viscosity-temperature susceptibility test data. The RTFO aged binder viscosities were used as it was the recommendation made by the Design Guide (2004). The variables were then input into the Witczak predictive equation to determine the reliability of the equation to the mixes that were tested for this project. Figure 7.18 shows the measured versus the predicted dynamic modulus.
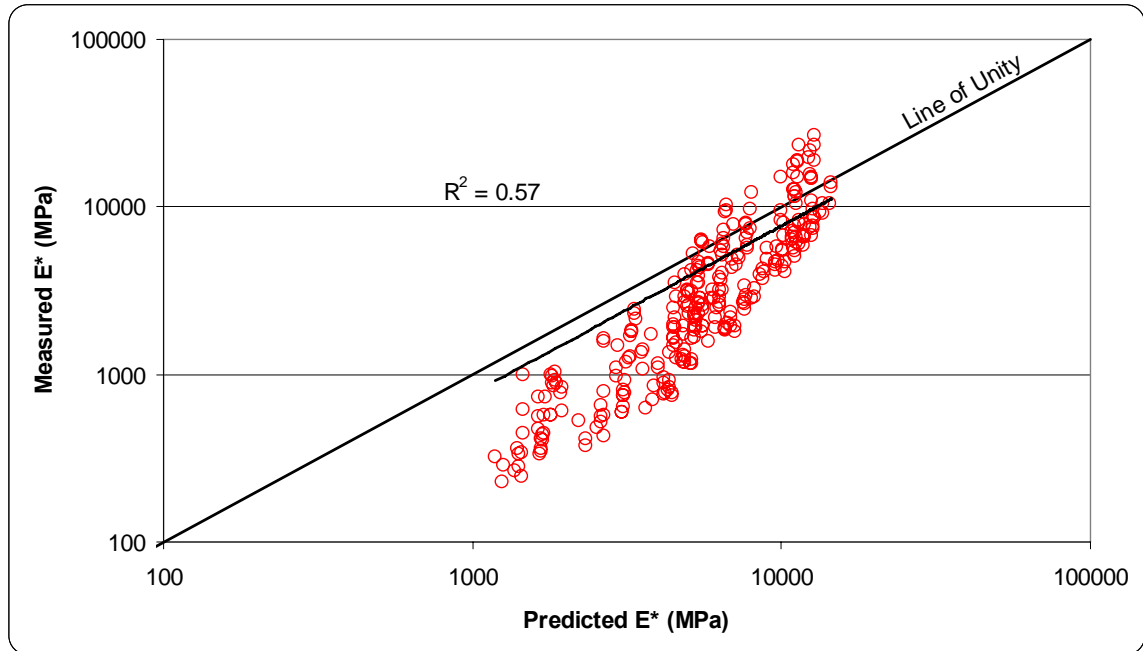
Figure 7.18 Witczak Predictive Equation for Wisconsin Mixtures Tested

Three mixes were tested and are shown in the above figure and totals 288 data points. A general linear regression equation was fit to the dataset and was forced through a zero intercept and was found to have a coefficient of determination (R^2) of 0.57. This regression equation was not meant to be a predictive equation, but rather show the deviation of the predicted data points from that of the measured. Caution should also be exercised with the R^2 value stated as forcing the intercept to zero can result in a negative value which is an unreasonable result. Some software packages address this issue by using an uncorrected sum of squares total and a meaningful interpretation of the data lost (Kutner et al, 2004). The general trend in Figure 7.18 was that as temperature increased and frequency decreased, the dynamic modulus value decreased. What the plot indicates was that on the whole the Witczak predictive equation tends to overestimate dynamic modulus especially at the high temperature and low frequency regimens.

In an effort to try to determine if one of the parameters used in the Witczak predictive equation was the source of the difference between the measured and predicted, plots of the residuals versus each parameter were developed (Appendix H). For all of the parameters considered in the Witczak predictive equation there appeared to be bias. This means that the errors in the predictive equation are not attributable to one or two parameters which would indicate an error in measuring the parameters.

The Witczak predictive equation was recalibrated to resolve the issue of overestimating dynamic modulus using the same form of the original equation.

7.7.2 Recalibration Procedure for the Witczak Predictive Equation

The base equation was used and only the coefficients that were present were manipulated (equation 7.1) to recalibrate the Witczak predictive equation.

$$\log|E*| = c_1 + c_2(\rho_{200}) + c_3(\rho_{200})^2 + c_4(\rho_4) + c_5(V_a)$$

$$+ \frac{c_6(V_{beff})}{V_{beff} + V_a} + \frac{c_7 + c_8(\rho_4) + c_9(\rho_{3/8}) + c_{10}(\rho_{3/8})^2 + c_{11}(\rho_{3/4})}{1 + e^{(c_{12} + c_{13} \times \log(f) + c_{14} \times \log(\eta))}} \quad (7.1)$$

The variables are explained Section 2.4.2. The program Solver which is available with Microsoft Excel was used to solve for the optimal coefficients to yield the best fit to the dynamic modulus dataset for this project.

Table 7.16 Witczak and Recalibrated Predictive Equation Coefficients

Coefficient	Witczak Coefficient	Recalibrated Coefficient	Coefficient	Witczak Coefficient	Recalibrated Coefficient
c_1	-2.629597	-0.581708	c_8	-0.002100	-0.543369
c_2	-4.967135	-3.788632	c_9	0.003958	1.947495
c_3	0.707892	0.529424	c_{10}	-0.000017	-0.019402
c_4	-0.003028	0.001826	c_{11}	0.005470	-3.140048
c_5	0.026752	0.062760	c_{12}	-0.603313	0.294474
c_6	1.501822	2.376609	c_{13}	-0.313351	-0.126005
c_7	1.114406	1.221728	c_{14}	-0.393353	-0.115625

With the new coefficients for the base Witczak predictive equation, the new equation was calibrated to the three mixtures tested and would be referred to as a local calibration of the predictive equation.

Comparisons were made between the measured dynamic modulus and that of the Witczak and recalibrated Witczak predictive equation. To perform the analysis the ANOVA procedure was used to measure the mean of the datasets. The ANOVA yielded an F_{stat} of 94.42 (F_{crit} = 3.00 at an α = 0.05), which meant that there was a significant difference between the means of the three groups. It was noted that the comparisons of the variances among the three groups were equal as found by the Levene's test (F_{stat} = 0.32).

The recalibration of the Witczak predictive equation was meant to reduce the differences between that of the uncalibrated predicted and measured dynamic modulus, thus a comparison was conducted between the two. The ANOVA showed that there was a significant difference between the mean of the two datasets (F_{stat} = 140.04 and a p-value = <0.0001). To ensure that the recalibrated model produced a statistically similar mean to that of the measured values, an ANOVA was performed on the datasets. The analysis

showed an F_{stat} of 0.00 (p-value = 0.99) and the Levene's test found an F_{stat} = 0.04 (p-value = 0.38). This demonstrates that the recalibrated equation is representative of the measured dataset, while the Witczak predictive equation does not accurately predict dynamic modulus for the three mixtures tested.

A comparison was also made between the coefficients of the two predictive equations. As with any predictive equation, the coefficients are expected to change with additional data factored into the recalibrated model. Table 7.17 shows the percent difference in the coefficients based on the uncalibrated Witczak predictive equation.

Table 7.17 Percent Difference in Predictive Equation Coefficients

Coefficient	Percent Difference	Coefficient	Percent Difference
c_1	-53	c_8	25,775
c_2	-13,061	c_9	49,104
c_3	-30,062	c_{10}	114,030
c_4	-164	c_{11}	-57,505
c_5	-208	c_{12}	-149
c_6	-396	c_{13}	-60
c_7	-68	c_{14}	-71

As can be seen in Table 7.17, there were significant changes in the coefficients and the negative percent difference indicates a sign change. These significant changes do not refute the reliability of the developed model as previous iterations of the predictive equation have undergone significant changes as were seen by Witczak and Fonseca (1996).

Figure 7.19 shows a plot of the measured versus predicted data using the recalibrated Witczak predictive equation.
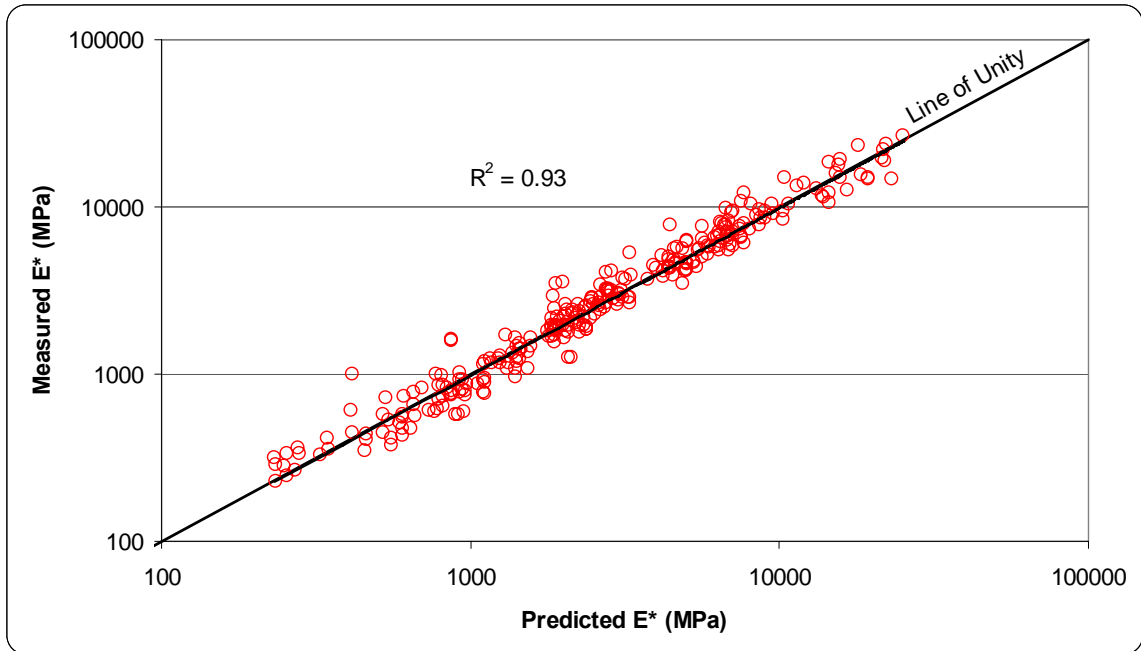
Figure 7.19 Recalibration of the Witczak Predictive Equation

Again, a linear regression equation was fit to the recalibrated predictive results and as can

be seen the R^2 was significantly increased to 0.933.

The plot of the residuals for each of the parameters appear to be unbiased

(Appendix H). With the recalibration, the residuals increased with an increase in the

measured dynamic modulus. Additionally, the residuals were evenly distributed around

zero. This model appears to better represent the test results. Further emphasis needs to

be placed on the fact that this model only applies to the three mixtures tested. Like any

predictive equation, it should only be applied within the limits of the parameters from

which it was created.

The recalibration of the predictive equation resolved the issues that were seen

with the uncalibrated Witczak predictive equation, in that at the higher temperatures and

lower frequencies overpredict dynamic modulus. This recalibration now makes it

possible to apply future predictions to these asphalt mixtures and with further testing.

The recalibration procedure that has been presented is applicable to typical mixtures in the State of Wisconsin and can be further expanded with additional testing.

7.8 Pavement Design

In addition to analyzing the results of the dynamic modulus and flow number testing, the pavement designs were analyzed using the actual constructed pavement structure and traffic information supplied by WisDOT. The measured dynamic modulus values were used as direct inputs in the Level 1 design, whereas the other pavement layers used either a Level 2 or 3 design input depending on the available information. Several assumptions had to be made during the pavement analysis as not all information was present. These assumptions are explained where applicable. The performance criteria that was used as default values in the Design Guide software are presented in Table 7.17.

Table 7.17 Design Guide Software Performance Criteria

Distress	Performance Criteria
Permanent Deformation AC Layer Only (mm)	6.0
Permanent Deformation Total Pavement (mm)	19.0
IRI (mm/km)	2,715.0
Longitudinal Cracking (m/500)	305.0
Alligator Cracking (%)	25.0

What follows describes the pavement design analysis that was conducted for this project.

7.8.1 Bloomville E-1 19.0mm

The Bloomville E-1 19.0-mm pavement design consisted 114.3-mm (4.5-in) of HMA on 304.8-mm (12-in) of crushed gravel on a subgrade of A-4 soil. The main

151

composition of an A-4 soil is silt under the AASHTO soil classification system. There was no breakdown in the HMA layer as to whether a 12.5-mm NMAS mixture was used as a surface course for the pavement structure, however, it probably was used for ride quality purposes. For ease of analysis, the 19.0-mm NMAS mixture was used for the entire HMA layer. This would be a safe assumption as any surface course would have a higher stiffness and thus make the pavement structure less prone to permanent deformation. A Level 1 analysis was used for the 19.0-mm NMAS layer and utilized the dynamic modulus test results, which are found in Appendix G. A modulus value of 275.8MPa (40ksi) was used for the crushed gravel layer, this particular layer was divided into two identical 152.4-mm (6-in layers). The reason for this division was previous simulations with the Design Guide software had problems handling the thick layers. A plasticity index of 1, with 10% passing the #200 sieve, 30% passing the #4 sieve, and a D60 of 2-mm were also used as inputs for the crushed gravel. The D60 refers to the grain size that corresponds to 60 percent passing (Coduto, 1999). The subgrade was reported to have a support value of 5.2 and using the Design Guide software yielded an analogous modulus value of 204.4MPa (29.6ksi), this layer was divided into a 152.4-mm (6-in) layer followed by an identical semi-infinite layer. The subgrade support value refers to the in-situ strength of a fine-grained soil (Coduto, 1999). A plasticity index of 3, with 60% passing the #200 sieve, 90% passing the #4 sieve, and a D60 of 0.05-mm were also used as inputs for the subgrade. The plasticity index refers to the range of moisture contents that compose the plastic state (Cuduto, 1999).

The traffic data was supplied by WisDOT as shown in Table 7.18 and shows that this particular roadway is not expected to have a considerable amount of truck traffic.

Table 7.18 Traffic Characteristics – Bloomville E-1 19.0mm

Traffic Characteristic	
AADT (veh./day)	3,800
Growth (%)	1.37
% of Traffic Greater Than Class 4	6.0
AADTT (trucks/day)	228
Truck Traffic Distribution	
2D (%)	1.5
3-SU (%)	1.5
2S-1 (%)	0.7
2S-2 (%)	0.7
3S-2 (%)	1.3
2-S1-2 (%)	0.3

The AADT refers to average annual daily traffic and measured through traffic counts.

The AADTT refers to average annual daily truck traffic for vehicles larger than a

passenger vehicle. The truck traffic distribution nomenclature used in Table 7.18 was

that used by WisDOT. The Wisconsin Asphalt Pavement Association has provided

running definitions for these truck classifications and listed as follows:

- 2D - WISDOT designation for a heavy single unit truck with two axles and 6 tires.
- 3SU - WISDOT designation for a heavy single unit truck with three axles.
- 2S-1 - WISDOT designation for a heavy tractor-semitrailer truck with three axles.
- 2S-2 - WISDOT designation for a heavy tractor-semitrailer with four axles.
- 3S-2 - WISDOT designation for a heavy tractor-semitrailer with five or more axles.
- 2-S1-2 - WISDOT designation for a heavy tractor-semitrailer-trailer combination with five or more axles. The 2-S1-2 is also known as a Double-Bottom truck.

A new climatic station had to be interpolated for the exact location of this project.

A latitude of 45.18-degrees and a longitude of -89.18-degrees were used along with an

estimated elevation of 362.4-m (1189-ft) and an annual depth to the water table of 1.8-m

(6ft). The water table information was derived from the soil surveys from the United

States Department of Agriculture for Lincoln County, WI (2000). The weather stations that were used for the interpolation were Wausau, WI, Iron Mountain, MI, and Green Bay, WI.

The aforementioned were inputted into the Design Guide software where applicable and a total of 24 simulations were conducted. The simulations were run at varying layer thicknesses to their determine the effects on pavement distress for 4.0 and 7.0% air voids along with the asphalt binder content increase of 0.3% at 7.0% air voids. The 10.0% air void specimen data was eliminated from the analysis as it was resulting in an instantaneous permanent deformation equal to the thickness of the entire HMA layer. This was not the first time that this problem was encountered, and at the current time there are no available solutions, and as a result it was omitted. It should be noted that MTU was working closely with the National Cooperative Highway Research Program to try to resolve this issue. Figures 7.20 through 7.24 shows what the effects of changing the HMA's layer thickness had on permanent deformation in the AC layer only and the entire pavement structure, as well as IRI, longitudinal cracking, and alligator cracking. The nomenclature used in the following figures shows the air void content as a number (4.0 and 7.0%) followed by the asphalt binder content (optimum 'Opt.' or +0.3% asphalt binder content 'Bump').
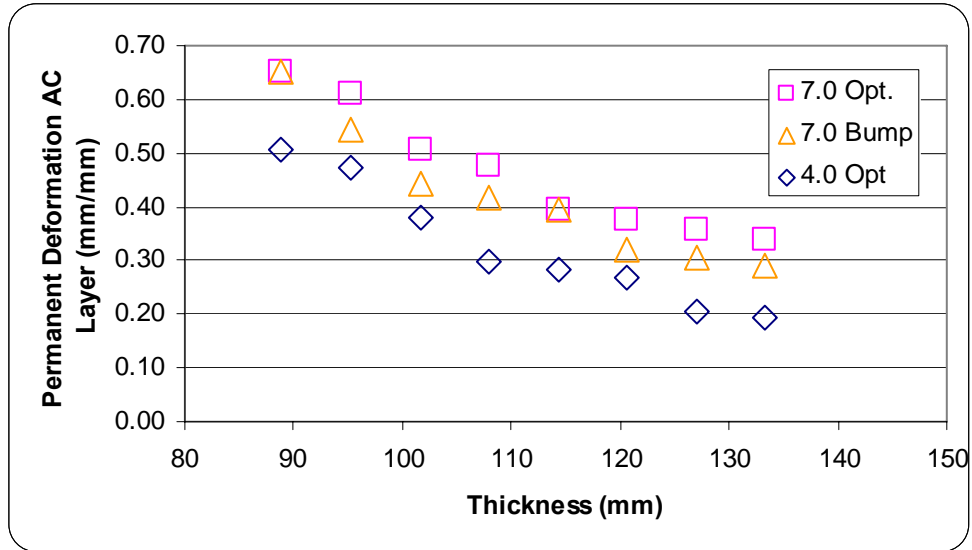
Figure 7.20 Bloomville E-1 Permanent Deformation AC Layer
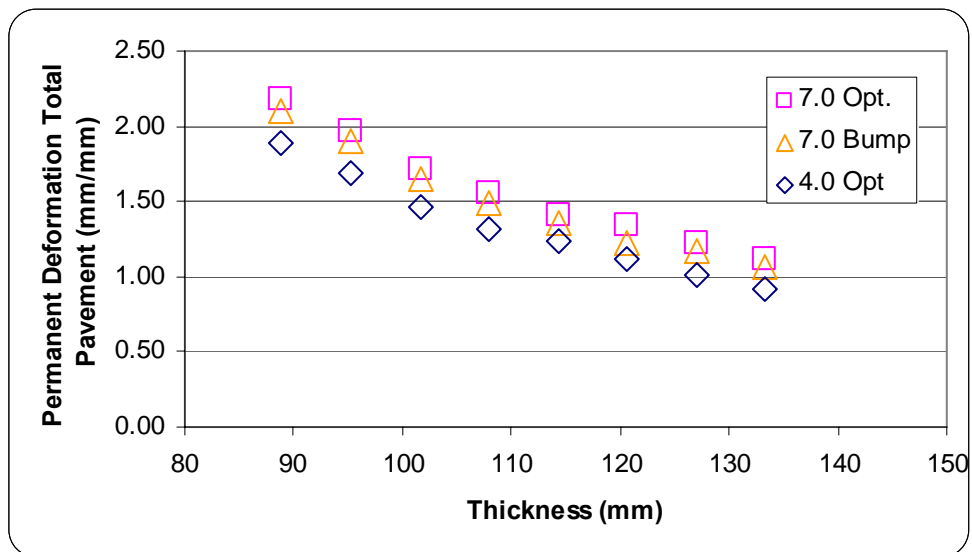
Figure 7.21 Bloomville E-1 Permanent Deformation Total Pavement
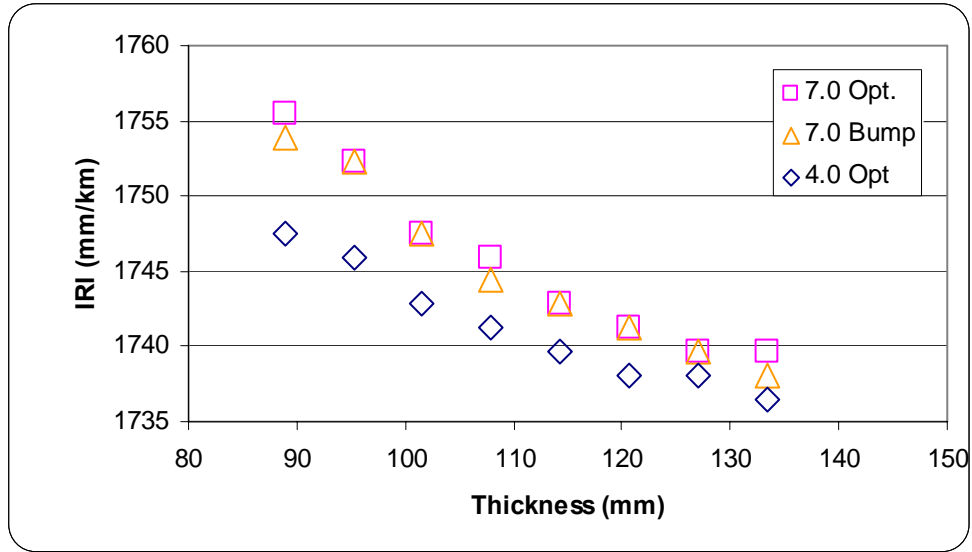
Figure 7.22 Bloomville E-1 IRI
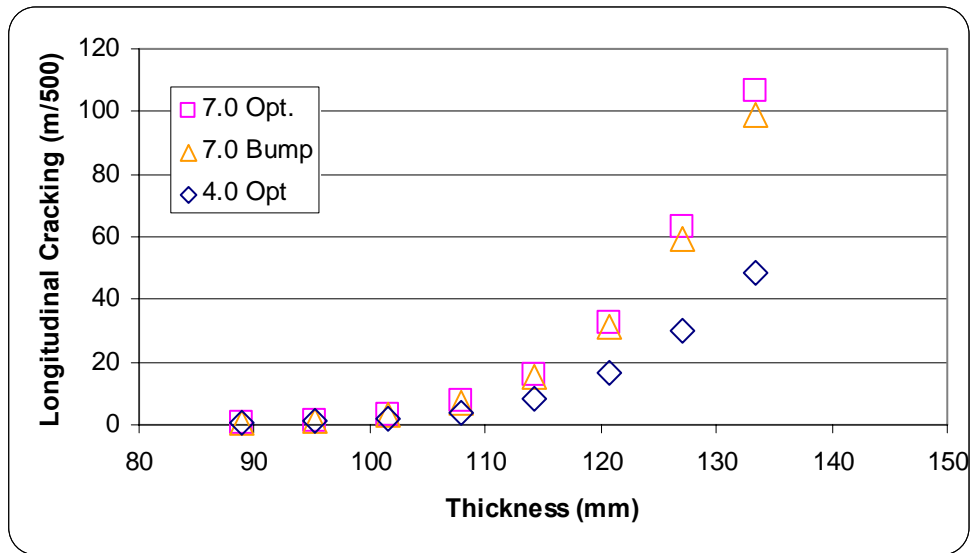
Figure 7.23 Bloomville E-1 Longitudinal Cracking
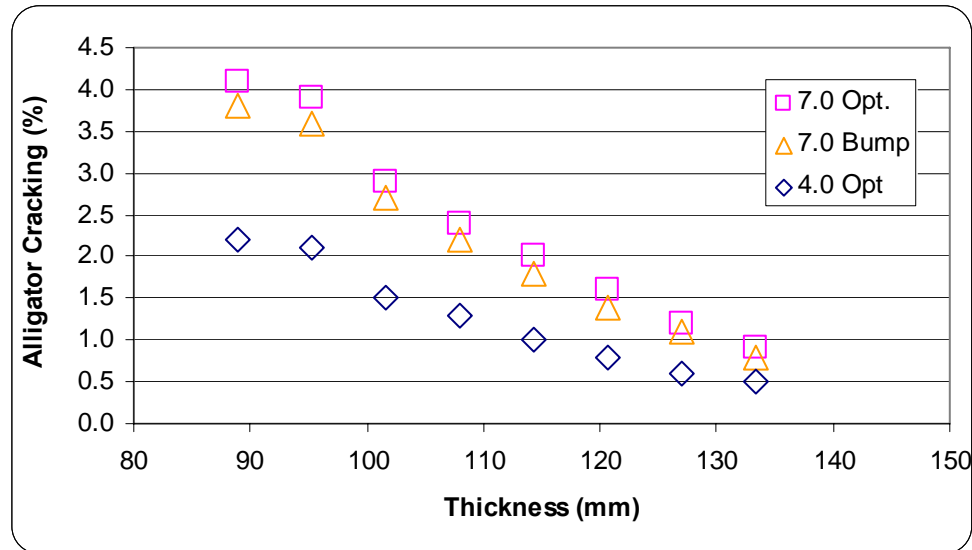
Figure 7.24 Bloomville E-1 Alligator Cracking

Figures 7.20 and 7.21 were normalized so that the trends in the permanent deformation could be more efficiently measured. The normalization was done by dividing the predicted permanent deformation by that of the thickness of the layer in question, thus a unitless quantity was presented. Based on the performance criteria for each distress, it appears as though the pavement was sufficiently designed if paved between 4 and 7% air voids and within the asphalt binder content tolerances.

Figures 7.20 and 7.21 shows that as the air void content increases in the pavement, there was a corresponding increase in the normalized permanent deformation and was consistent with the work of Basyouny et al (2005). The asphalt binder content increase resulted in a higher dynamic modulus, thus a stiffer mix. As a consequence, the asphalt binder bump resulted in lower permanent deformation (Figure 8.20). It should be noted that Basyouny et al found that with an increase in the effective asphalt binder content, there should be an increase in the amount of rutting predicted.

The analysis indicated that the IRI was insensitive to changes in the air void content, asphalt binder content, and thickness. The overall IRI number at the pavement design thickness was well within the performance criteria used in the Design Guide software of 2,715-mm/km.

Increasing the air void content was shown to increase both longitudinal and alligator cracking (Figures 7.23 and 7.24). Longitudinal cracking initiates at the surface of the pavement and propagates down and is partly a function of the stiffness of the subgrade. Figure 7.23 indicates that the subgrade is stiff and does not allow the pavement to flex substantially when loaded and increasing the pavement thickness compounds the situation. According to the analysis, the pavement is sufficiently designed to mitigate longitudinal cracking, but with construction variability, the pavement could be paved thicker than 114.3-mm (4.5-in). In any event, the pavement must balance both longitudinal and alligator cracking as they are competing distresses, in that, changes in pavement thickness has the conflicting effects on the two fatigue distresses. Based on the analysis, the designed thickness has found an ideal thickness to balance the two distresses.

The asphalt binder content increase resulted in a higher dynamic modulus and was expected to make the pavement more prone to fatigue cracking as opposed to the optimum binder content, but this was not the case (Figures 7.23 and 7.24). The greater controlling factor had to be the change in asphalt content, and Basyouny and Witczak (2005) showed that an increase in the effective asphalt binder content resulted in both lower longitudinal and alligator cracking, thus supporting the findings above.

The predicted longevity of this particular roadway is tied to its low volume of truck traffic and its low growth rate. The truck traffic and growth rate are simply estimates and it would be beneficial to measure the predicted distresses if the actual pavement saw an increase in truck traffic either through the base number due to its rehabilitation or in terms of growth. For the 7.0% air voids at the optimum asphalt binder content for the as designed pavement thickness, changes were made to the truck traffic and growth rate. An AADTT of 500 and a growth rate of 4% were considered separately and are presented in Table 7.19.

Table 7.19 Predicted Distresses for Changes in Truck Traffic Characteristics

Distress	Design AADTT = 228 Growth = 1.37%	Traffic Growth AADTT = 228 Growth = 4.00%	Truck Base AADTT = 500 Growth = 1.37%
Permanent Deformation AC Layer Only (mm)	1.8	2.0	2.8
Permanent Deformation Total Pavement (mm)	6.4	6.9	7.9
IRI (mm/km)	1,742.8	1,746.0	1,753.8
Longitudinal Cracking (m/500)	16.1	23.9	52.4
Alligator Cracking (%)	2.0	2.7	4.8
Cumulative Truck Traffic Over 20-yrs. of Service	903,076	1,177,920	1,980,430

The changes in truck traffic and traffic growth do not indicate that the pavement will fail due to these changes, but designs that are made that allow little room for error will be at the mercy of the actual traffic volume and composition. Table 7.19 indicates that changing the base traffic volume has the most prominent impact upon all of the predicted

distresses. This result was reasonable considering the total volume of traffic that the pavement is expected to see during its service life of 20-yrs.

7.8.2 Mosinee E-3 19.0mm

The Mosinee E-3 19.0mm pavement design consisted of 44.45-mm (1.75-in) of HMA on 177.8-mm (7-in) of existing asphalt pavement on an A-4 soil subgrade. The main composition of an A-4 soil is silt under the AASHTO soil classification system. The HMA design thickness of 44.5-mm (1.75-in) was suspect for this pavement. As a rule-of-thumb the thickness should be three times the NMAS of the mixture as a result the thickness should be at least 57.0-mm (2.24-in) through recommended construction practice. However, this was the information that was provided by WisDOT and thus is used in the analysis. It was assumed that the entire HMA layer consisted of the 19.0-mm mixture as no other information from WisDOT contradicts this assumption. A Level 1 analysis is used for the 19.0-mm NMAS layer and utilizes the dynamic modulus test results, these results can be found in Appendix G. The exist pavement layer was designed using a Level 3 analysis and using the gradation and volumetric information from the JMF for this specific project at 4.0% air voids. The A-4 subgrade was listed as having a subgrade support value of 4.2 and the Design Guide software was used to determine an analogous modulus value of 238.2MPa (34.6ksi). A plasticity index of 3, with 60% passing the #200 sieve, 90% passing the #4 sieve, and a D60 of 0.05-mm were also used as inputs for the subgrade. The D60 refers to the grain size that corresponds to 60 percent passing, the plasticity index refers to the range of moisture contents that compose the plastic state (Cuduto, 1999).

A breakdown of the truck traffic as well as the AADT for the roadway was supplied by WisDOT. The Design Guide software was then used to determine the analogous average annual daily truck traffic (AADTT) and was found to be 893. The truck traffic composition and the AADT can be found in Table 7.20.

Table 7.20 Traffic Characteristics – Mosinee E-3 19.0mm

Traffic Characteristic	
AADT (veh./day)	6,868
Growth (%)	1.37
% of Traffic Greater Than Class 4	13.0
AADTT (trucks/day)	893
Truck Traffic Distribution	
2D (%)	2.3
3-SU (%)	1.0
2S-1 (%)	0.7
2S-2 (%)	0.7
3S-2 (%)	8.2
2-S1-2 (%)	0.1

The AADT refers to average annual daily traffic and measured through traffic counts. The AADTT refers to average annual daily truck traffic for vehicles larger than a passenger vehicle. The truck traffic distribution nomenclature used in Table 7.20 was that used by WisDOT. The Wisconsin Asphalt Pavement Association has provided running definitions for these truck classifications and listed as follows:

- 2D - WISDOT designation for a heavy single unit truck with two axles and 6 tires.
- 3SU - WISDOT designation for a heavy single unit truck with three axles.
- 2S-1 - WISDOT designation for a heavy tractor-semitrailer truck with three axles.
- 2S-2 - WISDOT designation for a heavy tractor-semitrailer with four axles.
- 3S-2 - WISDOT designation for a heavy tractor-semitrailer with five or more axles.
- 2-S1-2 - WISDOT designation for a heavy tractor-semitrailer-trailer combination with five or more axles. The 2-S1-2 is also known as a Double-Bottom truck.

The Wausau, WI climatic file was used for the climatic input as the actual mix was placed on US-153 in the Wausau city limits. The ground water table was estimated to be at a depth of 1.829-m (6-ft) or greater based on the information from the soils surveys from the United States Department of Agriculture (2000) for Marathon County, WI.

A total of eight simulations were run for each of the air voids and asphalt binder contents, amounting to a total of 32 simulations. Figures 7.25 through 7.29 show the effects of changing the pavement thickness has on the predicted pavement distresses of AC only permanent deformation, IRI, total pavement deformation, longitudinal cracking (bottom-up cracking), and alligator cracking (top-down cracking). The nomenclature used in the following figures shows the air void content as a number (4.0, 7.0, and 10.0%) followed by the asphalt binder content (optimum 'Opt.' or +0.3% asphalt binder content 'Bump').
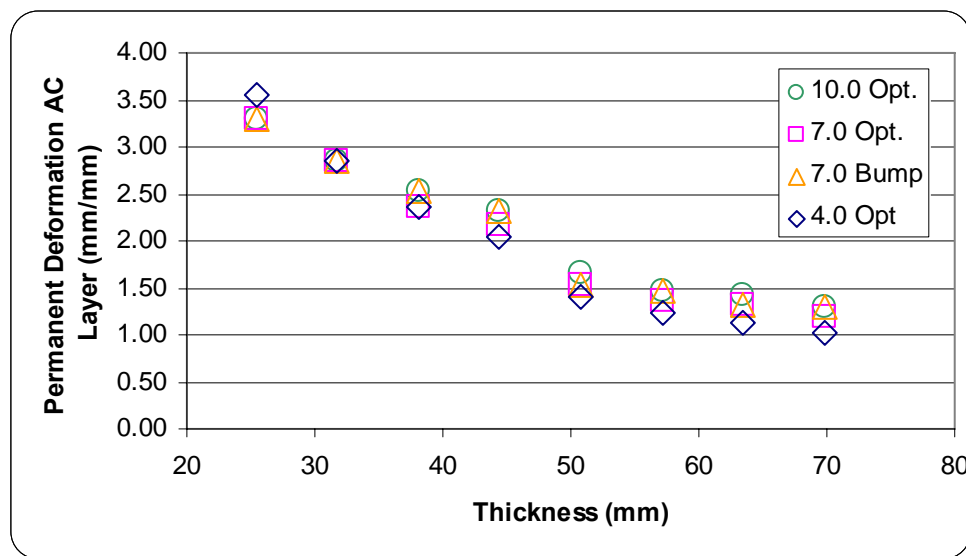
Figure 7.25 Mosinee E-3 Permanent Deformation AC Layer
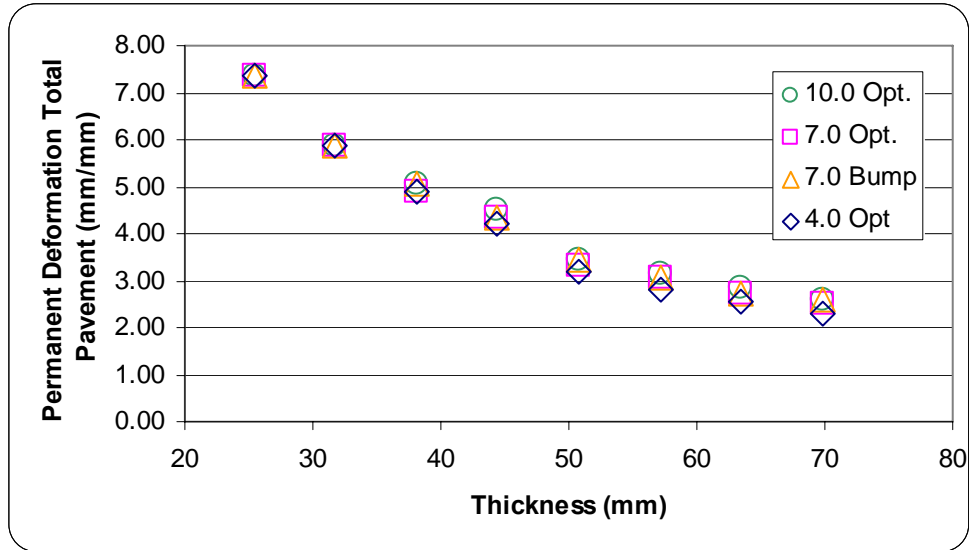
Figure 7.26 Mosinee E-3 Permanent Deformation Total Pavement
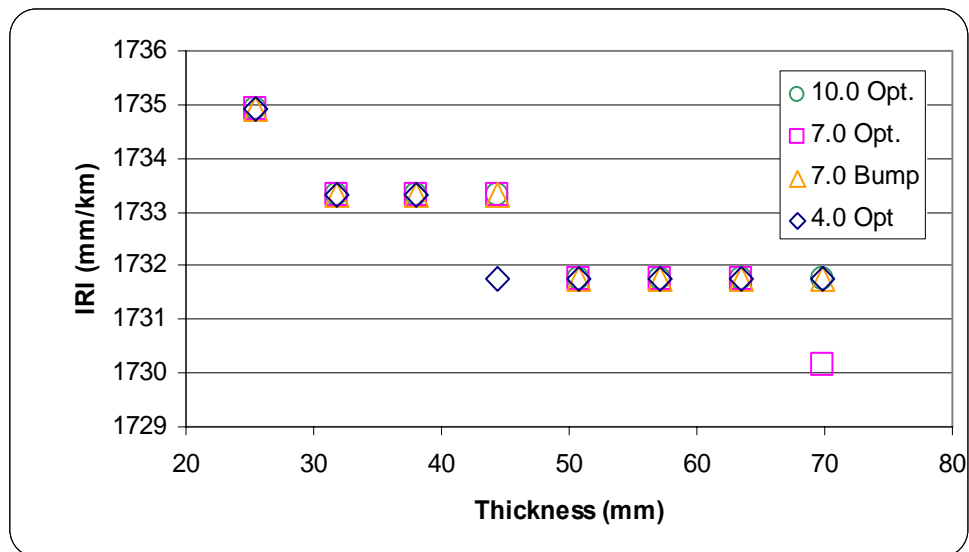
Figure 7.27 Mosinee E-3 IRI
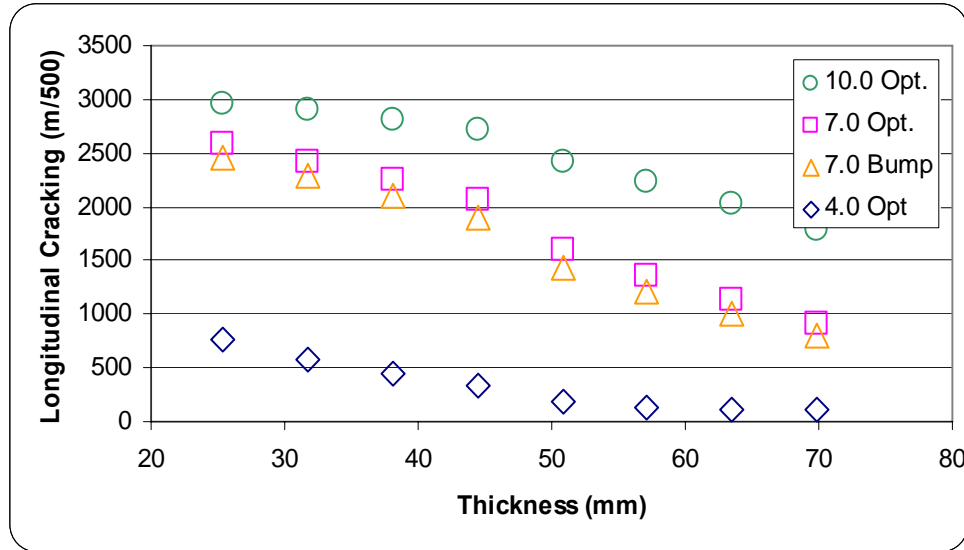
Figure 7.28 Mosinee E-3 Longitudinal Cracking
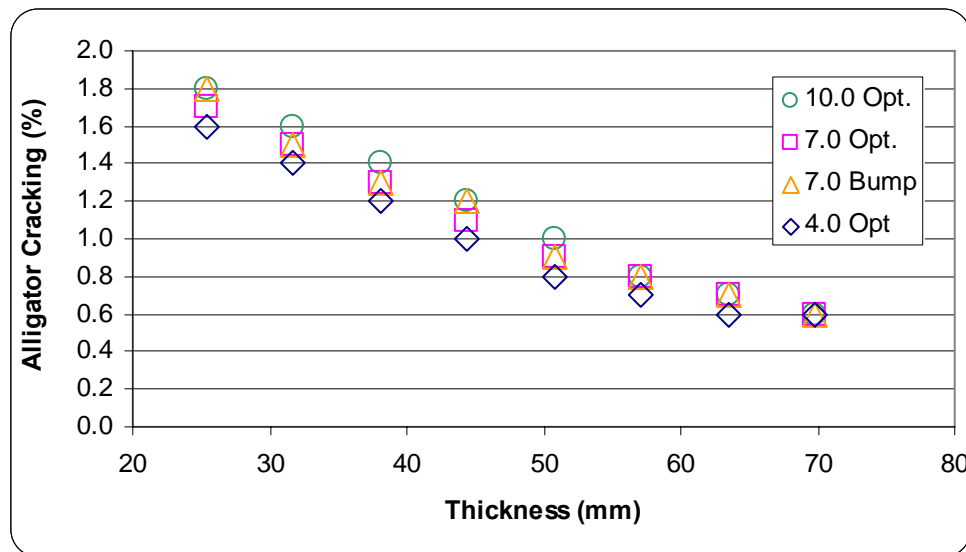
Figure 7.29 Mosinee E-3 Alligator Cracking

What is found is that the low air voids (4.0%) had the highest performing configuration in terms of all of the distresses considered. The respective predicted distress gets progressively worse as the air void content increases. The pavement design with the

asphalt binder content increase has a higher predicted resistance to all of the distresses considered in comparison to the pavement design with the optimum asphalt content.

Figures 7.25 and 7.26 indicates that adding a ¼-in of HMA may have a greater impact on mitigating the distresses of permanent deformation in the AC layer and total permanent deformation, respectively. In most instances the high air void content (10.0%) pavement design expectedly results in the highest predicted permanent deformation with the low air void content (4.0%) with the lowest. Examining the permanent deformation was rather difficult as most of the predictions fall near each other, indicating that the pavement is relatively insensitive to changes in air voids or asphalt content.

Again, IRI appears to be insensitive to changes in the air void content, asphalt binder content, and the pavement thickness. The predicted pavement IRI is significantly lower than the performance criteria used in the Design Guide software of 2,715-mm/km.

Figure 7.29 indicates that the thicknesses examined may not be sufficient to mitigate longitudinal cracking unless the pavement is compacted to less than 4% air voids. The performance criteria that is used by the Design Guide software was 305 m/500. Increasing the thickness would in-effect decrease longitudinal cracking. By iteration, the pavement thickness would need to be at least 95.3-mm (3.75-in) thick to bring the pavement within the performance criteria for a pavement with 7.0% air voids at the optimum asphalt binder content. The other distresses at 95.3-mm of pavement are shown in Table 7.21 and indicate the pavement would function within the performance criteria for each distress.

Table 7.21 Pavement Distress at Optimal Longitudinal Cracking Thickness

Distress	Prediction
Permanent Deformation AC Layer Only (mm)	2.8
Permanent Deformation Total Pavement (mm)	5.8
IRI (mm/km)	1,730.2
Longitudinal Cracking (m/500)	246.9
Alligator Cracking (%)	0.3

If the pavement were actually constructed to 10.0%, which is not likely, it would have to be considerably thicker and may be cost inhibitive.

7.8.3 Northfield E-30 19.0mm

The Northfield pavement is an extremely complex design structure and is not typical. The design consisted 44.5-mm (1.75-in) of a 12.5-mm NMAS SMA on 57.2-mm (2.25-in) of 19.0-mm dense-graded HMA on 254.0-mm (10-in) of continuously reinforced concrete pavement (CRCP) on 25.4-mm (1.0-in) of HMA on 228.6-mm (9-in) of joint reinforced concrete pavement (JRCP) on an A-4 subgrade. The main composition of an A-4 soil is silt under the AASHTO soil classification system. This presents a difficult pavement to analyze and in fact the Design Guide software was unable to process the pavement design as constructed. The difficulties with the pavement analysis were further compounded by the 19.0-mm mixture having a high dynamic modulus, which was found previously to cause problems with the software. Many approaches were developed to try and tackle the problems that were occurring for this pavement and in most instances they failed. The final pavement structure that was used to simulate the aforementioned pavement consisted of the two HMA layers as is on a 25.4-mm (1-in) high modulus subgrade on bedrock. The SMA layer was inputted as a

Level 3 design, but the Design Guide software does not give the ability to input this as a stiff layer as most SMA's are in fact stiff at their in-situ temperatures. A Level 1 analysis was used for the 19.0-mm NMAS layer and utilized the dynamic modulus results, these results can be found in Appendix G. The thin subgrade used a modulus 1724MPa (200ksi) with a plasticity index of 1, with 3% passing the #200 sieve, 20% passing the #4 sieve, and a D60 of 8-mm. It was realized that this subgrade would not exist, but was necessary in order to analyze the pavement and was meant to act as a stiff layer like that of concrete. The bedrock had a modulus of 5171MPa (750ksi), Poisson's ratio of 0.15, and a unit weight of 22kN/m^3 (140pcf).

The traffic characteristics were supplied by WisDOT and is shown in Table 7.22 and as can be seen by the truck traffic distribution constitutes a major trunkline.

Table 7.22 Traffic Characteristics – Northfield E-30 19.0mm

Traffic Characteristic	
AADT (veh./day)	11,550
Growth (%)	1.11
% of Traffic Greater Than Class 4	38.1
AADTT (trucks/day)	4,401
Truck Traffic Distribution	
2D (%)	3.1
3-SU (%)	0.7
2S-1 (%)	1.2
2S-2 (%)	1.2
3S-2 (%)	29.1
2-S1-2 (%)	2.8

The AADT refers to average annual daily traffic and measured through traffic counts. The AADTT refers to average annual daily truck traffic for vehicles larger than a passenger vehicle. The truck traffic distribution nomenclature used in Table 7.22 was

that used by WisDOT. The Wisconsin Asphalt Pavement Association has provided

running definitions for these truck classifications and listed as follows:

- 2D - WISDOT designation for a heavy single unit truck with two axles and 6 tires.
- 3SU - WISDOT designation for a heavy single unit truck with three axles.
- 2S-1 - WISDOT designation for a heavy tractor-semitrailer truck with three axles.
- 2S-2 - WISDOT designation for a heavy tractor-semitrailer with four axles.
- 3S-2 - WISDOT designation for a heavy tractor-semitrailer with five or more axles.
- 2-S1-2 - WISDOT designation for a heavy tractor-semitrailer-trailer combination with five or more axles. The 2-S1-2 is also known as a Double-Bottom truck.

A new climatic station had to be interpolated for the exact location of this project.

A latitude of 44.27-degrees and longitude of -91.20-degrees were used along with an

estimated elevation of 213.4-m (700-ft) and an annual depth to the water table of 1.829-m

(6ft). This information was once again derived from the soil survey made by the United

States Department of Agriculture for Jackson County (1990). The weather stations of

Eau Claire, WI, La Crosse, WI, Rochester, MN, and Wausau, WI were used to interpolate

a virtual weather station for this project.

A total of 16 simulations were run on the pavement structure, with simulation

issues for the pavement at 7.0% air voids for both the optimum and +0.3% optimum

asphalt binder content. With the 4.0 and 10.0% air void pavement structures running

correctly, there would be enough information to interpolate between the predicted

distresses for a 7.0% air void pavement. Figures 7.30 through 7.35 show the measured

distresses in the pavement structure for the Northfield E-30 19.0-mm mixture.
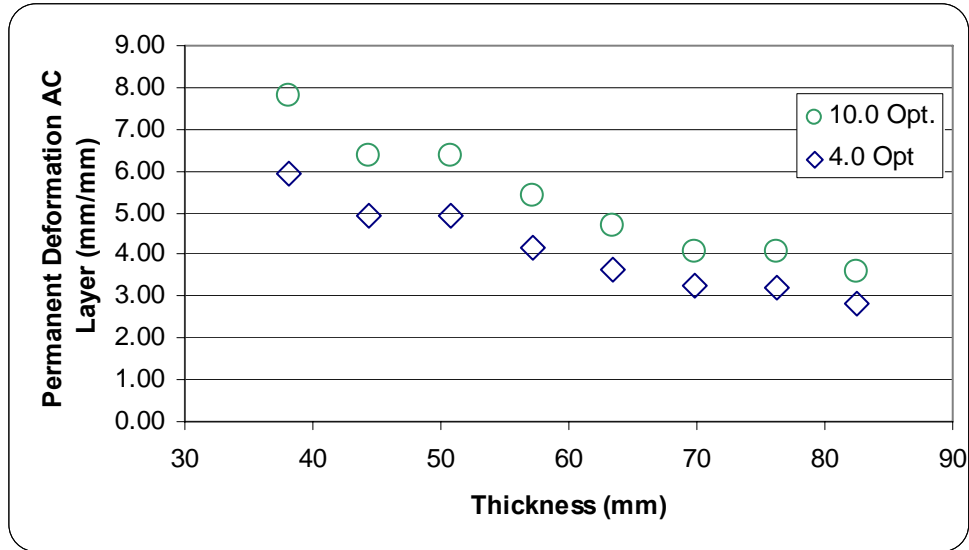
Figure 7.30 Northfield E-30 Permanent Deformation AC Layers
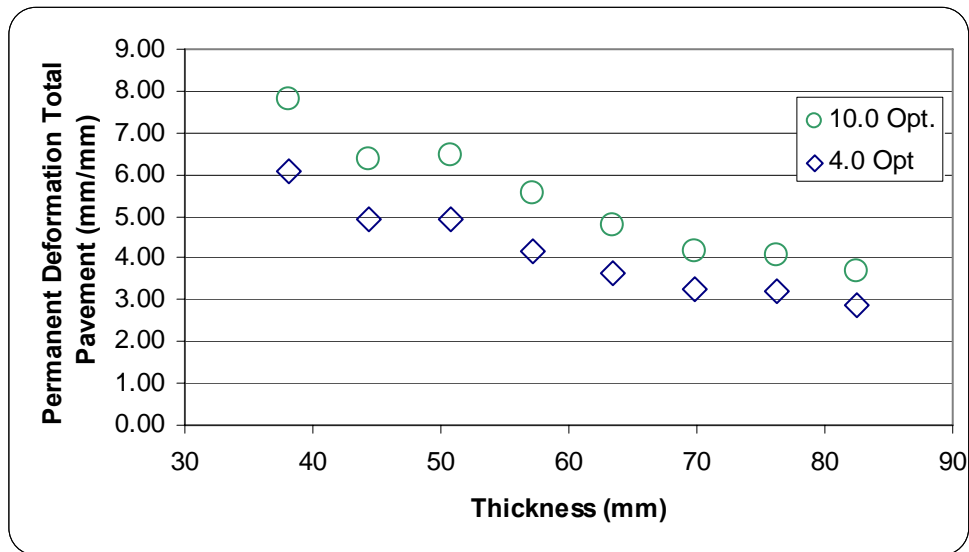
Figure 7.31 Northfield E-30 Permanent Deformation Total Pavement
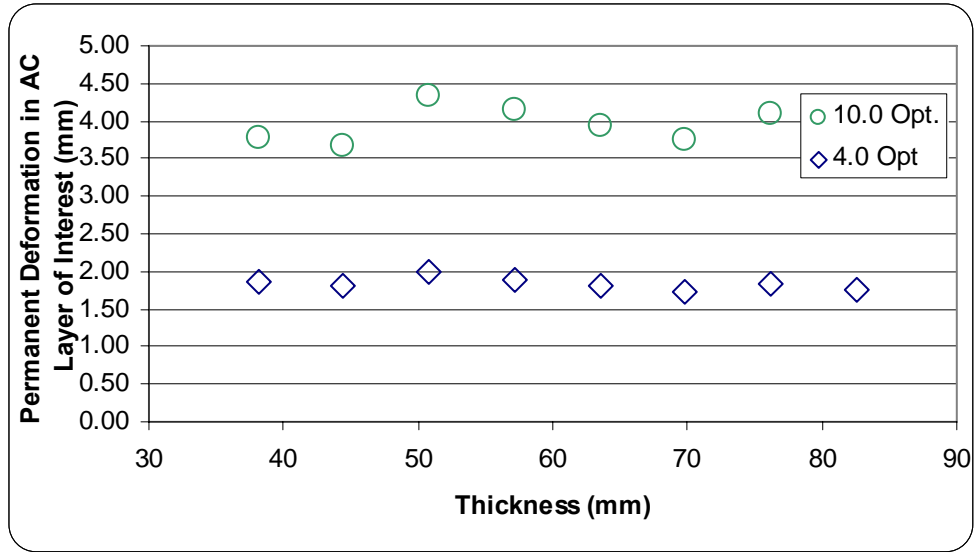
Figure 7.32 Northfield E-30 Permanent Deformation Layer of Interest
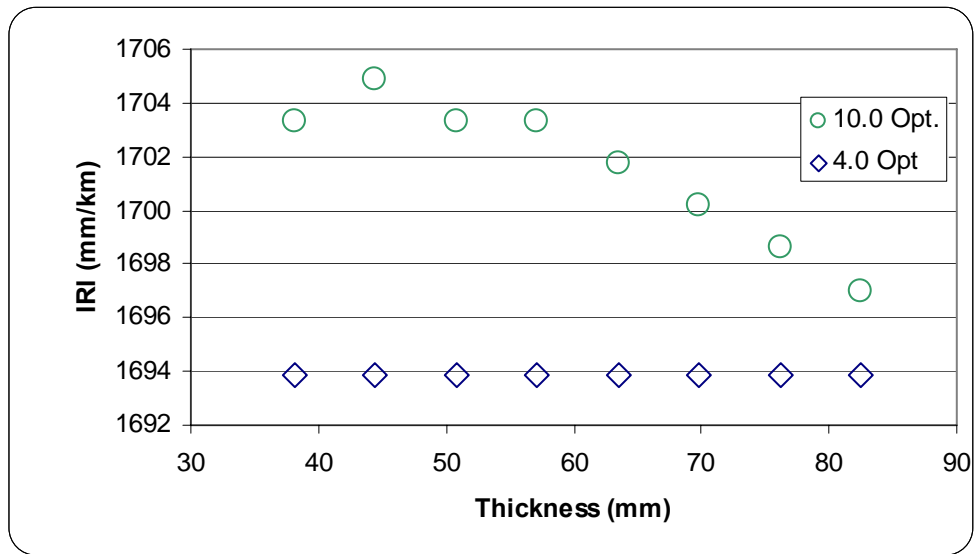
Figure 7.33 Northfield E-30 IRI
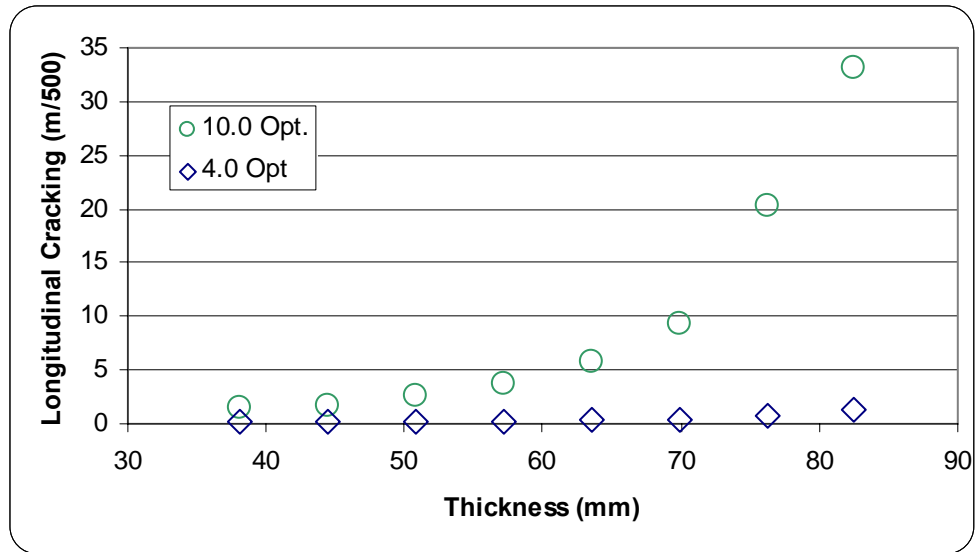
Figure 7.34 Northfield E-30 Longitudinal Cracking
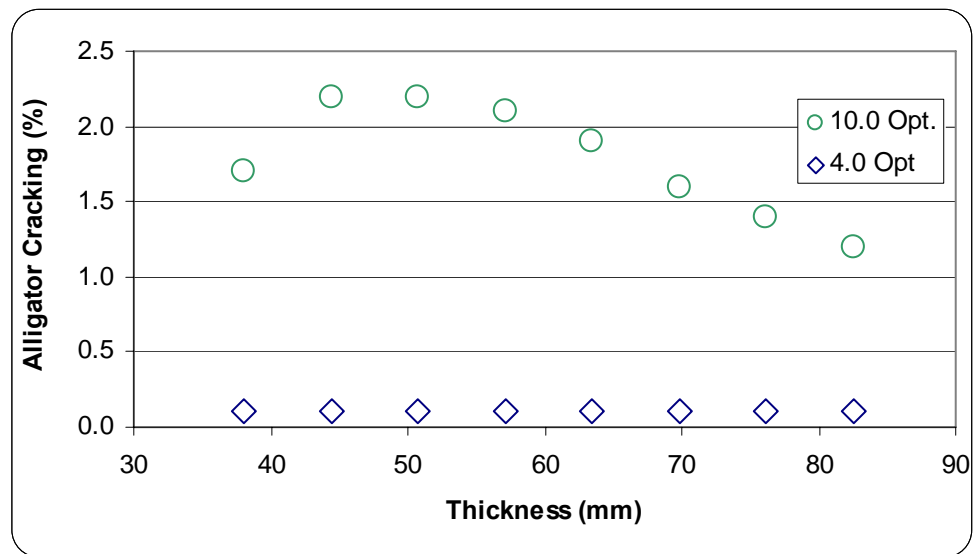
Figure 7.35 Northfield E-30 Alligator Cracking

The same trends are present; that at the low (4.0%) air void content the pavement has the greatest resistance to the predicted distresses. No interpolation was conducted to show where a pavement with 7.0% air voids would lie on the plots, but sufficient information has been presented to know that the pavement may be susceptible to permanent deformation (Figures 7.30 and 7.31).

171

The 12.5-mm SMA layer was used in a Level 3 design, where only the basic aggregate and asphalt binder characteristics were used for simulation. As a consequence, the true strength of this layer was not fully recognized in the analysis. As previously mentioned, the SMA promotes stone-on-stone contact to provide a high resistance to permanent deformation and the angularity required was not fully quantified in a Level 3 design. For this reason there appears to be excessive rutting in the pavement structure (Figures 7.30 and 7.31). To isolate the analysis to only the 19.0-mm dense-graded mixture, Figure 7.32 displays only the permanent deformation in this particular layer. With the performance criteria of 6.0-mm of permanent deformation in the AC layers, the performance of this layer is within the criteria, but the permanent deformation in the 12.5-mm SMA layer would have to be considered. At this time, the 12.5-mm SMA for this pavement structure has not been tested, thus the Design Guide software's prediction for permanent deformation in this layer is not available. The permanent deformation in the 19.0-mm dense-graded layer is rather insensitive to changes in thickness. Thus in order to reduce the permanent deformation in this pavement structure, the 19.0-mm dense-graded mixture needs to be compacted to a low air void content and/or the 12.5-mm SMA needs to be of equal or greater stiffness than the base course.

Again, the IRI of the pavement structure appears to be insensitive to the changes in the layer thickness (Figure 7.33). At the higher air void content (10.0%), the IRI can be reduced by increasing the pavement thickness, but the cost to benefit of such an approach may not be worthwhile.

The predicted fatigue cracking may have some inadequacies as the pavement structure had to be significantly altered in order to properly run the Design Guide

software. Additionally, the existing pavement condition plays a significant role in the development of fatigue related distresses as they can propagate through to the surface and by assuming a continuous and massive bedrock subgrade in which the pavement was placed, negates the effects of the existing pavements condition. In short, the predicted fatigue distress shown in Figures 7.34 and 7.35 should be carefully considered as the developed pavement design probably does not accurately reflect their potential for more (or less) expected fatigue cracking.

7.8.4 Pavement Design Test of Hypothesis

The hypothesis stated that the mechanistic-empirical pavement design should yield a thinner pavement recommendation as compared to that of the purely empirical design procedure. This hypothesis is hard to test as construction variability can play a significant role in whether a pavement has been sufficiently designed in order to mitigate pavement distresses. The current Design Guide is a design check and does not provide the optimal pavement design, thus different pavement alternatives and thicknesses must be examined to determine the changes in predicted distresses so as to better tailor the pavement to mitigate their occurrence. The only pavement analyzed that would not be suitable for its intended application would be the Mosinee E-3 19.0-mm as the layer thickness does appear to be sufficient and may have issues with fatigue. The Northfield E-30 19.0-mm pavement exhibits a complex pavement structure and as a result makes it difficult to determine the suitability of the design.

CHAPTER 8: CONCLUSIONS

The mechanistic-empirical pavement design procedure has been developed to the point where it is ready for understanding and verification by outside researchers prior to implementation by owner/agencies. The work outlined in this thesis has formed a basis on which WisDOT will evaluate the newly developed design approach.

The objectives of this project were to examine hot mix asphalt mixtures that are typically paved in the State of Wisconsin in terms of traffic level, gradation, and nominal maximum aggregate size. Additionally, volumetric properties of the pavement were considered (air voids and asphalt content). In total 19 of the 20 mixes outlined in the project matrix were sampled during the 2004 construction season.

Prior to testing of the Wisconsin asphalt mixtures, extensive research was conducted on the method of specimen preparation and testing history. This preliminary testing was meant to verify that the same specimen could be used throughout the testing sequence without statistically affecting later testing. The conclusions from this preliminary testing are reported as follows:

- The test history of the Superpave SPT (fatigue and permanent deformation dynamic modulus) does not affect the mean response for both dynamic modulus and flow number, but does increase the variability in the test results of the flow number.
- The method of specimen preparation, compacting to test geometry versus sawing/coring to test geometry, does not statistically appear to affect the intermediate and high temperature dynamic modulus and flow number test results.
- The 2002 AASHTO Design Guide simulations support the findings of the statistical analyses that the method of specimen preparation did not impact the

performance of the HMA as a structural layer as predicted by the Design Guide software.

The HMA that was sampled from Wisconsin was split and compacted to the project parameters and three specimens were sawed/cored to the testing geometries for each factor considered. The same specimen was tested throughout the testing sequence for both intermediate and high temperature dynamic modulus and flow number. Extensive testing was conducted on the asphalt binder with the rotational viscometer for direct input into the current Design Guide as well as the Witczak predictive equation. The Design Guide simulations that were conducted included the dynamic modulus testing results where applicable, as well as information gathered from the job mix formula, WisDOT, and soil surveys. The conclusions of the results reported herein are as follows:

- The methodologies for determining the temperature-viscosity relationship as stipulated by Witczak are sensitive to the viscosity test temperatures employed.
- The increase in asphalt binder content by 0.3% was found to actually increase the dynamic modulus at the intermediate and high test temperature as well as flow number. This result was based the testing that was conducted and was contradictory to previous research and the hypothesis that was put forth for this thesis. This result should be used with caution and requires further review.
- Based on the limited results presented herein, the asphalt binder grade appears to have a greater impact on performance in the Superpave SPT than aggregate angularity.
- Dynamic modulus and flow number was shown to increase with traffic level (requiring an increase in aggregate angularity) and with a decrease in air voids and confirm the hypotheses regarding these two factors.
- Accumulated micro-strain at flow number as opposed to the use of flow number appeared to be a promising measure for comparing the quality of specimens within a specific mixture.

- At the current time the Design Guide and its associate software needs to be further improved prior to implementation by owner/agencies.

CHAPTER 9: RECOMMENDATIONS

Extensive testing has been conducted as part of this research project. This testing has brought to light many issues that are involved in the implementation of the Superpave SPT. These issues should be addressed prior to their implementation by owner/agencies and industry. Additional research is needed as discussed in the following points:

- Only three of the 20 mixtures that have been sampled for this project have been tested. Testing needs to continue to examine the effects of NMAS and to make the analysis more robust by the inclusion of more results in the experimental plan.

- An examination should be undertaken to apply the Hirsh predictive model. The Hirsh model is a newer predictive equation developed by Don Christensen and Ramon Bonaquist (2003) and has been shown to address the issues of over prediction seen with the Witczak model.

- Examine the temperature selection used to determine the temperature-viscosity susceptibility of asphalt binder for the Witczak predictive model.

- Examine asphalt binder content changes greater than +0.3%. The testing in this study was not significant enough to statistically demonstrate any differences or the effects of asphalt binder content changes. However, greater asphalt binder content changes would not be practical in the field as construction limits are set at ±0.3% of the optimum value stated in the JMF.

- Examine the effects of laboratory versus field prepared specimens to validate the use of the SSPT as a design and QC/QA test.

- Develop a flow number predictive equation that uses key aggregate, asphalt binder, and volumetric characteristics.

- Further testing should be conducted on the method of preparation (sawed/cored and compacted to the test geometry) as it pertains to the NMAS of the mixture as well as gradation type. Further testing could validate the conclusion reached: that the method of preparation does not matter. An additional factor for specimen preparation would be to consider specimens that have been compacted to 150-mm in diameter and height and then were only cored. This type of preparation would provide a quality surface in which to mount the LVDTs to the sides of the specimen.

- Examine the application of accumulated micro-strain as a means of comparison within a mixture type to changes in volumetric properties.

REFERENCES

1. Akhter, G. F., and M.W. Witczak, "Sensitivity of Flexible Pavement Performance to Bituminous Mix Properties," Washington D.C.: Transportation Research Board (Transportation Research Record 1034) pp. 70-79, 1985.
2. "An Introduction to Aggregate Testing", Materials Certification and Training Program, Transportation Institute, Michigan Technological University, 2002.
3. Anderson, R.M., R.J. Cominsky, B.M. Killingsworth, "Sensitivity of Superpave Mixture Tests to Changes in Mixture Components," Journal of the Association of Asphalt Paving Technologists, Vol. 67, pp.153-188, 1998.
4. Annual Book of ASTM Standards, American Society for Testing and Materials (ASTM), Vol. 04.03, 2003.
5. Asphalt Institute, "Superpave Mix Design Series No. 2 (SP-2)", 1996.
6. Ayyub, B.M., R.H. McCuen, Probability, Statistics, and Reliability for Engineers and Scientists 2nd Ed., Chapman & Hall/CRC, Boca Raton, FL, 2003.
7. Azari, H., R. McCuen, and K. Stuart, "The Effect of Vertical Inhomogeneity on Compressive Properties of Asphalt Mixtures," Journal of the Association of Asphalt Paving Technologists, Vol. 73, pp.121-146, 2004.
8. Basyouny, M.M., M.W. Witczak, "Verification of the Calibrated Fatigue Cracking Models for the 2002 Design Guide," Journal of the Association of Asphalt Paving Technologists, 2005.
9. Basyouny, M.M., M.W. Witczak, S. El-Badawy, "Verification for the Calibrated Permanent Deformation Models for the 2002 Design Guide," Journal of the Association of Asphalt Paving Technologists, 2005.
10. Birgisson, B, G. Sholar, R. Roque, "Evaluation of Predicted Dynamic Modulus for Florida Mixtures," Washington D.C.: Transportation Research Board (Transportation Research Record 84th Annual Meeting) pp. 1-21, 2005.
11. Bonaquist, R., D. Christensen, W. Stump III, C. Antle, "Simple Performance Tester for Superpave Mixture Design," Interim Report for NCHRP 9-29, Advanced Asphalt Technologies, LLC, Sterling VA, September 2001.
12. Bonaquist, R., Personal Conversation, Fall 2004.
13. Brown, E.R., P.S. Kandhal, J. Zhang, "Performance Testing for Hot Mix Asphalt," National Center for Asphalt Technology (NCAT) Report 2001-05, 2001.
14. Brown, E.R.,R.B. Mallick, J.E. Haddock, J. Bukowski, "Performance of Stone Matrix Asphalt (SMA) Mixtures in the United States," Journal of the Association of Asphalt Paving Technologists, Vol. 66, pp.426-457, 1997.
15. Brown, S.F., and M.S. Snaith, "The Permanent Deformation Characteristics of a Dense Bitumen Macadam Subjected to Repeated Loading," Journal of the Association of Asphalt Paving Technologists, Vol. 43, pp.224-252, 1974.
16. Brown, S. F., and K. E. Cooper, "The Mechanical Properties of Bituminous Materials for Road Bases and Basecourses," Journal of the Association of Asphalt Paving Technologists, Vol. 53, pp.415-439, 1984.
17. Brown, S. F., and J. M. Gibb. "Validation Experiments for Permanent Deformation Testing of Bituminous Mixtures," Journal of the Association of Asphalt Paving Technologists, Vol.65, pp.255-299, 1996.

18. Burmister, D.M., "The Theory of Stresses and Displacement in Layered Systems and Applications to the Design of Airport Runways," Highway Research Record, Vol. 23, pp. 126-148, 1943.
19. Buttlar, W.G., R. Roque, B. Reid, "Automated Procedure for Generation of Creep Compliance Master Curve for Asphalt Mixtures," Washington D.C.: Transportation Research Board (Transportation Research Record 1630) pp. 28-36, 1998.
20. Christensen, D., Personal Conversation, Fall 2004.
21. Clyne, T.R., X. Li, M.O. Marasteanu, E.L. Skok, "Dynamic and Resilient Modulus of MN/DOT Asphalt Mixtures," Minnesota Department of Transportation, MN/RC-2003-09, 2003.
22. Coduto, D.P., Geotechnical Engineering: Principles and Practices, Prentice Hall, Upper Saddle River, New Jersey, 1999.
23. Coffman, B.S., D.C. Kraft, J. Tamayo, "A Comparison of Calculated and Measured Deflections for the AASHO Test Road," Proceedings of the Association of Asphalt Paving Technologists, Vol.33, pp.54-91, 1964.
24. Collop, A.C., A. Scarpas, C. Kasbergen, A. de Bondt, "Development and Finitie Element Implementation of Stress-Dependent Elastoviscoplastic Constitutive Model with Damage for Asphalt", Washington D.C.: Transportation Research Board (Transportation Research Record 1832) pp. 96-104, 2003.
25. Crockford, W.W., C. Berthelot, B. Tritt, C. Sinadinos, "Rapid Triaxial Test," Journal of the Association of Asphalt Paving Technologists, Vol.71, pp.712-724, 2001.
26. DATAPAVE, http://www.datapave.com, LTPP DataPave Online, 2004.
27. Dougan, C.E., J.E. Stephens, J. Mahoney, G. Hansen, "E* - DYNAMIC MODULUS Test Protocol – Problems and Solutions," Connecticut Transportation Institute, Report CT-SPR-0003084-F-03-3, 2003.
28. Dukatz, E., "Aggregate Production for Superpave HMA," The Superpave Asphalt Research Program, The University of Texas at Austin, 1996.
29. Epps, A.L., and A.J. Hand, "A Comparison of HMA Field Performance and Laboratory Volumetric Sensitivities," Journal of the Association of Asphalt Paving Technologists, Vol.70, pp.675-711, 2001.
30. Epps, J.A., R.B. Leahy, T. Mitchell, C. Ashmore, S. Seeds, S. Alavi, C.L. Monismith, "WesTrack – The Road to Performance-Related Specifications," International Conference on Accelerated Pavement Testing, Reno, NV, 1999.
31. Foster, C.R., and R.G. Ahlvin, "Stresses and Deflections Induced by a Uniform Circular Load," Highway Research Board, Vol. 33, pp. 467-470, 1954.
32. Guide for Mechanistic-Empirical Design of New and Rehabilitated Pavement Structures, National Cooperative Highway Research Program, NCHRP 1-37A, March 2004.
33. Hills, J.F., "The Creep of Asphalt Mixes," Journal of the Institute of Petroleum, V59, No. 570, 1973.
34. Hills, J.F., D. Brien, P.J. van de Loo, "The Correlation of Rutting and Creep Test on Asphalt Mixes," Journal of the Institute of Petroleum, Paper IP 74-001, 1974.
35. Huang, Y.H, Pavement Analysis and Design, Prentice Hall, Upper Saddle River, New Jersey, 2003.

36. Jones, A., "Tables of Stresses in Three-Layered Elastic Systems," Washington D.C.: Highway Research Board (1025), pp. 176-214, 1962.

37. Kaloush, K.E., and M.W. Witczak, " Tertiary Flow Characteristics of Asphalt Mixtures," Journal of the Association of Asphalt Paving Technologists, Vol. 71, pp.248-276, 2002.

38. Kerkhoven, R.E., G.M. Dormon, "Some Considerations on the California Bearing Ratio Method for the Design of Flexible Pavement," Shell Bitumen Monograph No. 1, 1953.

39. Krutz, N.C., and P.E. Sebaaly, "The Effects of Aggregate Gradation on Permanent Deformation of Asphalt Concrete," Journal of the Association of Asphalt Paving Technologists, Vol.62, pp.450-480, 1993.

40. Kutner, M.H., C.J. Nachtheim, J. Neter, Applied Regression Models, McGraw Hill/Irwin, 2004.

41. Levene, H. (1960). In Contributions to Probability and Statistics: Essays in Honor of Harold Hotelling, I. Olkin et al. eds., Stanford University Press, pp. 278-292.

42. Lytton, R.L., J. Uzan, E.G. Femando, R. Roque, D. Hiltunen, S.M. Stoffels, "Development and Validation of Performance Prediction Models and Specifications for Asphalt Binders and Paving Mixes", Strategic Highway Research Program 357, National Research Council, Washington D.C., 1993.

43. Mahoney, J., and J. Stephens, "Connecticut Superpave Gyratory Round Robin – 2003," Connecticut Transportation Institute, Report CAP Lab 1-2003, 2003.

44. Mallick, R.B., R. Ahlrich, E.R. Brown, "Potential of Dynamic Creep to Predict Rutting," Engineering Properties of Asphalt Mixtures and the Relationship to their Performance, ASTM STP 1265, G.A. Huber and D.S. Decker Eds., American Society for Testing and Materials, Philadelphia, 1995.

45. McClave, J.T., T. Sinich, Statistics 9th Ed., Prentice Hall, Upper Saddle River, NJ, 2003.

46. McGhee, K. H. "Summary of Proposed 2002 Pavement Design Guide," National Highway Cooperative Research Program 1-37A, 1999.

47. Mirza, M.W., M.W. Witczak, "Development of a Global Aging System for Short and Long Term Aging of Asphalt Cements," Journal of the Association of Asphalt Paving Technologists, Vol.64, pp.393-430, 1995.

48. Mohammad, L.N., Z. Wu, L. Myers, S. Cooper, C. Abadie, "A Practical Look at the Simple Performance Tests: Louisiana's Experience," Journal of the Association of Asphalt Paving Technologists, 2005.

49. Molenaar, A.A.A. and Ch. A. P. M. Van Gurp, "Structural Performance Model and Overlay Design Method for Asphalt Concrete Pavements," Washington D.C.: Transportation Research Board (Transportation Research Record 888) pp. 31-37, 1982.

50. Monismith, C.L., A.A. Tayabali "Permanent Deformation (Rutting) Considerations in Asphalt Concrete Pavement Actions," Journal of the Association of Asphalt Paving Technologists, Vol. 57 pp. 414-446, 1988.

51. Myers, L., Federal Highway Administration Engineer, Personal Conversation, Fall 2004.

52. Newcomb, D.E. and D.H. Timm, "Mechanistic Pavement Design: The Next Wave," Hot Mix Asphalt Technology, pp. 49-51, September/October 2001.

53. Owen, D.R.J., E. Hinton, <u>Finite Elements in Plasticity: Theory and Practice</u>, Pineridge Press Limited, Swansea, U.K., 1980.

54. Papazian, H.S., "The Response of Linear Viscoelastic Materials in the Frequency Domain with Emphasis on Asphaltic Concrete," International Conference on the Structural Design of Asphalt Pavements, University of Michigan, pp. 454-463, 1962.

55. Peattie, K.R., "Stress and Strain Factors for Three-Layered Elastic Systems," Washington D.C.: Highway Research Board (1025), pp. 214-253, 1962.

56. Pellinen, T.K, M.W. Witczak, "Stress Dependent Master Curve Construction for Dynamic (Complex) Modulus," Journal of the Association of Asphalt Paving Technologists, Vol. 71, pp.281-309, 2002.

57. Roberts, F. L. <u>Hot Mix Asphalt Materials, Mixture Design, and Construction</u>, Lanham: NAPA Research and Education Foundation, 1996.

58. Roberts, F.L., L.N. Mohammad, L.B. Wang, "History of Hot Mix Asphalt Mixture Design in the United States," American Society of Civil Engineers, Journal of Civil Engineering Materials, July 2002.

59. Saal R.N.J., and P.S. Pell, "Kolloid-Zeitschrift MI," Heft 1, pp. 61-71, 1960.

60. Shenoy, A., and P. Romero, "Standardized Procedure for Analysis of Dynamic Modulus $|E*|$ Data to Predict Asphalt Pavement Distresses," Washington D.C.: Transportation Research Board (Transportation Research Record 1789) pp. 173-182, 2002.

61. Shook J.F., and B.F. Kallas. "Factors Influencing Dynamic Modulus of Asphalt Concrete," Journal of the Association of Asphalt Paving Technologists, Vol. 38, pp.140-178, 1969.

62. Soil Survey of Lincoln County Wisconsin, United States Department of Agriculture, 1990.

63. Soil Survey of Lincoln County Wisconsin, United States Department of Agriculture, 2000.

64. Soil Survey of Marathon County Wisconsin, United States Department of Agriculture, 2000.

65. Superpave Mix Design Series No.2 (SP-2), The Asphalt Institute, 1996.

66. Timm, D., B. Birgisson, D. Newcomb, "Development of Mechanistic-Empirical Pavement Design in Minnesota," Washington D.C.: Transportation Research Board (Transportation Research Record 1629) pp. 181-188, 1998.

67. Uzan, J., A. Sides, M. Perl, "Viscoelastoplastic Model for Predicting Performance of Asphaltic Mixtures," Washington D.C.: Transportation Research Board (Transportation Research Record 1043) pp. 78-89, 1985.

68. Uzan, J., "Permanent Deformation in Flexible Pavements", American Society of Civil Engineering, Journal of Transportation Engineering, Vol. 130, No. 1, January 1, 2004.

69. Van Cauwelaert, F., D.R. Alexander, T.D. White, W.R. Barker, "Multilayer Elastic Program for Backcalculating Layer Moduli in Pavement Evaluation," Nondestructive Testing of Pavements and Backcalculating Moduli , ASTM STP

1026, A.J. Bush III and G.Y. Baladi, American Society for Testing and Materials, Philadelphia, 1989, pp. 171-188.

70. Van de Loo, P.J., "Creep Testing, a Simple Tool to Judge Asphalt Mix Stability," Proceedings of the Association of Asphalt Paving Technologists, Vol. 43, pp.253-284, 1974.

71. Vesic, A.S., and L. Domaschuk, "Theoretical Analysis of Structural Behavior of Road Test Flexible Pavements," National Cooperative Highway Research Program, Report 10, 1964.

72. Wisconsin Department of Transportation: Standard Specifications for Highway and Structure Construction, Wisconsin Department of Transportation, 2002.

73. Wisconsin State Climatology Office, http://www.aos.wisc.edu/~sco/, 1/7/2005.

74. Witczak, M. W., R. Bonaquist, H. Von Quintus, K. Kaloush. "Specimen Geometry and Aggregate Size Effects in Uniaxial Compression and Constant Height Shear Tests," Journal of the Association of Asphalt Paving Technologists, Vol. 69, pp.733-793, 2000.

75. Witczak, M.W., and O.A. Fonseca, "Revised Predictive Model for Dynamic (Complex) Modulus of Asphalt Mixtures," Washington D.C.: Transportation Research Board (Transportation Research Record 1540) pp. 15-23, 1996.

76. Witczak, M.W., K.E. Kaloush, H. Von Quintus, "Pursuit of the Simple Performance Test for Asphalt Mixture Rutting," Journal of the Association of Asphalt Paving Technologists, Vol. 71, pp.671-691, 2002a.

77. Witczak, M. W., K. Kaloush, T. Pellinen, M. El-Basyouny, H. Von Quintus, "Simple Performance Test for Superpave Mix Design," National Cooperative Highway Research Program 465, pp.6-100, 2002b.

78. WSDOT Pavement Guide Vol. 2 Pavement Notes For Design, Evaluation and Rehabilitation, Washington Department of Transportation, February 1995.

79. Zhou, F., T. Scullion, "Preliminary Field Validation of Simple Performance Tests for Permanent Deformation: Case Study," Washington D.C.: Transportation Research Board (Transportation Research Record 1832) pp. 209-216, 2003.

80. Zhou, F., T. Scullion, L. Sun, "Verification and Modelling of Three-Stage Permanent Deformation Behavior of Asphalt Mixtures," Journal of Transportation Engineering, Vol. 130 Issue 4, pp. 486-494, 2004.

APPENDIX A PROJECT JMF'S

Project: Sauk County - Baraboo USH 12

Project No.:	5300-03-77
Location:	Sauk County
Contractor:	D.L. Gasser
Traffic Volume (ESALs):	300,000
NMAS (mm):	12.5
Mix Type:	Dense
Date:	6/16/2004
G_{se}	2.701
G_{sb}	2.652
G_{sa}	N/A
Absorption (%)	0.8
Sand Equivalency (%)	41.5
Flat & Elongated (%)	4.7
NAA	79.0
1 Face Crush (%)	89.5
2 Face Crush (%)	87.4

Temperatures:	
Mixing:	N/A
Compacting:	143

Sieve Size in (mm):	3/4" Gravel	5/8" Quartzite	Blend Sand	Agg Source 4	Agg Source 5	Agg Source 6	Agg Source 7	Mix
1 (25)	100.0	100.0	100.0					100.0
3/4 (19)	100.0	100.0	100.0					100.0
1/2 (12.5)	90.0	91.0	99.0					95.3
3/8 (9.5)	73.0	75.0	94.0					85.2
#4 (4.75)	45.0	47.0	82.0					66.2
#8 (2.36)	31.0	31.0	72.0					54.0
#16 (1.18)	23.0	22.0	67.0					47.4
#30 (0.60)	19.0	16.0	56.0					39.1
#50 (0.30)	14.0	12.0	23.0					18.6
#100 (0.15)	8.4	9.0	5.1					6.7
#200 (0.075)	5.7	6.5	3.0					4.4
Percentages	22%	22%	56%					100%

Asphalt & Additives:

Asphalt Source:	MIF-LaCrosse
Asphalt Grade (PG):	58-28
Asphalt Content (%):	6.0
Specific Gravity:	1.029
Asphalt Additives:	None
Asphalt Additives (%):	N/A

Compactive Effort:

N_{ini}:	6
N_{des}:	40
N_{max}:	60
%G_{mm} @ N_{ini}:	91.7
%G_{mm} @ N_{max}:	96.7
CF:	1.020

Volumetrics:

VMA @ N_{des}:	16.2
VFA @ N_{des}:	75.4
AV @ N_{des}:	4.0
F/P_{be}:	0.8
P_{be} (%):	5.3

12.5 mm Nominal Sieve Size

Blend 1

Project: Taylor County Medford WI STH 102

Project No.:	9225-05-70
Location:	Taylor County
Contractor:	American - Mathy
Traffic Volume (ESALs):	1,000,000
NMAS (mm):	12.5
Mix Type:	Dense
Date:	7/8/2004
G_{se}	2.747
G_{sb}	2.697
G_{sa}	N/A
Absorption (%)	1.0
Sand Equivalency (%)	75.0
Flat & Elongated (%)	3.3
NAA	42.9
1 Face Crush (%)	96.5
2 Face Crush (%)	96.4

Temperatures:	
Mixing:	N/A
Compacting:	143

Sieve Size in (mm):	11/16" Rock	5/8 Sand	RAP (5.0% AC)	Agg Source 4	Agg Source 5	Agg Source 6	Agg Source 7	Mix
1 (25)	100.0	100.0	100.0					100.0
3/4 (19)	100.0	100.0	100.0					100.0
1/2 (12.5)	89.0	99.0	93.0					94.9
3/8 (9.5)	67.0	91.0	79.0					81.4
#4 (4.75)	39.0	75.0	60.0					60.9
#8 (2.36)	25.0	63.0	49.0					48.3
#16 (1.18)	18.0	48.0	40.0					36.7
#30 (0.60)	13.0	30.0	31.0					24.2
#50 (0.30)	9.0	12.0	20.0					11.8
#100 (0.15)	5.9	3.5	13.0					5.3
#200 (0.075)	3.9	3.2	9.5					4.1
Percentages	35%	55%	10%					100%

Asphalt & Additives:

Asphalt Source:	MIF-LaCrosse
Asphalt Grade (PG):	58-28
Asphalt Content (%):	5.2
Specific Gravity:	1.03
Asphalt Additives:	None
Asphalt Additives (%):	N/A

Compactive Effort:

N_{ini}:	7
N_{des}:	60
N_{max}:	75
%G_{mm} @ N_{ini}:	90
%G_{mm} @ N_{max}:	96.8
C.F.:	1.020

Volumetrics:

VMA @ N_{des}:	15.3
VFA @ N_{des}:	73.9
AV @ N_{des}:	4.0
F/P$_{be}$:	0.9
P_{be} (%):	4.5

12.5 mm Nominal Sieve Size

Project: Waushara County Wautoma STH 22

Sieve Size in (mm):	Millings	5/8x1/2 Chip	1/2x1/4 Chip	1/4" Screen	Screen Sand	Agg Source 6	Agg Source 7	Mix
Project No.: 6300-03-60								
1 (25)	100.0	100.0	100.0	100.0	100.0			100.0
3/4 (19)	100.0	100.0	100.0	100.0	100.0			100.0
1/2 (12.5)	96.5	63.7	100.0	100.0	100.0			96.8
3/8 (9.5)	90.8	7.7	81.8	93.6	95.4			87.9
#4 (4.75)	77.6	1.6	8.3	60.8	86.1			66.1
#8 (2.36)	64.5	1.3	2.4	43.3	79.1			52.8
#16 (1.18)	52.2	1.2	2.1	33.6	62.5			44.7
#30 (0.60)	38.5	1.2	1.9	25.0	19.8			34.8
#50 (0.30)	18.3	1.1	1.8	16.5	3.0			15.3
#100 (0.15)	11.0	0.9	1.5	11.3	1.1			6.7
#200 (0.075)	8.1	0.7	1.2					4.4
Percentages	18%	7%	22%	20%	33%			100%

Location: Waushara County
Contractor: Northeast Asphalt
Traffic Volume (ESALs): 1,000,000
NMAS (mm): 12.5
Mix Type: Dense
Date: 6/20/2004
G_{se}: 2.733
G_{sb}: 2.713
G_{sa}: 2.765
Absorption (%): 0.7
Sand Equivalency (%): 84.0
Flat & Elongated (%): 2.5
NAA: 41.0
1 Face Crush (%): 96.7
2 Face Crush (%): 96.0

Temperatures:
Mixing: N/A
Compacting: 143

Asphalt & Additives:
Asphalt Source:	Koch, Stevens Point
Asphalt Grade (PG):	58-28
Asphalt Content (%):	4.7
Specific Gravity:	1.032
Asphalt Additives:	None
Asphalt Additives (%):	N/A

Compactive Effort:
N_{ini}:	7
N_{des}:	60
N_{max}:	75
%G_{mm} @ N_{ini}:	91.2
%G_{mm} @ N_{max}:	96.5
C.F.:	1.020

Volumetrics:
VMA @ N_{des}:	14.5
VFA @ N_{des}:	72.4
AV @ N_{des}:	4.0
F/P$_{be}$:	1
P_{be} (%):	4.4

12.5 mm Nominal Sieve Size

Blend 1

Project: Iron County Hurley STH 169

Project No.:	9311-13-60
Location:	Iron County
Contractor:	Northwoods Paving
Traffic Volume (ESALs):	300,000
NMAS (mm):	12.5
Mix Type:	Dense
Date:	7/21/2004
G_{se}	2.760
G_{sb}	2.689
G_{sa}	N/A
Absorption (%)	1.3
Sand Equivalency (%)	74.0
Flat & Elongated (%)	4.0
NAA	
1 Face Crush (%)	93.6
2 Face Crush (%)	93.4

Temperatures:

Mixing:	N/A
Compacting:	143

Sieve Size in (mm):	3/4" Rock	5/8x3/8 Rock	3/8 Minus	5/8 Nat Sand	RAP (6.0% AC)	Agg Source 6	Agg Source 7	Mix
1 (25)	100.0	100.0	100.0	100.0	100.0			100.0
3/4 (19)	100.0	100.0	100.0	100.0	100.0			100.0
1/2 (12.5)	78.0	77.0	100.0	99.0	98.0			92.7
3/8 (9.5)	62.0	35.0	100.0	97.0	91.0			83.4
#4 (4.75)	34.0	2.4	73.0	94.0	70.0			62.8
#8 (2.36)	19.0	2.0	48.0	90.0	54.0			49.3
#16 (1.18)	12.0	1.8	28.0	83.0	43.0			38.9
#30 (0.60)	9.0	1.7	18.0	65.0	32.0			29.1
#50 (0.30)	7.0	1.5	13.0	19.0	17.0			13.0
#100 (0.15)	6.0	1.4	9.0	6.7	11.0			7.5
#200 (0.075)	5.0	1.0	7.0	1.0	8.8			4.9
Percentages	20%	10%	25%	25%	20%			100%

Asphalt & Additives:

Asphalt Source:	Murphy
Asphalt Grade (PG):	58-28
Asphalt Content (%):	6.3
Specific Gravity:	1.03
Asphalt Additives:	None
Asphalt Additives (%):	N/A

Compactive Effort:

N_{ini}:	6
N_{des}:	40
N_{max}:	60
%G_{mm} @ N_{ini}:	90.6
%G_{mm} @ N_{max}:	96.7
CF:	1.020

Volumetrics:

VMA @ N_{des}:	16.5
VFA @ N_{des}:	75.8
AV @ N_{des}:	4.0
F/P_{be}:	0.9
P_{be} (%):	5.4

12.5 mm Nominal Sieve Size

Project: Sawyer County Hayward WI State Highway 77

Project No.:	8520-13-71
Location:	Sawyer County
Contractor:	B. R. Amon
Traffic Volume (ESALs):	3,000,000
NMAS (mm):	12.5
Mix Type:	Dense
Date:	6/3/2004
G_{se}	2.779
G_{sb}	2.728
G_{sa}	N/A
Absorption (%)	0.9
Sand Equivalency (%)	81.0
Flat & Elongated (%)	2.1
NAA	44.0
1 Face Crush (%)	74.7
2 Face Crush (%)	70.4

Temperatures:	
Mixing:	148
Compacting:	135

Sieve Size in (mm):	7/8" Stone	5/8" Stone	3/8" Stone	Sand	Dust	RAP	Agg Source 7	Mix
1 (25)	100.0	100.0	100.0	100.0	100.0	100.0		100.0
3/4 (19)	95.8	100.0	100.0	100.0	100.0	100.0		100.0
1/2 (12.5)	18.2	91.9	100.0	100.0	100.0	100.0		98.8
3/8 (9.5)	3.0	25.7	96.0	99.2	100.0	100.0		87.8
#4 (4.75)	2.3	3.3	8.4	89.2	88.6	100.0		62.4
#8 (2.36)	2.2	3.1	4.2	76.1	57.9	100.0		48.4
#16 (1.18)	2.1	3.0	4.0	61.2	41.8	100.0		37.9
#30 (0.60)	2.0	2.9	3.7	37.8	31.4	100.0		25.2
#50 (0.30)	1.8	2.5	3.2	16.5	21.3	100.0		13.3
#100 (0.15)	1.3	1.8	2.5	4.3	12.4	100.0		5.6
#200 (0.075)	1.1	1.6	2.0	3.9	9.4	100.0		4.6
Percentages	0%	15%	17%	43%	25%	0%		100%

Asphalt & Additives:

Asphalt Source:	Murphy
Asphalt Grade (PG):	58-28
Asphalt Content (%):	5.3
Specific Gravity:	1.031
Asphalt Additives:	None
Asphalt Additives (%):	N/A

Compactive Effort:

N_{ini}:	7
N_{des}:	75
N_{max}:	115
%G_{mm} @ N_{ini}:	89.1
%G_{mm} @ N_{max}:	96.7
CF:	1.020

Volumetrics:

VMA @ N_{des}:	15.0
VFA @ N_{des}:	73.3
AV @ N_{des}:	4.0
F/P_{be}:	0.99
P_{be} (%):	4.6

12.5 mm Nominal Sieve Size

— Blend 1

Project: Marathon County Wausau WI CTH 12

Project No.:	6675-00-70
Location:	Marathon County
Contractor:	American - Mathy
Traffic Volume (ESALs):	3,000,000
NMAS (mm):	12.5
Mix Type:	Dense
Date:	6/15/2004
G_{se}	2.698
G_{sb}	2.647
G_{sa}	N/A
Absorption (%)	0.5
Sand Equivalency (%)	87.0
Flat & Elongated (%)	1.8
NAA	43.2
1 Face Crush (%)	96.7
2 Face Crush (%)	96.5

Temperatures:

Mixing:	N/A
Compacting:	143

Sieve Size in (mm):	1/2" Rock	3/8" Rock	3/16 Screening	Blend Sand	Man Sand	RAP (4.0% AC)	Agg Source 7	Mix
1 (25)	100.0	100.0	100.0	100.0	100.0	100.0		100.0
3/4 (19)	100.0	100.0	100.0	100.0	100.0	100.0		100.0
1/2 (12.5)	81.0	100.0	100.0	99.0	100.0	97.0		95.7
3/8 (9.5)	36.0	100.0	100.0	98.0	100.0	90.0		85.8
#4 (4.75)	6.0	29.0	97.0	94.0	100.0	73.0		66.1
#8 (2.36)	3.0	10.0	66.0	88.0	67.0	58.0		48.8
#16 (1.18)	2.2	5.6	42.0	77.0	43.0	47.0		36.2
#30 (0.60)	1.9	4.4	28.0	58.0	24.0	36.0		25.4
#50 (0.30)	1.8	3.5	17.0	10.0	10.0	18.0		9.6
#100 (0.15)	1.5	3.0	11.0	1.2	3.5	11.0		4.8
#200 (0.075)	1.3	2.4	10.0	0.7	1.5	8.0		3.8
Percentages	20%	15%	20%	20%	15%	10%		100%

Asphalt & Additives:

Asphalt Source:	MIF-LaCrosse
Asphalt Grade (PG):	64-22
Asphalt Content (%):	5.9
Specific Gravity:	1.029
Asphalt Additives:	Polymer
Asphalt Additives (%):	N/A

Compactive Effort:

N_{ini}:	7
N_{des}:	75
N_{max}:	115
$\%G_{mm}$ @ N_{ini}:	89.5
$\%G_{mm}$ @ N_{max}:	96.9
CF:	1.020

Volumetrics:

VMA @ N_{des}:	15.9
VFA @ N_{des}:	74.9
AV @ N_{des}:	4.0
F/P_{be}:	0.7
P_{be} (%):	5.2

12.5 mm Nominal Sieve Size

Legend: Blend 1

X-axis: Sieve Size (mm) — 0.075, 0.15, 0.3, 0.6, 1.18, 2.36, 4.75, 9.5, 12.5, 19.0

Y-axis: Percent Passing — 0, 20, 40, 60, 80, 100, 120

Project: Iron County Hurley WI West County Line - CTH B US 2

Project No.:	1185-02-70
Location:	Iron County
Contractor:	Northwoods Paving
Traffic Volume (ESALs):	3,000,000
NMAS (mm):	12.5
Mix Type:	Dense
Date:	6/24/2004
G_{se}	2.748
G_{sb}	2.696
G_{sa}	N/A
Absorption (%)	1.3
Sand Equivalency (%)	66.0
Flat & Elongated (%)	3.9
NAA	
1 Face Crush (%)	95.4
2 Face Crush (%)	95.3

Temperatures:	
Mixing:	
Compacting:	

Sieve Size in (mm):	3/4" Rock	5/8x3/8 Rock	3/8 Minus	5/8 Nat Sand	RAP (5.9% AC)	Agg Source 6	Agg Source 7	Mix
1 (25)	100.0	100.0	100.0	100.0	100.0			100.0
3/4 (19)	100.0	100.0	100.0	100.0	100.0			100.0
1/2 (12.5)	78.0	77.0	100.0	99.0	95.0			93.4
3/8 (9.5)	62.0	35.0	100.0	97.0	90.0			83.0
#4 (4.75)	34.0	2.4	73.0	94.0	75.0			61.4
#8 (2.36)	19.0	2.0	48.0	90.0	50.0			46.1
#16 (1.18)	12.0	1.8	28.0	83.0	40.0			34.8
#30 (0.60)	9.0	1.7	18.0	65.0	30.0			25.5
#50 (0.30)	7.0	1.5	13.0	19.0	25.0			13.4
#100 (0.15)	6.0	1.4	9.0	6.7	17.0			8.1
#200 (0.075)	5.0	1.0	7.0	1.0	12.0			5.3
Percentages	5%	20%	40%	20%	15%			100%

Asphalt & Additives:

Asphalt Source:	MIF-LaCrosse
Asphalt Grade (PG):	64-34
Asphalt Content (%):	5.6
Specific Gravity:	1.029
Asphalt Additives:	Polymer
Asphalt Additives (%):	N/A

Compactive Effort:

N_{ini}:	7
N_{des}:	75
N_{max}:	115
%G_{mm} @ N_{ini}:	89.3
%G_{mm} @ N_{max}:	96.7
CF:	1.020

Volumetrics:

VMA @ N_{des}:	15.5
VFA @ N_{des}:	74.2
AV @ N_{des}:	4.0
F/P_{be}	1.1
P_{be} (%):	4.9

12.5 mm Nominal Sieve Size

Percent Passing vs. Sieve Size (mm) — Blend 1

Project: Langlade County WI City of Antigo

Project No.:	1605-04-70
Location:	Langlade County
Contractor:	Northeast Asphalt
Traffic Volume (ESALs):	10,000,000
NMAS (mm):	12.5
Mix Type:	Dense
Date:	6/2/2004
G_{se}	2.700
G_{sb}	2.690
G_{sa}	2.721
Absorption (%)	0.4
Sand Equivalency (%)	86.0
Flat & Elongated (%)	0.4
NAA	45.2
1 Face Crush (%)	95.4
2 Face Crush (%)	93.8

Temperatures:

Mixing:	N/A
Compacting:	142

Sieve Size in (mm):	5/8"x1/2" Chip	1/2"x1/4" Chip	1/4" Screenings	MFGD Sand	Screened Sand	Agg Source 6	Agg Source 7	Mix
1 (25)	100.0	100.0	100.0	100.0	100.0			100.0
3/4 (19)	100.0	100.0	100.0	100.0	100.0			100.0
1/2 (12.5)	83.4	100.0	100.0	100.0	100.0			98.0
3/8 (9.5)	27.6	85.8	88.5	76.0	99.3			89.6
#4 (4.75)	6.9	10.3	60.4	44.7	84.6			64.5
#8 (2.36)	5.1	6.0	44.2	27.1	68.1			43.9
#16 (1.18)	4.2	4.9	33.3	17.0	55.8			31.7
#30 (0.60)	3.8	4.2	24.5	9.0	37.2			21.5
#50 (0.30)	3.3	3.6	15.7	3.7	15.2			11.6
#100 (0.15)	2.7	3.0	10.2	1.7	6.4			6.0
#200 (0.075)	2.0	2.2	7.2	0.9	3.9			4.1
Percentages	12%	11%	15%	37%	25%			100%

Asphalt & Additives:

Asphalt Source:	CRM Gladstone
Asphalt Grade (PG):	58-34
Asphalt Content (%):	5.0
Specific Gravity:	1.03
Asphalt Additives:	Polymer
Asphalt Additives (%):	N/A

Compactive Effort:

N_{ini}:	8
N_{des}:	100
N_{max}:	160
%G_{mm} @ N_{ini}:	89
%G_{mm} @ N_{max}:	97
C.F.:	1.020

Volumetrics:

VMA @ N_{des}:	14.7
VFA @ N_{des}:	72.8
AV @ N_{des}:	4.0
F/P$_{be}$:	0.8
P_{be} (%):	4.9

12.5 mm Nominal Sieve Size
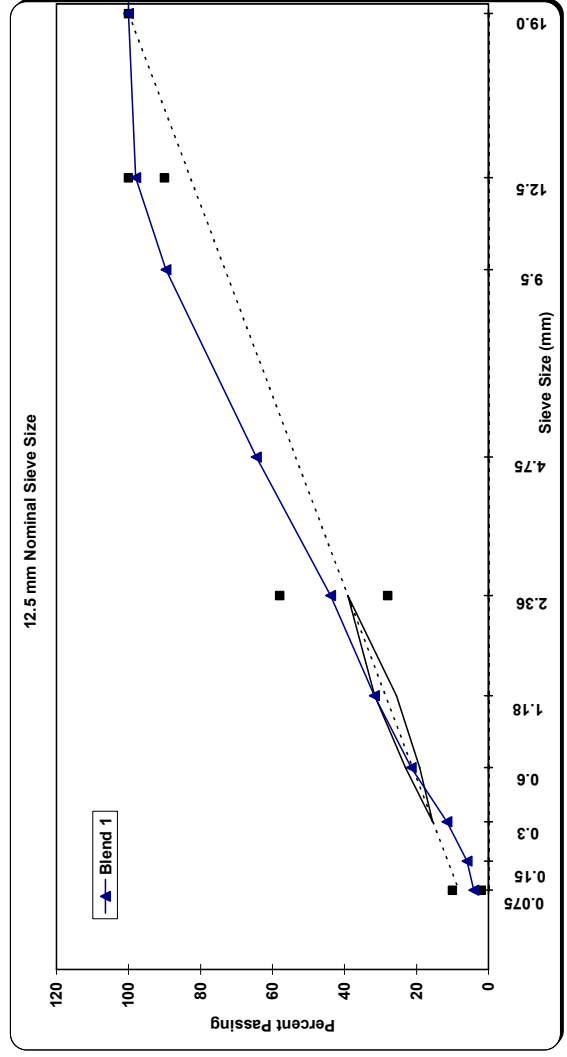
Project: Sheboygan County Plymouth WI STH 23

Project No.:	4840-02-71
Location:	Sheboygan County
Contractor:	Northeast Asphalt
Traffic Volume (ESALs):	10,000,000
NMAS (mm):	12.5
Mix Type:	Dense
Date:	6/8/2004
G_{se}	2.812
G_{sb}	2.768
G_{sa}	2.838
Absorption (%)	0.9
Sand Equivalency (%)	83.7
Flat & Elongated (%)	1.0
NAA	
1 Face Crush (%)	97.0
2 Face Crush (%)	95.0

Temperatures:

Mixing:	N/A
Compacting:	155

Sieve Size in (mm)	5/8x1/2 Chip	1/2x1/4 Chip	Wash Man Sand	Wash Nat Sand	1/4" Screen	Agg Source 6	Agg Source 7	Mix
1 (25)	100.0	100.0	100.0	100.0	100.0			100.0
3/4 (19)	100.0	100.0	100.0	100.0	100.0			100.0
1/2 (12.5)	80.8	100.0	100.0	100.0	100.0			97.9
3/8 (9.5)	14.8	93.9	100.0	100.0	100.0			89.9
#4 (4.75)	2.6	18.1	90.9	90.2	93.7			72.5
#8 (2.36)	2.1	3.4	52.6	72.1	69.7			45.3
#16 (1.18)	2.0	2.8	36.4	54.1	53.8			32.5
#30 (0.60)	1.9	2.6	24.3	37.5	44.7			22.6
#50 (0.30)	1.9	2.5	15.3	19.0	37.4			14.2
#100 (0.15)	1.8	2.3	7.6	5.4	29.1			7.3
#200 (0.075)	1.8	2.1	4.0	2.3	20.4			4.2
Percentages	11%	12%	55%	16%	6%			100%

Asphalt & Additives:

Asphalt Source:	Amoco
Asphalt Grade (PG):	64-22
Asphalt Content (%):	4.9
Specific Gravity:	1.029
Asphalt Additives:	None
Asphalt Additives (%):	N/A

Compactive Effort:

N_{ini}:	8
N_{des}:	100
N_{max}:	160
$\%G_{mm}$ @ N_{ini}:	87.7
$\%G_{mm}$ @ N_{max}:	97
C.F.:	1.020

Volumetrics:

VMA @ N_{des}:	14.5
VFA @ N_{des}:	72.4
AV @ N_{des}:	4.0
F/P_{be}:	1.0
P_{be} (%):	4.2

12.5 mm Nominal Sieve Size — Blend 1

Project: Racine County Racine WI

Project No.:	3230-06-60							
Location:	Racine County							
Contractor:	Payne & Dolan							
Traffic Volume (ESALs):	10,000,000							
NMAS (mm):	12.5							
Mix Type:	Dense							
Date:	10/14/2004							
G_{se}	2.723							
G_{sb}	2.671							
G_{sa}	2.795							
Absorption (%)	1.7							
Sand Equivalency (%)	93.0							
Flat & Elongated (%)	1.0							
NAA	45.1							
1 Face Crush (%)	95.8							
2 Face Crush (%)	95.0							

Temperatures:

Mixing:	N/A
Compacting:	160

Sieve Size in (mm):	RAP (3.52% AC)	5/8" Chip	3/8" Chip	Mfg'd Sand	Nat Sand	Agg Source 6	Agg Source 7	Mix
1 (25)	100.0	100.0	100.0	100.0	100.0			100.0
3/4 (19)	100.0	100.0	100.0	100.0	100.0			100.0
1/2 (12.5)	96.5	82.2	100.0	100.0	100.0			97.2
3/8 (9.5)	87.5	33.6	97.9	100.0	100.0			89.1
#4 (4.75)	67.7	4.6	26.2	97.1	86.7			69.2
#8 (2.36)	51.8	3.6	7.6	63.7	69.7			46.8
#16 (1.18)	40.6	3.3	6.5	34.4	52.9			29.2
#30 (0.60)	31.5	3.1	6.1	16.8	32.9			16.8
#50 (0.30)	22.3	3.0	5.7	8.0	12.6			8.4
#100 (0.15)	15.4	2.9	5.3	4.5	6.3			5.2
#200 (0.075)	12.2	2.7	4.5	3.2	4.9			4.1
Percentages	5%	15%	15%	47%	18%			100%

Asphalt & Additives:

Asphalt Source:	CRM Milwaukee
Asphalt Grade (PG):	64-28
Asphalt Content (%):	5.8
Specific Gravity:	1.029
Asphalt Additives:	Polymer
Asphalt Additives (%):	N/A

Compactive Effort:

N_{ini}:	8
N_{des}:	100
N_{max}:	160
%G_{mm} @ N_{ini}:	87.3
%G_{mm} @ N_{max}:	97.4
CF:	1.020

Volumetrics:

VMA @ N_{des}:	15.5
VFA @ N_{des}:	74.2
AV @ N_{des}:	4.0
F/P$_{be}$:	0.8
P_{be} (%):	5.1

12.5 mm Nominal Sieve Size

Project: Jackson County Northfield WI I-94 Westbound Northfield to Osseo

Project No.:	1023-04-12
Location:	Jackson County
Contractor:	Mathy - Milestone
Traffic Volume (ESALs):	10,000,000
NMAS (mm):	12.5
Mix Type:	Open
Date:	10/1/2004
G_{se}	2.719
G_{sb}	2.694
G_{sa}	N/A
Absorption (%)	0.6
Sand Equivalency (%)	68.0
Flat & Elongated (%)	18.8
NAA	46.1
1 Face Crush (%)	100.0
2 Face Crush (%)	99.8

Temperatures:	
Mixing:	N/A
Compacting:	155

Sieve Size in (mm):	5/8x3/8 Rock	3/8 Minus Rock	3/8" Chip	Fly Ash	Agg Source 5	Agg Source 6	Agg Source 7	Mix
1 (25)	100.0	100.0	100.0	100.0				100.0
3/4 (19)	100.0	100.0	100.0	100.0				100.0
1/2 (12.5)	89.0	100.0	100.0	100.0				92.4
3/8 (9.5)	48.0	100.0	100.0	100.0				64.1
#4 (4.75)	6.9	76.0	41.0	100.0				26.2
#8 (2.36)	4.3	51.0	8.2	100.0				17.5
#16 (1.18)	3.5	35.0	2.6	100.0				14.3
#30 (0.60)	3.0	24.0	1.2	100.0				12.3
#50 (0.30)	2.5	17.0	0.8	99.0				11.0
#100 (0.15)	2.0	12.0	0.6	97.0				9.8
#200 (0.075)	1.5	8.0	0.3	91.0				8.5
Percentages	69%	13%	11%	7%				100%

Asphalt & Additives:

Asphalt Source:	MIF-LaCrosse
Asphalt Grade (PG):	70-22
Asphalt Content (%):	5.9
Specific Gravity:	1.029
Asphalt Additives:	None
Asphalt Additives (%):	N/A

Compactive Effort:

N_{ini}:	8
N_{des}:	100
N_{max}:	160
%G_{mm} @ N_{ini}:	85.8
%G_{mm} @ N_{max}:	96.8
CF:	1.020

Volumetrics:

VMA @ N_{des}:	16.9
VFA @ N_{des}:	76.3
AV @ N_{des}:	4.0
F/P_{be}:	1.5
P_{be} (%):	5.5

12.5 mm Nominal Sieve Size

Project: Sheboygan County Cascade WI STH32

Project No.:	4540-14-71
Location:	Sheboygan County
Contractor:	B. R. Amon
Traffic Volume (ESALs):	1,000,000
NMAS (mm):	19.0
Mix Type:	Dense
Date:	8/5/2004
G_{se}	2.759
G_{sb}	2.721
G_{sa}	N/A
Absorption (%)	1.3
Sand Equivalency (%)	89.0
Flat & Elongated (%)	2.1
NAA	42.4
1 Face Crush (%)	71.0
2 Face Crush (%)	0.0

Temperatures:	
Mixing:	N/A
Compacting:	143

Sieve Size in (mm):	RAP (4.1%)	7/8" Stone	5/8" Stone	3/8" Stone	Sand	Dust	Agg Source 7	Mix
1 (25)	100.0	100.0	100.0	100.0	100.0	100.0		100.0
3/4 (19)	100.0	97.3	100.0	100.0	100.0	100.0		99.8
1/2 (12.5)	97.9	3.2	59.0	100.0	100.0	100.0		88.8
3/8 (9.5)	92.6	1.7	9.4	87.6	99.7	100.0		81.7
#4 (4.75)	72.5	1.4	2.2	5.0	88.0	91.0		64.0
#8 (2.36)	54.6	1.3	1.8	2.0	71.7	59.4		49.1
#16 (1.18)	41.1	1.2	1.7	1.9	55.6	40.6		37.1
#30 (0.60)	31.9	1.2	1.6	1.8	35.3	30.9		25.4
#50 (0.30)	23.4	1.1	1.6	1.8	12.0	24.1		12.8
#100 (0.15)	16.3	1.1	1.5	1.7	3.2	18.1		6.9
#200 (0.075)	12.0	0.9	1.2	1.4	1.7	13.0		4.8
Percentages	15%	7%	10%	9%	44%	15%		100%

Asphalt & Additives:

|	
Asphalt Source:	Amoco
Asphalt Grade (PG):	58-28
Asphalt Content (%):	4.4
Specific Gravity:	1.026
Asphalt Additives:	None
Asphalt Additives (%):	N/A

Compactive Effort:

N_{ini}:	7
N_{des}:	60
N_{max}:	75
%G_{mm} @ N_{ini}:	90.3
%G_{mm} @ N_{max}:	96.4
CF:	1.020

Volumetrics:

VMA @ N_{des}:	13.4
VFA @ N_{des}:	70.9
AV @ N_{des}:	4.0
F/P$_{be}$:	1.2
P_{be} (%):	3.9

19.0 mm Nominal Sieve Size

Blend 1

Project: Lincoln County Bloomville WI STH 17

Project No.:	9030-08-70
Location:	Lincoln County
Contractor:	American Asphalt
Traffic Volume (ESALs):	1,000,000
NMAS (mm):	19.0
Mix Type:	Dense
Date:	8/26/2004
G_{se}	2.742
G_{sb}	2.696
G_{sa}	2.742
Absorption (%)	1.2
Sand Equivalency (%)	49.0
Flat & Elongated (%)	1.8
NAA	42.2
1 Face Crush (%)	71.0
2 Face Crush (%)	69.4

Temperatures:

Mixing:	N/A
Compacting:	143

Sieve Size in (mm):	3/4" Rock	Blend Sand	Agg Source 3	Agg Source 4	Agg Source 5	Agg Source 6	Agg Source 7	Mix
1 (25)	100.0	100.0						100.0
3/4 (19)	98.0	100.0						99.2
1/2 (12.5)	70.0	99.0						87.4
3/8 (9.5)	52.0	92.0						76.0
#4 (4.75)	32.0	72.0						56.0
#8 (2.36)	22.0	56.0						42.4
#16 (1.18)	17.0	40.0						30.8
#30 (0.60)	13.0	26.0						20.8
#50 (0.30)	7.0	14.0						11.2
#100 (0.15)	5.0	8.0						6.8
#200 (0.075)	3.5	5.8						4.9
Percentages	40%	60%						100%

Asphalt & Additives:

Asphalt Source:	MIF-LaCrosse
Asphalt Grade (PG):	58-34
Asphalt Content (%):	4.8
Specific Gravity:	1.028
Asphalt Additives:	None
Asphalt Additives (%):	N/A

Compactive Effort:

N_{ini}:	7
N_{des}:	60
N_{max}:	75
%G_{mm} @ N_{ini}:	89.6
%G_{mm} @ N_{max}:	96.2
CF:	1.020

Volumetrics:

VMA @ N_{des}:	13.9
VFA @ N_{des}:	71.2
AV @ N_{des}:	4.0
F/P$_{be}$:	1.2
P_{be} (%):	4.1

19.0 mm Nominal Sieve Size

Legend: Blend 1

X-axis: Sieve Size (mm) — 0.075, 0.15, 0.3, 0.6, 1.18, 2.36, 4.75, 9.5, 12.5, 19.0, 25.0

Y-axis: Percent Passing — 0 to 120

Project: Douglas County Brule WI CTH 13

Project No.:	8510-14-71
Location:	Douglas County
Contractor:	Northwoods Paving
Traffic Volume (ESALs):	300,000
NMAS (mm):	19.0
Mix Type:	Dense
Date:	9/9/2004
G_{se}	2.811
G_{sb}	2.772
G_{sa}	2.811
Absorption (%)	0.9
Sand Equivalency (%)	71.0
Flat & Elongated (%)	2.0
NAA	42.4
1 Face Crush (%)	96.3
2 Face Crush (%)	96.1

Temperatures:

Mixing:	N/A
Compacting:	143

Sieve Size in (mm):	15/16 Rock	3/8 Minus	Nat Sand	RAP (4.4% AC)	Agg Source 5	Agg Source 6	Agg Source 7	Mix
1 (25)	100.0	100.0	100.0	100.0				100.0
3/4 (19)	92.0	100.0	100.0	100.0				97.4
1/2 (12.5)	43.0	100.0	99.0	93.0				79.9
3/8 (9.5)	19.0	100.0	98.0	88.0				70.9
#4 (4.75)	2.0	68.0	96.0	69.0				53.9
#8 (2.36)	1.8	40.0	94.0	57.0				44.5
#16 (1.18)	1.7	26.0	91.0	45.0				38.4
#30 (0.60)	1.6	16.0	78.0	32.0				30.4
#50 (0.30)	1.5	11.0	42.0	21.0				17.7
#100 (0.15)	1.4	7.6	9.0	13.0				6.7
#200 (0.075)	1.0	5.0	2.0	9.0				3.5
Percentages	33%	25%	27%	15%				100%

Compactive Effort:

N_{ini}:	6
N_{des}:	40
N_{max}:	60
%G_{mm} @ N_{ini}:	91.2
%G_{mm} @ N_{max}:	96.8
CF:	1.020

Asphalt & Additives:

Asphalt Source:	Murphy
Asphalt Grade (PG):	58-28
Asphalt Content (%):	5.4
Specific Gravity:	1.03
Asphalt Additives:	None
Asphalt Additives (%):	N/A

Volumetrics:

VMA @ N_{des}:	15.8
VFA @ N_{des}:	74.6
AV @ N_{des}:	4.0
F/P_{be}:	0.7
P_{be} (%):	4.9

19.0 mm Nominal Sieve Size

Blend 1

Project:	Dane County Waunakee WI STH 113									
Project No.:	5992-04-14	Sieve Size in (mm):	5/8" Chip	3/8" Chip	1/4" Screenings	Man Sand	Nat Sand	RAP	Agg Source 7	Mix
Location:	Dane County	1 (25)	100.0	100.0	100.0	100.0	100.0	100.0		100.0
Contractor:	Payne & Dolan	3/4 (19)	99.3	100.0	100.0	100.0	100.0	100.0		99.9
Traffic Volume (ESALs):	3,000,000	1/2 (12.5)	40.0	95.3	99.8	100.0	100.0	98.3		89.6
NMAS (mm):	19.0	3/8 (9.5)	16.8	74.7	99.3	99.1	100.0	87.8		81.9
Mix Type:	Dense	#4 (4.75)	5.0	13.1	83.3	77.9	99.5	65.7		62.1
Date:	6/30/2004	#8 (2.36)	4.2	7.3	63.6	48.8	84.6	51.3		46.1
G_{se}	2.737	#16 (1.18)	4.0	6.4	50.7	28.1	70.7	42.1		34.5
G_{sb}	2.648	#30 (0.60)	3.9	6.1	42.7	16.2	59.3	36.0		26.9
G_{sa}	2.765	#50 (0.30)	3.7	5.7	34.6	7.8	32.4	25.6		16.0
Absorption (%)	1.6	#100 (0.15)	3.3	4.8	25.1	4.5	8.4	16.1		7.3
Sand Equivalency (%)	80.0	#200 (0.075)	2.5	3.5	15.3	2.5	1.9	10.7		3.8
Flat & Elongated (%)	0.0	Percentages	16%	14%	5%	31%	26%	8%		100%
NAA	43.9									
1 Face Crush (%)	100.0									
2 Face Crush (%)	100.0									

Temperatures:

Mixing:	N/A
Compacting:	142

Asphalt & Additives:

Asphalt Source:	Koch
Asphalt Grade (PG):	58-28
Asphalt Content (%):	5.11
Specific Gravity:	1.032
Asphalt Additives:	None
Asphalt Additives (%):	N/A

Compactive Effort:

N_{ini} :	7
N_{des} :	75
N_{max} :	115
%G_{mm} @ N_{ini} :	89.7
%G_{mm} @ N_{max} :	96.7
CF:	1.020

Volumetrics:

VMA @ N_{des} :	13.2
VFA @ N_{des} :	69.6
AV @ N_{des} :	4.0
F/P$_{be}$:	1.1
P$_{be}$ (%):	3.9

19.0 mm Nominal Sieve Size

Project: Marathon County Mosinee WI USH 51

Sieve Size in (mm):	3/4" Rock	3/8" Rock	3/16 Screen	Blend Sand	Man Sand	RAP (4.0% AC)	Agg Source 7	Mix
1 (25)	100.0	100.0	100.0	100.0	100.0	100.0		100.0
3/4 (19)	98.0	100.0	100.0	100.0	100.0	100.0		99.4
1/2 (12.5)	61.0	100.0	100.0	99.0	100.0	97.0		87.8
3/8 (9.5)	29.0	100.0	100.0	98.0	100.0	90.0		77.3
#4 (4.75)	6.6	29.0	97.0	94.0	100.0	73.0		60.5
#8 (2.36)	3.8	10.0	66.0	88.0	67.0	58.0		45.5
#16 (1.18)	2.9	5.6	42.0	77.0	43.0	47.0		34.3
#30 (0.60)	2.4	4.4	28.0	58.0	24.0	36.0		24.2
#50 (0.30)	2.1	3.5	17.0	10.0	10.0	18.0		8.8
#100 (0.15)	1.8	3.0	11.0	1.2	3.5	11.0		4.4
#200 (0.075)	1.5	2.4	10.0	0.7	1.5	8.0		3.4
Percentages	30%	10%	15%	20%	15%	10%		100%

Project No.:	6370-00-60
Location:	Marathon County
Contractor:	American - Mathy
Traffic Volume (ESALs):	3,000,000
NMAS (mm):	19.0
Mix Type:	Dense
Date:	7/7/2004
G_{se}	2.699
G_{sb}	2.649
G_{sa}	N/A
Absorption (%)	0.4
Sand Equivalency (%)	88.0
Flat & Elongated (%)	2.1
NAA	43.3
1 Face Crush (%)	97.1
2 Face Crush (%)	97.0

Temperatures:

Mixing:	N/A
Compacting:	143

Asphalt & Additives:

Asphalt Source:	MIF-LaCrosse
Asphalt Grade (PG):	58-28
Asphalt Content (%):	5.0
Specific Gravity:	1.029
Asphalt Additives:	None
Asphalt Additives (%):	N/A

Compactive Effort:

N_{ini}:	7
N_{des}:	75
N_{max}:	115
$\%G_{mm}$ @ N_{ini}:	90.1
$\%G_{mm}$ @ N_{max}:	96.5
CF:	1.020

Volumetrics:

VMA @ N_{des}:	14.9
VFA @ N_{des}:	73.1
AV @ N_{des}:	4.0
F/P_{be}:	0.7
P_{be} (%):	4.3

19.0 mm Nominal Sieve Size

Blend 1

A-17

Project: Barron County Cumberland USH 63

Project No.:	1550-17-71
Location:	Barron County
Contractor:	Monarch Paving
Traffic Volume (ESALs):	3,000,000
NMAS (mm):	19.0
Mix Type:	Dense
Date:	9/9/2004
G_{se}	2.781
G_{sb}	2.738
G_{sa}	2.781
Absorption (%)	0.8
Sand Equivalency (%)	74.0
Flat & Elongated (%)	1.7
NAA	43.2
1 Face Crush (%)	63.3
2 Face Crush (%)	61.1

Temperatures:

Mixing:	N/A
Compacting:	143

Sieve Size in (mm):	7/8x3/8 Rock	5/8x3/8 Rock	Man Sand	Nat Sand	RAP (4.2%)	Agg Source 6	Agg Source 7	Mix
1 (25)	100.0	100.0	100.0	100.0	100.0			100.0
3/4 (19)	100.0	100.0	100.0	100.0	98.0			99.5
1/2 (12.5)	52.0	81.0	100.0	98.0	93.0			92.5
3/8 (9.5)	6.5	30.0	100.0	92.0	85.0			80.7
#4 (4.75)	1.2	2.4	67.0	77.0	68.0			60.2
#8 (2.36)	1.0	2.0	42.0	65.0	57.0			47.1
#16 (1.18)	1.0	1.0	28.0	50.0	46.0			35.7
#30 (0.60)	0.9	1.0	21.0	31.0	35.0			24.7
#50 (0.30)	0.9	1.0	14.0	11.0	21.0			12.6
#100 (0.15)	0.8	1.0	9.8	4.6	11.0			6.9
#200 (0.075)	0.8	1.0	6.5	3.1	7.6			4.7
Percentages	7%	9%	25%	34%	25%			100%

Compactive Effort:

N_{ini}:	7
N_{des}:	75
N_{max}:	115
%G_{mm} @ N_{ini}:	89.7
%G_{mm} @ N_{max}:	97.1
CF:	1.020

Asphalt & Additives:

Asphalt Source:	Koch
Asphalt Grade (PG):	58-28
Asphalt Content (%):	4.6
Specific Gravity:	1.03
Asphalt Additives:	None
Asphalt Additives (%):	N/A

Volumetrics:

VMA @ N_{des}:	13.5
VFA @ N_{des}:	70.3
AV @ N_{des}:	4.0
F/P_{be}:	1.2
P_{be} (%):	4

19.0 mm Nominal Sieve Size

Blend 1

Project: Langlade County Antigo WI City of Antigo

Project No.:	1605-04-70
Location:	Langlade County
Contractor:	Northeast Asphalt
Traffic Volume (ESALs):	10,000,000
NMAS (mm):	19.0
Mix Type:	Dense
Date:	6/15/2004
G_{se}	2.700
G_{sb}	2.688
G_{sa}	2.723
Absorption (%)	0.5
Sand Equivalency (%)	85.0
Flat & Elongated (%)	0.4
NAA	44.9
1 Face Crush (%)	93.8
2 Face Crush (%)	91.5

Temperatures:

Mixing:	N/A
Compacting:	143

Sieve Size in (mm):	3/4" Chip	5/8"x1/2" Chip	1/2"x1/4" Chip	1/4" Screenings	Man Sand	Screened Sand	Agg Source 7	Mix
1 (25)	100.0	100.0	100.0	100.0	100.0	100.0		100.0
3/4 (19)	97.9	100.0	100.0	100.0	100.0	100.0		99.7
1/2 (12.5)	41.8	83.4	100.0	100.0	100.0	100.0		89.6
3/8 (9.5)	13.2	27.6	85.8	100.0	100.0	99.5		78.2
#4 (4.75)	3.5	6.9	10.3	88.5	76.0	84.6		55.3
#8 (2.36)	2.6	5.1	6.0	60.4	44.7	68.1		43.2
#16 (1.18)	2.3	4.2	4.9	44.2	27.1	55.8		28.0
#30 (0.60)	2.2	3.8	4.2	33.3	17.0	37.2		19.1
#50 (0.30)	2.0	3.3	3.6	24.5	9.0	15.2		10.3
#100 (0.15)	1.7	2.7	3.0	15.7	3.7	6.4		5.4
#200 (0.075)	1.3	2.0	2.2	10.2	1.7	3.9		3.9
Percentages	15%	10%	10%	13%	28%	24%		100%

Asphalt & Additives:

Asphalt Source:	CRM Gladstone
Asphalt Grade (PG):	58-34
Asphalt Content (%):	4.3
Specific Gravity:	1.03
Asphalt Additives:	Polymer
Asphalt Additives (%):	N/A

Compactive Effort:

N_{ini}	8
N_{des}	100
N_{max}	160
%G_{mm} @ N_{ini}	89
%G_{mm} @ N_{max}	96.9
CF:	1.020

Volumetrics:

VMA @ N_{des}:	13.7
VFA @ N_{des}:	70.8
AV @ N_{des}:	4.0
F/P_{be}:	0.951219512
P_{be} (%):	4.1

19.0 mm Nominal Sieve Size

Percent Passing vs. Sieve Size (mm) — Blend 1

Project: Jackson County Northfield WI I-94 Westbound Northfield to Osseo

Project No.:	1023-04-12
Location:	Jackson County
Contractor:	Mathy - Milestone
Traffic Volume (ESALs):	30,000,000
NMAS (mm):	19.0
Mix Type:	Dense
Date:	9/29/2004
G_{se}	2.648
G_{sb}	2.635
G_{sa}	N/A
Absorption (%)	0.7
Sand Equivalency (%)	75.0
Flat & Elongated (%)	3.7
NAA	45.1
1 Face Crush (%)	100.0
2 Face Crush (%)	93.3

Temperatures:

Mixing:	N/A
Compacting:	155

Sieve Size in (mm):	7/8"x3/8" Rock	3/8" Minus Rock	Washed Sand	Agg Source 4	Agg Source 5	Agg Source 6	Agg Source 7	Mix
1 (25)	100.0	100.0	100.0					100.0
3/4 (19)	99.0	100.0	100.0					99.4
1/2 (12.5)	54.0	100.0	100.0					72.4
3/8 (9.5)	23.0	100.0	100.0					53.8
#4 (4.75)	1.2	76.0	100.0					33.5
#8 (2.36)	0.7	51.0	86.0					24.3
#16 (1.18)	0.6	35.0	78.0					18.7
#30 (0.60)	0.5	24.0	60.0					13.5
#50 (0.30)	0.5	16.0	26.0					7.7
#100 (0.15)	0.5	10.0	4.4					3.7
#200 (0.075)	0.4	8.0	1.4					2.8
Percentages	60%	30%	10%					100%

Asphalt & Additives:

Asphalt Source:	MIF-LaCrosse
Asphalt Grade (PG):	64-28
Asphalt Content (%):	4.5
Specific Gravity:	1.029
Asphalt Additives:	None
Asphalt Additives (%):	N/A

Compactive Effort:

N_{ini}:	8
N_{des}:	100
N_{max}:	160
%G_{mm} @ N_{ini}:	86.4
%G_{mm} @ N_{max}:	97.7
CF:	1.020

Volumetrics:

VMA @ N_{des}:	13.9
VFA @ N_{des}:	71.3
AV @ N_{des}:	4.0
F/P$_{be}$:	0.6
P$_{be}$ (%):	4.3

19.0 mm Nominal Sieve Size

Project: Oneida County Tomahawk USH 8 - Birchwood Drive STH 17

Project No.:	9040-05-70
Location:	Oneida County
Contractor:	American - Mathy
Traffic Volume (ESALs):	3,000,000
NMAS (mm):	25.0
Mix Type:	Open
Date:	6/16/2004
G_{se}	2.723
G_{sb}	2.693
G_{sa}	N/A
Absorption (%)	0.7
Sand Equivalency (%)	N/A
Flat & Elongated (%)	0.7
NAA	43.4
1 Face Crush (%)	80.1
2 Face Crush (%)	70.4

Temperatures:	
Mixing:	N/A
Compacting:	142

Sieve Size in (mm):	3/4" Gravel	Blend Sand	RAP (3.8%AC)	Agg Source 4	Agg Source 5	Agg Source 6	Agg Source 7	Mix
1 (25)	100.0	100.0	100.0					100.0
3/4 (19)	72.0	100.0	98.0					81.3
1/2 (12.5)	9.5	99.0	89.0					38.3
3/8 (9.5)	6.0	94.0	83.0					34.1
#4 (4.75)	5.3	81.0	69.0					28.8
#8 (2.36)	5.0	69.0	57.0					24.4
#16 (1.18)	4.8	55.0	47.0					20.4
#30 (0.60)	4.5	39.0	39.0					16.6
#50 (0.30)	3.3	17.0	24.0					9.8
#100 (0.15)	2.1	7.5	13.0					5.4
#200 (0.075)	1.4	4.0	9.0					3.6
Percentages	65%	10%	25%					100%

Asphalt & Additives:

Asphalt Source:	MIF-LaCrosse
Asphalt Grade (PG):	58-28
Asphalt Content (%):	3.4
Specific Gravity:	1.029
Asphalt Additives:	None
Asphalt Additives (%):	N/A

Compactive Effort:

N_{ini}:	7
N_{des}:	75
N_{max}:	115
%G_{mm} @ N_{ini}:	87.6
%G_{mm} @ N_{max}:	96.6
CF:	1.020

Volumetrics:

VMA @ N_{des}:	11.2
VFA @ N_{des}:	64.3
AV @ N_{des}:	4.0
F/P_{be}:	1.2
P_{be} (%):	3.0

25.0 mm Nominal Sieve Size

Blend 1

A-21
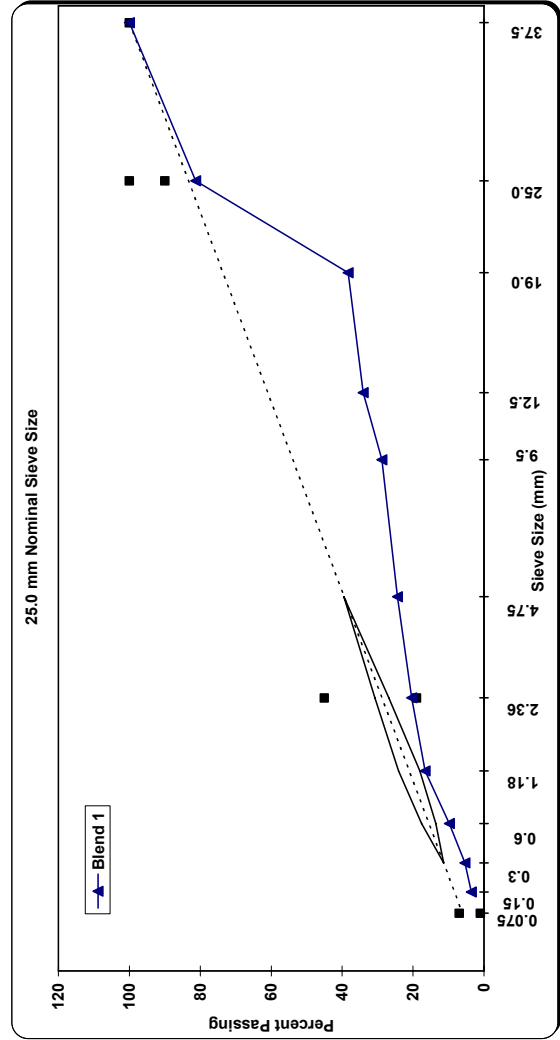
APPENDIX B SPECIMEN VOLUMETRICS BEFORE SAWING/CORING

Project	Specimen ID	Compacted	AC%	Target AV%	Bulk Specific Gravity					MTSG	Done	Air Voids	Gry. Ht.	Gmb Est.	Actual Corr. Fac.
					Dry Wt.	Submerged Wt.	SSD Wt.	BSG	Done						
Sauk Cty Baraboo 12.5mm E-0.3	BAR-OP-7.0-12.5-E0.3-A	√	-	7.0	6792.8	3859.2	6801.3	2.309	√	2.486	√	7.1	168.4	2.283	1.011
	BAR-OP-7.0-12.5-E0.3-B	√	-	7.0	6796.2	3861.2	6812.3	2.303	√	2.486	√	7.4	169.0	2.276	1.012
	BAR-OP-7.0-12.5-E0.3-C	√	-	7.0	6794.6	3866.3	6805.8	2.311	√	2.486	√	7.0	168.3	2.285	1.012
	BAR-OP-7.0-12.5-E0.3-D	√	-	7.0	6794.7	3863.3	6809	2.307	√	2.486	√	7.2	168.8	2.278	1.013
	BAR-OP-7.0-12.5-E0.3-E	√	-	7.0	6803.1	3865.5	6815.9	2.306	√	2.486	√	7.2	168.9	2.279	1.012
	BAR-OP-7.0-12.5-E0.3-F	√	-	7.0	6800.3	3864.4	6812.9	2.306	√	2.486	√	7.2	168.9	2.278	1.012
	BAR-OP-4.0-12.5-E0.3-A	√	-	4.0	7047.9	4080.1	7055.3	2.369	√	2.486	√	4.7	170.2	2.343	1.011
	BAR-OP-4.0-12.5-E0.3-B	√	-	4.0	7050.3	4078.2	7054.9	2.368	√	2.486	√	4.7	170.4	2.341	1.012
	BAR-OP-4.0-12.5-E0.3-C	√	-	4.0	7050.9	4084.9	7056.5	2.373	√	2.486	√	4.5	170.4	2.342	1.013
	BAR-OP-4.0-12.5-E0.3-D	√	-	4.0	7046	4082.2	7053.8	2.371	√	2.486	√	4.6	170.3	2.341	1.013
	BAR-OP-4.0-12.5-E0.3-E	√	-	4.0	7048.8	4082.1	7054	2.372	√	2.486	√	4.6	170.2	2.344	1.012
	BAR-OP-4.0-12.5-E0.3-F	√	-	4.0	7054.5	4083.6	7059.9	2.370	√	2.486	√	4.6	170.4	2.343	1.012
	BAR-OP-10.0-12.5-E0.3-A	√	-	10.0	6587.6	3709	6617.4	2.265	√	2.486	√	8.9	167.1	2.231	1.015
	BAR-OP-10.0-12.5-E0.3-B	√	-	10.0	6606	3699.8	6629.3	2.255	√	2.486	√	9.3	167.9	2.226	1.013
	BAR-OP-10.0-12.5-E0.3-C	√	-	10.0	6611.5	3717.8	6637.3	2.265	√	2.486	√	8.9	167.4	2.235	1.013
	BAR-OP-10.0-12.5-E0.3-D	√	-	10.0	6602.2	3698	6628.7	2.253	√	2.486	√	9.4	168.0	2.224	1.013
	BAR-OP-10.0-12.5-E0.3-E	√	-	10.0	6598.6	3714.7	6628	2.265	√	2.486	√	8.9	167.3	2.232	1.015
	BAR-OP-10.0-12.5-E0.3-F	√	-	10.0	6607.9	3704.3	6643.3	2.248	√	2.486	√	9.6	168.6	2.218	1.014
	BAR-BU-7.0-12.5-E0.3-A	√	+0.3	7.0	6741.9	3823.5	6754.2	2.300	√	2.474	√	7.0	168.1	2.270	1.014
	BAR-BU-7.0-12.5-E0.3-B	√	+0.3	7.0	6723.3	3813.8	6735.5	2.301	√	2.474	√	7.0	167.5	2.271	1.013
	BAR-BU-7.0-12.5-E0.3-C	√	+0.3	7.0	6777.8	3849.6	6792.1	2.303	√	2.474	√	6.9	169.8	2.259	1.020
	BAR-BU-7.0-12.5-E0.3-D	√	+0.3	7.0	6768.3	3851.3	6782.4	2.309	√	2.474	√	6.7	168.1	2.278	1.013
	BAR-BU-7.0-12.5-E0.3-E	√	+0.3	7.0	6767.6	3847.4	6782.4	2.306	√	2.474	√	6.8	168.6	2.271	1.015
	BAR-BU-7.0-12.5-E0.3-F	√	+0.3	7.0	6756.3	3847.4	6771.9	2.310	√	2.474	√	6.6	167.9	2.277	1.015

Project	Specimen ID	Compacted	AC%	Target AV%	Bulk Specific Gravity					MTSG	Done	Air Voids	Gry. Ht.	Gmb Est.	Actual Corr. Fac.
					Dry Wt.	Submerged Wt.	SSD Wt.	BSG	Done						
Taylor Cty Medford 12.5mm E-1	MED-OP-7.0-12.5-E1-A	√	-	7.0	6850.1	3928.2	6879.4	2.321	√	2.502	√	7.2	168.7	2.298	1.010
	MED-OP-7.0-12.5-E1-B	√	-	7.0	6841.2	3921.2	6870.6	2.320	√	2.502	√	7.3	168.4	2.299	1.009
	MED-OP-7.0-12.5-E1-C	√	-	7.0	6843.9	3930.3	6875	2.324	√	2.502	√	7.1	168.4	2.300	1.011
	MED-OP-7.0-12.5-E1-D	√	-	7.0	6844.9	3940.1	6883.3	2.326	√	2.502	√	7.1	168.6	2.297	1.012
	MED-OP-7.0-12.5-E1-E	√	-	7.0	6847.4	3943.8	6887.8	2.326	√	2.502	√	7.0	168.5	2.300	1.011
	MED-OP-7.0-12.5-E1-F	√	-	7.0	6846.5	3937.6	6877.8	2.329	√	2.502	√	6.9	169.4	2.287	1.018
	MED-OP-4.0-12.5-E1-A	√	-	4.0	7066.1	4122.5	7075.2	2.393	√	2.502	√	4.4	168.5	2.373	1.008
	MED-OP-4.0-12.5-E1-B	√	-	4.0	7069.6	4118.3	7076.3	2.390	√	2.502	√	4.5	168.4	2.376	1.006
	MED-OP-4.0-12.5-E1-C	√	-	4.0	7064.9	4123.4	7074.6	2.394	√	2.502	√	4.3	168.8	2.368	1.011
	MED-OP-4.0-12.5-E1-D	√	-	4.0	7064.6	4123.7	7075.8	2.393	√	2.502	√	4.4	168.9	2.367	1.011
	MED-OP-4.0-12.5-E1-E	√	-	4.0	7075.7	4132.4	7083.6	2.398	√	2.502	√	4.2	168.7	2.373	1.010
	MED-OP-4.0-12.5-E1-F	√	-	4.0	7071.1	4123.5	7079.4	2.392	√	2.502	√	4.4	168.9	2.369	1.010
	MED-OP-10.0-12.5-E1-A	√	-	10.0	6617.4	3778.2	6718.1	2.251	√	2.502	√	10.0	168.7	2.220	1.014
	MED-OP-10.0-12.5-E1-B	√	-	10.0	6617	3768.8	6705.8	2.253	√	2.502	√	10.0	168.4	2.224	1.013
	MED-OP-10.0-12.5-E1-C	√	-	10.0	6616.8	3772.8	6704.8	2.257	√	2.502	√	9.8	168.4	2.223	1.015
	MED-OP-10.0-12.5-E1-D	√	-	10.0	6627.2	3785.2	6719.4	2.259	√	2.502	√	9.7	168.6	2.224	1.015
	MED-OP-10.0-12.5-E1-E	√	-	10.0	6617.3	3789.4	6709.5	2.266	√	2.502	√	9.4	168.5	2.222	1.020
	MED-OP-10.0-12.5-E1-F	√	-	10.0	6617.1	3785.7	6726.4	2.250	√	2.502	√	10.1	169.4	2.210	1.018
	MED-BU-7.0-12.5-E1-A	√	+0.3	7.0	6784.2	3888.6	6817.1	2.317	√	2.489	√	6.9	168.5	2.278	1.017
	MED-BU-7.0-12.5-E1-B	√	+0.3	7.0	6791.3	3880.6	6815.8	2.314	√	2.489	√	7.0	168.4	2.282	1.014
	MED-BU-7.0-12.5-E1-C	√	+0.3	7.0	6815	3905.6	6839.7	2.323	√	2.489	√	6.7	168.8	2.285	1.017
	MED-BU-7.0-12.5-E1-D	√	+0.3	7.0	6807.6	3899.7	6834.7	2.319	√	2.489	√	6.8	168.9	2.281	1.017
	MED-BU-7.0-12.5-E1-E	√	+0.3	7.0	6819	3909.8	6845.8	2.323	√	2.489	√	6.7	168.7	2.287	1.015
	MED-BU-7.0-12.5-E1-F	√	+0.3	7.0	6815.1	3909.6	6847.5	2.320	√	2.489	√	6.8	168.9	2.283	1.016

Project	Specimen ID	Compacted	AC%	Target AV%	Bulk Specific Gravity					MTSG	Done	Air Voids	Gry. Ht.	Gmb Est.	Actual Corr. Fac.
					Dry Wt.	Submerged Wt.	SSD Wt.	BSG	Done						
Waushara Cty Wautoma 12.5mm E-1	OMA-OP-7.0-12.5-E1-A	✓	-	7.0	6946.1	3985.5	6960.3	2.335	✓	2.532	✓	7.8	169.8	2.315	1.009
	OMA-OP-7.0-12.5-E1-B	✓	-	7.0	6939.4	3990.8	6956.9	2.340	✓	2.532	✓	7.6	169.5	2.317	1.010
	OMA-OP-7.0-12.5-E1-C	✓	-	7.0	6939.5	3997.6	6957.3	2.345	✓	2.532	✓	7.4	169.3	2.320	1.011
	OMA-OP-7.0-12.5-E1-D	✓	-	7.0	6939	3985	6957.1	2.335	✓	2.532	✓	7.8	169.4	2.318	1.007
	OMA-OP-7.0-12.5-E1-E	✓	-	7.0	6934.2	3990.1	6956.7	2.337	✓	2.532	✓	7.7	169.6	2.314	1.010
	OMA-OP-7.0-12.5-E1-F	✓	-	7.0	6935.7	3991.8	6955.9	2.340	✓	2.532	✓	7.6	169.5	2.316	1.011
	OMA-OP-4.0-12.5-E1-A	✓	-	4.0	7162	4190.9	7166.4	2.407	✓	2.532	✓	4.9	169.9	2.385	1.009
	OMA-OP-4.0-12.5-E1-B	✓	-	4.0	7160.5	4197.4	7165.6	2.412	✓	2.532	✓	4.7	169.9	2.385	1.012
	OMA-OP-4.0-12.5-E1-C	✓	-	4.0	7162.5	4196.4	7167.6	2.411	✓	2.532	✓	4.8	169.8	2.387	1.010
	OMA-OP-4.0-12.5-E1-D	✓	-	4.0	7157.2	4190.6	7161.5	2.409	✓	2.532	✓	4.8	169.7	2.387	1.009
	OMA-OP-4.0-12.5-E1-E	✓	-	4.0	7160.5	4197	7166.3	2.412	✓	2.532	✓	4.7	169.8	2.386	1.011
	OMA-OP-4.0-12.5-E1-F	✓	-	4.0	7160.2	4196.5	7165.4	2.412	✓	2.532	✓	4.7	169.8	2.386	1.011
	OMA-OP-10.0-12.5-E1-A	✓	-	10.0	6721.2	3824.5	6764	2.287	✓	2.532	✓	9.7	168.3	2.260	1.012
	OMA-OP-10.0-12.5-E1-B	✓	-	10.0	6715.9	3822.3	6775.4	2.274	✓	2.532	✓	10.2	169.2	2.246	1.013
	OMA-OP-10.0-12.5-E1-C	✓	-	10.0	6712.3	3802.2	6758.8	2.270	✓	2.532	✓	10.3	169.0	2.248	1.010
	OMA-OP-10.0-12.5-E1-D	✓	-	10.0	6717.2	3795.9	6768.8	2.259	✓	2.532	✓	10.8	169.8	2.239	1.009
	OMA-OP-10.0-12.5-E1-E	✓	-	10.0	6717.2	3791	6766.3	2.258	✓	2.532	✓	10.8	170.1	2.235	1.010
	OMA-OP-10.0-12.5-E1-F	✓	-	10.0	6713.9	3823.3	6779.6	2.271	✓	2.532	✓	10.3	169.5	2.241	1.013
	OMA-BU-7.0-12.5-E1-A	✓	+0.3	7.0	6903.5	3965.6	6921.8	2.335	✓	2.521	✓	7.4	169.3	2.307	1.012
	OMA-BU-7.0-12.5-E1-B	✓	+0.3	7.0	6903.8	3970.3	6920.1	2.340	✓	2.521	✓	7.2	169.0	2.312	1.012
	OMA-BU-7.0-12.5-E1-C	✓	+0.3	7.0	6910.7	3973.4	6931.2	2.336	✓	2.521	✓	7.3	169.3	2.310	1.011
	OMA-BU-7.0-12.5-E1-D	✓	+0.3	7.0	6921	3973.2	6938.4	2.334	✓	2.521	✓	7.4	169.5	2.311	1.010
	OMA-BU-7.0-12.5-E1-E	✓	+0.3	7.0	6926.1	3974.2	6942.8	2.333	✓	2.521	✓	7.5	169.7	2.310	1.010
	OMA-BU-7.0-12.5-E1-F	✓	+0.3	7.0	6928.9	3980.4	6945.6	2.337	✓	2.521	✓	7.3	169.7	2.311	1.011

Project: **Iron Cty Hurley 12.5mm E-3**

Specimen ID	Compacted	AC%	Target AV%	Bulk Specific Gravity					MTSG	Done	Air Voids	Gry. Ht.	Gmb Est.	Actual Corr. Fac.
				Dry Wt.	Submerged Wt.	SSD Wt.	BSG	Done						
HUR-OP-7.0-12.5-E0.3-A	✓	-	7.0	6813.6	3913.2	6841.4	2.327	✓	2.498	✓	6.9	168.3	2.291	1.016
HUR-OP-7.0-12.5-E0.3-B	✓	-	7.0	6826.4	3907	6851.5	2.318	✓	2.498	✓	7.2	169.1	2.284	1.015
HUR-OP-7.0-12.5-E0.3-C	✓	-	7.0	6830.1	3916.3	6865.3	2.316	✓	2.498	✓	7.3	169.2	2.284	1.014
HUR-OP-7.0-12.5-E0.3-D	✓	-	7.0	6828.9	3909.5	6854.3	2.319	✓	2.498	✓	7.2	169.0	2.287	1.014
HUR-OP-7.0-12.5-E0.3-E	✓	-	7.0	6827.3	3909.1	6852	2.320	✓	2.498	✓	7.1	169.0	2.286	1.015
HUR-OP-7.0-12.5-E0.3-F	✓	-	7.0	6830	3919.2	6859.8	2.323	✓	2.498	✓	7.0	169.1	2.286	1.016
HUR-OP-4.0-12.5-E0.3-A	✓	-	4.0	7045.6	4100.9	7053.4	2.386	✓	2.498	✓	4.5	169.4	2.354	1.014
HUR-OP-4.0-12.5-E0.3-B	✓	-	4.0	7049.3	4108.4	7055.1	2.392	✓	2.498	✓	4.2	169.4	2.355	1.016
HUR-OP-4.0-12.5-E0.3-C	✓	-	4.0	7039.6	4096.7	7044.8	2.388	✓	2.498	✓	4.4	169.2	2.354	1.014
HUR-OP-4.0-12.5-E0.3-D	✓	-	4.0	7049.9	4106.4	7055.5	2.391	✓	2.498	✓	4.3	169.2	2.358	1.014
HUR-OP-4.0-12.5-E0.3-E	✓	-	4.0	7052.7	4110.6	7059.8	2.391	✓	2.498	✓	4.3	169.4	2.356	1.015
HUR-OP-4.0-12.5-E0.3-F	✓	-	4.0	7047.8	4107.8	7054.1	2.392	✓	2.498	✓	4.2	169.4	2.354	1.016
HUR-OP-10.0-12.5-E0.3-A	✓	-	10.0	6607	3750.4	6698.2	2.241	✓	2.498	✓	10.3	169.3	2.208	1.015
HUR-OP-10.0-12.5-E0.3-B	✓	-	10.0	6607.7	3754.1	6696.4	2.246	✓	2.498	✓	10.1	169.4	2.207	1.017
HUR-OP-10.0-12.5-E0.3-C	✓	-	10.0	6611.4	3760.5	6691.3	2.256	✓	2.498	✓	9.7	168.9	2.215	1.018
HUR-OP-10.0-12.5-E0.3-D	✓	-	10.0	6620.9	3750.6	6717.4	2.232	✓	2.498	✓	10.7	169.8	2.207	1.011
HUR-OP-10.0-12.5-E0.3-E	✓	-	10.0	6608.9	3744.8	6683.7	2.249	✓	2.498	✓	10.0	168.7	2.217	1.014
HUR-OP-10.0-12.5-E0.3-F	✓	-	10.0	6619.9	3757.5	6703	2.247	✓	2.498	✓	10.0	169.0	2.217	1.014
HUR-BU-7.0-12.5-E0.3-A	✓	+0.3	7.0	6762.8	3874.5	6793.4	2.317	✓	2.476	✓	6.4	168.4	2.273	1.020
HUR-BU-7.0-12.5-E0.3-B	✓	+0.3	7.0	6783.4	3886.3	6812	2.319	✓	2.476	✓	6.4	168.6	2.277	1.018
HUR-BU-7.0-12.5-E0.3-C	✓	+0.3	7.0	6800.8	3890.7	6830.4	2.313	✓	2.476	✓	6.6	169.0	2.277	1.016
HUR-BU-7.0-12.5-E0.3-D	✓	+0.3	7.0	6772.5	3864.2	6798.1	2.308	✓	2.476	✓	6.8	168.6	2.273	1.016
HUR-BU-7.0-12.5-E0.3-E	✓	+0.3	7.0	6784.8	3881.3	6807.3	2.319	✓	2.476	✓	6.3	168.6	2.277	1.018
HUR-BU-7.0-12.5-E0.3-F	✓	+0.3	7.0	6786.8	3878.8	6813.6	2.313	✓	2.476	✓	6.6	169.1	2.271	1.018

Project	Specimen ID	Compacted	AC%	Target AV%	Bulk Specific Gravity					MTSG	Done	Air Voids	Gry. Ht.	Gmb Est.	Actual Corr. Fac.
					Dry Wt.	Submerged Wt.	SSD Wt.	BSG	Done						
Sawyer Cty Hayward 12.5mm E-3	HAY-OP-7.0-12.5-E3-A	✓	-	7.0	6997	4075.6	7016.2	2.379	✓	2.543	✓	6.4	169.4	2.337	1.018
	HAY-OP-7.0-12.5-E3-B	✓	-	7.0	6942	4039.2	6976.6	2.363	✓	2.543	✓	7.1	168.9	2.326	1.016
	HAY-OP-7.0-12.5-E3-C	✓	-	7.0	6990.2	4056.1	7016.6	2.361	✓	2.543	✓	7.2	170.1	2.325	1.015
	HAY-OP-7.0-12.5-E3-D	✓	-	7.0	6973.3	4066.2	7016	2.364	✓	2.543	✓	7.0	169.6	2.327	1.016
	HAY-OP-7.0-12.5-E3-E	✓	-	7.0	6961.6	4031.9	6989.5	2.354	✓	2.543	✓	7.5	169.9	2.319	1.015
	HAY-OP-7.0-12.5-E3-F	✓	-	7.0	7005	4065.9	7035.5	2.359	✓	2.543	✓	7.2	170.3	2.328	1.013
	HAY-OP-4.0-12.5-E3-A	✓	-	4.0	6984.9	4126.2	6995	2.435	✓	2.543	✓	4.3	164.7	2.400	1.015
	HAY-OP-4.0-12.5-E3-B	✓	-	4.0	7205.8	4265	7218.8	2.440	✓	2.543	✓	4.1	169.7	2.403	1.015
	HAY-OP-4.0-12.5-E3-C	✓	-	4.0	7182.8	4248.6	7192.7	2.440	✓	2.543	✓	4.1	169.3	2.401	1.016
	HAY-OP-4.0-12.5-E3-D	✓	-	4.0	7183.7	4245.5	7194	2.436	✓	2.543	✓	4.2	169.4	2.400	1.015
	HAY-OP-4.0-12.5-E3-E	✓	-	4.0	7205.4	4256.1	7214	2.436	✓	2.543	✓	4.2	169.9	2.400	1.015
	HAY-OP-4.0-12.5-E3-F	✓	-	4.0	7207.7	4267.4	7221.6	2.440	✓	2.543	✓	4.1	169.9	2.401	1.016
	HAY-OP-10.0-12.5-E3-A	✓	-	10.0	6794.8	3950.4	6885.1	2.315	✓	2.543	✓	9.0	169.9	2.263	1.023
	HAY-OP-10.0-12.5-E3-B	✓	-	10.0	6816.5	3935.8	6899.1	2.300	✓	2.543	✓	9.6	169.6	2.274	1.011
	HAY-OP-10.0-12.5-E3-C	✓	-	10.0	6792.4	3907.7	6862.7	2.299	✓	2.543	✓	9.6	168.3	2.284	1.006
	HAY-OP-10.0-12.5-E3-D	✓	-	10.0	6818.8	3948.5	6901.1	2.309	✓	2.543	✓	9.2	168.8	2.286	1.010
	HAY-OP-10.0-12.5-E3-E	✓	-	10.0	6802.8	3947.9	6888.1	2.314	✓	2.543	✓	9.0	169.6	2.270	1.019
	HAY-OP-10.0-12.5-E3-F	✓	-	10.0	6744.7	3898.3	6813.8	2.313	✓	2.543	✓	9.0	167.7	2.276	1.016
	HAY-BU7-7.0-12.5-E3-A	✓	+0.3	7.0	6783	3931.2	6841.3	2.331	✓	2.483	✓	6.1	167.6	2.290	1.018
	HAY-BU-7.0-12.5-E3-B	✓	+0.3	7.0	6769.2	3921.4	6831.8	2.326	✓	2.483	✓	6.3	167.1	2.292	1.015
	HAY-BU-7.0-12.5-E3-C	✓	+0.3	7.0	6748	3916.6	6819.8	2.324	✓	2.483	✓	6.4	167.9	2.274	1.022
	HAY-BU-7.0-12.5-E3-D	✓	+0.3	7.0	6775.8	3915.5	6844	2.314	✓	2.483	✓	6.8	168.3	2.278	1.016
	HAY-BU-7.0-12.5-E3-E	✓	+0.3	7.0	6770.3	3911.8	6825.7	2.323	✓	2.483	✓	6.4	168.1	2.279	1.019
	HAY-BU-7.0-12.5-E3-F	✓	+0.3	7.0	6788.4	3926.7	6842.3	2.328	✓	2.483	✓	6.2	167.4	2.295	1.015

Project	Specimen ID	Compacted	AC%	Target AV%	Bulk Specific Gravity					MTSG	Done	Air Voids	Gry. Ht.	Gmb Est.	Actual Corr. Fac.
					Dry Wt.	Submerged Wt.	SSD Wt.	BSG	Done						
Marathon Cty Wausau 12.5mm E-3	WAU-OP-7.0-12.5-E3-A	✓	-	7.0	6688.3	3753.5	6713	2.260	✓	2.450	✓	7.7	169.0	2.240	1.009
	WAU-OP-7.0-12.5-E3-B	✓	-	7.0	6697.1	3765.8	6718.2	2.268	✓	2.450	✓	7.4	169.1	2.241	1.012
	WAU-OP-7.0-12.5-E3-C	✓	-	7.0	6692.7	3758.5	6713.8	2.265	✓	2.450	✓	7.6	170.4	2.223	1.019
	WAU-OP-7.0-12.5-E3-D	✓	-	7.0	6697.5	3763.8	6721.9	2.264	✓	2.450	✓	7.6	169.2	2.240	1.011
	WAU-OP-7.0-12.5-E3-E	✓	-	7.0	6689.5	3762.2	6713.3	2.267	✓	2.450	✓	7.5	169.3	2.236	1.014
	WAU-OP-7.0-12.5-E3-F	✓	-	7.0	6688.1	3765.9	6712.8	2.270	✓	2.450	✓	7.4	169.0	2.239	1.013
	WAU-OP-4.0-12.5-E3-A	✓	-	4.0	6958.6	3981.7	6963.7	2.334	✓	2.450	✓	4.7	169.0	2.330	1.002
	WAU-OP-4.0-12.5-E3-B	✓	-	4.0	6933.4	3973.9	6939	2.338	✓	2.450	✓	4.5	171.0	2.294	1.019
	WAU-OP-4.0-12.5-E3-C	✓	-	4.0	6942.9	3977.4	6949.3	2.336	✓	2.450	✓	4.6	170.1	2.310	1.011
	WAU-OP-4.0-12.5-E3-D	✓	-	4.0	6943.5	3975.7	6949.7	2.335	✓	2.450	✓	4.7	170.6	2.303	1.014
	WAU-OP-4.0-12.5-E3-E	✓	-	4.0	6945.5	3982.6	6951.2	2.340	✓	2.450	✓	4.5	170.5	2.305	1.015
	WAU-OP-4.0-12.5-E3-F	✓	-	4.0	6940.7	3978.9	6947.4	2.338	✓	2.450	✓	4.6	170.5	2.304	1.015
	WAU-OP-10.0-12.5-E3-A	✓	-	10.0	6327.5	3536.8	6419.1	2.195	✓	2.450	✓	10.4	164.9	2.171	1.011
	WAU-OP-10.0-12.5-E3-B	✓	-	10.0	6482.6	3621.1	6553.5	2.211	✓	2.450	✓	9.8	168.0	2.184	1.012
	WAU-OP-10.0-12.5-E3-C	✓	-	10.0	6498.6	3645.6	6581.2	2.214	✓	2.450	✓	9.6	168.7	2.180	1.016
	WAU-OP-10.0-12.5-E3-D	✓	-	10.0	6486.4	3629.2	6570.4	2.205	✓	2.450	✓	10.0	168.5	2.178	1.012
	WAU-OP-10.0-12.5-E3-E	✓	-	10.0	6515.5	3644.3	6604.7	2.201	✓	2.450	✓	10.2	169.3	2.178	1.011
	WAU-OP-10.0-12.5-E3-F	✓	-	10.0	6485.7	3636.7	6584.3	2.200	✓	2.450	✓	10.2	168.9	2.173	1.013
	WAU-BU-7.0-12.5-E3-A	✓	+0.3	7.0	6674	3752.3	6700.6	2.264	✓	2.436	✓	7.1	169.3	2.231	1.015
	WAU-BU-7.0-12.5-E3-B	✓	+0.3	7.0	6706.8	3774.5	6737.1	2.264	✓	2.436	✓	7.1	170.3	2.229	1.016
	WAU-BU-7.0-12.5-E3-C	✓	+0.3	7.0	6697.6	3755.8	6725.8	2.255	✓	2.436	✓	7.4	170.3	2.226	1.013
	WAU-BU-7.0-12.5-E3-D	✓	+0.3	7.0	6738.1	3784.9	6759.9	2.265	✓	2.436	✓	7.0	170.8	2.232	1.015
	WAU-BU-7.0-12.5-E3-E	✓	+0.3	7.0	6727.3	3770.9	6754.9	2.254	✓	2.436	✓	7.5	171.1	2.225	1.013
	WAU-BU-7.0-12.5-E3-F	✓	+0.3	7.0	6761.9	3791.5	6793.1	2.253	✓	2.436	✓	7.5	171.9	2.226	1.012

Project: Iron Cty Hurley 12.5mm E-3

Specimen ID	Compacted	AC%	Target AV%	Bulk Specific Gravity					MTSG	Done	Air Voids	Gry. Ht.	Gmb Est.	Actual Corr. Fac.
				Dry Wt.	Submerged Wt.	SSD Wt.	BSG	Done						
HUR-OP-7.0-12.5-E3-A	✓	-	7.0	6789.4	3880	6821.9	2.308	✓	2.484	✓	7.1	169.4	2.268	1.018
HUR-OP-7.0-12.5-E3-B	✓	-	7.0	6797.6	3901.3	6836.7	2.316	✓	2.484	✓	6.8	169.4	2.271	1.020
HUR-OP-7.0-12.5-E3-C	✓	-	7.0	6793.1	3890.5	6829.5	2.311	✓	2.484	✓	6.9	169.5	2.268	1.019
HUR-OP-7.0-12.5-E3-D	✓	-	7.0	6789.7	3888.7	6828.2	2.310	✓	2.484	✓	7.0	169.4	2.268	1.018
HUR-OP-7.0-12.5-E3-E	✓	-	7.0	6791.9	3888.3	6822.9	2.314	✓	2.484	✓	6.8	169.3	2.270	1.019
HUR-OP-7.0-12.5-E3-F	✓	-	7.0	6794.6	3902.2	6834.4	2.317	✓	2.484	✓	6.7	169.4	2.270	1.021
HUR-OP-4.0-12.5-E3-A	✓	-	4.0	6985.3	4071.7	6994.7	2.390	✓	2.484	✓	3.8	168.0	2.353	1.016
HUR-OP-4.0-12.5-E3-B	✓	-	4.0	6998.6	4077.9	7005.7	2.390	✓	2.484	✓	3.8	168.4	2.352	1.016
HUR-OP-4.0-12.5-E3-C	✓	-	4.0	6988.8	4077.9	6997.9	2.393	✓	2.484	✓	3.6	168.1	2.353	1.017
HUR-OP-4.0-12.5-E3-D	✓	-	4.0	6991.9	4083.3	7003.3	2.394	✓	2.484	✓	3.6	168.3	2.351	1.019
HUR-OP-4.0-12.5-E3-E	✓	-	4.0	6986.7	4085.2	6997.5	2.399	✓	2.484	✓	3.4	168.1	2.352	1.020
HUR-OP-4.0-12.5-E3-F	✓	-	4.0	7008.1	4078.4	7014.1	2.387	✓	2.484	✓	3.9	168.6	2.352	1.015
HUR-OP-10.0-12.5-E3-A	✓	-	10.0	6576.5	3724.2	6655.9	2.243	✓	2.484	✓	9.7	169.2	2.199	1.020
HUR-OP-10.0-12.5-E3-B	✓	-	10.0	6578.6	3743.8	6663.1	2.253	✓	2.484	✓	9.3	168.9	2.204	1.022
HUR-OP-10.0-12.5-E3-C	✓	-	10.0	6594.6	3736.7	6666	2.251	✓	2.484	✓	9.4	169.2	2.206	1.021
HUR-OP-10.0-12.5-E3-D	✓	-	10.0	6586.5	3754.3	6670.6	2.259	✓	2.484	✓	9.1	169.1	2.204	1.025
HUR-OP-10.0-12.5-E3-E	✓	-	10.0	6592.2	3738.7	6675.1	2.245	✓	2.484	✓	9.6	169.2	2.205	1.018
HUR-OP-10.0-12.5-E3-F	✓	-	10.0	6584.3	3762.4	6675.6	2.260	✓	2.484	✓	9.0	169.1	2.203	1.026
HUR-BU-7.0-12.5-E3-A	✓	+0.3	7.0	6701.4	3829.8	6736.9	2.305	✓	2.472	✓	6.7	167.9	2.259	1.021
HUR-BU-7.0-12.5-E3-B	✓	+0.3	7.0	6661.8	3799.9	6694.6	2.301	✓	2.472	✓	6.9	166.9	2.259	1.019
HUR-BU-7.0-12.5-E3-C	✓	+0.3	7.0	6674.8	3820.6	6704.9	2.314	✓	2.472	✓	6.4	167.1	2.260	1.024
HUR-BU-7.0-12.5-E3-D	✓	+0.3	7.0	6687.1	3814.6	6720.5	2.301	✓	2.472	✓	6.9	167.7	2.256	1.020
HUR-BU-7.0-12.5-E3-E	✓	+0.3	7.0	6664.7	3808.2	6697.9	2.306	✓	2.472	✓	6.7	166.8	2.261	1.020
HUR-BU-7.0-12.5-E3-F	✓	+0.3	7.0	6694.8	3817.7	6727.4	2.301	✓	2.472	✓	6.9	167.9	2.256	1.020

Project	Specimen ID	Compacted	AC%	Target AV%	Bulk Specific Gravity					MTSG	Done	Air Voids	Gry. Ht.	Gmb Est.	Actual Corr. Fac.
					Dry Wt.	Submerged Wt.	SSD Wt.	BSG	Done						
Langlade Cty Antigo 12.5mm E-10	ANT-OP-7.0-12.5-E10-A	✓	-	7.0	6996.9	4048.3	7010.6	2.362	✓	2.551	✓	7.4	170.2	2.326	1.015
	ANT-OP-7.0-12.5-E10-B	✓	-	7.0	6985	4039.9	7001.6	2.358	✓	2.551	✓	7.5	170.1	2.324	1.015
	ANT-OP-7.0-12.5-E10-C	✓	-	7.0	6754.7	3900	6771.6	2.352	✓	2.551	✓	7.8	164.4	2.325	1.012
	ANT-OP-7.0-12.5-E10-D	✓	-	7.0	6798	3931	6809.9	2.361	✓	2.551	✓	7.4	165.4	2.326	1.015
	ANT-OP-7.0-12.5-E10-E	✓	-	7.0	6844.9	3956.5	6857.3	2.360	✓	2.551	✓	7.5	166.6	2.325	1.015
	ANT-OP-7.0-12.5-E10-F	✓	-	7.0	6976.8	4038.8	6991.7	2.363	✓	2.551	✓	7.4	169.8	2.325	1.016
	ANT-OP-4.0-12.5-E10-A	✓	-	4.0	7240.3	4217.8	7248.8	2.389	✓	2.551	✓	6.4	174.1	2.353	1.015
	ANT-OP-4.0-12.5-E10-B	✓	-	4.0	7180.9	4212.2	7185.3	2.415	✓	2.551	✓	5.3	170.5	2.383	1.013
	ANT-OP-4.0-12.5-E10-C	✓	-	4.0	6984.8	4091.6	6988.3	2.411	✓	2.551	✓	5.5	166.3	2.377	1.015
	ANT-OP-4.0-12.5-E10-D	✓	-	4.0	7192.2	4208.8	7197.6	2.406	✓	2.551	✓	5.7	171.6	2.372	1.015
	ANT-OP-4.0-12.5-E10-E	✓	-	4.0	7182.3	4207.7	7186.6	2.411	✓	2.551	✓	5.5	170.7	2.381	1.013
	ANT-OP-4.0-12.5-E10-F	✓	-	4.0	7106.8	4165.7	7111.6	2.412	✓	2.551	✓	5.4	168.9	2.381	1.013
	ANT-OP-10.0-12.5-E10-A	✓	-	10.0	6765.2	3860.5	6817.5	2.288	✓	2.551	✓	10.3	169.9	2.253	1.015
	ANT-OP-10.0-12.5-E10-B	✓	-	10.0	6733	3846.8	6788.8	2.289	✓	2.551	✓	10.3	169.1	2.253	1.016
	ANT-OP-10.0-12.5-E10-C	✓	-	10.0	6730	3841.8	6788.8	2.284	✓	2.551	✓	10.5	169.3	2.249	1.015
	ANT-OP-10.0-12.5-E10-D	✓	-	10.0	6580.4	3753.8	6629.9	2.288	✓	2.551	✓	10.3	165.2	2.254	1.015
	ANT-OP-10.0-12.5-E10-E	✓	-	10.0	6697.8	3832	6761.1	2.287	✓	2.551	✓	10.4	168.3	2.252	1.015
	ANT-OP-10.0-12.5-E10-F	✓	-	10.0	6711.8	3841	6767	2.294	✓	2.551	✓	10.1	168.4	2.255	1.017
	ANT-BU-7.0-12.5-E10-A	✓	+0.3	7.0	6809.7	3901.9	6823.9	2.330	✓	2.492	✓	6.5	168.1	2.292	1.017
	ANT-BU-7.0-12.5-E10-B	✓	+0.3	7.0	6786	3880.2	6826	2.304	✓	2.492	✓	7.6	169.5	2.266	1.017
	ANT-BU-7.0-12.5-E10-C	✓	+0.3	7.0	6851.1	3911.8	6882.6	2.306	✓	2.492	✓	7.5	170.6	2.273	1.015
	ANT-BU-7.0-12.5-E10-D	✓	+0.3	7.0	6798.6	3890	6830.5	2.312	✓	2.492	✓	7.2	169.3	2.272	1.017
	ANT-BU-7.0-12.5-E10-E	✓	+0.3	7.0	6774.6	3880.4	6797	2.323	✓	2.492	✓	6.8	167.8	2.285	1.017
	ANT-BU-7.0-12.5-E10-F	✓	+0.3	7.0	6828.3	3898.5	6855.6	2.309	✓	2.492	✓	7.3	170.0	2.273	1.016

Project: Sheboygan Cty Plymouth 12.5mm E-10

Specimen ID	Compacted	AC%	Target AV%	Bulk Specific Gravity					MTSG	Done	Air Voids	Gry. Ht.	Gmb Est.	Actual Corr. Fac.
				Dry Wt.	Submerged Wt.	SSD Wt.	BSG	Done						
PLY-OP-7.0-12.5-E10-A	✓	-	7.0	7079.4	4177.8	7124.4	2.403	✓	2.588	✓	7.2	169.5	2.363	1.017
PLY-OP-7.0-B12.5-E10-	✓	-	7.0	7076.2	4170.6	7121.6	2.398	✓	2.588	✓	7.4	169.6	2.361	1.016
PLY-OP-7.0-12.5-E10-C	✓	-	7.0	7074	4167.7	7110.5	2.404	✓	2.588	✓	7.1	169.3	2.364	1.017
PLY-OP-7.0-12.5-E10-D	✓	-	7.0	7075.7	4179.1	7117.2	2.408	✓	2.588	✓	7.0	169.2	2.366	1.018
PLY-OP-7.0-12.5-E10-E	✓	-	7.0	7079.7	4185.8	7128.7	2.406	✓	2.588	✓	7.1	169.3	2.366	1.017
PLY-OP-7.0-12.5-E10-F	✓	-	7.0	7079.8	4180.7	7126.9	2.403	✓	2.588	✓	7.2	169.7	2.361	1.018
ANT-OP-4.0-12.5-E10-A	✓	-	4.0	7314.2	4371.8	7324.4	2.477	✓	2.588	✓	4.3	169.7	2.439	1.016
PLY-OP-4.0-12.5-E10-B	✓	-	4.0	7316.9	4383.1	7329.6	2.483	✓	2.588	✓	4.1	169.8	2.438	1.018
PLY-OP-4.0-12.5-E10-C	✓	-	4.0	7310.3	4372.6	7320.4	2.480	✓	2.588	✓	4.2	169.6	2.439	1.017
PLY-OP-4.0-12.5-E10-D	✓	-	4.0	7307.8	4370.3	7318.4	2.479	✓	2.588	✓	4.2	169.5	2.440	1.016
PLY-OP-4.0-12.5-E10-E	✓	-	4.0	7309.6	4371.8	7326.1	2.474	✓	2.588	✓	4.4	169.8	2.436	1.016
PLY-OP-4.0-12.5-E10-F	✓	-	4.0	7317.7	4375.2	7327.2	2.479	✓	2.588	✓	4.2	169.8	2.439	1.016
PLY-OP-10.0-12.5-E10-A	✓	-	10.0	6857.6	4037.6	6975.2	2.334	✓	2.588	✓	9.8	169.1	2.295	1.017
PLY-OP-10.0-12.5-E10-B	✓	-	10.0	6861.5	4038.7	6976.8	2.335	✓	2.588	✓	9.8	169.4	2.292	1.019
PLY-OP-10.0-12.5-E10-C	✓	-	10.0	6856.5	4045.5	6974.7	2.341	✓	2.588	✓	9.6	169.1	2.294	1.020
PLY-OP-10.0-12.5-E10-D	✓	-	10.0	6856.1	4029.3	6970.8	2.331	✓	2.588	✓	9.9	169.1	2.294	1.016
PLY-OP-10.0-12.5-E10-E	✓	-	10.0	6853	4036.1	6964.8	2.340	✓	2.588	✓	9.6	168.9	2.296	1.019
PLY-OP-10.0-12.5-E10-F	✓	-	10.0	6860.2	4035.7	6970.5	2.338	✓	2.588	✓	9.7	169.4	2.292	1.020
PLY-BU-7.0-12.5-E10-A	✓	+0.3	7.0	7084.3	4156.6	7105.8	2.402	✓	2.581	✓	6.9	169.8	2.361	1.017
PLY-BU-7.0-12.5-E10-B	✓	+0.3	7.0	7082.1	4163.8	7114.7	2.400	✓	2.581	✓	7.0	169.9	2.359	1.017
PLY-BU-7.0-12.5-E10-C	✓	+0.3	7.0	7084.8	4166.8	7114.7	2.403	✓	2.581	✓	6.9	169.9	2.360	1.018
PLY-BU-7.0-12.5-E10-D	✓	+0.3	7.0	7082.8	4169.5	7114.8	2.405	✓	2.581	✓	6.8	169.8	2.360	1.019
PLY-BU-7.0-12.5-E10-E	✓	+0.3	7.0	7084.7	4169.2	7111.4	2.408	✓	2.581	✓	6.7	169.8	2.361	1.020
PLY-BU-7.0-12.5-E10-F	✓	+0.3	7.0	7103.7	4177.3	7133.9	2.403	✓	2.581	✓	6.9	170.3	2.360	1.018

Project	Specimen ID	Compacted	AC%	Target AV%	Bulk Specific Gravity					MTSG	Done	Air Voids	Gry. Ht.	Gmb Est.	Actual Corr. Fac.
					Dry Wt.	Submerged Wt.	SSD Wt.	BSG	Done						
Kenosha Cty Racine 12.5mm E-10	RAC-OP-7.0-12.5-E10-A	✓	-	7.0	6865.6	3952.5	6903.8	2.326	✓	2.510	✓	7.3	168.9	2.300	1.011
	RAC-OP-7.0-12.5-E10-B	✓	-	7.0	6860.8	3953.9	6901.2	2.328	✓	2.510	✓	7.2	169.8	2.286	1.018
	RAC-OP-7.0-12.5-E10-C	✓	-	7.0	6873	3958.4	6913.5	2.326	✓	2.510	✓	7.3	169.2	2.299	1.012
	RAC-OP-7.0-12.5-E10-D	✓	-	7.0	6869.6	3954.5	6905.5	2.328	✓	2.510	✓	7.2	169	2.300	1.012
	RAC-OP-7.0-12.5-E10-E	✓	-	7.0	6855.6	3957.8	6893.4	2.335	✓	2.510	✓	6.9	168.9	2.297	1.017
	RAC-OP-7.0-12.5-E10-F	✓	-	7.0	6877.1	3959.9	6903.6	2.336	✓	2.510	✓	6.9	169	2.303	1.015
	RAC-OP-4.0-12.5-E10-A	✓	-	4.0	7071.6	4136.1	7085.7	2.397	✓	2.510	✓	4.5	168.8	2.371	1.011
	RAC-OP-4.0-12.5-E10-B	✓	-	4.0	7082.3	4136	7093.4	2.395	✓	2.510	✓	4.6	169.1	2.370	1.010
	RAC-OP-4.0-12.5-E10-C	✓	-	4.0	7078.8	4143.7	7092.5	2.401	✓	2.510	✓	4.3	168.9	2.372	1.012
	RAC-OP-4.0-12.5-E10-D	✓	-	4.0	7093.7	4152.9	7104.6	2.403	✓	2.510	✓	4.2	169.1	2.374	1.012
	RAC-OP-4.0-12.5-E10-E	✓	-	4.0	7064.2	4127.5	7076.1	2.396	✓	2.510	✓	4.5	168.8	2.368	1.012
	RAC-OP-4.0-12.5-E10-F	✓	-	4.0	7096.4	4152.7	7110.3	2.399	✓	2.510	✓	4.4	169.4	2.371	1.012
	RAC-OP-10.0-12.5-E10-A	✓	-	10.0	6626.1	3781.2	6739.4	2.240	✓	2.510	✓	10.7	169.3	2.215	1.011
	RAC-OP-10.0-12.5-E10-B	✓	-	10.0	6651.8	3808.7	6768.5	2.247	✓	2.510	✓	10.5	170	2.214	1.015
	RAC-OP-10.0-12.5-E10-C	✓	-	10.0	6640.5	3786.9	6755.8	2.237	✓	2.510	✓	10.9	169.8	2.213	1.011
	RAC-OP-10.0-12.5-E10-D	✓	-	10.0	6623.1	3779.3	6736.7	2.240	✓	2.510	✓	10.8	169.4	2.212	1.012
	RAC-OP-10.0-12.5-E10-E	✓	-	10.0	6642.2	3802.6	6771.1	2.238	✓	2.510	✓	10.8	170.1	2.210	1.013
	RAC-OP-10.0-12.5-E10-F	✓	-	10.0	6655.2	3801.4	6762.2	2.248	✓	2.510	✓	10.4	170	2.215	1.015
	RAC-BU-7.0-12.5-E10-A	✓	+0.3	7.0	6735.7	3872.4	6788.6	2.310	✓	2.486	✓	7.1	167.4	2.277	1.014
	RAC-BU-7.0-12.5-E10-B	✓	+0.3	7.0	6781.9	3896.8	6826.5	2.315	✓	2.486	✓	6.9	168.3	2.280	1.015
	RAC-BU-7.0-12.5-E10-C	✓	+0.3	7.0	6753.6	3880.2	6797.3	2.315	✓	2.486	✓	6.9	167.5	2.282	1.015
	RAC-BU-7.0-12.5-E10-D	✓	+0.3	7.0	6752.8	3876	6797.9	2.311	✓	2.486	✓	7.0	167.6	2.280	1.014
	RAC-BU-7.0-12.5-E10-E	✓	+0.3	7.0	6771.5	3883.5	6808.9	2.315	✓	2.486	✓	6.9	168	2.281	1.015
	RAC-BU-7.0-12.5-E10-F	✓	+0.3	7.0	6786.7	3896.7	6827.5	2.316	✓	2.486	✓	6.9	168.2	2.283	1.014

Project	Specimen ID	Compacted	AC%	Target AV%	Bulk Specific Gravity					MTSG	Done	Air Voids	Gry. Ht.	Gmb Est.	Actual Corr. Fac.
					Dry Wt.	Submerged Wt.	SSD Wt.	BSG	Done						
Sheboygan Cty Cascade 19.0mm E-1	CAS-OP-7.0-19.0-E1-A	✓	-	7.0	7062.2	4140.1	7096.6	2.389	✓	2.578	✓	7.4	169.3	2.361	1.012
	CAS-OP-7.0-19.0-E1-B	✓	-	7.0	7058.1	4144.9	7102.9	2.386	✓	2.578	✓	7.5	169.2	2.361	1.011
	CAS-OP-7.0-19.0-E1-C	✓	-	7.0	7059.7	4152.8	7095.9	2.399	✓	2.578	✓	7.0	169.2	2.361	1.016
	CAS-OP-7.0-19.0-E1-D	✓	-	7.0	7065.4	4168.6	7109.9	2.402	✓	2.578	✓	6.8	169.5	2.359	1.018
	CAS-OP-7.0-19.0-E1-E	✓	-	7.0	7062.3	4143.7	7094.3	2.394	✓	2.578	✓	7.2	169.5	2.358	1.015
	CAS-OP-7.0-19.0-E1-F	✓	-	7.0	7060.3	4138.4	7094.8	2.388	✓	2.578	✓	7.4	169.3	2.360	1.012
	CAS-OP-4.0-19.0-E1-A	✓	-	4.0	7290.1	4342.3	7300.5	2.464	✓	2.578	✓	4.4	169.8	2.430	1.014
	CAS-OP-4.0-19.0-E1-B	✓	-	4.0	7286.6	4346.8	7296.6	2.470	✓	2.578	✓	4.2	169.8	2.428	1.017
	CAS-OP-4.0-19.0-E1-C	✓	-	4.0	7291.1	4337.2	7298.5	2.462	✓	2.578	✓	4.5	169.9	2.428	1.014
	CAS-OP-4.0-19.0-E1-D	✓	-	4.0	7293.1	4339.4	7302	2.462	✓	2.578	✓	4.5	169.9	2.429	1.013
	CAS-OP-4.0-19.0-E1-E	✓	-	4.0	7290.7	4341.7	7302.2	2.463	✓	2.578	✓	4.5	169.9	2.428	1.014
	CAS-OP-4.0-19.0-E1-F	✓	-	4.0	7293.5	4341.2	7302.1	2.463	✓	2.578	✓	4.5	169.8	2.431	1.013
	CAS-OP-10.0-19.0-E1-A	✓	-	10.0	6828.1	3988.9	6917.5	2.332	✓	2.578	✓	9.6	169.1	2.285	1.020
	CAS-OP-10.0-19.0-E1-B	✓	-	10.0	6826.2	3982.1	6912.2	2.330	✓	2.578	✓	9.6	169.4	2.280	1.022
	CAS-OP-10.0-19.0-E1-C	✓	-	10.0	6830.6	3992.3	6933.7	2.322	✓	2.578	✓	9.9	169.9	2.275	1.021
	CAS-OP-10.0-19.0-E1-D	✓	-	10.0	6832	3969.5	6936.1	2.303	✓	2.578	✓	10.7	170.1	2.273	1.013
	CAS-OP-10.0-19.0-E1-E	✓	-	10.0	6830.4	3960	6919.6	2.308	✓	2.578	✓	10.5	169.8	2.276	1.014
	CAS-OP-10.0-19.0-E1-F	✓	-	10.0	6831.8	3989.4	6924.7	2.327	✓	2.578	✓	9.7	169.8	2.277	1.022
	CAS-BU-7.0-19.0-E1-A	✓	+0.3	7.0	6996.4	4086.3	7034	2.374	✓	2.554	✓	7.1	169.2	2.340	1.014
	CAS-BU-7.0-19.0-E1-B	✓	+0.3	7.0	7006.6	4094.7	7044	2.376	✓	2.554	✓	7.0	169.4	2.341	1.015
	CAS-BU-7.0-19.0-E1-C	✓	+0.3	7.0	7004.3	4105.8	7050.7	2.378	✓	2.554	✓	6.9	170.0	2.332	1.020
	CAS-BU-7.0-19.0-E1-D	✓	+0.3	7.0	6997.9	4104.7	7048	2.378	✓	2.554	✓	6.9	169.7	2.334	1.019
	CAS-BU-7.0-19.0-E1-E	✓	+0.3	7.0	7012.1	4096.3	7051.1	2.373	✓	2.554	✓	7.1	170.1	2.333	1.017
	CAS-BU-7.0-19.0-E1-F	✓	+0.3	7.0	7005.3	4103.1	7043.1	2.383	✓	2.554	✓	6.7	169.6	2.337	1.019

Project	Specimen ID	Compacted	AC%	Target AV%	Bulk Specific Gravity					MTSG	Done	Air Voids	Gry. Ht.	Gmb Est.	Actual Corr. Fac.
					Dry Wt.	Submerged Wt.	SSD Wt.	BSG	Done						
Lincoln Cty Bloomville 19.0mm E-1	BLO-OP-7.0-19.0-E1-A	✓	-	7.0	6904.9	3993	6946.9	2.338	✓	2.521	✓	7.3	169.4	2.307	1.013
	BLO-OP-7.0-19.0-E1-B	✓	-	7.0	6910.2	3967.8	6932.2	2.331	✓	2.521	✓	7.5	169.5	2.307	1.010
	BLO-OP-7.0-19.0-E1-C	✓	-	7.0	6902.6	3963.7	6945.1	2.315	✓	2.521	✓	8.2	171.9	2.272	1.019
	BLO-OP-7.0-19.0-E1-D	✓	-	7.0	6911	3986.7	6945	2.336	✓	2.521	✓	7.3	169.5	2.307	1.013
	BLO-OP-7.0-19.0-E1-E	✓	-	7.0	6908.8	3977.5	6936.3	2.335	✓	2.521	✓	7.4	169.4	2.308	1.012
	BLO-OP-7.0-19.0-E1-F	✓	-	7.0	6908.9	3971.2	6933.6	2.332	✓	2.521	✓	7.5	169.4	2.308	1.011
	BLO-OP-4.0-19.0-E1-A	✓	-	4.0	7130	4175.5	7138.4	2.406	✓	2.521	✓	4.5	169.7	2.378	1.012
	BLO-OP-4.0-19.0-E1-B	✓	-	4.0	7129	4182.8	7144	2.407	✓	2.521	✓	4.5	169.8	2.376	1.013
	BLO-OP-4.0-19.0-E1-C	✓	-	4.0	7124	4172	7133.4	2.406	✓	2.521	✓	4.6	169.6	2.377	1.012
	BLO-OP-4.0-19.0-E1-D	✓	-	4.0	7121.4	4183.7	7135.9	2.412	✓	2.521	✓	4.3	169.6	2.376	1.015
	BLO-OP-4.0-19.0-E1-E	✓	-	4.0	7120.7	4177.8	7134.2	2.409	✓	2.521	✓	4.5	169.8	2.373	1.015
	BLO-OP-4.0-19.0-E1-F	✓	-	4.0	7136.4	4187.6	7149.5	2.409	✓	2.521	✓	4.4	169.9	2.377	1.014
	BLO-OP-10.0-19.0-E1-A	✓	-	10.0	6686.9	3837	6771	2.279	✓	2.521	✓	9.6	168.6	2.244	1.015
	BLO-OP-10.0-19.0-E1-B	✓	-	10.0	6687.9	3832	6767.6	2.278	✓	2.521	✓	9.6	168.6	2.245	1.015
	BLO-OP-10.0-19.0-E1-C	✓	-	10.0	6682.8	3829.3	6766.4	2.275	✓	2.521	✓	9.7	168.9	2.239	1.016
	BLO-OP-10.0-19.0-E1-D	✓	-	10.0	6691.4	3831.1	6773.1	2.274	✓	2.521	✓	9.8	169.0	2.241	1.015
	BLO-OP-10.0-19.0-E1-E	✓	-	10.0	6686.3	3828.4	6770.6	2.273	✓	2.521	✓	9.9	168.8	2.242	1.014
	BLO-OP-10.0-19.0-E1-F	✓	-	10.0	6682.9	3837.5	6762.1	2.285	✓	2.521	✓	9.4	168.4	2.246	1.018
	BLO-BU-7.0-19.0-E1-A	✓	+0.3	7.0	6865.3	3960.1	6909.5	2.328	✓	2.505	✓	7.1	169.3	2.295	1.014
	BLO-BU-7.0-19.0-E1-B	✓	+0.3	7.0	6864.6	3951.5	6890.9	2.335	✓	2.505	✓	6.8	169.2	2.296	1.017
	BLO-BU-7.0-19.0-E1-C	✓	+0.3	7.0	6856.5	3956.2	6901.3	2.328	✓	2.505	✓	7.0	169.0	2.296	1.014
	BLO-BU-7.0-19.0-E1-D	✓	+0.3	7.0	6854.6	3948	6892.4	2.328	✓	2.505	✓	7.1	169.0	2.295	1.014
	BLO-BU-7.0-19.0-E1-E	✓	+0.3	7.0	6890.1	3967.2	6924.1	2.330	✓	2.505	✓	7.0	169.7	2.298	1.014
	BLO-BU-7.0-19.0-E1-F	✓	+0.3	7.0	6875.3	3949.9	6903.9	2.327	✓	2.505	✓	7.1	169.5	2.295	1.014

Douglas Cty Brule 19.0mm E-0.3

Project	Specimen ID	Compacted	AC%	Target AV%	Bulk Specific Gravity					MTSG	Done	Air Voids	Gry. Ht.	Gmb Est.	Actual Corr. Fac.
					Dry Wt.	Submerged Wt.	SSD Wt.	BSG	Done						
	BRU-OP-7.0-19.0-E0.3-A	✓	-	7.0	7032.6	4136.9	7064.3	2.402	✓	2.569	✓	6.5	169.4	2.349	1.023
	BRU-OP-7.0-19.0-E0.3-B	✓	-	7.0	7034	4144.2	7073.2	2.402	✓	2.569	✓	6.5	169.2	2.352	1.021
	BRU-OP-7.0-19.0-E0.3-C	✓	-	7.0	7030.5	4137.5	7067.1	2.400	✓	2.569	✓	6.6	168.8	2.357	1.018
	BRU-OP-7.0-19.0-E0.3-D	✓	-	7.0	7033.3	4138.3	7066.5	2.402	✓	2.569	✓	6.5	169.2	2.352	1.021
	BRU-OP-7.0-19.0-E0.3-E	✓	-	7.0	7027.8	4113.5	7061.2	2.384	✓	2.569	✓	7.2	169.1	2.352	1.014
	BRU-OP-7.0-19.0-E0.3-F	✓	-	7.0	7029.4	4128.8	7067.8	2.392	✓	2.569	✓	6.9	169.3	2.350	1.018
	BRU-OP-4.0-19.0-E0.3-A	✓	-	4.0	7248.3	4304.2	7262.1	2.450	✓	2.569	✓	4.6	169.5	2.420	1.013
	BRU-OP-4.0-19.0-E0.3-B	✓	-	4.0	7250.2	4308	7266	2.451	✓	2.569	✓	4.6	169.6	2.419	1.013
	BRU-OP-4.0-19.0-E0.3-C	✓	-	4.0	7248.5	4305.5	7260.5	2.453	✓	2.569	✓	4.5	169.6	2.419	1.014
	BRU-OP-4.0-19.0-E0.3-D	✓	-	4.0	7255.9	4324.2	7273.5	2.460	✓	2.569	✓	4.2	169.5	2.422	1.016
	BRU-OP-4.0-19.0-E0.3-E	✓	-	4.0	7243.3	4300	7256	2.450	✓	2.569	✓	4.6	169.5	2.418	1.013
	BRU-OP-4.0-19.0-E0.3-F	✓	-	4.0	7248.1	4302.4	7263.7	2.448	✓	2.569	✓	4.7	169.4	2.421	1.011
	BRU-OP-10.0-19.0-E0.3-A	✓	-	10.0	6807.7	3927.7	6867.2	2.316	✓	2.569	✓	9.8	169.2	2.277	1.017
	BRU-OP-10.0-19.0-E0.3-B	✓	-	10.0	6810.1	3925.5	6868.2	2.314	✓	2.569	✓	9.9	169.1	2.279	1.015
	BRU-OP-10.0-19.0-E0.3-C	✓	-	10.0	6800.1	3923.1	6862.2	2.314	✓	2.569	✓	9.9	169.0	2.277	1.016
	BRU-OP-10.0-19.0-E0.3-D	✓	-	10.0	6811	3945.5	6881.5	2.320	✓	2.569	✓	9.7	169.1	2.279	1.018
	BRU-OP-10.0-19.0-E0.3-E	✓	-	10.0	6789.9	3914.6	6857.1	2.308	✓	2.569	✓	10.2	169.2	2.271	1.016
	BRU-OP-10.0-19.0-E0.3-F	✓	-	10.0	6802.9	3932.9	6859.4	2.325	✓	2.569	✓	9.5	168.4	2.286	1.017
	BRU-BU-7.0-19.0-E0.3-A	✓	+0.3	7.0	7019.6	4084	7042.6	2.373	✓	2.553	✓	7.1	169.9	2.338	1.015
	BRU-BU-7.0-19.0-E0.3-B	✓	+0.3	7.0	7006.6	4105.8	7038.8	2.389	✓	2.553	✓	6.4	169.9	2.334	1.024
	BRU-BU-7.0-19.0-E0.3-C	✓	+0.3	7.0	6994.2	4096.1	7031.2	2.383	✓	2.553	✓	6.7	170.2	2.325	1.025
	BRU-BU-7.0-19.0-E0.3-D	✓	+0.3	7.0	7006	4089	7038.8	2.375	✓	2.553	✓	7.0	170.1	2.331	1.019
	BRU-BU-7.0-19.0-E0.3-E	✓	+0.3	7.0	7010.3	4090.8	7049.4	2.369	✓	2.553	✓	7.2	170.2	2.331	1.017
	BRU-BU-7.0-19.0-E0.3-F	✓	+0.3	7.0	7010.5	4086.1	7041.8	2.372	✓	2.553	✓	7.1	170.1	2.332	1.017

Project	Specimen ID	Compacted	AC%	Target AV%	Bulk Specific Gravity					MTSG	Done	Air Voids	Gry. Ht.	Gmb Est.	Actual Corr. Fac.
					Dry Wt.	Submerged Wt.	SSD Wt.	BSG	Done						
Dane Cty Waunakee 19.0mm E-3	KEE-OP-7.0-19.0-E3-A	✓	-	7.0	6876.7	3965.7	6905.2	2.339	✓	2.511	✓	6.8	168.7	2.307	1.014
	KEE-OP-7.0-19.0-E3-B	✓	-	7.0	6870.5	3973.9	6906.5	2.343	✓	2.511	✓	6.7	168.3	2.310	1.014
	KEE-OP-7.0-19.0-E3-C	✓	-	7.0	6870.1	3964.1	6902.5	2.338	✓	2.511	✓	6.9	168.8	2.303	1.015
	KEE-OP-7.0-19.0-E3-D	✓	-	7.0	6873.2	3983.5	6912.6	2.347	✓	2.511	✓	6.5	168.4	2.310	1.016
	KEE-OP-7.0-19.0-E3-E	✓	-	7.0	6870	3983.5	6908.1	2.349	✓	2.511	✓	6.4	168.5	2.307	1.018
	KEE-OP-7.0-19.0-E3-F	✓	-	7.0	6868.3	3971.6	6903.2	2.343	✓	2.511	✓	6.7	168.8	2.303	1.018
	KEE-OP-4.0-19.0-E3-A	✓	-	4.0	7096.7	4163.6	7109.3	2.409	✓	2.511	✓	4.1	169.8	2.365	1.019
	KEE-OP-4.0-19.0-E3-B	✓	-	4.0	7093.7	4168.4	7107.3	2.414	✓	2.511	✓	3.9	169.4	2.370	1.019
	KEE-OP-4.0-19.0-E3-C	✓	-	4.0	7098.3	4160.2	7110.2	2.406	✓	2.511	✓	4.2	170.3	2.359	1.020
	KEE-OP-4.0-19.0-E3-D	✓	-	4.0	7094	4165.2	7107.2	2.411	✓	2.511	✓	4.0	170.4	2.356	1.024
	KEE-OP-4.0-19.0-E3-E	✓	-	4.0	7099.4	4163.2	7108.6	2.410	✓	2.511	✓	4.0	170.2	2.360	1.021
	KEE-OP-4.0-19.0-E3-F	✓	-	4.0	7096	4160.5	7105.3	2.410	✓	2.511	✓	4.0	169.9	2.363	1.020
	KEE-OP-10.0-19.0-E3-A	✓	-	10.0	6643.4	3794.1	6714.7	2.275	✓	2.511	✓	9.4	169.4	2.219	1.025
	KEE-OP-10.0-19.0-E3-B	✓	-	10.0	6648.9	3809.4	6717.1	2.287	✓	2.511	✓	8.9	169.3	2.222	1.029
	KEE-OP-10.0-19.0-E3-C	✓	-	10.0	6656.9	3809.8	6728.7	2.281	✓	2.511	✓	9.2	169.4	2.224	1.026
	KEE-OP-10.0-19.0-E3-D	✓	-	10.0	6652.2	3809.9	6719.8	2.286	✓	2.511	✓	9.0	169.6	2.220	1.030
	KEE-OP-10.0-19.0-E3-E	✓	-	10.0	6647.1	3822.4	6717.6	2.296	✓	2.511	✓	8.6	169.4	2.220	1.034
	KEE-OP-10.0-19.0-E3-F	✓	-	10.0	6649.4	3809.9	6721.6	2.284	✓	2.511	✓	9.0	169.2	2.224	1.027
	KEE-BU-7.0-19.0-E3-A	✓	+0.3	7.0	6852	3948.5	6886	2.333	✓	2.495	✓	6.5	169.9	2.282	1.022
	KEE-BU-7.0-19.0-E3-B	✓	+0.3	7.0	6844.5	3951.4	6877.2	2.339	✓	2.495	✓	6.3	169.8	2.281	1.026
	KEE-BU-7.0-19.0-E3-C	✓	+0.3	7.0	6883.4	3972.4	6918.5	2.336	✓	2.495	✓	6.4	169.8	2.294	1.019
	KEE-BU-7.0-19.0-E3-D	✓	+0.3	7.0	6881.6	3969.3	6916.3	2.335	✓	2.495	✓	6.4	169.7	2.295	1.018
	KEE-BU-7.0-19.0-E3-E	✓	+0.3	7.0	6882.4	3979.3	6921	2.340	✓	2.495	✓	6.2	169.8	2.294	1.020
	KEE-BU-7.0-19.0-E3-F	✓	+0.3	7.0	6862.9	3968.6	6902.4	2.339	✓	2.495	✓	6.3	169.8	2.287	1.023

Project	Specimen ID	Compacted	AC%	Target AV%	Bulk Specific Gravity					MTSG	Done	Air Voids	Gry. Ht.	Gmb Est.	Actual Corr. Fac.
					Dry Wt.	Submerged Wt.	SSD Wt.	BSG	Done						
Marathon Cty Mosinee 19.0mm E-3	MOS-OP-7.0-19.0-E3-A	✓	-	7.0	6686.5	3752.4	6712.4	2.259	✓	2.445	✓	7.6	169.4	2.234	1.011
	MOS-OP-7.0-19.0-E3-B	✓	-	7.0	6697.9	3751.7	6716.7	2.259	✓	2.445	✓	7.6	169.6	2.235	1.011
	MOS-OP-7.0-19.0-E3-C	✓	-	7.0	6703.2	3765.3	6734.1	2.258	✓	2.445	✓	7.7	169.8	2.234	1.011
	MOS-OP-7.0-19.0-E3-D	✓	-	7.0	6699.3	3755.8	6723	2.258	✓	2.445	✓	7.7	169.8	2.233	1.011
	MOS-OP-7.0-19.0-E3-E	✓	-	7.0	6691.6	3764.1	6723.2	2.261	✓	2.445	✓	7.5	169.5	2.234	1.012
	MOS-OP-7.0-19.0-E3-F	✓	-	7.0	6695.3	3758.4	6722.8	2.259	✓	2.445	✓	7.6	169.5	2.235	1.010
	MOS-OP-4.0-19.0-E3-A	✓	-	4.0	6921.2	3960.2	6927.6	2.332	✓	2.445	✓	4.6	170.1	2.303	1.013
	MOS-OP-4.0-19.0-E3-B	✓	-	4.0	6922	3964.5	6928.3	2.336	✓	2.445	✓	4.5	170.2	2.301	1.015
	MOS-OP-4.0-19.0-E3-C	✓	-	4.0	6919.6	3949.1	6925.2	2.325	✓	2.445	✓	4.9	170.3	2.299	1.011
	MOS-OP-4.0-19.0-E3-D	✓	-	4.0	6925.2	3962.4	6930.8	2.333	✓	2.445	✓	4.6	170.3	2.301	1.014
	MOS-OP-4.0-19.0-E3-E	✓	-	4.0	6915.7	3953.1	6921.6	2.330	✓	2.445	✓	4.7	170.0	2.302	1.012
	MOS-OP-4.0-19.0-E3-F	✓	-	4.0	6916.7	3958	6922.5	2.333	✓	2.445	✓	4.6	170.0	2.302	1.013
	MOS-OP-10.0-19.0-E3-A	✓	-	10.0	6474.2	3615.3	6559.3	2.199	✓	2.445	✓	10.1	168.5	2.174	1.011
	MOS-OP-10.0-19.0-E3-B	✓	-	10.0	6468.6	3604.9	6561.8	2.188	✓	2.445	✓	10.5	169.4	2.161	1.012
	MOS-OP-10.0-19.0-E3-C	✓	-	10.0	6465.6	3596.5	6566.7	2.177	✓	2.445	✓	11.0	169.7	2.156	1.010
	MOS-OP-10.0-19.0-E3-D	✓	-	10.0	6466.9	3586.6	6572.6	2.166	✓	2.445	✓	11.4	170.2	2.150	1.007
	MOS-OP-10.0-19.0-E3-E	✓	-	10.0	6445.5	3597.4	6555.7	2.179	✓	2.445	✓	10.9	169.5	2.152	1.013
	MOS-OP-10.0-19.0-E3-F	✓	-	10.0	6468.2	3605.7	6571.1	2.181	✓	2.445	✓	10.8	169.8	2.156	1.012
	MOS-BU-7.0-19.0-E3-A	✓	+0.3	7.0	6661.6	3740.1	6684.2	2.263	✓	2.438	✓	7.2	168.9	2.232	1.014
	MOS-BU-7.0-19.0-E3-B	✓	+0.3	7.0	6659.2	3732.3	6682.4	2.257	✓	2.438	✓	7.4	169.0	2.230	1.012
	MOS-BU-7.0-19.0-E3-C	✓	+0.3	7.0	6704	3750.3	6729.1	2.251	✓	2.438	✓	7.7	170.3	2.228	1.010
	MOS-BU-7.0-19.0-E3-D	✓	+0.3	7.0	6707.2	3761.4	6737.1	2.254	✓	2.438	✓	7.5	170.2	2.230	1.011
	MOS-BU-7.0-19.0-E3-E	✓	+0.3	7.0	6684	3742.1	6709.8	2.252	✓	2.438	✓	7.6	169.9	2.226	1.012
	MOS-BU-7.0-19.0-E3-F	✓	+0.3	7.0	6682.1	3739.2	6702.9	2.255	✓	2.438	✓	7.5	169.7	2.228	1.012

Project	Specimen ID	Compacted	AC%	Target AV%	Bulk Specific Gravity					MTSG	Done	Air Voids	Gry. Ht.	Gmb Est.	Actual Corr. Fac.
					Dry Wt.	Submerged Wt.	SSD Wt.	BSG	Done						
Barron Cty Cumberland 19.0mm E-3	UMB-OP-7.0-19.0-E3-A	✓	-	7.0	7068.5	4132.9	7086.4	2.393	✓	2.586	✓	7.5	169.3	2.363	1.013
	UMB-OP-7.0-19.0-E3-B	✓	-	7.0	7082.5	4153.2	7106.6	2.398	✓	2.586	✓	7.3	169.5	2.365	1.014
	UMB-OP-7.0-19.0-E3-C	✓	-	7.0	7075.1	4146.4	7100.4	2.395	✓	2.586	✓	7.4	169.5	2.362	1.014
	UMB-OP-7.0-19.0-E3-D	✓	-	7.0	7068.6	4146.7	7095.4	2.397	✓	2.586	✓	7.3	169.3	2.363	1.015
	UMB-OP-7.0-19.0-E3-E	✓	-	7.0	7073.3	4149.8	7094.9	2.402	✓	2.586	✓	7.1	169.4	2.363	1.016
	UMB-OP-7.0-19.0-E3-F	✓	-	7.0	7075.5	4144.9	7096	2.398	✓	2.586	✓	7.3	169.5	2.362	1.015
	UMB-OP-4.0-19.0-E3-A	✓	-	4.0	7310	4362.6	7319.1	2.473	✓	2.586	✓	4.4	169.8	2.436	1.015
	UMB-OP-4.0-19.0-E3-B	✓	-	4.0	7316.7	4365.3	7325.3	2.472	✓	2.586	✓	4.4	170.0	2.436	1.015
	UMB-OP-4.0-19.0-E3-C	✓	-	4.0	7309.6	4365.2	7319.1	2.475	✓	2.586	✓	4.3	169.7	2.437	1.015
	UMB-OP-4.0-19.0-E3-D	✓	-	4.0	7309.1	4361.5	7316.8	2.473	✓	2.586	✓	4.4	169.8	2.436	1.015
	UMB-OP-4.0-19.0-E3-E	✓	-	4.0	7312.9	4357.8	7319	2.470	✓	2.586	✓	4.5	169.8	2.437	1.013
	UMB-OP-4.0-19.0-E3-F	✓	-	4.0	7312.6	4359.1	7319.6	2.470	✓	2.586	✓	4.5	169.8	2.437	1.014
	UMB-OP-10.0-19.0-E3-A	✓	-	10.0	6851.6	3948.4	6921.1	2.305	✓	2.586	✓	10.9	170.4	2.275	1.013
	UMB-OP-10.0-19.0-E3-B	✓	-	10.0	6853.5	3973.7	6927.3	2.320	✓	2.586	✓	10.3	169.9	2.283	1.017
	UMB-OP-10.0-19.0-E3-C	✓	-	10.0	6851.5	3957.2	6923.2	2.310	✓	2.586	✓	10.7	170.1	2.279	1.013
	UMB-OP-10.0-19.0-E3-D	✓	-	10.0	6845.1	3949.6	6915.7	2.308	✓	2.586	✓	10.8	170.2	2.276	1.014
	UMB-OP-10.0-19.0-E3-E	✓	-	10.0	6856.1	3986.4	6941.1	2.320	✓	2.586	✓	10.3	169.9	2.284	1.016
	UMB-OP-10.0-19.0-E3-F	✓	-	10.0	6846.9	3945.5	6917.3	2.304	✓	2.586	✓	10.9	169.8	2.282	1.010
	UMB-BU-7.0-19.0-E3-A	✓	+0.3	7.0	7031.1	4114.6	7063.2	2.385	✓	2.572	✓	7.3	169.9	2.342	1.018
	UMB-BU-7.0-19.0-E3-B	✓	+0.3	7.0	7053.3	4122.7	7076.6	2.388	✓	2.572	✓	7.2	170.0	2.348	1.017
	UMB-BU-7.0-19.0-E3-C	✓	+0.3	7.0	7056.4	4131.9	7083.4	2.391	✓	2.572	✓	7.0	170.1	2.347	1.018
	UMB-BU-7.0-19.0-E3-D	✓	+0.3	7.0	7049.2	4112.3	7073.9	2.380	✓	2.572	✓	7.5	170.2	2.344	1.016
	UMB-BU-7.0-19.0-E3-E	✓	+0.3	7.0	7054	4124.3	7079.7	2.387	✓	2.572	✓	7.2	170.1	2.347	1.017
	UMB-BU-7.0-19.0-E3-F	✓	+0.3	7.0	7054	4116.6	7076	2.384	✓	2.572	✓	7.3	170.0	2.348	1.015

Langlade Cty Antigo 19.0mm E-10

Project	Specimen ID	Compacted	AC%	Target AV%	Bulk Specific Gravity					MTSG	Done	Air Voids	Gry. Ht.	Gmb Est.	Actual Corr. Fac.
					Dry Wt.	Submerged Wt.	SSD Wt.	BSG	Done						
Langlade Cty Antigo 19.0mm E-10	ANT-OP-7.0-19.0-E10-A	✓	-	7.0	6934.4	4034.2	6969.9	2.362	✓	2.535	✓	6.8	170.0	2.308	1.023
	ANT-OP-7.0-19.0-E10-B	✓	-	7.0	6940.8	4038.5	6973.6	2.365	✓	2.535	✓	6.7	170.0	2.310	1.024
	ANT-OP-7.0-19.0-E10-C	✓	-	7.0	6946	4041.6	6979.3	2.364	✓	2.535	✓	6.7	169.9	2.313	1.022
	ANT-OP-7.0-19.0-E10-D	✓	-	7.0	6946.7	4047.3	6979.2	2.369	✓	2.535	✓	6.5	170.0	2.312	1.025
	ANT-OP-7.0-19.0-E10-E	✓	-	7.0	6937.1	4040.9	6973.7	2.365	✓	2.535	✓	6.7	169.8	2.312	1.023
	ANT-OP-7.0-19.0-E10-F	✓	-	7.0	6947.5	4051.3	6988.1	2.366	✓	2.535	✓	6.7	170.0	2.313	1.023
	ANT-OP-4.0-19.0-E10-A	✓	-	4.0	6991.9	4131.6	7003.3	2.435	✓	2.535	✓	4.0	165.9	2.385	1.021
	ANT-OP-4.0-19.0-E10-B	✓	-	4.0	7170.6	4229.3	7183.4	2.427	✓	2.535	✓	4.2	170.2	2.384	1.018
	ANT-OP-4.0-19.0-E10-C	✓	-	4.0	7166.8	4222.6	7174	2.428	✓	2.535	✓	4.2	169.9	2.387	1.017
	ANT-OP-4.0-19.0-E10-D	✓	-	4.0	7176.6	4235.9	7189.7	2.430	✓	2.535	✓	4.2	170.3	2.385	1.019
	ANT-OP-4.0-19.0-E10-E	✓	-	4.0	7169.4	4243.9	7186.3	2.437	✓	2.535	✓	3.9	170.2	2.384	1.022
	ANT-OP-4.0-19.0-E10-F	✓	-	4.0	7173.5	4222.9	7182.9	2.423	✓	2.535	✓	4.4	170.3	2.384	1.017
	ANT-OP-10.0-19.0-E10-A	✓	-	10.0	6712.5	3879.4	6807.6	2.292	✓	2.535	✓	9.6	169.4	2.242	1.022
	ANT-OP-10.0-19.0-E10-B	✓	-	10.0	6720.9	3887.2	6802.1	2.306	✓	2.535	✓	9.0	169.7	2.241	1.029
	ANT-OP-10.0-19.0-E10-C	✓	-	10.0	6722	3873.3	6801.8	2.295	✓	2.535	✓	9.5	169.7	2.242	1.024
	ANT-OP-10.0-19.0-E10-D	✓	-	10.0	6722.3	3870.9	6791.8	2.301	✓	2.535	✓	9.2	169.2	2.248	1.024
	ANT-OP-10.0-19.0-E10-E	✓	-	10.0	6719.2	3876.4	6798.3	2.300	✓	2.535	✓	9.3	168.8	2.253	1.021
	ANT-OP-10.0-19.0-E10-F	✓	-	10.0	6713.9	3876.6	6794.1	2.301	✓	2.535	✓	9.2	169.4	2.243	1.026
	ANT-BU-7.0-19.0-E10-A	✓	+0.3	7.0	6903.5	4005.1	6938.1	2.354	✓	2.521	✓	6.6	169.9	2.299	1.024
	ANT-BU-7.0-19.0-E10-B	✓	+0.3	7.0	6913.1	4017.9	6953.7	2.355	✓	2.521	✓	6.6	170.0	2.301	1.023
	ANT-BU-7.0-19.0-E10-C	✓	+0.3	7.0	6914.5	4016.7	6960.3	2.349	✓	2.521	✓	6.8	170.3	2.298	1.022
	ANT-BU-7.0-19.0-E10-D	✓	+0.3	7.0	6911.6	4007.3	6954.2	2.345	✓	2.521	✓	7.0	169.8	2.303	1.018
	ANT-BU-7.0-19.0-E10-E	✓	+0.3	7.0	6929.6	4031.9	6967.2	2.361	✓	2.521	✓	6.4	170.4	2.301	1.026
	ANT-BU-7.0-19.0-E10-F	✓	+0.3	7.0	6974	4044.7	7014.5	2.348	✓	2.521	✓	6.9	171.5	2.301	1.020

Project	Specimen ID	Compacted	AC%	Target AV%	Bulk Specific Gravity					MTSG	Done	Air Voids	Gry. Ht.	Gmb Est.	Actual Corr. Fac.
					Dry Wt.	Submerged Wt.	SSD Wt.	BSG	Done						
Jackson Cty Northfield 19.0mm E-30	NOR-OP-7.0-19.0-E30-A	✓	-	7.0	6857.1	4005.5	6884.5	2.381	✓	2.505	✓	4.9	169.8	2.285	1.042
	NOR-OP-7.0-19.0-E30-B	✓	-	7.0	6853.5	3991.8	6881.1	2.372	✓	2.505	✓	5.3	169.8	2.284	1.039
	NOR-OP-7.0-19.0-E30-C	✓	-	7.0	6847.9	4029.5	6881.5	2.401	✓	2.505	✓	4.2	170.1	2.278	1.054
	NOR-OP-7.0-19.0-E30-D	✓	-	7.0	6853.2	4011.5	6881.3	2.388	✓	2.505	✓	4.7	170.1	2.280	1.047
	NOR-OP-7.0-19.0-E30-E	✓	-	7.0	6850.9	3998.6	6876.3	2.381	✓	2.505	✓	5.0	169.7	2.285	1.042
	NOR-OP-7.0-19.0-E30-F	✓	-	7.0	6852.6	4008.1	6883.1	2.384	✓	2.505	✓	4.9	169.7	2.285	1.043
	NOR-OP-4.0-19.0-E30-A	✓	-	4.0	7074.9	4156.6	7106.9	2.398	✓	2.505	✓	4.3	174.7	2.292	1.046
	NOR-OP-4.0-19.0-E30-B	✓	-	4.0	7072.4	4170.8	7098	2.416	✓	2.505	✓	3.6	173.3	2.309	1.046
	NOR-OP-4.0-19.0-E30-C	✓	-	4.0	7063.8	4166.4	7081.3	2.423	✓	2.505	✓	3.3	171.7	2.328	1.041
	NOR-OP-4.0-19.0-E30-D	✓	-	4.0	7066.2	4171.2	7079.4	2.430	✓	2.505	✓	3.0	171.1	2.337	1.040
	NOR-OP-4.0-19.0-E30-E	✓	-	4.0	7060.4	4147	7083.3	2.405	✓	2.505	✓	4.0	173.3	2.305	1.043
	NOR-OP-4.0-19.0-E30-F	✓	-	4.0	7066.5	4170	7079.8	2.429	✓	2.505	✓	3.1	170.1	2.351	1.033
	NOR-OP-10.0-19.0-E30-A	✓	-	10.0	6618.9	3846.1	6676.1	2.339	✓	2.505	✓	6.6	169.9	2.205	1.061
	NOR-OP-10.0-19.0-E30-B	✓	-	10.0	6621.9	3852.5	6688.4	2.335	✓	2.505	✓	6.8	170.0	2.204	1.059
	NOR-OP-10.0-19.0-E30-C	✓	-	10.0	6623.8	3849.4	6684.8	2.336	✓	2.505	✓	6.7	169.6	2.210	1.057
	NOR-OP-10.0-19.0-E30-D	✓	-	10.0	6611.1	3826.2	6687.6	2.310	✓	2.505	✓	7.8	170.2	2.198	1.051
	NOR-OP-10.0-19.0-E30-E	✓	-	10.0	6613.8	3847.1	6664.8	2.347	✓	2.505	✓	6.3	169.1	2.213	1.061
	NOR-OP-10.0-19.0-E30-F	✓	-	10.0	6633.8	3875.9	6689.9	2.357	✓	2.505	✓	5.9	170.0	2.208	1.068
	NOR-BU-7.0-19.0-E30-A	✓	+0.3	7.0	6791.2	3984.6	6824.8	2.391	✓	2.493	✓	4.1	169.6	2.266	1.055
	NOR-BU-7.0-19.0-E30-B	✓	+0.3	7.0	6828.8	3986.1	6857.6	2.378	✓	2.493	✓	4.6	170.2	2.270	1.047
	NOR-BU-7.0-19.0-E30-C	✓	+0.3	7.0	6803.1	3984.9	6828.9	2.392	✓	2.493	✓	4.0	169.4	2.273	1.053
	NOR-BU-7.0-19.0-E30-D	✓	+0.3	7.0	6803.6	3969.3	6830.3	2.378	✓	2.493	✓	4.6	169.7	2.269	1.048
	NOR-BU-7.0-19.0-E30-E	✓	+0.3	7.0	6806.8	3973.5	6832.8	2.381	✓	2.493	✓	4.5	169.5	2.272	1.048
	NOR-BU-7.0-19.0-E30-F	✓	+0.3	7.0	6816.6	3997.6	6843.8	2.395	✓	2.493	✓	3.9	169.7	2.273	1.054

Project	Specimen ID	Compacted	AC%	Target AV%	Bulk Specific Gravity					MTSG	Done	Air Voids	Gry. Ht.	Gmb Est.	Actual Corr. Fac.
					Dry Wt.	Submerged Wt.	SSD Wt.	BSG	Done						
Lincoln Cty Tomahawk 25.0mm E-3	TOM-OP-7.0-25.0-E3-OPEN-A	✓	-	7.0	7000.2	4211.5	7048.4	2.468	✓	2.560	✓	3.6	169.7	2.334	1.057
	TOM-OP-7.0-25.0-E3-OPEN-B	✓	-	7.0	7001.1	4212.5	7052	2.466	✓	2.560	✓	3.7	169.7	2.335	1.056
	TOM-OP-7.0-25.0-E3-OPEN-C	✓	-	7.0	6996.2	4238.3	7058.2	2.481	✓	2.560	✓	3.1	171.2	2.313	1.073
	TOM-OP-7.0-25.0-E3-OPEN-D	✓	-	7.0	6987.5	4207	7035.6	2.470	✓	2.560	✓	3.5	169.9	2.327	1.061
	TOM-OP-7.0-25.0-E3-OPEN-E	✓	-	7.0	6994	4198.8	7039.3	2.462	✓	2.560	✓	3.8	169.7	2.332	1.056
	TOM-OP-7.0-25.0-E3-OPEN-F	✓	-	7.0	6982.7	4212.3	7027.1	2.481	✓	2.560	✓	3.1	169.9	2.326	1.067
	TOM-OP-4.0-25.0-E3-OPEN-A	✓	-	4.0	7226.5	4347.6	7252	2.488	✓	2.560	✓	2.8	169.8	2.408	1.033
	TOM-OP-4.0-25.0-E3-OPEN-B	✓	-	4.0	7227.7	4342.2	7249.2	2.486	✓	2.560	✓	2.9	169.7	2.410	1.032
	TOM-OP-4.0-25.0-E3-OPEN-C	✓	-	4.0	7229	4380.2	7263.9	2.507	✓	2.560	✓	2.1	171.8	2.381	1.053
	TOM-OP-4.0-25.0-E3-OPEN-D	✓	-	4.0	7232.1	4381.2	7265.3	2.508	✓	2.560	✓	2.1	170.1	2.406	1.042
	TOM-OP-4.0-25.0-E3-OPEN-E	✓	-	4.0	7234.4	4370	7264.4	2.499	✓	2.560	✓	2.4	169.9	2.410	1.037
	TOM-OP-4.0-25.0-E3-OPEN-F	✓	-	4.0	7226.9	4380.8	7258	2.512	✓	2.560	✓	1.9	169.8	2.408	1.043
	TOM-OP-10.0-25.0-E3-OPEN-A	✓	-	10.0	6766.4	4017.5	6829.1	2.407	✓	2.560	✓	6.0	169.1	2.264	1.063
	TOM-OP-10.0-25.0-E3-OPEN-B	✓	-	10.0	6774.1	4014.2	6837.4	2.399	✓	2.560	✓	6.3	169.1	2.267	1.058
	TOM-OP-10.0-25.0-E3-OPEN-C	✓	-	10.0	6765.8	4006.5	6827.4	2.398	✓	2.560	✓	6.3	168.8	2.268	1.057
	TOM-OP-10.0-25.0-E3-OPEN-D	✓	-	10.0	6764.9	4029.8	6820.5	2.424	✓	2.560	✓	5.3	169.2	2.262	1.071
	TOM-OP-10.0-25.0-E3-OPEN-E	✓	-	10.0	6773.8	4015.6	6834.2	2.403	✓	2.560	✓	6.1	168.9	2.269	1.059
	TOM-OP-10.0-25.0-E3-OPEN-F	✓	-	10.0	6764.4	4072.1	6816.4	2.465	✓	2.560	✓	3.7	169.7	2.256	1.093
	TOM-BU-7.0-25.0-E3-OPEN-A	✓	+0.3	7.0	6924.8	4080	6953.7	2.410	✓	2.529	✓	4.7	168.7	2.323	1.037
	TOM-BU-7.0-25.0-E3-OPEN-B	✓	+0.3	7.0	6929.2	4097.9	6961.7	2.420	✓	2.529	✓	4.3	169.4	2.315	1.045
	TOM-BU-7.0-25.0-E3-OPEN-C	✓	+0.3	7.0	6933.6	4099.8	6964.2	2.421	✓	2.529	✓	4.3	168.8	2.324	1.041
	TOM-BU-7.0-25.0-E3-OPEN-D	✓	+0.3	7.0	6924.4	4183.6	6962.6	2.492	✓	2.529	✓	1.5	170.0	2.305	1.081
	TOM-BU-7.0-25.0-E3-OPEN-E	✓	+0.3	7.0	6918	4168.3	6960.5	2.478	✓	2.529	✓	2.0	169.9	2.304	1.075
	TOM-BU-7.0-25.0-E3-OPEN-F	✓	+0.3	7.0	6921.4	4107.3	6960.4	2.426	✓	2.529	✓	4.1	168.5	2.324	1.044

APPENDIX C SPECIMEN VOLUMETRICS AFTER SAWING/CORING

Project: Lincoln Cty Bloomville 19.0mm E-1

Specimen ID	Diameter Bottom 1	Diameter Bottom 2	Diameter Midpoint 1	Diameter Midpoint 2	Diameter Top 1	Diameter Top 2	Diameter Average	Diameter Std. Dev.	Height 1	Height 2	Height 3	Height 4	Height Average	Height Std. Dev.
BLO-OP-7.0-19.0-E1-A	101.44	101.51	101.44	101.55	101.47	101.37	101.46	0.06	150.63	150.83	150.97	150.77	150.80	0.14
BLO-OP-7.0-19.0-E1-D	101.67	101.45	100.97	101.25	101.33	101.01	101.28	0.27	150.73	150.83	150.62	150.70	150.72	0.09
BLO-OP-7.0-19.0-E1-E	101.43	101.42	101.52	101.51	101.34	101.22	101.41	0.11	150.96	150.69	150.85	150.67	150.79	0.14
BLO-OP-4.0-19.0-E1-D	101.42	101.49	101.51	101.49	101.49	101.37	101.46	0.05	151.36	150.59	150.68	150.77	150.85	0.35
BLO-OP-4.0-19.0-E1-E	101.48	101.45	101.52	101.48	101.54	101.48	101.49	0.03	150.94	150.71	150.64	150.70	150.75	0.13
BLO-OP-4.0-19.0-E1-F	101.43	101.31	101.41	101.44	101.38	101.37	101.39	0.05	150.84	150.73	150.76	150.64	150.74	0.08
BLO-OP-10.0-19.0-E1-A	101.46	101.44	101.52	101.46	101.37	101.36	101.44	0.06	150.74	150.75	150.84	150.78	150.78	0.04
BLO-OP-10.0-19.0-E1-C	101.50	101.55	101.54	101.21	101.23	101.20	101.37	0.17	150.67	150.83	150.88	150.94	150.83	0.12
BLO-OP-10.0-19.0-E1-E	101.33	101.44	101.43	101.50	101.40	101.45	101.43	0.06	150.88	150.67	150.88	150.70	150.78	0.11
BLO-BU-7.0-19.0-E1-C	101.25	101.46	101.42	101.45	101.43	101.44	101.41	0.08	150.77	150.84	150.64	150.74	150.75	0.08
BLO-BU-7.0-19.0-E1-D	101.57	101.50	101.47	101.57	101.37	101.27	101.46	0.12	150.62	150.69	150.70	150.66	150.67	0.04
BLO-BU-7.0-19.0-E1-F	101.60	101.47	101.53	101.38	101.47	101.39	101.47	0.08	150.77	150.95	150.88	150.93	150.88	0.08

Project: Lincoln Cty Bloomville 19.0mm E-1

Specimen ID	Cut down	AC%	Target AV%	Bulk Specific Gravity Dry Wt.	Sub Wt.	SSD Wt.	BSG	Done	MTSG	Done	Air Voids	Ht.	Dia.	Gmb Est.	Actual Corr. Fac.
BLO-OP-7.0-19.0-E1-A	√	-	7.0	2855.2	1652	2861.8	2.360	√	2.521	√	6.4	150.8	101.5	2.342	1.008
BLO-OP-7.0-19.0-E1-D	√	-	7.0	2849.8	1648.5	2856	2.360	√	2.521	√	6.4	150.7	101.3	2.347	1.006
BLO-OP-7.0-19.0-E1-E	√	-	7.0	2854.3	1647	2859.3	2.354	√	2.521	√	6.6	150.8	101.4	2.344	1.005
BLO-OP-4.0-19.0-E1-D	√	-	4.0	2972.3	1762.6	2975.6	2.450	√	2.521	√	2.8	150.9	101.5	2.437	1.005
BLO-OP-4.0-19.0-E1-E	√	-	4.0	2963.7	1754.2	2967.3	2.443	√	2.521	√	3.1	150.7	101.5	2.430	1.005
BLO-OP-4.0-19.0-E1-F	√	-	4.0	2954.3	1744.2	2957.6	2.435	√	2.521	√	3.4	150.7	101.4	2.427	1.003
BLO-OP-10.0-19.0-E1-A	√	-	10.0	2793.9	1597.8	2810	2.305	√	2.521	√	8.6	150.8	101.4	2.293	1.005
BLO-OP-10.0-19.0-E1-C	√	-	10.0	2740.3	1565.7	2753.8	2.306	√	2.521	√	8.5	150.8	101.4	2.251	1.025
BLO-OP-10.0-19.0-E1-E	√	-	10.0	2793.4	1592.4	2803.5	2.306	√	2.521	√	8.5	150.8	101.4	2.293	1.006
BLO-BU-7.0-19.0-E1-C	√	+0.3	7.0	2870.2	1660.3	2874.7	2.363	√	2.505	√	5.6	150.7	101.4	2.357	1.003
BLO-BU-7.0-19.0-E1-D	√	+0.3	7.0	2860	1651.3	2863.7	2.359	√	2.505	√	5.8	150.7	101.5	2.348	1.005
BLO-BU-7.0-19.0-E1-F	√	+0.3	7.0	2862.4	1653.1	2866.4	2.359	√	2.505	√	5.8	150.9	101.5	2.346	1.006

Project: Marathon Cty Mosinee 19.0mm E-3

Specimen ID	Diameter Bottom 1	Diameter Bottom 2	Diameter Midpoint 1	Diameter Midpoint 2	Diameter Top 1	Diameter Top 2	Diameter Average	Diameter Std. Dev.	Height 1	Height 2	Height 3	Height 4	Height Average	Height Std. Dev.
MOS-OP-7.0-19.0-E3-A	101.29	101.43	101.26	101.16	101.53	101.30	101.33	0.13	150.78	150.64	150.65	150.64	150.68	0.07
MOS-OP-7.0-19.0-E3-B	101.46	101.51	101.47	101.62	101.46	101.56	101.51	0.07	150.69	150.67	150.50	150.31	150.54	0.18
MOS-OP-7.0-19.0-E3-E	101.20	101.36	101.34	101.37	101.41	101.37	101.34	0.07	150.49	150.54	150.69	150.70	150.61	0.11
MOS-OP-4.0-19.0-E3-A	101.30	101.26	101.29	101.34	101.40	101.42	101.34	0.06	150.68	150.74	150.57	150.69	150.67	0.07
MOS-OP-4.0-19.0-E3-B	101.36	101.27	101.29	101.31	101.40	101.40	101.34	0.06	150.64	150.65	150.59	150.56	150.61	0.04
MOS-OP-4.0-19.0-E3-D	101.30	101.39	101.37	101.36	101.40	101.40	101.37	0.04	150.71	150.65	150.47	150.41	150.56	0.14
MOS-OP-10.0-19.0-E3-A	101.35	101.29	101.30	101.20	101.46	101.25	101.31	0.09	150.70	150.40	150.40	150.54	150.51	0.14
MOS-OP-10.0-19.0-E3-B	101.25	101.24	101.18	101.26	101.40	101.29	101.27	0.07	150.58	150.48	150.72	150.67	150.61	0.11
MOS-OP-10.0-19.0-E3-F	101.16	101.27	101.16	101.37	101.35	101.39	101.28	0.10	150.57	150.66	150.54	150.77	150.64	0.10
MOS-BU-7.0-19.0-E3-A	101.22	101.20	101.16	101.25	101.25	101.32	101.23	0.05	150.64	150.52	150.73	150.83	150.68	0.13
MOS-BU-7.0-19.0-E3-E	101.39	101.22	101.30	101.27	101.33	101.30	101.30	0.06	150.52	150.61	150.59	150.50	150.56	0.05
MOS-BU-7.0-19.0-E3-F	101.31	101.32	101.27	101.29	101.35	101.28	101.30	0.03	150.58	150.43	150.48	150.55	150.51	0.07

Project: Marathon Cty Mosinee 19.0mm E-3

Specimen ID	Cut down	AC%	Target AV%	Bulk Specific Gravity					MTSG	Done	Air Voids	Ht.	Dia.	Gmb Est.	Actual Corr. Fac.
				Dry Wt.	Sub Wt.	SSD Wt.	BSG	Done							
MOS-OP-7.0-19.0-E3-A	✓	-	7.0	2763.9	1558.2	2771.7	2.278	✓	2.445	✓	6.9	150.7	101.3	2.275	1.001
MOS-OP-7.0-19.0-E3-B	✓	-	7.0	2756.6	1547.3	2763	2.268	✓	2.445	✓	7.3	150.5	101.5	2.262	1.002
MOS-OP-7.0-19.0-E3-E	✓	-	7.0	2757.4	1552.2	2762.6	2.278	✓	2.445	✓	6.8	150.6	101.3	2.270	1.004
MOS-OP-4.0-19.0-E3-A	✓	-	4.0	2846.4	1637	2849	2.349	✓	2.445	✓	4.0	150.7	101.3	2.342	1.003
MOS-OP-4.0-19.0-E3-B	✓	-	4.0	2846.6	1638.2	2849.7	2.350	✓	2.445	✓	3.9	150.6	101.3	2.343	1.003
MOS-OP-4.0-19.0-E3-D	✓	-	4.0	2834.1	1626.2	2838	2.339	✓	2.445	✓	4.4	150.6	101.4	2.332	1.003
MOS-OP-10.0-19.0-E3-A	✓	-	10.0	2691	1495.5	2702.4	2.230	✓	2.445	✓	8.8	150.5	101.3	2.218	1.005
MOS-OP-10.0-19.0-E3-B	✓	-	10.0	2693.6	1502.6	2711.4	2.228	✓	2.445	✓	8.9	150.6	101.3	2.220	1.004
MOS-OP-10.0-19.0-E3-F	✓	-	10.0	2668.4	1479.1	2685.4	2.212	✓	2.445	✓	9.5	150.6	101.3	2.199	1.006
MOS-BU-7.0-19.0-E3-A	✓	+0.3	7.0	2746.5	1542.7	2752.1	2.271	✓	2.438	✓	6.9	150.7	101.2	2.265	1.003
MOS-BU-7.0-19.0-E3-E	✓	+0.3	7.0	2747.7	1544.1	2753.4	2.272	✓	2.438	✓	6.8	150.6	101.3	2.264	1.003
MOS-BU-7.0-19.0-E3-F	✓	+0.3	7.0	2737	1533.2	2743	2.262	✓	2.438	✓	7.2	150.5	101.3	2.256	1.003

Project: Jackson Cty Northfield 19.0mm E-30

Specimen ID	Diameter Bottom 1	Diameter Bottom 2	Diameter Midpoint 1	Diameter Midpoint 2	Diameter Top 1	Diameter Top 2	Diameter Average	Diameter Std. Dev.	Height 1	Height 2	Height 3	Height 4	Height Average	Height Std. Dev.
NOR-OP-7.0-19.0-E30-A	101.45	101.41	101.42	101.37	101.40	101.31	101.39	0.05	150.74	150.70	150.85	150.72	150.75	0.07
NOR-OP-7.0-19.0-E30-E	101.46	101.37	101.43	101.32	101.36	101.30	101.37	0.06	150.59	150.75	150.67	150.92	150.73	0.14
NOR-OP-7.0-19.0-E30-F	101.37	101.40	101.36	101.35	101.39	101.33	101.37	0.03	150.63	150.73	150.72	150.52	150.65	0.10
NOR-OP-4.0-19.0-E30-A	101.37	101.55	101.36	101.58	101.33	101.48	101.45	0.11	150.71	150.68	150.73	150.58	150.68	0.07
NOR-OP-4.0-19.0-E30-B	101.12	101.21	101.24	101.13	101.16	101.14	101.17	0.05	150.80	150.80	150.55	150.50	150.66	0.16
NOR-OP-4.0-19.0-E30-E	101.20	101.15	101.29	101.30	101.33	101.23	101.25	0.07	150.83	150.76	150.91	150.72	150.81	0.08
NOR-OP-10.0-19.0-E30-A	101.31	101.27	101.12	101.19	101.17	101.22	101.21	0.07	150.87	150.74	150.39	150.47	150.62	0.23
NOR-OP-10.0-19.0-E30-B	101.30	101.51	101.50	101.30	101.15	101.24	101.33	0.14	150.70	150.84	150.41	150.39	150.59	0.22
NOR-OP-10.0-19.0-E30-C	101.25	101.26	101.28	101.25	101.59	101.23	101.31	0.14	151.01	150.80	150.89	150.80	150.88	0.10
NOR-BU-7.0-19.0-E30-B	101.41	101.53	101.37	101.49	101.39	101.43	101.44	0.06	150.72	150.73	150.78	150.94	150.79	0.10
NOR-BU-7.0-19.0-E30-D	101.32	101.44	101.25	101.28	101.29	101.22	101.30	0.08	150.86	150.66	150.67	150.54	150.68	0.13
NOR-BU-7.0-19.0-E30-E	101.26	101.27	101.22	101.47	101.26	101.43	101.32	0.10	150.62	150.73	150.64	150.72	150.68	0.06

Project: Jackson Cty Northfield 19.0mm E-30

Specimen ID	Cut down	AC%	Target AV%	Bulk Specific Gravity					MTSG	Done	Air Voids	Ht.	Dia.	Gmb Est.	Actual Corr. Fac.
				Dry Wt.	Sub Wt.	SSD Wt.	BSG	Done							
NOR-OP-7.0-19.0-E30-A	✓	-	7.0	2917.9	1712.1	2920.2	2.415	✓	2.505	✓	3.6	150.8	101.4	2.397	1.008
NOR-OP-7.0-19.0-E30-E	✓	-	7.0	2907.9	1702.9	2910.7	2.408	✓	2.505	✓	3.9	150.7	101.4	2.390	1.007
NOR-OP-7.0-19.0-E30-F	✓	-	7.0	2916	1712	2918.8	2.416	✓	2.505	✓	3.5	150.7	101.4	2.398	1.007
NOR-OP-4.0-19.0-E30-A	✓	-	4.0	2937.6	1733.9	2940.5	2.435	✓	2.505	✓	2.8	150.7	101.4	2.412	1.009
NOR-OP-4.0-19.0-E30-B	✓	-	4.0	2963.1	1755.9	2965.2	2.450	✓	2.505	✓	2.2	150.7	101.2	2.447	1.001
NOR-OP-4.0-19.0-E30-E	✓	-	4.0	2947.5	1740	2951.1	2.434	✓	2.505	✓	2.9	150.8	101.3	2.427	1.003
NOR-OP-10.0-19.0-E30-A	✓	-	10.0	2825	1633.1	2832.9	2.355	✓	2.505	✓	6.0	150.6	101.2	2.331	1.010
NOR-OP-10.0-19.0-E30-B	✓	-	10.0	2818.8	1633.9	2831.1	2.354	✓	2.505	✓	6.0	150.6	101.3	2.321	1.014
NOR-OP-10.0-19.0-E30-C	✓	-	10.0	2813.2	1629.7	2823.6	2.356	✓	2.505	✓	5.9	150.9	101.3	2.313	1.019
NOR-BU-7.0-19.0-E30-B	✓	+0.3	7.0	2915.5	1717.5	2921.6	2.421	✓	2.493	✓	2.9	150.8	101.4	2.393	1.012
NOR-BU-7.0-19.0-E30-D	✓	+0.3	7.0	2896.9	1700	2902.2	2.410	✓	2.493	✓	3.3	150.7	101.3	2.385	1.010
NOR-BU-7.0-19.0-E30-E	✓	+0.3	7.0	2916.5	1711.1	2920.4	2.412	✓	2.493	✓	3.2	150.7	101.3	2.401	1.005

APPENDIX D SAS ANALYSIS OF PRELIMINARY DYNAMIC MODULUS RESULTS

Round Two Preliminary Testing

Frequency	0.1Hz				
Temperature	21.3ºC				
Group	N. Obs.	Mean	Std. Dev.	Min.	Max.
1st Exp.	8	3450.7	1165.9	2200.3	5240.3
2nd Exp.	7	3345.9	838.5	2231.5	4515.4
ANOVA		Bartlett's		Bonferroni	
ANOVA F_{stat}=	0.57	$\chi2_{stat}$=	0.0007	α=0.05	Equal
Levene's F_{stat}=	0.00				
$F_{crit}@\alpha$=0.05	3.59	$\chi^2_{crit}@\alpha$=0.05	3.8415	α=0.10	Equal
$F_{crit}@\alpha$=0.10	2.64	$\chi^2_{crit}@\alpha$=0.10	2.7055		

Frequency	1Hz				
Temperature	39.2ºC				
Group	N. Obs.	Mean	Std. Dev.	Min.	Max.
1st Exp.	8	2137.7	849.2	1242.0	3309.1
2nd Exp.	7	2266.8	451.8	1661.6	3031.3
ANOVA		Bartlett's		Bonferroni	
ANOVA F_{stat}=	0.13	$\chi2_{stat}$=	2.1905	α=0.05	Equal
Levene's F_{stat}=	5.77				
$F_{crit}@\alpha$=0.05	4.67	$\chi^2_{crit}@\alpha$=0.05	3.8415	α=0.10	Equal
$F_{crit}@\alpha$=0.10	3.14	$\chi^2_{crit}@\alpha$=0.10	2.7055		

Frequency	10Hz				
Temperature	39.2ºC				
Group	N. Obs.	Mean	Std. Dev.	Min.	Max.
1st Exp.	8	5103.7	1751.4	3145.5	7951.4
2nd Exp.	7	5408.2	974.3	4037.3	6990.4
ANOVA		Bartlett's		Bonferroni	
ANOVA F_{stat}=	0.17	$\chi2_{stat}$=	1.9011	α=0.05	Equal
Levene's F_{stat}=	3.30				
$F_{crit}@\alpha$=0.05	4.67	$\chi^2_{crit}@\alpha$=0.05	3.8415	α=0.10	Equal
$F_{crit}@\alpha$=0.10	3.14	$\chi^2_{crit}@\alpha$=0.10	2.7055		

Frequency	25Hz				
Temperature	39.2ºC				
Group	N. Obs.	Mean	Std. Dev.	Min.	Max.
1st Exp.	8	9518.6	3872.4	6566.5	18454.5
2nd Exp.	6	10332.7	2690.2	6463.9	13272.2
ANOVA		Bartlett's		Bonferroni	
ANOVA F_{stat}=	0.19	$\chi2_{stat}$=	0.6709	α=0.05	Equal
Levene's F_{stat}=	0.39				
$F_{crit}@\alpha$=0.05	4.75	$\chi^2_{crit}@\alpha$=0.05	3.8415	α=0.10	Equal
$F_{crit}@\alpha$=0.10	3.18	$\chi^2_{crit}@\alpha$=0.10	2.7055		

Round Three Preliminary Testing

Frequency			0.1Hz			
Temperature			21.3ºC			
Group		N. Obs.	Mean	Std. Dev.	Min.	Max.
2nd Exp.		8	3450.7	1165.9	2200.3	5240.3
5th Exp.		7	3345.9	838.5	2231.5	4515.4
Aged		4	3901.5	1132.4	2674.7	5292.4
ANOVA			Bartlett's		Bonferroni	
ANOVA F_{stat}=		0.24	$\chi2_{stat}$=	0.2602	α=0.05	Equal
Levene's F_{stat}=		0.30				
$F_{crit}@\alpha$=0.05		3.59	$\chi^2_{crit}@\alpha$=0.05	3.8415	α=0.10	Equal
$F_{crit}@\alpha$=0.10		2.64	$\chi^2_{crit}@\alpha$=0.10	2.7055		
Group	75% C.I.		90% C.I.		95% C.I.	
2nd Exp.	1,988.7	4,912.6	1,241.3	5,660.0	693.4	6,207.9
5th Exp.	2,342.7	4,746.7	1,728.3	5,361.2	1,277.8	5,811.7
Aged	2,290.1	5,512.9	1,235.8	6,567.2	299.4	7,503.6

Frequency		0.1Hz				
Temperature		39.2ºC				
Group	N. Obs.	Mean	Std. Dev.	Min.	Max.	
2nd Exp.	8	925.3	321.1	601.8	1468.8	
3rd Exp.	7	1050.0	317.5	774.7	1699.4	
5th Exp.	8	1082.1	308.4	767.5	1607.7	
Aged	4	1379.8	317.1	1039.1	1806.0	

ANOVA		Bartlett's		Bonferroni		
ANOVA $F_{stat}=$	1.86	$\chi2_{stat}=$	0.0113	$\alpha=0.05$	Equal	
Levene's $F_{stat}=$	0.02					
$F_{crit}@\alpha=0.05$	2.98	$\chi^2_{crit}@\alpha=0.05$	3.8415	$\alpha=0.10$	Equal	
$F_{crit}@\alpha=0.10$	2.31	$\chi^2_{crit}@\alpha=0.10$	2.7055			

Group	75% C.I.		90% C.I.		95% C.I.	
2nd Exp.	522.6	1,328.0	316.7	1,533.8	165.8	1,684.8
3rd Exp.	645.7	1,454.2	433.0	1,667.0	272.9	1,827.0
5th Exp.	695.4	1,468.8	497.7	1,666.4	352.8	1,811.3
Aged	928.6	1,831.0	633.5	2,126.1	371.2	2,388.4

Frequency			1Hz			
Temperature			21.3ºC			
Group		N. Obs.	Mean	Std. Dev.	Min.	Max.
2nd Exp.		8	7352.2	2278.7	5065.8	11454.8
5th Exp.		7	7154.2	1641.3	4783.9	9447.7
Aged		4	8177.2	2259.3	5774.9	10454.5
ANOVA			Bartlett's		Bonferroni	
ANOVA F_{stat}=		0.18	$\chi 2_{stat}$=	0.0657	α=0.05	Equal
Levene's F_{stat}=		0.10				
F_{crit}@α=0.05		3.59	χ^2_{crit}@α=0.05	3.8415	α=0.10	Equal
F_{crit}@α=0.10		2.64	χ^2_{crit}@α=0.10	2.7055		
Group	75% C.I.		90% C.I.		95% C.I.	
2nd Exp.	4,494.7	10,209.6	3,034.1	11,670.3	1,963.1	12,741.2
5th Exp.	4,726.1	10,980.6	3,127.6	12,579.1	1,955.5	13,751.2
Aged	4,962.2	11,392.2	2,858.8	13,495.7	990.3	15,364.1

Frequency			1Hz			
Temperature			39.2ºC			
Group		N. Obs.	Mean	Std. Dev.	Min.	Max.
2nd Exp.		8	2137.7	849.2	1242.0	3309.1
3rd Exp.		7	2266.8	451.8	1661.6	3031.3
5th Exp.		8	2215.2	578.2	1685.8	3147.7
Aged		4	2888.5	648.7	2161.0	3490.4
ANOVA			Bartlett's		Bonferroni	
ANOVA F_{stat}=		1.29	$\chi 2_{stat}$=	2.4431	α=0.05	Equal
Levene's F_{stat}=		2.92				
$F_{crit}@\alpha$=0.05		2.98	$\chi^2_{crit}@\alpha$=0.05	3.8415	α=0.10	Equal
$F_{crit}@\alpha$=0.10		2.31	$\chi^2_{crit}@\alpha$=0.10	2.7055		
Group		75% C.I.	90% C.I.		95% C.I.	
2nd Exp.	1,072.8	3,202.7	528.5	3,747.0	129.3	4,146.2
3rd Exp.	1,691.7	2,841.9	1,389.1	3,144.6	1,161.4	3,372.3
5th Exp.	1,490.1	2,940.2	1,119.5	3,310.8	847.7	3,582.6
Aged	1,965.3	3,811.6	1,361.3	4,415.6	824.8	4,952.1

Frequency			10Hz			
Temperature			21.3ºC			
Group		N. Obs.	Mean	Std. Dev.	Min.	Max.
2nd Exp.		8	13465.0	4467.3	10114.3	23030.4
5th Exp.		7	12686.5	2553.2	8645.5	15932.2
Aged		4	14170.3	3839.8	10245.6	17746.8
ANOVA			Bartlett's		Bonferroni	
ANOVA F_{stat}=		0.05	$\chi2_{stat}$=	0.1298	α=0.05	Equal
Levene's F_{stat}=		0.10				
$F_{crit}@\alpha$=0.05		3.59	$\chi^2_{crit}@\alpha$=0.05	3.8415	α=0.10	Equal
$F_{crit}@\alpha$=0.10		2.64	$\chi^2_{crit}@\alpha$=0.10	2.7055		
Group	75% C.I.		90% C.I.		95% C.I.	
2nd Exp.	7,863.0	19,067.0	4,999.5	21,930.6	2,899.9	24,030.2
5th Exp.	8,284.9	19,906.3	5,314.6	22,876.5	3,136.8	25,054.4
Aged	8,706.3	19,634.3	5,131.5	23,209.2	1,956.0	26,384.7

Frequency	10Hz				
Temperature	39.2ºC				
Group	N. Obs.	Mean	Std. Dev.	Min.	Max.
2nd Exp.	8	5103.7	1751.4	3145.5	7951.4
3rd Exp.	7	5408.2	974.3	4037.3	6990.4
5th Exp.	8	4952.3	1020.2	3796.1	6162.2
Aged	4	6041.1	1198.7	4851.8	7427.3

ANOVA		Bartlett's		Bonferroni	
ANOVA F_{stat}=	0.70	$\chi2_{stat}$=	2.8683	α=0.05	Equal
Levene's F_{stat}=	2.51				
$F_{crit}@\alpha$=0.05	2.98	$\chi^2_{crit}@\alpha$=0.05	3.8415	α=0.10	Equal
$F_{crit}@\alpha$=0.10	2.31	$\chi^2_{crit}@\alpha$=0.10	2.7055		

Group	75% C.I.		90% C.I.		95% C.I.	
2nd Exp.	2,907.5	7,299.9	1,784.9	8,422.5	961.7	9,245.7
3rd Exp.	4,168.0	6,648.5	3,515.2	7,301.3	3,024.2	7,792.3
5th Exp.	3,673.0	6,231.6	3,019.0	6,885.6	2,539.6	7,365.0
Aged	4,335.3	7,746.9	3,219.3	8,862.9	2,227.9	9,854.3

Frequency			25Hz			
Temperature			21.3ºC			
Group		N. Obs.	Mean	Std. Dev.	Min.	Max.
2nd Exp.		8	16924.3	5089.1	12301.2	27670.6
5th Exp.		7	15972.6	2851.0	10924.5	18697.6
Aged		4	17237.6	4765.3	12449.1	22303.1
ANOVA			Bartlett's		Bonferroni	
ANOVA F_{stat}=		0.12	$\chi 2_{stat}$=	0.5945	α=0.05	Equal
Levene's F_{stat}=		0.35				
$F_{crit}@\alpha$=0.05		3.59	$\chi^2_{crit}@\alpha$=0.05	3.8415	α=0.10	Equal
$F_{crit}@\alpha$=0.10		2.64	$\chi^2_{crit}@\alpha$=0.10	2.7055		
Group	75% C.I.		90% C.I.		95% C.I.	
2nd Exp.	10,542.5	23,306.1	7,280.3	26,568.2	4,888.5	28,960.1
5th Exp.	9,318.3	27,358.1	4,707.7	31,968.8	1,327.0	35,349.4
Aged	10,456.7	24,018.6	6,020.2	28,455.0	2,079.3	32,395.9

Frequency	25Hz				
Temperature	39.2ºC				
Group	N. Obs.	Mean	Std. Dev.	Min.	Max.
2nd Exp.	8	9518.6	3872.4	6566.5	18454.5
3rd Exp.	6	10332.7	2690.2	6463.9	13272.2
5th Exp.	8	8439.8	3087.3	5294.2	14405.6
Aged	4	8215.5	1434.1	6666.3	9584.3
ANOVA			Bartlett's		Bonferroni
ANOVA F_{stat}=	0.58	$\chi 2_{stat}$=	0.3917	α=0.05	Equal
Levene's F_{stat}=	0.47				
$F_{crit}@\alpha$=0.05	3.05	$\chi^2_{crit}@\alpha$=0.05	3.8415	α=0.10	Equal
$F_{crit}@\alpha$=0.10	2.35	$\chi^2_{crit}@\alpha$=0.10	2.7055		
Group	75% C.I.		90% C.I.		95% C.I.
2nd Exp.	4,662.6	14,374.5	2,180.4	16,856.7	360.4	18,676.7
3rd Exp.	6,832.8	13,832.6	4,912.0	15,753.4	3,416.2	17,249.1
5th Exp.	4,568.3	12,311.3	2,589.4	14,290.3	1,138.3	15,741.3
Aged	6,174.8	10,256.1	4,839.7	11,591.2	3,653.7	12,777.2

APPENDIX E PAVEMENT DESIGN INPUTS

Structure--Layers
Layer 1 -- Asphalt concrete
Material type: Asphalt concrete

Layer thickness (in):   3

General Properties

<u>General</u>

Reference temperature (F°):   70

<u>Volumetric Properties as Built</u>

Effective binder content (%):   3.96

Air voids (%):   7

Total unit weight (pcf):   148

<u>Poisson's ratio:</u>   0.35 (user entered)

<u>Thermal Properties</u>

Thermal conductivity asphalt (BTU/hr-ft-F°):   0.67

Heat capacity asphalt (BTU/lb-F°):   0.23

Asphalt Mix

Number of temperatures: 3

Number of frequencies: 4

Temperature	Mixture E* (psi)			
°F	0.1	1	10	25
70	348875	770023	1372039	1792838
86	224543	493474	955293	1348843
103	92440	199640	512500	877097

Asphalt Binder

Option: Conventional binder

Number of penetrations: 0

Number of Brookfield viscosities: 4

Test	Temp. °F	Binder Property
Softening point (P)	0	13000
Absolute viscosity (P)	140	0
Kinematic viscosity (CS)	275	0
Specific gravity	77	1.029
Brookfield viscosity	176	32833
Brookfield viscosity	212	5791
Brookfield viscosity	250	1308
Brookfield viscosity	275	625

Layer 2 -- Asphalt concrete

Material type: Asphalt concrete
Layer thickness (in): 5

General Properties

General
Reference temperature (F°): 70

Volumetric Properties as Built
Effective binder content (%): 4.31
Air voids (%): 2.6
Total unit weight (pcf): 148

Poisson's ratio: 0.35 (user entered)

Thermal Properties
Thermal conductivity asphalt (BTU/hr-ft-F°): 0.67
Heat capacity asphalt (BTU/lb-F°): 0.23

Asphalt Mix

Number of temperatures: 3
Number of frequencies: 4

Temperature	Mixture E* (psi)			
°F	0.1	1	10	25
65.1	607666	1417854	2766581	3353125
81.4	370919	872681.3	1829218	2373657
97.7	136774	333500	902156	1404953

Asphalt Binder

Option: Conventional binder
Number of penetrations: 0
Number of Brookfield viscosities: 4

Test	Temp. °F	Binder Property
Softening point (P)	0	13000
Absolute viscosity (P)	140	0
Kinematic viscosity (CS)	275	0
Specific gravity	77	1.029
Brookfield viscosity	176	45997
Brookfield viscosity	212	8216
Brookfield viscosity	250	2141
Brookfield viscosity	275	892

Layer 3 -- Asphalt concrete

Material type:	Asphalt concrete
Layer thickness (in):	5

General Properties

General

Reference temperature (F°):	70

Volumetric Properties as Built

Effective binder content (%):	4.31
Air voids (%):	7
Total unit weight (pcf):	148

Poisson's ratio: 0.35 (user

Thermal Properties

Thermal conductivity asphalt (BTU/hr-ft-F°):	0.67
Heat capacity asphalt (BTU/lb-F°):	0.23

Asphalt Mix

Cumulative % Retained 3/4 inch sieve:	0.6
Cumulative % Retained 3/8 inch sieve:	46.2
Cumulative % Retained #4 sieve:	66.5
% Passing #200 sieve:	2.8

Asphalt Binder

Option:	Superpave binder grading
A	10.3120 (correlated)
VTS:	-3.4400 (correlated)

High temp. °C	Low temperature, °C				
	-10	-16	-22	-28	-34
46					
52					
58					
64					
70					
76					
82					

Layer 4 -- Crushed stone

Unbound Material: Crushed stone
Thickness(in): 12

Strength Properties

Input Level: Level 3
Analysis Type: ICM inputs (ICM Calculated
Poisson's ratio: 0.35
Coefficient of lateral pressure,Ko: 0.5
Modulus (input) (psi): 40000

ICM Inputs

<u>Gradation and Plasticity Index</u>
Plasticity Index, PI: 1
Passing #200 sieve (%): 8
Passing #4 sieve (%): 25
D60 (mm): 2

<u>Calculated/Derived Parameters</u>
Maximum dry unit weight (pcf): 122.3 (derived)
Specific gravity of solids, Gs: 2.67 (derived)
Saturated hydraulic conductivity (ft/hr): 37 (derived)
Optimum gravimetric water content (%): 11.2 (derived)
Calculated degree of saturation (%): 82.7 (calculated)

Soil water characteristic curve parameters: Default values

Parameters	Value
a	11.3
b	1.74
c	0.516
Hr.	368

Layer 5 -- A-3

Unbound Material: A-3
Thickness(in):   6

Strength Properties

Input Level: Level 3
Analysis Type: ICM inputs (ICM Calculated
Poisson's ratio: 0.35
Coefficient of lateral pressure,Ko: 0.5
Modulus (input) (psi):   29000

ICM Inputs

Gradation and Plasticity Index
Plasticity Index, PI: 0
Passing #200 sieve (%):   10
Passing #4 sieve (%):   80
D60 (mm):   0.2

Calculated/Derived Parameters
Maximum dry unit weight (pcf):   126 (derived)
Specific gravity of solids, Gs: 2.65 (derived)
Saturated hydraulic conductivity (ft/hr):   0.0223 (derived)
Optimum gravimetric water content (%):   9.2 (derived)
Calculated degree of saturation (%):   78 (calculated)

Soil water characteristic curve parameters: Default values

Parameters	Value
a	2.89
b	7.5
c	0.488
Hr.	7.65

APPENDIX F BITUMEN TEMPERATURE SUSCEPTIBILITY

Job:	Baraboo
Mix Type:	12.5mm Dense
Traffic Level:	E-0.3
Binder Grade (PG):	58-28

		A	VTS
Original Binder	η_{orig}	9.941	-3.321
Mix/Laydown Condition	$\eta_{t=0}$	9.718	-3.228
RTFO Aged Viscosity Tested	η_{vis}	9.828	-3.281
Fonesca and Witczak	$\eta_{t=0}$	11.010	-3.701

A = regression intercept

VTS = Regression slope of viscosity temperature susceptibility

Viscosity (10^6 Poise):		Int. Temperature (°C)	High Temperature (°C)
		19.0	36.6
Original Binder	η_{orig}	115.5	4.4
Mix/Laydown Condition	$\eta_{t=0}$	417.4	13.7
RTFO Aged Viscosity Tested	η_{vis}	89.5	3.7
Fonesca and Witczak	$\eta_{t=0}$	513.1	10.3
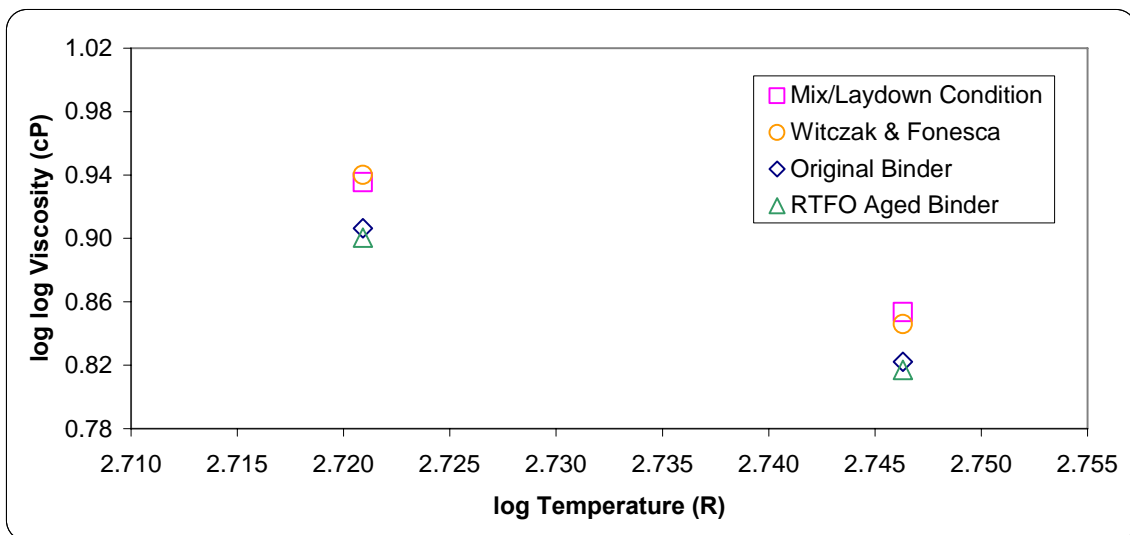
Job: Medford

Mix Type: 12.5mm Dense

Traffic Level: E-1

Binder Grade (PG): 58-28

		A	VTS
Original Binder	η_{orig}	11.802	-3.997
Mix/Laydown Condition	$\eta_{t=0}$	11.527	-3.885
RTFO Aged Viscosity Tested	η_{vis}	10.218	-3.419
Fonesca and Witczak	$\eta_{t=0}$	11.010	-3.701

A = regression intercept

VTS = Regression slope of viscosity temperature susceptibility

Viscosity (10^6 Poise):		Int. Temperature (°C)	High Temprature (°C)
		17.6	35.7
Original Binder	η_{orig}	422.3	6.0
Mix/Laydown Condition	$\eta_{t=0}$	1,603.5	19.1
RTFO Aged Viscosity Tested	η_{vis}	222.6	6.2
Fonesca and Witczak	$\eta_{t=0}$	735.3	12.3

Job: Wautoma

Mix Type: 12.5mm Dense

Traffic Level: E-1

Binder Grade (PG): 58-28

		A	VTS
Original Binder	η_{orig}	9.933	-3.317
Mix/Laydown Condition	$\eta_{t=0}$	9.710	-3.225
RTFO Aged Viscosity Tested	η_{vis}	10.002	-3.340
Fonesca and Witczak	$\eta_{t=0}$	11.010	-3.701

A = regression intercept

VTS = Regression slope of viscosity temperature susceptibility

Viscosity (10^6 Poise):		Int. Temperature (°C)	High Temeprature (°C)
		18.8	37.7
Original Binder	η_{orig}	123.5	3.7
Mix/Laydown Condition	$\eta_{t=0}$	447.4	11.7
RTFO Aged Viscosity Tested	η_{vis}	170.5	4.7
Fonesca and Witczak	$\eta_{t=0}$	539.9	8.4

		A	**VTS**
Original Binder	η_{orig}	9.725	-3.243
Mix/Laydown Condition	$\eta_{t=0}$	9.507	-3.152
RTFO Aged Viscosity Tested	η_{vis}	9.750	-3.251
Fonesca and Witczak	$\eta_{t=0}$	11.010	-3.701

A = regression intercept

VTS = Regression slope of viscosity temperature susceptibility

Viscosity (10^6Poise):		**Int. Temperature (°C)**	**High Temeprature (°C)**
		16.6	**35.7**
Original Binder	η_{orig}	153.0	4.5
Mix/Laydown Condition	$\eta_{t=0}$	559.0	14.2
RTFO Aged Viscosity Tested	η_{vis}	171.7	4.9
Fonesca and Witczak	$\eta_{t=0}$	955.5	12.3

Job: Hayward

Mix Type: 12.5mm Dense

Traffic Level: E-3

Binder Grade (PG): 58-28

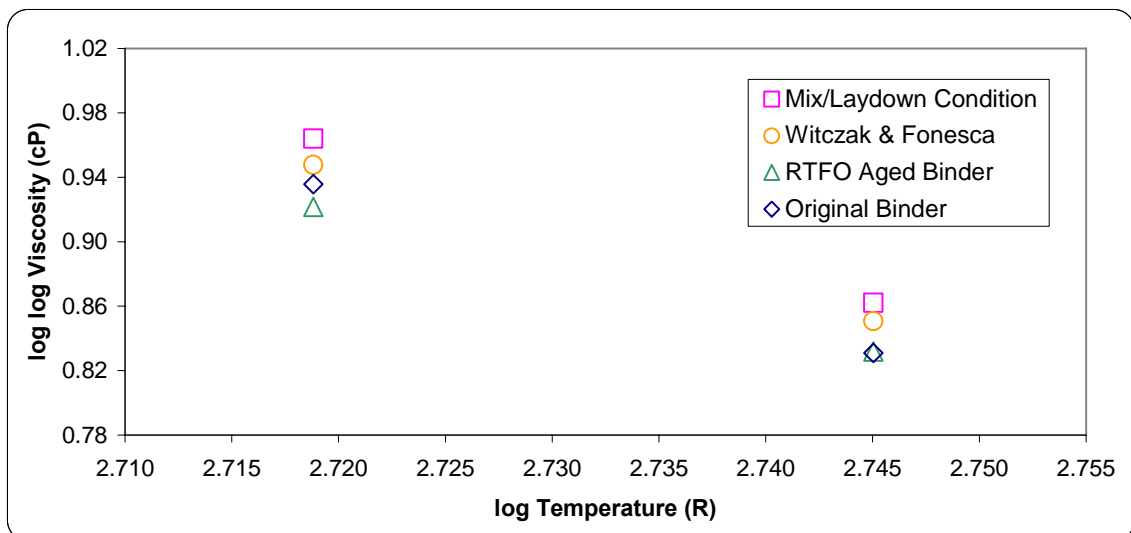|		A	VTS
Original Binder	η_{orig}	9.778	-3.263
Mix/Laydown Condition	$\eta_{t=0}$	9.559	-3.171
RTFO Aged Viscosity Tested	η_{vis}	9.806	-3.272
Fonesca and Witczak	$\eta_{t=0}$	11.010	-3.701

A = regression intercept

VTS = Regression slope of viscosity temperature susceptibility

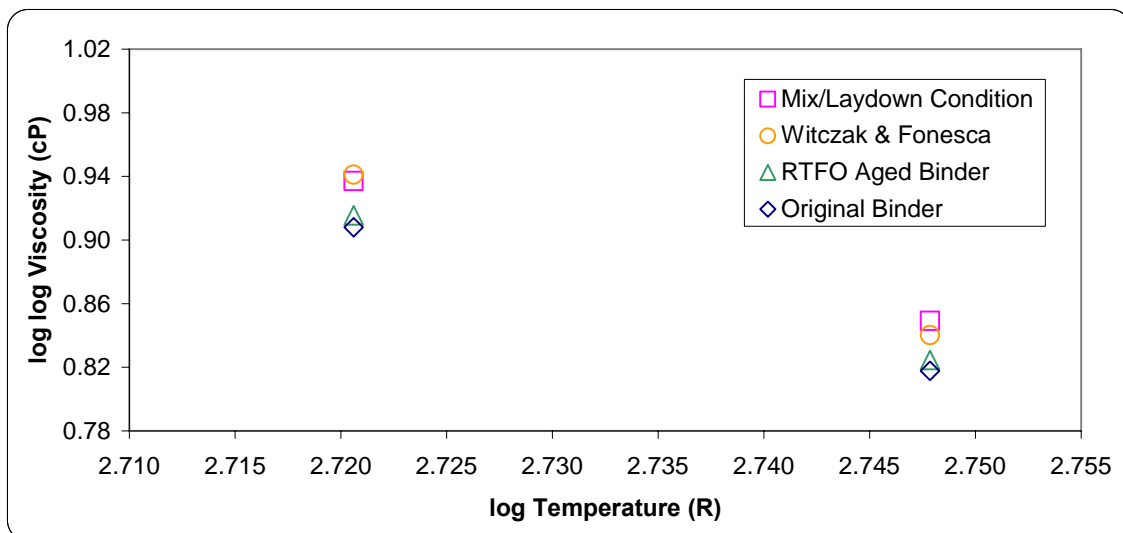| Viscosity (10^6 Poise):		Int. Temperature (°C)	High Temperature (°C)
		19.0	36.6
Original Binder	η_{orig}	90.7	3.8
Mix/Laydown Condition	$\eta_{t=0}$	324.5	11.7
RTFO Aged Viscosity Tested	η_{vis}	106.5	4.3
Fonesca and Witczak	$\eta_{t=0}$	513.1	10.3
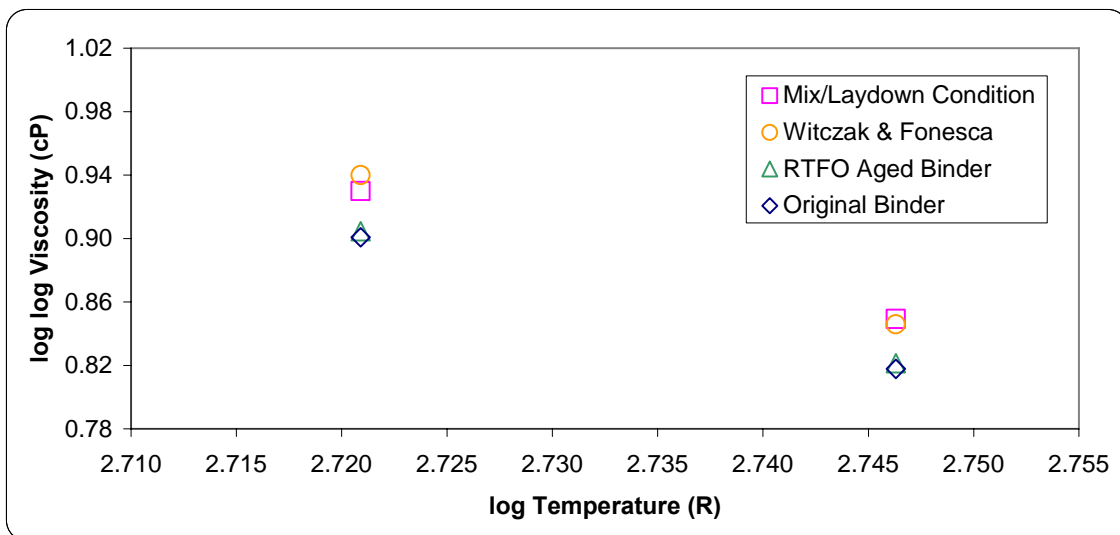
Job:	Wausau
Mix Type:	12.5mm Dense
Traffic Level:	E-3
Binder Grade (PG):	64-22

		A	VTS
Original Binder	η_{orig}	10.171	-3.395
Mix/Laydown Condition	$\eta_{t=0}$	9.941	-3.300
RTFO Aged Viscosity Tested	η_{vis}	9.995	-3.332
Fonesca and Witczak	$\eta_{t=0}$	11.010	-3.701

A = regression intercept

VTS = Regression slope of viscosity temperature susceptibility

Viscosity (10^6 Poise):		Int. Temperature (°C)	High Temeprature (°C)
		19.0	36.6
Original Binder	η_{orig}	397.9	11.2
Mix/Laydown Condition	$\eta_{t=0}$	1,507.5	36.9
RTFO Aged Viscosity Tested	η_{vis}	312.2	9.8
Fonesca and Witczak	$\eta_{t=0}$	513.1	10.3

Job: Hurley

Mix Type: 12.5mm Dense

Traffic Level: E-3

Binder Grade (PG): 64-34

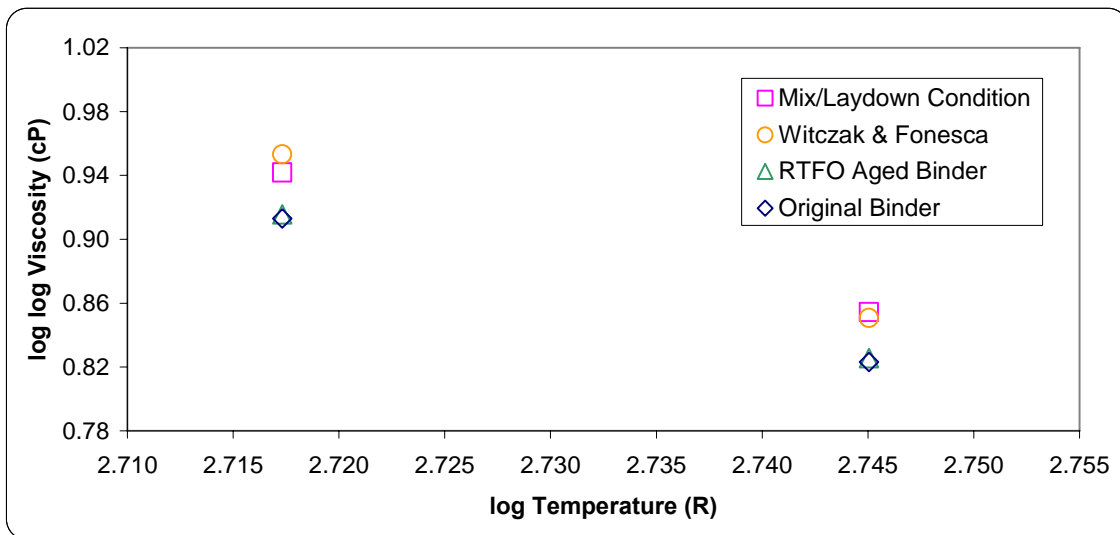|		A	VTS
Original Binder	η_{orig}	10.172	-3.397
Mix/Laydown Condition	$\eta_{t=0}$	9.942	-3.302
RTFO Aged Viscosity Tested	η_{vis}	9.461	-3.127
Fonesca and Witczak	$\eta_{t=0}$	11.010	-3.701

A = regression intercept

VTS = Regression slope of viscosity temperature susceptibility

Viscosity (10^6Poise):		Int. Temperature (°C)	High Temprature (°C)
		19.0	36.6
Original Binder	η_{orig}	324.8	9.5
Mix/Laydown Condition	$\eta_{t=0}$	1,221.0	31.0
RTFO Aged Viscosity Tested	η_{vis}	898.5	28.6
Fonesca and Witczak	$\eta_{t=0}$	513.1	10.3
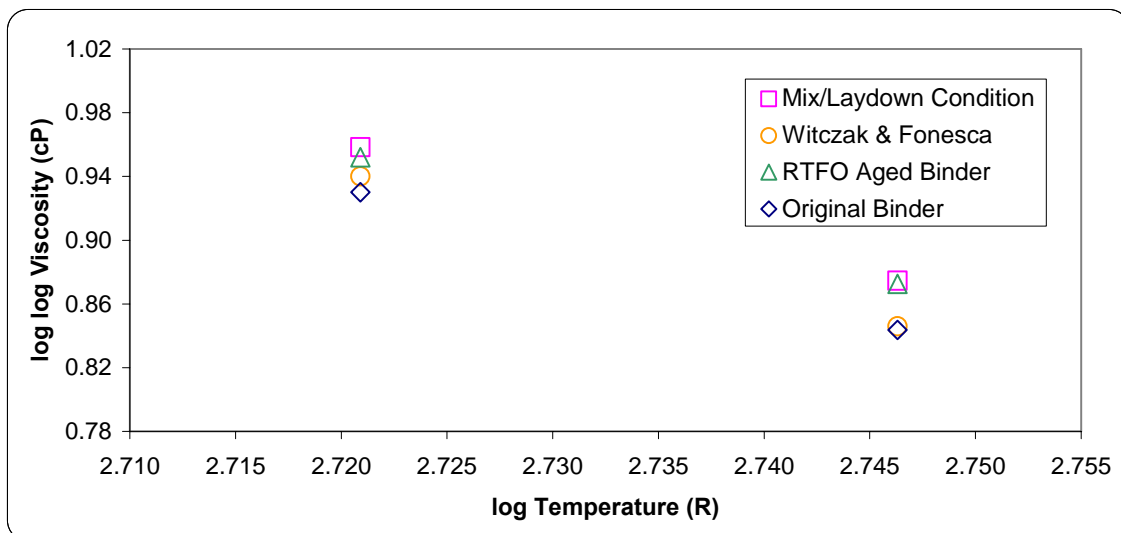
Job: Antigo

Mix Type: 12.5mm Dense

Traffic Level: E-10

Binder Grade (PG): 58-34

		A	VTS
Original Binder	η_{orig}	8.969	-2.970
Mix/Laydown Condition	$\eta_{t=0}$	8.772	-2.887
RTFO Aged Viscosity Tested	η_{vis}	8.533	-2.808
Fonesca and Witczak	$\eta_{t=0}$	10.035	-3.350

A = regression intercept

VTS = Regression slope of viscosity temperature susceptibility

| Viscosity (10^6 Poise):		Int. Temperature (°C)	High Temperature (°C)
		17.3	35.2
Original Binder	η_{orig}	69.4	3.7
Mix/Laydown Condition	$\eta_{t=0}$	245.5	11.5
RTFO Aged Viscosity Tested	η_{vis}	85.0	5.1
Fonesca and Witczak	$\eta_{t=0}$	304.1	8.8

Job:	Plymouth
Mix Type:	12.5mm Dense
Traffic Level:	E-10
Binder Grade (PG):	64-22

		A	VTS
Original Binder	η_{orig}	9.916	-3.312
Mix/Laydown Condition	$\eta_{t=0}$	9.693	-3.219
RTFO Aged Viscosity Tested	η_{vis}	9.665	-3.221
Fonesca and Witczak	$\eta_{t=0}$	10.980	-3.680

A = regression intercept

VTS = Regression slope of viscosity temperature susceptibility

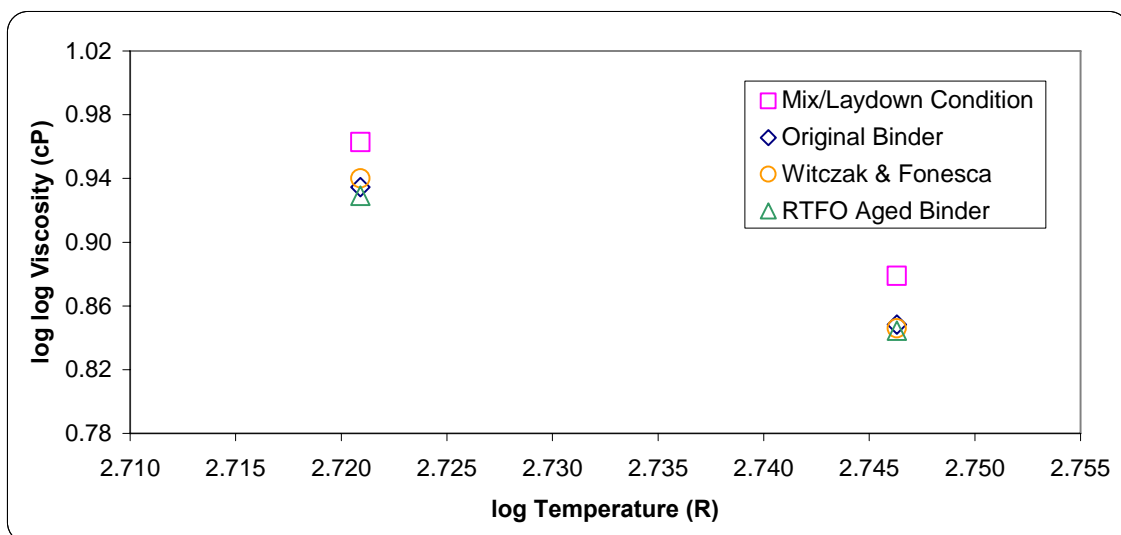| Viscosity (10^6 Poise):		Int. Temperature (°C)	High Temeprature (°C)
		19.7	37.6
Original Binder	η_{orig}	90.8	3.5
Mix/Laydown Condition	$\eta_{t=0}$	325.0	10.8
RTFO Aged Viscosity Tested	η_{vis}	80.1	3.4
Fonesca and Witczak	$\eta_{t=0}$	1,550.9	24.4
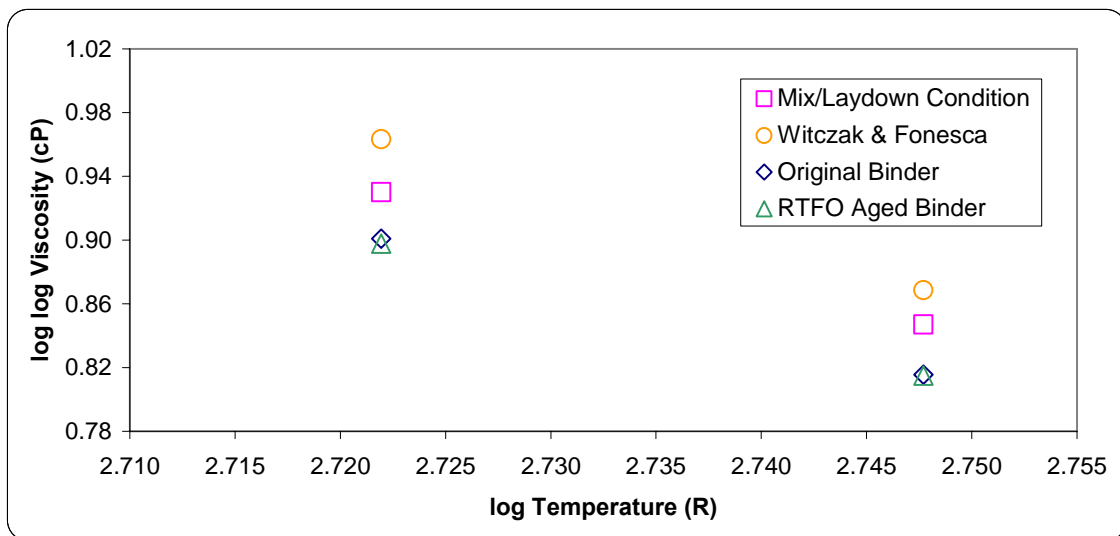
Job: Racine

Mix Type: 12.5mm Dense

Traffic Level: E-10

Binder Grade (PG): 64-28

		A	VTS
Original Binder	η_{orig}	9.313	-3.084
Mix/Laydown Condition	$\eta_{t=0}$	9.106	-2.998
RTFO Aged Viscosity Tested	η_{vis}	9.093	-2.998
Fonesca and Witczak	$\eta_{t=0}$	10.312	-3.440

A = regression intercept

VTS = Regression slope of viscosity temperature susceptibility

Viscosity (10^6 Poise):		Int. Temperature (°C)	High Temperature (°C)
		20.9	39.2
Original Binder	η_{orig}	148.9	6.1
Mix/Laydown Condition	$\eta_{t=0}$	543.4	19.5
RTFO Aged Viscosity Tested	η_{vis}	302.6	11.9
Fonesca and Witczak	$\eta_{t=0}$	575.2	13.1
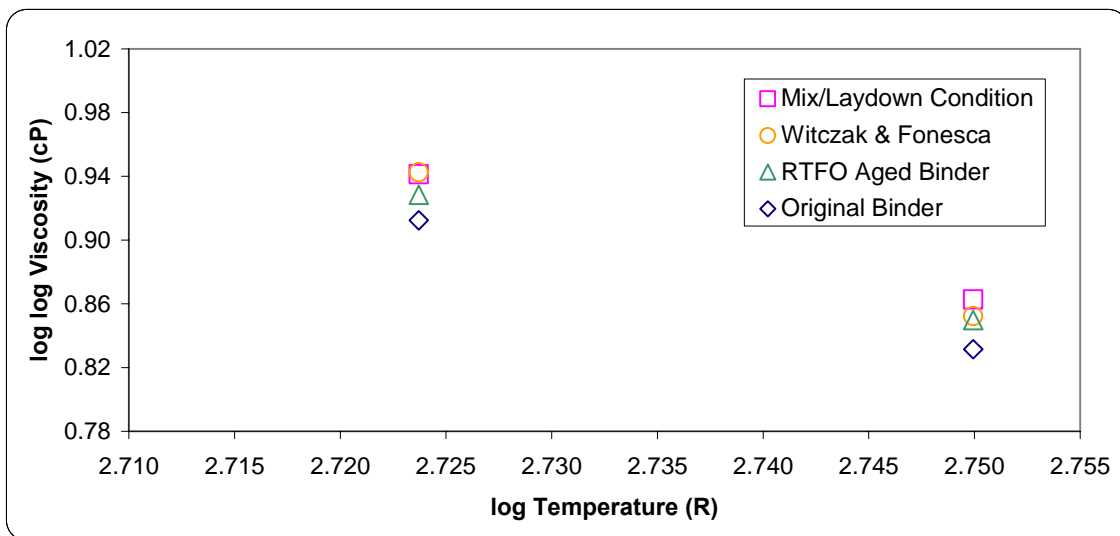
Job:	Northfield
Mix Type:	12.5mm Open
Traffic Level:	E-10
Binder Grade (PG):	70-22

		A	VTS
Original Binder	η_{orig}	8.347	-2.725
Mix/Laydown Condition	$\eta_{t=0}$	8.168	-2.649
RTFO Aged Viscosity Tested	η_{vis}	9.065	-2.964
Fonesca and Witczak	$\eta_{t=0}$	10.299	-3.426

A = regression intercept

VTS = Regression slope of viscosity temperature susceptibility

Viscosity (10^6Poise):		Int. Temperature (°C)	High Temeprature (°C)
		18.4	36.5
Original Binder	η_{orig}	400.2	20.0
Mix/Laydown Condition	$\eta_{t=0}$	1,516.3	67.1
RTFO Aged Viscosity Tested	η_{vis}	12,307.7	275.9
Fonesca and Witczak	$\eta_{t=0}$	3,607.2	59.6

Job:	Cascade
Mix Type:	19.0mm Dense
Traffic Level:	E-1
Binder Grade (PG):	58-28

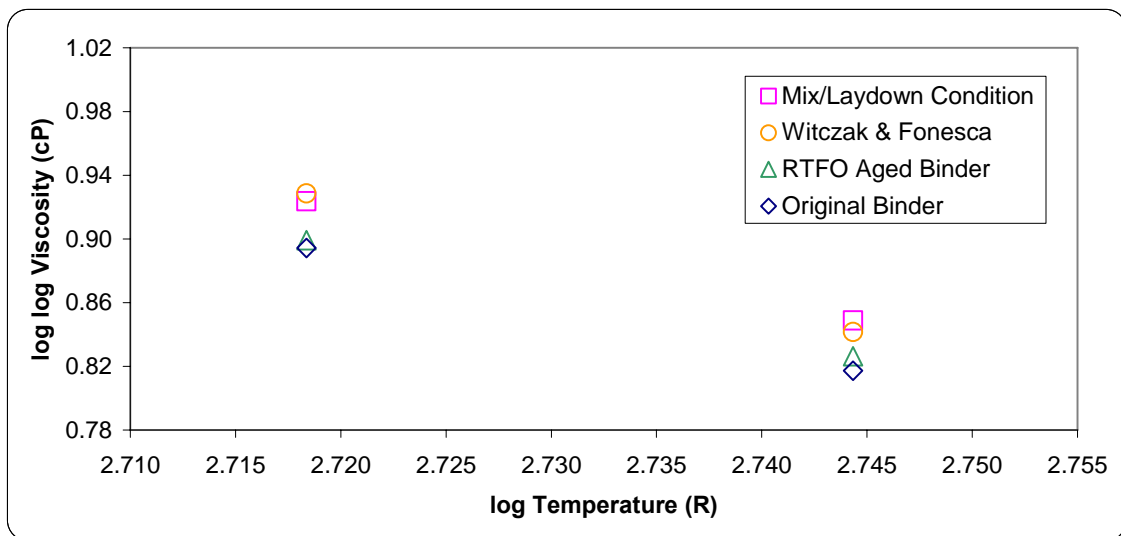|		A	VTS
Original Binder	η_{orig}	12.124	-4.116
Mix/Laydown Condition	$\eta_{t=0}$	11.840	-4.001
RTFO Aged Viscosity Tested	η_{vis}	9.279	-3.086
Fonesca and Witczak	$\eta_{t=0}$	11.010	-3.701

A = regression intercept

VTS = Regression slope of viscosity temperature susceptibility

| Viscosity (10^6Poise):		Int. Temperature (°C)	High Temprature (°C)
		19.8	37.7
Original Binder	η_{orig}	216.2	3.4
Mix/Laydown Condition	$\eta_{t=0}$	800.4	10.5
RTFO Aged Viscosity Tested	η_{vis}	36.3	2.0
Fonesca and Witczak	$\eta_{t=0}$	419.3	8.4
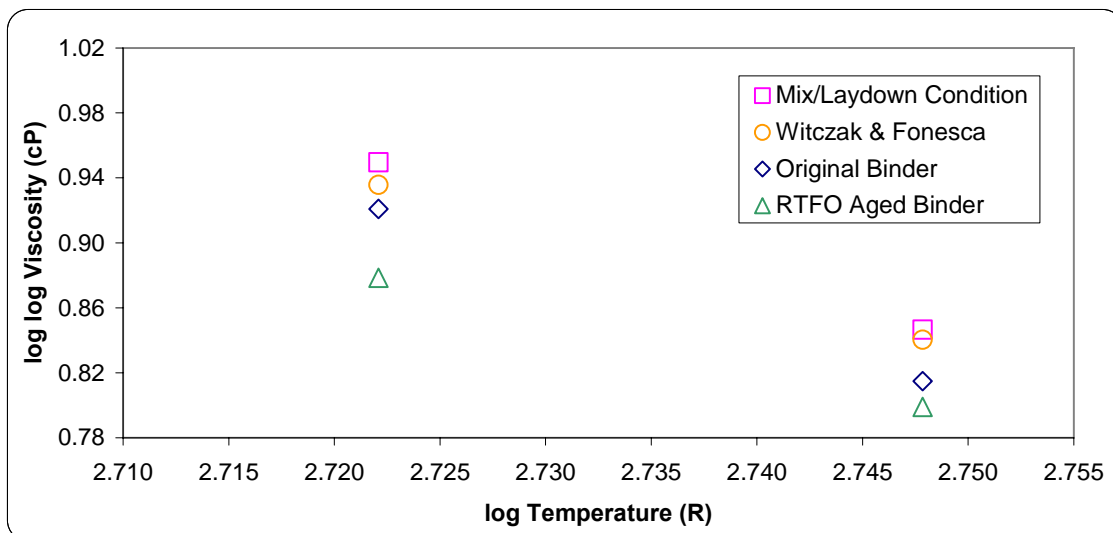
Job: **Bloomville**
Mix Type: **19.0mm Dense**
Traffic Level: **E-1**
Binder Grade (PG):   **58-34**

		A	VTS
Original Binder	η_{orig}	9.188	-3.048
Mix/Laydown Condition	$\eta_{t=0}$	8.985	-2.963
RTFO Aged Viscosity Tested	η_{vis}	9.207	-3.049
Fonesca and Witczak	$\eta_{t=0}$	10.035	-3.350

A = regression intercept

VTS = Regression slope of viscosity temperature susceptibility

Viscosity (10^6Poise):		Int. Temperature (°C)	High Temeprature (°C)
		17.5	36.6
Original Binder	η_{orig}	89.6	3.5
Mix/Laydown Condition	$\eta_{t=0}$	320.3	11.1
RTFO Aged Viscosity Tested	η_{vis}	201.2	6.9
Fonesca and Witczak	$\eta_{t=0}$	290.7	6.9
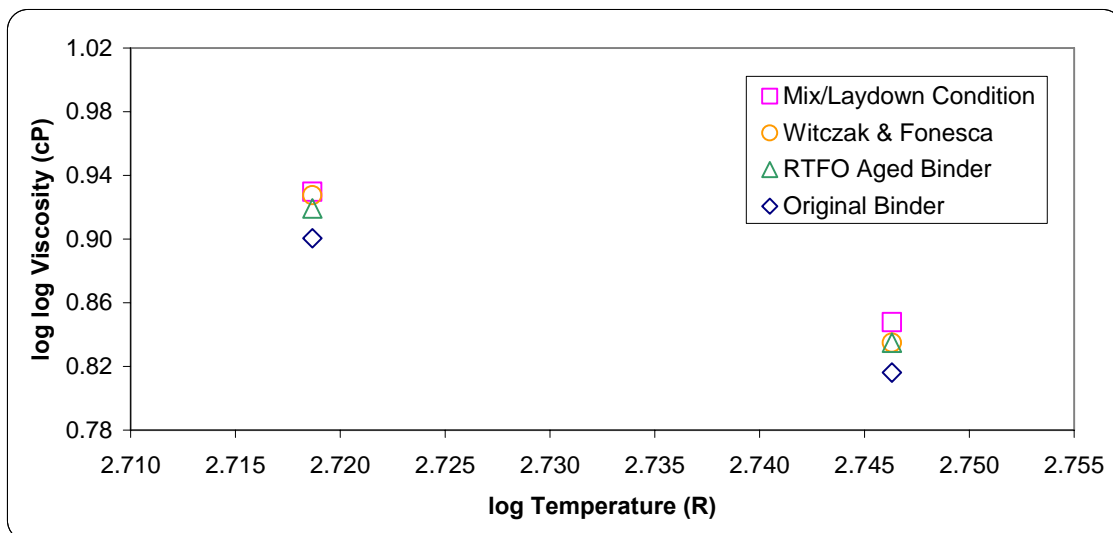
Job: Brule

Mix Type: 19.0mm Dense

Traffic Level: E-0.3

Binder Grade (PG): 58-28

		A	VTS
Original Binder	η_{orig}	10.300	-3.451
Mix/Laydown Condition	$\eta_{t=0}$	10.067	-3.355
RTFO Aged Viscosity Tested	η_{vis}	9.587	-3.191
Fonesca and Witczak	$\eta_{t=0}$	11.010	-3.701

A = regression intercept

VTS = Regression slope of viscosity temperature susceptibility

| Viscosity (10^6Poise):		Int. Temperature (°C)	High Temeprature (°C)
		18.8	37.7
Original Binder	η_{orig}	139.9	3.6
Mix/Laydown Condition	$\eta_{t=0}$	509.1	11.3
RTFO Aged Viscosity Tested	η_{vis}	103.7	3.6
Fonesca and Witczak	$\eta_{t=0}$	539.9	8.4
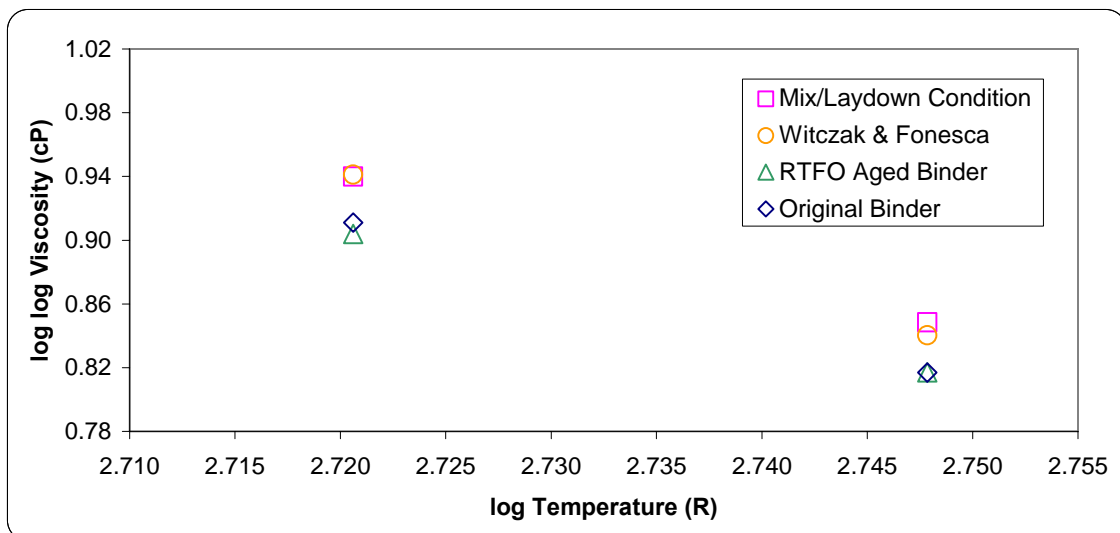
Job: Waunakee

Mix Type: 19.0mm Dense

Traffic Level: E-3

Binder Grade (PG): 58-28

		A	VTS
Original Binder	η_{orig}	9.890	-3.302
Mix/Laydown Condition	$\eta_{t=0}$	9.668	-3.210
RTFO Aged Viscosity Tested	η_{vis}	9.711	-3.234
Fonesca and Witczak	$\eta_{t=0}$	11.010	-3.701

A = regression intercept

VTS = Regression slope of viscosity temperature susceptibility

Viscosity (10^6 Poise):		Int. Temperature (°C)	High Temeprature (°C)
		20.1	37.9
Original Binder	η_{orig}	88.1	3.5
Mix/Laydown Condition	$\eta_{t=0}$	314.7	10.8
RTFO Aged Viscosity Tested	η_{vis}	118.0	4.7
Fonesca and Witczak	$\eta_{t=0}$	389.0	8.1
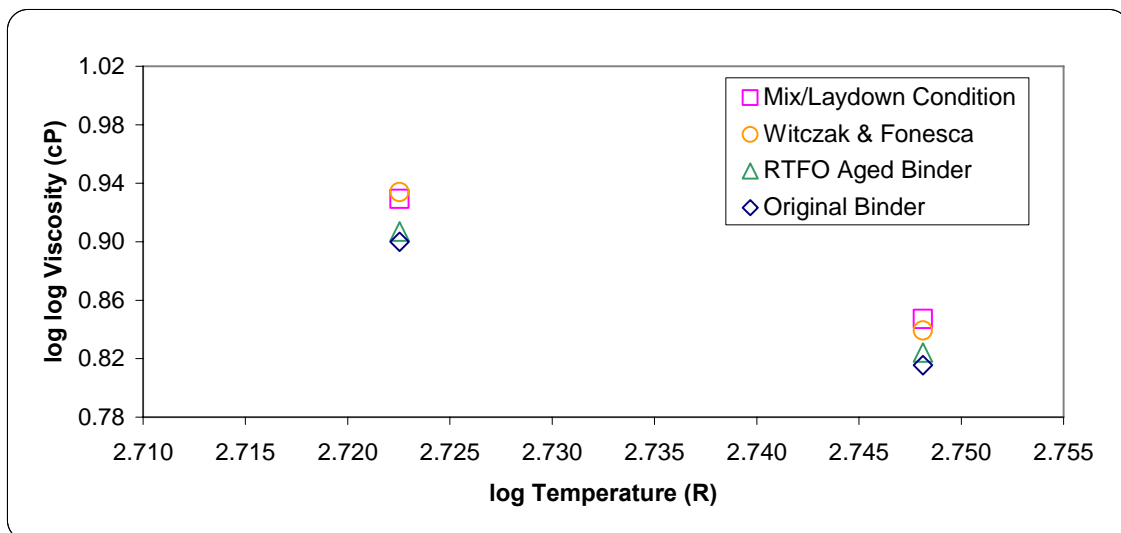
Job: Mosinee

Mix Type: 19.0mm Dense

Traffic Level: E-3

Binder Grade (PG): 58-28

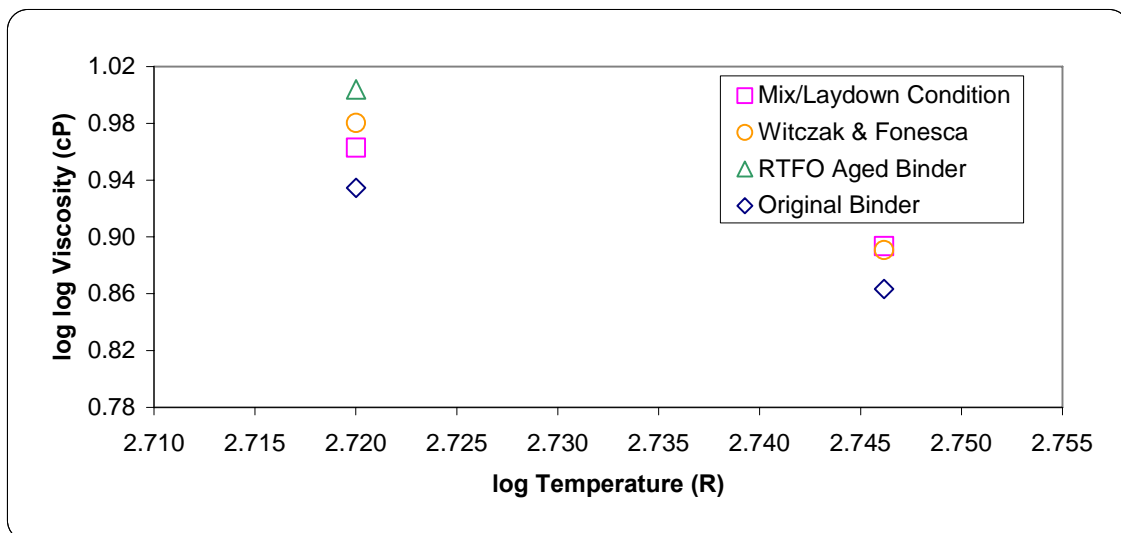|		A	VTS
Original Binder	η_{orig}	11.605	-3.925
Mix/Laydown Condition	$\eta_{t=0}$	11.335	-3.816
RTFO Aged Viscosity Tested	η_{vis}	10.218	-3.419
Fonesca and Witczak	$\eta_{t=0}$	11.010	-3.701

A = regression intercept

VTS = Regression slope of viscosity temperature susceptibility

Viscosity (10^6 Poise):		Int. Temperature (°C)	High Temprature (°C)
		18.7	36.9
Original Binder	η_{orig}	283.4	4.6
Mix/Laydown Condition	$\eta_{t=0}$	1,060.0	14.6
RTFO Aged Viscosity Tested	η_{vis}	174.0	5.0
Fonesca and Witczak	$\eta_{t=0}$	553.9	9.8
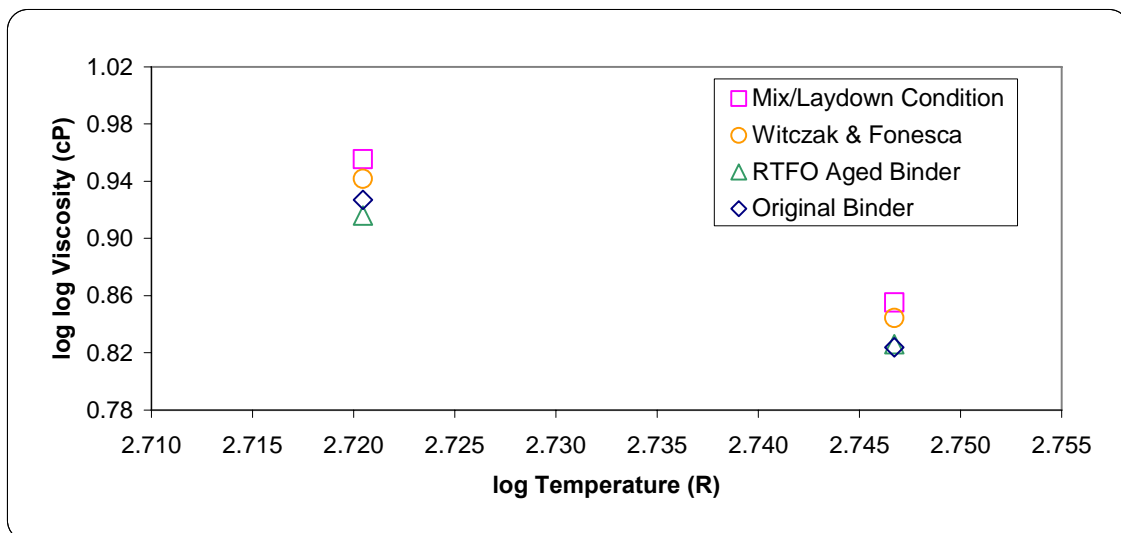
Job: Cumberland

Mix Type: 19.0mm Dense

Traffic Level: E-3

Binder Grade (PG): 58-28

		A	VTS
Original Binder	η_{orig}	9.906	-3.308
Mix/Laydown Condition	$\eta_{t=0}$	9.683	-3.215
RTFO Aged Viscosity Tested	η_{vis}	9.958	-3.324
Fonesca and Witczak	$\eta_{t=0}$	11.010	-3.701

A = regression intercept

VTS = Regression slope of viscosity temperature susceptibility

| Viscosity (10^6 Poise):		Int. Temperature (°C)	High Temeprature (°C)
		17.7	36.0
Original Binder	η_{orig}	146.6	4.7
Mix/Laydown Condition	$\eta_{t=0}$	534.8	14.9
RTFO Aged Viscosity Tested	η_{vis}	223.6	6.6
Fonesca and Witczak	$\eta_{t=0}$	716.4	11.6
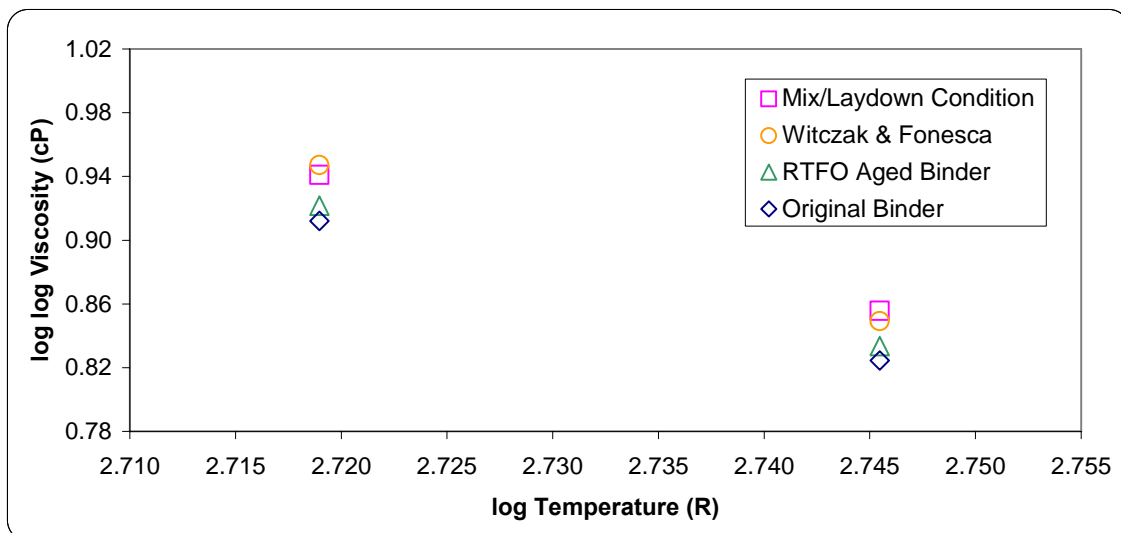
Job: Antigo

Mix Type: 19.0mm Dense

Traffic Level: E-10

Binder Grade (PG): 58-34

		A	VTS
Original Binder	η_{orig}	8.969	-2.970
Mix/Laydown Condition	$\eta_{t=0}$	8.772	-2.887
RTFO Aged Viscosity Tested	η_{vis}	8.533	-2.808
Fonesca and Witczak	$\eta_{t=0}$	11.010	-3.701

A = regression intercept

VTS = Regression slope of viscosity temperature susceptibility

| Viscosity (10^6 Poise):		Int. Temperature (°C)	High Temperature (°C)
		17.7	36.0
Original Binder	η_{orig}	64.4	3.3
Mix/Laydown Condition	$\eta_{t=0}$	227.4	10.2
RTFO Aged Viscosity Tested	η_{vis}	79.2	4.5
Fonesca and Witczak	$\eta_{t=0}$	716.4	11.6
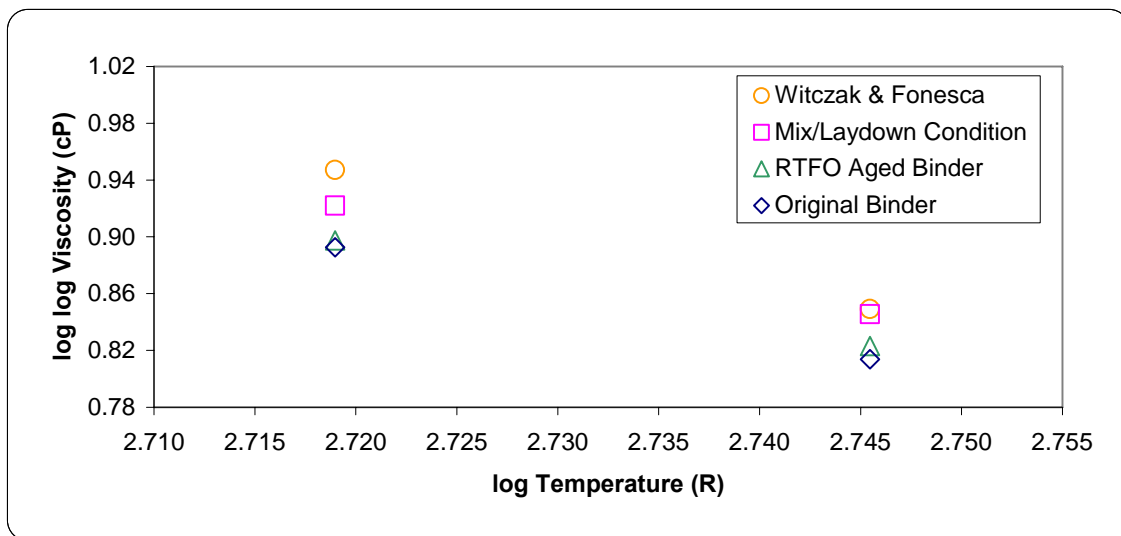
Job:	**Northfield**
Mix Type:	**19.0mm Dense**
Traffic Level:	**E-30**
Binder Grade (PG):	**64-28**

		A	**VTS**
Original Binder	η_{orig}	**10.124**	**-3.377**
Mix/Laydown Condition	$\eta_{t=0}$	**9.896**	**-3.283**
RTFO Aged Viscosity Tested	η_{vis}	**9.448**	**-3.132**
Fonesca and Witczak	$\eta_{t=0}$	**10.312**	**-3.426**

A = regression intercept

VTS = Regression slope of viscosity temperature susceptibility

Viscosity (10^6Poise):		**Int. Temperature (°C)**	**High Temeprature (°C)**
		18.4	**36.5**
Original Binder	η_{orig}	**491.2**	**12.3**
Mix/Laydown Condition	$\eta_{t=0}$	**1,875.4**	**40.7**
RTFO Aged Viscosity Tested	η_{vis}	**317.6**	**11.0**
Fonesca and Witczak	$\eta_{t=0}$	**7,040.1**	**102.7**
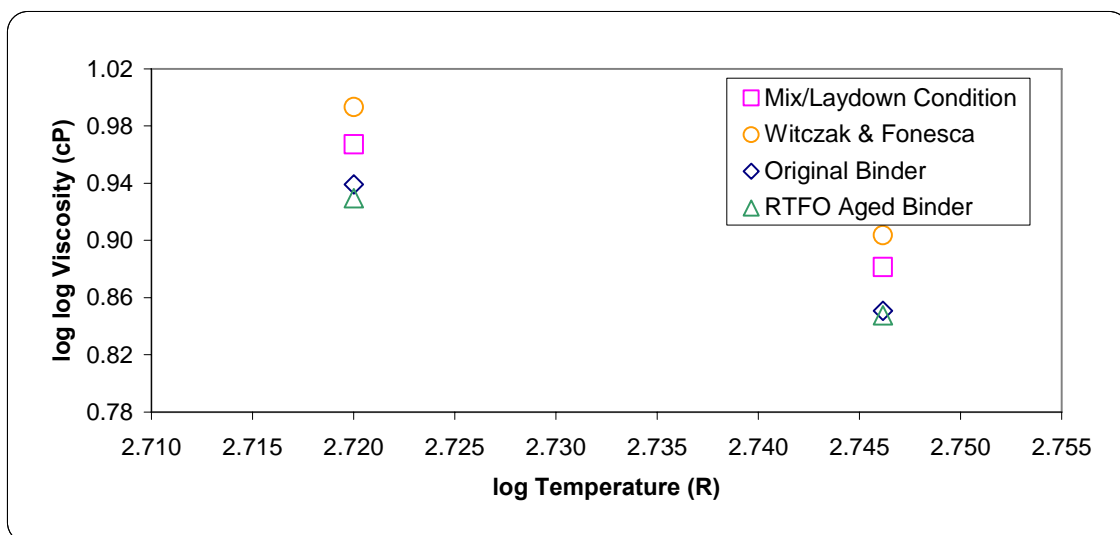
Job: Tomahawk

Mix Type: 25.0mm Open

Traffic Level: E-3

Binder Grade (PG): 58-28

		A	VTS
Original Binder	η_{orig}	11.664	-3.950
Mix/Laydown Condition	$\eta_{t=0}$	11.392	-3.840
RTFO Aged Viscosity Tested	η_{vis}	9.370	-3.117
Fonesca and Witczak	$\eta_{t=0}$	11.010	-3.701

A = regression intercept

VTS = Regression slope of viscosity temperature susceptibility

| Viscosity (10^6 Poise):		Int. Temperature (°C)	High Temeprature (°C)
		17.3	35.6
Original Binder	η_{orig}	276.9	4.3
Mix/Laydown Condition	$\eta_{t=0}$	1,034.6	13.5
RTFO Aged Viscosity Tested	η_{vis}	77.6	3.3
Fonesca and Witczak	$\eta_{t=0}$	795.1	12.6
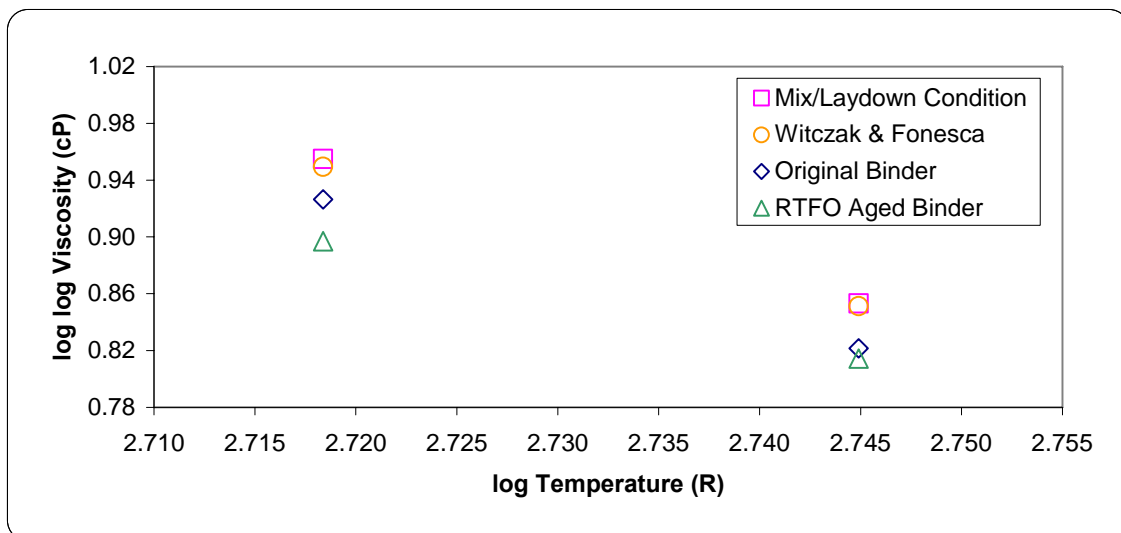
APPENDIX G SPECIMEN TEST RESULTS

Bloomvile E-1 19.0mm

7.0% Air Voids Opt. Asphalt
Dynamic Modulus

Specimen	BLO-OP-7.0-19.0-E Stress		103 kPa	
Temperature	17.5 C			
		Frequency		
	0.1	1	10	25
E*	1291.4	3409.2	7669.4	10862.2
φ	40.68	37.45	30.2	5.77

Specimen	BLO-OP-7.0-19.0-E1-D			
Temperature	17.5 C			
		Frequency		
	0.1	1	10	25
E*	1171	2433.6	5034.5	6745.9
φ	33.65	31.46	29.98	31.59

Specimen	BLO-OP-7.0-19.0-E1-E			
Temperature	17.5 C			
		Frequency		
	0.1	1	10	25
E*	1229.7	2681.6	5622.5	7606.5
φ	35.24	31.5	27.72	28.86

		Frequency		
	0.1	1	10	25
E* Mean	1230.7	2841.5	6108.8	8404.9
E* Std. Dev.	60.2	507.1	1383.1	2171.2
COV (%)	4.89	17.85	22.64	25.83
φ Mean	36.52	33.47	29.30	22.07
φ Std. Dev.	3.69	3.45	1.37	14.18
COV (%)	10.09	10.30	4.69	64.26

Specimen	BLO-OP-7.0-19.0-E Stress		35 kPa	
Temperature	36.6 C			
		Frequency		
	0.1	1	10	25
E*	407.3	797.5	2295.2	3216.9
φ	29.82	35.51	26.76	28.66

Specimen	BLO-OP-7.0-19.0-E1-D			
Temperature	36.6 C			
		Frequency		
	0.1	1	10	25
E*	438.8	743	1822.8	2664.1
φ	26.01	29.72	29.46	28.95

Specimen	BLO-OP-7.0-19.0-E1-E			
Temperature	36.6 C			
		Frequency		
	0.1	1	10	25
E*	344.8	591.8	1638.4	2498.5
φ	25.37	30.51	29.41	28.9

		Frequency		
	0.1	1	10	25
E* Mean	397.0	710.8	1918.8	2793.2
E* Std. Dev.	47.8	106.6	338.8	376.2
COV (%)	12.05	14.99	17.65	13.47
φ Mean	27.07	31.91	28.54	28.84
φ Std. Dev.	2.41	3.14	1.54	0.16
COV (%)	8.89	9.84	5.41	0.54

Flow Number

Specimen	BLO-OP-7.0-19.0-E1-A	
Temperature	36.6 C	
FN	Min Slope	Acc. Strain at Min Slope
114	77.7925	15449

Specimen	BLO-OP-7.0-19.0-E1-D	
Temperature	36.6 C	
FN	Min Slope	Acc. Strain at Min Slope
164	68.0494	18325

Specimen	BLO-OP-7.0-19.0-E1-E	
Temperature	36.6 C	
FN	Min Slope	Acc. Strain at Min Slope
169	62.7402	17577

FN		Min Slope	Acc. Strain at Min Slope	
149	Mean	69.5274	17117	
30	Std. Dev.	7.6342	1492	
20.41	COV (%)	10.9802	8.72	

G-2

4.0% Air Voids Opt. Asphalt

Dynamic Modulus

Specimen BLO-OP-4.0-19.0-E1-D Temperature 18.4 C

	Frequency			
	0.1	1	10	25
E*	1954.2	4122.2	8630.5	13818.2
φ	33.33	31.08	30.7	19.97

Specimen BLO-OP-4.0-19.0-E1-E Temperature 18.4 C

	Frequency			
	0.1	1	10	25
E*	1932.7	4287	8838	13278.2
φ	35.72	31.67	29.67	16.02

Specimen BLO-OP-4.0-19.0-E1-F Temperature 18.4 C

	Frequency			
	0.1	1	10	25
E*	1808	3693	7425	10382.4
φ	36.07	29.96	28.34	28.26

	Frequency			
	0.1	1	10	25
E* Mean	1898.3	4034.1	8297.8	12492.9
E* Std. Dev.	78.9	306.7	763.0	1847.6
COV (%)	4.16	7.60	9.19	14.79
φ Mean	35.04	30.90	29.57	21.42
φ Std. Dev.	1.49	0.87	1.18	6.25
COV (%)	4.26	2.81	4.00	29.17

Specimen BLO-OP-4.0-19.0-E1-D Temperature 36.5 C

	Frequency			
	0.1	1	10	25
E*	608.7	1082.3	2869.6	4997.7
φ	27.76	32.41	34.25	42.16

Specimen BLO-OP-4.0-19.0-E1-E Temperature 36.5 C

	Frequency			
	0.1	1	10	25
E*	833	1404.8	3170.8	5116.6
φ	25.28	27.75	30.79	27.93

Specimen BLO-OP-4.0-19.0-E1-F Temperature 36.5 C

	Frequency			
	0.1	1	10	25
E*	773.8	1340.4	2820.6	4496.4
φ	23.27	27.48	12.13	23.61

	Frequency			
	0.1	1	10	25
E* Mean	738.5	1275.8	2953.7	4870.2
E* Std. Dev.	116.2	170.7	189.6	329.2
COV (%)	15.74	13.38	6.42	6.76
φ Mean	25.44	29.21	25.72	31.23
φ Std. Dev.	2.25	2.77	11.90	9.71
COV (%)	8.84	9.49	46.26	31.08

Flow Number

Specimen BLO-OP-4.0-19.0-E1-D Temperature 36.5 C

FN	Min Slope	Acc. Strain at Min Slope
1028	5.3421	13404

Specimen BLO-OP-4.0-19.0-E1-E Temperature 36.5 C

FN	Min Slope	Acc. Strain at Min Slope
768	6.3176	12684

Specimen BLO-OP-4.0-19.0-E1-F Temperature 36.5 C

FN	Min Slope	Acc. Strain at Min Slope
946	4.374	12928

FN	Min Slope	Acc. Strain at Min Slope	
914.0	5.34	13005	Mean
132.9	0.97	366	Std. Dev.
14.54	18.18	2.82	COV (%)

G-3

Bloomvile E-1 19.0mm

10.0% Air Voids
Dynamic Modulus

Specimen	BLO-OP-10.0-19.0-E1-A			
Temperature	18.4 C			
		Frequency		
	0.1	1	10	25
E*	764.3	1844.6	4542.1	6633.6
φ	40.08	37.13	31.56	16.35

Specimen	BLO-OP-10.0-19.0-E1-C			
Temperature	18.4 C			
		Frequency		
	0.1	1	10	25
E*	952.6	1910.7	4652.2	7110.2
φ	41.73	34.08	30.6	12.36

Specimen	BLO-OP-10.0-19.0-E1-E			
Temperature	18.4 C			
		Frequency		
	0.1	1	10	25
E*	893.4	1856	4196.9	6300.6
φ	34.86	33.7	32.63	23.6

		Frequency		
	0.1	1	10	25
E* Mean	870.1	1870.4	4463.7	6681.5
E* Std. Dev.	96.3	35.3	237.6	406.9
COV (%)	11.07	1.89	5.32	6.09
φ Mean	38.89	34.97	31.60	17.44
φ Std. Dev.	3.59	1.88	1.02	5.70
COV (%)	9.22	5.38	3.21	32.68

Specimen	BLO-OP-10.0-19.0-E1-A			
Temperature	36.5 C			
		Frequency		
	0.1	1	10	25
E*	612.7	1621.5	1969.1	2694
φ	32.81	34.42	15.33	5.62

Specimen	BLO-OP-10.0-19.0-E1-C			
Temperature	36.5 C			
		Frequency		
	0.1	1	10	25
E*	1000.4	1577.1	2163	2847
φ	31.29	38.72	30.62	15

Specimen	BLO-OP-10.0-19.0-E1-E			
Temperature	36.5 C			
		Frequency		
	0.1	1	10	25
E*	448.1	789.6	1892.5	2827.1
φ	25.96	29	25.47	5.36

		Frequency		
	0.1	1	10	25
E* Mean	687.1	1329.4	2008.2	2789.4
E* Std. Dev.	283.6	468.0	139.4	83.2
COV (%)	41.27	35.20	6.94	2.98
φ Mean	30.02	34.05	23.81	8.66
φ Std. Dev.	3.60	4.87	7.78	5.49
COV (%)	11.98	14.31	32.68	63.42

Flow Number

Specimen	BLO-OP-10.0-19.0-E1-A		
Temperature	36.5 C		
FN		Min Slope	Acc. Strain at Min Slope
	74	154.2	17791

Specimen	BLO-OP-10.0-19.0-E1-C		
Temperature	36.5 C		
FN		Min Slope	Acc. Strain at Min Slope
	59	189.4	17168

Specimen	BLO-OP-10.0-19.0-E1-E		
Temperature	36.5 C		
FN		Min Slope	Acc. Strain at Min Slope
	79	153.9	18591

	FN	Min Slope	Acc. Strain at Min Slope
Mean	70.7	165.83	17850
Std. Dev.	10.4	20.41	713
COV (%)	14.73	12.31	4.00

Bloomvile E-1 19.0mm

7.0% Air Voids +0.3% Asphalt

Dynamic Modulus

Specimen	BLO-BU-7.0-19.0-E1-C			
Temperature	18.4 C			
		Frequency		
	0.1	1	10	25
E*	1405.8	2979.5	6162	8631.5
φ	32.56	30.37	29.17	31.99

Specimen	BLO-BU-7.0-19.0-E1-D			
Temperature	18.4 C			
		Frequency		
	0.1	1	10	25
E*	1270.1	2633.1	5474.9	7769.9
φ	32.43	29.57	29.67	28.98

Specimen	BLO-BU-7.0-19.0-E1-F			
Temperature	18.4 C			
		Frequency		
	0.1	1	10	25
E*	1190.7	2779.1	7036.5	9653.7
φ	40.1	37.97	29.98	23.17

	Frequency			
	0.1	1	10	25
E* Mean	1288.9	2797.2	6224.5	8685.0
E* Std. Dev.	108.8	173.9	782.7	943.0
COV (%)	8.44	6.22	12.57	10.86
φ Mean	35.03	32.64	29.61	28.05
φ Std. Dev.	4.39	4.64	0.41	4.48
COV (%)	12.54	14.21	1.38	15.99

Specimen	BLO-BU-7.0-19.0-E1-C			
Temperature	36.5 C			
		Frequency		
	0.1	1	10	25
E*	725.7	1189.1	2512.1	3654.2
φ	21.53	25.75	24.05	17.44

Specimen	BLO-BU-7.0-19.0-E1-D			
Temperature	36.5 C			
		Frequency		
	0.1	1	10	25
E*	575.7	923.1	2208.6	3762.3
φ	23.17	26.53	32	29.91

Specimen	BLO-BU-7.0-19.0-E1-F			
Temperature	36.5 C			
		Frequency		
	0.1	1	10	25
E*	446.9	773.5	1941.1	2899.4
φ	27.53	29.15	4.59	31.02

	Frequency			
	0.1	1	10	25
E* Mean	582.8	961.9	2220.6	3438.6
E* Std. Dev.	139.5	210.5	285.7	470.1
COV (%)	23.94	21.88	12.87	13.67
φ Mean	24.08	27.14	20.21	26.12
φ Std. Dev.	3.10	1.78	14.10	7.54
COV (%)	12.88	6.56	69.77	28.86

Flow Number

Specimen	BLO-BU-7.0-19.0-E1-C		
Temperature	36.5 C		
FN	Min Slope	Acc. Strain at Min Slope	
189	58.3165	19244	

Specimen	BLO-BU-7.0-19.0-E1-D		
Temperature	36.5 C		
FN	Min Slope	Acc. Strain at Min Slope	
214	60.2924	20665	

Specimen	BLO-BU-7.0-19.0-E1-F		
Temperature	36.5 C		
FN	Min Slope	Acc. Strain at Min Slope	
149	64.3209	16434	

	FN	Min Slope	Acc. Strain at Min Slope
Mean	184.0	60.98	18781
Std. Dev.	32.8	3.06	2153
COV (%)	17.82	5.02	11.46

Mosinee E-3 19.0mm

7.0% Air Voids Opt. Asphalt

Dynamic Modulus

Specimen	MOS-OP-7.0-19.0-E3-Stress			69 kPa
Temperature	18.7 C			
		Frequency		
	0.1	1	10	25
E*	750.2	1785.6	4108.8	5878.4
φ	35.73	35.47	33.12	32.33

Specimen	MOS-OP-7.0-19.0-E3-B			
Temperature	18.7 C			
		Frequency		
	0.1	1	10	25
E*	832.8	2178.1	5578.5	8278.5
φ	38.38	38.57	35.34	29.24

Specimen	MOS-OP-7.0-19.0-E3-E			
Temperature	18.7 C			
		Frequency		
	0.1	1	10	25
E*	770.5	1945.1	4683.7	6781.8
φ	37.57	36.84	33.77	32.75

		Frequency		
	0.1	1	10	25
E* Mean	784.5	1969.6	4790.3	6979.6
E* Std. Dev.	43.0	197.4	740.6	1212.2
COV (%)	5.49	10.02	15.46	17.37
φ Mean	37.23	36.96	34.08	31.44
φ Std. Dev.	1.36	1.55	1.14	1.92
COV (%)	3.65	4.20	3.35	6.10

Specimen	MOS-OP-7.0-19.0-E3-Stress			35 kPa
Temperature	36.9 C			
		Frequency		
	0.1	1	10	25
E*	337.1	574.4	1531	2693.2
φ	25.78	31	34.05	28.59

Specimen	MOS-OP-7.0-19.0-E3-B			
Temperature	36.9 C			
		Frequency		
	0.1	1	10	25
E*	281.6	514.8	1660.7	3522.9
φ	26.36	34.51	39.8	30.53

Specimen	MOS-OP-7.0-19.0-E3-E			
Temperature	36.9 C			
		Frequency		
	0.1	1	10	25
E*	244.1	426.5	1243.4	2436.9
φ	23.54	32.53	39.54	29.45

		Frequency		
	0.1	1	10	25
E* Mean	287.6	505.2	1478.4	2851.0
E* Std. Dev.	46.8	74.4	213.6	587.1
COV (%)	16.27	14.73	14.45	20.59
φ Mean	25.23	32.68	37.80	29.52
φ Std. Dev.	1.49	1.76	3.25	0.97
COV (%)	5.90	5.38	8.59	3.29

Flow Number

Specimen	MOS-OP-7.0-19.0-E3-A	
Temperature	36.9 C	
FN	Min Slope	Acc. Strain at Min Slope
59	173	14878

Specimen	MOS-OP-7.0-19.0-E3-B	
Temperature	36.9 C	
FN	Min Slope	Acc. Strain at Min Slope
69	165.5	15816

Specimen	MOS-OP-7.0-19.0-E3-E	
Temperature	36.9 C	
FN	Min Slope	Acc. Strain at Min Slope
59	169.27	14447

	FN	Min Slope	Acc. Strain at Min Slope
Mean	62	169.2567	15047
Std. Dev.	6	3.7500	700
COV (%)	9.26	2.2156	4.65

Mosinee E-3 19.0mm

4.0% Air Voids Opt. Asphalt

Dynamic Modulus

Specimen MOS-OP-4.0-19.0-E3-A, Temperature 18.7 C

	Frequency			
	0.1	1	10	25
E*	1232.2	3246.3	7823.6	10429
φ	40.01	37.59	31.35	30.05

Specimen MOS-OP-4.0-19.0-E3-B, Temperature 18.7 C

	Frequency			
	0.1	1	10	25
E*	1155.4	2913.3	6669.4	9058.8
φ	38.42	25.6	30.88	31.74

Specimen MOS-OP-4.0-19.0-E3-D, Temperature 18.7 C

	Frequency			
	0.1	1	10	25
E*	1150	2871.5	6653	9397.6
φ	36.46	35.64	32.93	33.84

	Frequency			
	0.1	1	10	25
E* Mean	1179.2	3010.4	7048.7	9628.5
E* Std. Dev.	46.0	205.4	671.2	713.7
COV (%)	3.90	6.82	9.52	7.41
φ Mean	38.30	32.94	31.72	31.88
φ Std. Dev.	1.78	6.43	1.07	1.90
COV (%)	4.64	19.53	3.39	5.96

Specimen MOS-OP-4.0-19.0-E3-A, Temperature 36.9 C

	Frequency			
	0.1	1	10	25
E*	414.2	741.9	2092.2	4024.2
φ	23.56	33.99	38.76	36.21

Specimen MOS-OP-4.0-19.0-E3-B, Temperature 36.9 C

	Frequency			
	0.1	1	10	25
E*	358	646	1911.8	3192.3
φ	27.02	32.96	12.15	34.66

Specimen MOS-OP-4.0-19.0-E3-D, Temperature 36.9 C

	Frequency			
	0.1	1	10	25
E*	330.8	597.1	1672.4	2580.6
φ	23.82	32.02	13.1	35.67

	Frequency			
	0.1	1	10	25
E* Mean	367.7	661.7	1892.1	3265.7
E* Std. Dev.	42.5	73.7	210.6	724.6
COV (%)	11.57	11.13	11.13	22.19
φ Mean	24.80	32.99	21.34	35.51
φ Std. Dev.	1.93	0.99	15.10	0.79
COV (%)	7.77	2.99	70.75	2.22

Flow Number

Specimen MOS-OP-4.0-19.0-E3-A, Temperature 36.9 C

FN	Min Slope	Acc. Strain at Min Slope
154	48.6229	12302
277		

Specimen MOS-OP-4.0-19.0-E3-B, Temperature 36.9 C

FN	Min Slope	Acc. Strain at Min Slope
109	60.3164	11431
227		

Specimen MOS-OP-4.0-19.0-E3-D, Temperature 36.9 C

FN	Min Slope	Acc. Strain at Min Slope
99	54.4974	9975
252		

FN	Min Slope	Acc. Strain at Min Slope
Mean	120.7	54.48	11236
Std. Dev.	29.3	5.85	1176
COV (%)	24.28	10.73	10.46

Mosinee E-3 19.0mm

7.0% Air Voids +0.3% Asphalt

Dynamic Modulus

Specimen MOS-BU-7.0-19.0-E3-A — Temperature 18.7 C

	Frequency			
	0.1	1	10	25
E*	802.9	1954.9	4379.6	6033.2
φ	36.81	35.3	31.47	31.65

Specimen MOS-BU-7.0-19.0-E3-E — Temperature 18.7 C

	Frequency			
	0.1	1	10	25
E*	922.7	2359.4	5499.7	7954
φ	39.7	37.06	32.76	31.98

Specimen MOS-BU-7.0-19.0-E3-F — Temperature 18.7 C

	Frequency			
	0.1	1	10	25
E*	782.2	2019.1	4762.7	6613.7
φ	38.91	36.48	32.33	33.6

	Frequency			
	0.1	1	10	25
E* Mean	835.9	2111.1	4880.7	6867.0
E* Std. Dev.	75.9	217.4	569.3	985.1
COV (%)	9.07	10.30	11.66	14.35
φ Mean	38.47	36.28	32.19	32.41
φ Std. Dev.	1.49	0.90	0.66	1.04
COV (%)	3.88	2.47	2.04	3.22

Specimen MOS-BU-7.0-19.0-E3-A — Temperature 36.9 C

	Frequency			
	0.1	1	10	25
E*	361.5	657.1	1632	2617
φ	29.07	30.49	15.09	37.24

Specimen MOS-BU-7.0-19.0-E3-E — Temperature 36.9 C

	Frequency			
	0.1	1	10	25
E*	333.5	558.8	1476.4	2284.9
φ	25.7	31.32	8.15	24.98

Specimen MOS-BU-7.0-19.0-E3-F — Temperature 36.9 C

	Frequency			
	0.1	1	10	25
E*	266	475.7	1351.5	2166.7
φ	26.32	32.23	4.72	0.26

	Frequency			
	0.1	1	10	25
E* Mean	320.3	563.9	1486.6	2356.2
E* Std. Dev.	49.1	90.8	140.5	233.5
COV (%)	15.33	16.10	9.45	9.91
φ Mean	27.03	31.35	9.32	20.83
φ Std. Dev.	1.79	0.87	5.28	18.84
COV (%)	6.64	2.78	56.69	90.44

Flow Number

Specimen MOS-BU-7.0-19.0-E3-A — Temperature 36.9 C

FN	Min Slope	Acc. Strain at Min Slope
69	155.5	15607
97		

Specimen MOS-BU-7.0-19.0-E3-E — Temperature 36.9 C

FN	Min Slope	Acc. Strain at Min Slope
69	181	17176
87		

Specimen MOS-BU-7.0-19.0-E3-F — Temperature 36.9 C

FN	Min Slope	Acc. Strain at Min Slope
79	146	16744
102		

FN	Min Slope	Acc. Strain at Min Slope
Mean	72.3	160.83	16509
Std. Dev.	5.8	18.10	810
COV (%)	7.98	11.25	4.91

Mosinee E-3 19.0mm

7.0% Air Voids +0.3% Asphalt
Dynamic Modulus

Flow Number

Specimen MOS-BU-7.0-19.0-E3-A
Temperature 36.9 C

FN	Min Slope	Acc. Strain at Min Slope
69	155.5	15607
97		

Specimen MOS-BU-7.0-19.0-E3-E
Temperature 36.9 C

FN	Min Slope	Acc. Strain at Min Slope
69	181	17176
87		

Specimen MOS-BU-7.0-19.0-E3-F
Temperature 36.9 C

FN	Min Slope	Acc. Strain at Min Slope
79	146	16744
102		

FN	Min Slope	Acc. Strain at Min Slope	
Mean	72.3	160.83	16509
Std. Dev.	5.8	18.10	810.4683831
COV (%)	7.98	11.25	4.909251821

Dynamic Modulus — 36.9 C

Specimen MOS-BU-7.0-19.0-E3-A
Temperature 36.9 C

	Frequency			
	0.1	1	10	25
E*	361.5	657.1	1632	2617
φ	29.07	30.49	15.09	37.24

Specimen MOS-BU-7.0-19.0-E3-E
Temperature 36.9 C

	Frequency			
	0.1	1	10	25
E*	333.5	558.8	1476.4	2284.9
φ	25.7	31.32	8.15	24.98

Specimen MOS-BU-7.0-19.0-E3-F
Temperature 36.9 C

	Frequency			
	0.1	1	10	25
E*	266	475.7	1351.5	2166.7
φ	26.32	32.23	4.72	0.26

	Frequency			
	0.1	1	10	25
E* Mean	320.3	563.9	1486.6	2356.2
E* Std. Dev.	49.1	90.8	140.5	233.5
COV (%)	15.33	16.10	9.45	9.91
φ Mean	27.03	31.35	9.32	20.83
φ Std. Dev.	1.79	0.87	5.28	18.84
COV (%)	6.64	2.78	56.69	90.44

Dynamic Modulus — 18.7 C

Specimen MOS-BU-7.0-19.0-E3-A
Temperature 18.7 C

	Frequency			
	0.1	1	10	25
E*	802.9	1954.9	4379.6	6033.2
φ	36.81	35.3	31.47	31.65

Specimen MOS-BU-7.0-19.0-E3-E
Temperature 18.7 C

	Frequency			
	0.1	1	10	25
E*	922.7	2359.4	5499.7	7954
φ	39.7	37.06	32.76	31.98

Specimen MOS-BU-7.0-19.0-E3-F
Temperature 18.7 C

	Frequency			
	0.1	1	10	25
E*	782.2	2019.1	4762.7	6613.7
φ	38.91	36.48	32.33	33.6

	Frequency			
	0.1	1	10	25
E* Mean	835.9	2111.1	4880.7	6867.0
E* Std. Dev.	75.9	217.4	569.3	985.1
COV (%)	9.07	10.30	11.66	14.35
φ Mean	38.47	36.28	32.19	32.41
φ Std. Dev.	1.49	0.90	0.66	1.04
COV (%)	3.88	2.47	2.04	3.22

Northfield E-30 19.0mm

7.0% Air Voids Opt. Asphalt
Dynamic Modulus

Dynamic Modulus — 18.4 C (173 kPa)

Specimen NOR-OP-7.0-19.0-E Stress, Temperature 18.4 C

	Frequency			
	0.1	1	10	25
E*	2586.9	5875.8	11600.3	14819.1
φ	40.72	31.53	27.46	26.19

Specimen NOR-OP-7.0-19.0-E30-E, Temperature 18.4 C

	Frequency			
	0.1	1	10	25
E*	2561.4	6446	12746.2	15586.3
φ	43.27	31.47	24.12	23.24

Specimen NOR-OP-7.0-19.0-E30-F, Temperature 18.4 C

	Frequency			
	0.1	1	10	25
E*	2295.2	5698.2	11545.5	14908.1
φ	42.32	31.1	27.38	27.05

	Frequency			
	0.1	1	10	25
E* Mean	2481.2	6006.7	11964.0	15104.5
E* Std. Dev.	161.6	390.7	678.0	419.6
COV (%)	6.51	6.50	5.67	2.78
φ Mean	42.10	31.37	26.32	25.49
φ Std. Dev.	1.29	0.23	1.91	2.00
COV (%)	3.06	0.74	7.24	7.84

Dynamic Modulus — 36.5 C (35 kPa)

Specimen NOR-OP-7.0-19.0-E Stress, Temperature 36.5 C

	Frequency			
	0.1	1	10	25
E*	983.2	1837.9	4381.6	6518.4
φ	22.26	25.99	30.71	23.83

Specimen NOR-OP-7.0-19.0-E30-E, Temperature 36.5 C

	Frequency			
	0.1	1	10	25
E*	1003	1683.9	3853.5	5196.7
φ	32.63	26.22	27.45	13.51

Specimen NOR-OP-7.0-19.0-E30-F, Temperature 36.5 C

	Frequency			
	0.1	1	10	25
E*	857	1796.2	4338.7	5764
φ	43.32	39.32	32.45	26.04

	Frequency			
	0.1	1	10	25
E* Mean	947.7	1772.7	4191.3	5826.4
E* Std. Dev.	79.2	79.7	293.3	663.1
COV (%)	8.36	4.49	7.00	11.38
φ Mean	32.74	30.51	30.20	21.13
φ Std. Dev.	10.53	7.63	2.54	6.69
COV (%)	32.17	25.01	8.40	31.66

Flow Number

Specimen NOR-OP-7.0-19.0-E30-A, Temperature 36.5 C

FN	Min Slope	Acc. Strain at Min Slope
1786	2.5918	13073
3707		

Specimen NOR-OP-7.0-19.0-E30-E, Temperature 36.5 C

FN	Min Slope	Acc. Strain at Min Slope
2296	2.9162	13901
3740		

Specimen NOR-OP-7.0-19.0-E30-F, Temperature 36.5 C

FN	Min Slope	Acc. Strain at Min Slope
2255	2.8867	14910
3630		

FN		Min Slope	Acc. Strain at Min Slope
Mean	2112	2.7982	13961
Std. Dev.	283	0.1794	920
COV (%)	13.41	6.4106	6.59

Northfield E-30 19.0mm

4.0% Air Voids Opt. Asphalt

Dynamic Modulus

Specimen NOR-OP-4.0-19.0-E30-A
Temperature 18.4 C

	Frequency			
	0.1	1	10	25
E*	4139.8	9738.7	19054.4	23558.4
φ	39.61	29.34	25.55	25.63

Specimen NOR-OP-4.0-19.0-E30-B
Temperature 18.4 C

	Frequency			
	0.1	1	10	25
E*	5270.9	12155.2	23182.5	26852.1
φ	36.45	29.5	22.93	22.42

Specimen NOR-OP-4.0-19.0-E30-E
Temperature 18.4 C

	Frequency			
	0.1	1	10	25
E*	3161.7	7441	15002.7	18964.5
φ	38.93	33.73	26.17	23.7

	Frequency			
	0.1	1	10	25
E* Mean	4190.8	9778.3	19079.9	23125.0
E* Std. Dev.	1055.5	2357.3	4090.0	3961.6
COV (%)	25.19	24.11	21.44	17.13
φ Mean	38.33	30.86	24.88	23.92
φ Std. Dev.	1.66	2.49	1.72	1.62
COV (%)	4.34	8.07	6.91	6.76

Specimen NOR-OP-4.0-19.0-E30-A
Temperature 36.5 C

	Frequency			
	0.1	1	10	25
E*	1026.1	2431.8	6239.6	9422.6
φ	36.27	38.39	34.01	7.94

Specimen NOR-OP-4.0-19.0-E30-B
Temperature 36.5 C

	Frequency			
	0.1	1	10	25
E*	880.6	2146	6075.8	10348.9
φ	38.65	42.66	29.76	13.22

Specimen NOR-OP-4.0-19.0-E30-E
Temperature 36.5 C

	Frequency			
	0.1	1	10	25
E*	923.1	2322.2	6349.9	9296.5
φ	37.54	25.26	17.92	4.48

	Frequency			
	0.1	1	10	25
E* Mean	943.3	2300.0	6221.8	9689.3
E* Std. Dev.	74.8	144.2	137.9	574.7
COV (%)	7.93	6.27	2.22	5.93
φ Mean	37.49	35.44	27.23	8.55
φ Std. Dev.	1.19	9.07	8.34	4.40
COV (%)	3.18	25.59	30.62	51.50

Flow Number

Specimen NOR-OP-4.0-19.0-E30-A
Temperature 36.5 C

FN	Min Slope	Acc. Strain at Min Slope
2767	2.0254	11767
5495		

Specimen NOR-OP-4.0-19.0-E30-B
Temperature 36.5 C

FN	Min Slope	Acc. Strain at Min Slope
3910	1.1345	11280
8805		

Specimen NOR-OP-4.0-19.0-E30-E
Temperature 36.5 C

FN	Min Slope	Acc. Strain at Min Slope
2278	1.9431	11853
5516		

FN	Min Slope	Acc. Strain at Min Slope	
2985.0	1.70	11633	Mean
837.6	0.49	309	Std. Dev.
28.06	28.94	2.66	COV (%)

Northfield E-30 19.0mm
Dynamic Modulus
10.0% Air Voids

18.4 C — Dynamic Modulus

Specimen NOR-OP-10.0-19.0-E30-A
Temperature 18.4 C

	Frequency			
	0.1	1	10	25
E*	2466.2	4851.6	9466.8	12158.6
φ	36.26	30.38	27.23	27.73

Specimen NOR-OP-10.0-19.0-E30-B
Temperature 18.4 C

	Frequency			
	0.1	1	10	25
E*	1907	4335.4	8340.4	10548
φ	37.72	30.63	25.92	26.41

Specimen NOR-OP-10.0-19.0-E30-C
Temperature 18.4 C

	Frequency			
	0.1	1	10	25
E*	3501.3	7811.6	15006.4	18623.3
φ	39.5	28.96	21.19	24.29

	Frequency			
	0.1	1	10	25
E* Mean	2624.8	5666.2	10937.9	13776.6
E* Std. Dev.	808.9	1875.8	3568.2	4273.9
COV (%)	30.82	33.11	32.62	31.02
φ Mean	37.83	29.99	24.78	26.14
φ Std. Dev.	1.62	0.90	3.18	1.74
COV (%)	4.29	3.00	12.82	6.64

36.5 C — Dynamic Modulus

Specimen NOR-OP-10.0-19.0-E30-A
Temperature 36.5 C

	Frequency			
	0.1	1	10	25
E*	475.5	971.5	2683.2	4542.9
φ	28	33.93	12.43	27.11

Specimen NOR-OP-10.0-19.0-E30-B
Temperature 36.5 C

	Frequency			
	0.1	1	10	25
E*	554.8	1088.3	2898.6	4599.1
φ	30.76	35.15	36.14	32

Specimen NOR-OP-10.0-19.0-E30-C
Temperature 36.5 C

	Frequency			
	0.1	1	10	25
E*	737.9	1474.2	3912.1	5784.9
φ	27.05	35.07	33.41	14.85

	Frequency			
	0.1	1	10	25
E* Mean	589.4	1178.0	3164.6	4975.6
E* Std. Dev.	134.6	263.1	656.2	701.4
COV (%)	22.83	22.33	20.74	14.10
φ Mean	28.60	34.72	27.33	24.65
φ Std. Dev.	1.93	0.68	12.97	8.83
COV (%)	6.74	1.97	47.47	35.84

Flow Number

Specimen NOR-OP-10.0-19.0-E30-A
Temperature 36.5 C

FN	Min Slope	Acc. Strain at Min Slope
2944	3.5669	21061
2704		

Specimen NOR-OP-10.0-19.0-E30-B
Temperature 36.5 C

FN	Min Slope	Acc. Strain at Min Slope
1875	6.789	23853
1432		

Specimen NOR-OP-10.0-19.0-E30-C
Temperature 36.5 C

FN	Min Slope	Acc. Strain at Min Slope
1426	4.5318	16363
2109		

FN	Min Slope	Acc. Strain at Min Slope	
2081.7	4.96	20426	Mean
779.8	1.65	3785	Std. Dev.
37.46	33.32	18.53	COV (%)

Northfield E-30 19.0mm

7.0% Air Voids +0.3% Asphalt
Dynamic Modulus

Temperature 18.4 C

Specimen NOR-BU-7.0-19.0-E30-B — Temperature 18.4 C

	Frequency			
	0.1	1	10	25
E*	3068.5	7029.3	12632.4	14773.5
φ	38.61	30.66	23.41	21.72

Specimen NOR-BU-7.0-19.0-E30-D — Temperature 18.4 C

	Frequency			
	0.1	1	10	25
E*	3198.4	7977	15841.4	19665.1
φ	40.34	33.06	24.62	23.72

Specimen NOR-BU-7.0-19.0-E30-E — Temperature 18.4 C

	Frequency			
	0.1	1	10	25
E*	3116.5	7811.9	17950.9	21841.6
φ	41.07	35.6	24.56	23.26

	Frequency			
	0.1	1	10	25
E* Mean	3127.8	7606.1	15474.9	18760.1
E* Std. Dev.	65.7	506.3	2678.1	3619.9
COV (%)	2.10	6.66	17.31	19.30
φ Mean	40.01	33.11	24.20	22.90
φ Std. Dev.	1.26	2.47	0.68	1.05
COV (%)	3.16	7.46	2.82	4.57

Temperature 36.5 C (Dynamic Modulus)

Specimen NOR-BU-7.0-19.0-E30-B — Temperature 36.5 C

	Frequency			
	0.1	1	10	25
E*	879.5	1789.3	4638.5	7298.2
φ	30.07	35.15	34.23	21.45

Specimen NOR-BU-7.0-19.0-E30-D — Temperature 36.5 C

	Frequency			
	0.1	1	10	25
E*	569	1249.8	3507.6	5485.5
φ	31.4	36.11	31.83	16.12

Specimen NOR-BU-7.0-19.0-E30-E — Temperature 36.5 C

	Frequency			
	0.1	1	10	25
E*	568	1264.7	4205	5975
φ	33.85	40.08	33.22	20.06

	Frequency			
	0.1	1	10	25
E* Mean	672.2	1434.6	4117.0	6252.9
E* Std. Dev.	179.6	307.3	570.6	937.8
COV (%)	26.71	21.42	13.86	15.00
φ Mean	31.77	37.11	33.09	19.21
φ Std. Dev.	1.92	2.61	1.21	2.76
COV (%)	6.03	7.04	3.64	14.39

Flow Number

Specimen NOR-BU-7.0-19.0-E30-B — Temperature 36.5 C

FN	Min Slope	Acc. Strain at Min Slope
5422	0.9717	15936
7914		

Specimen NOR-BU-7.0-19.0-E30-D — Temperature 36.5 C

FN	Min Slope	Acc. Strain at Min Slope
3934	1.4586	13905
7058		

Specimen NOR-BU-7.0-19.0-E30-E — Temperature 36.5 C

FN	Min Slope	Acc. Strain at Min Slope
4047	1.7216	14998
6188		

FN	Min Slope	Acc. Strain at Min Slope	
Mean	4467.7	1.38	14946
Std. Dev.	828.4	0.38	1016
COV (%)	18.54	27.49	6.80

APPENDIX H SPECIMEN TEST RESULTS
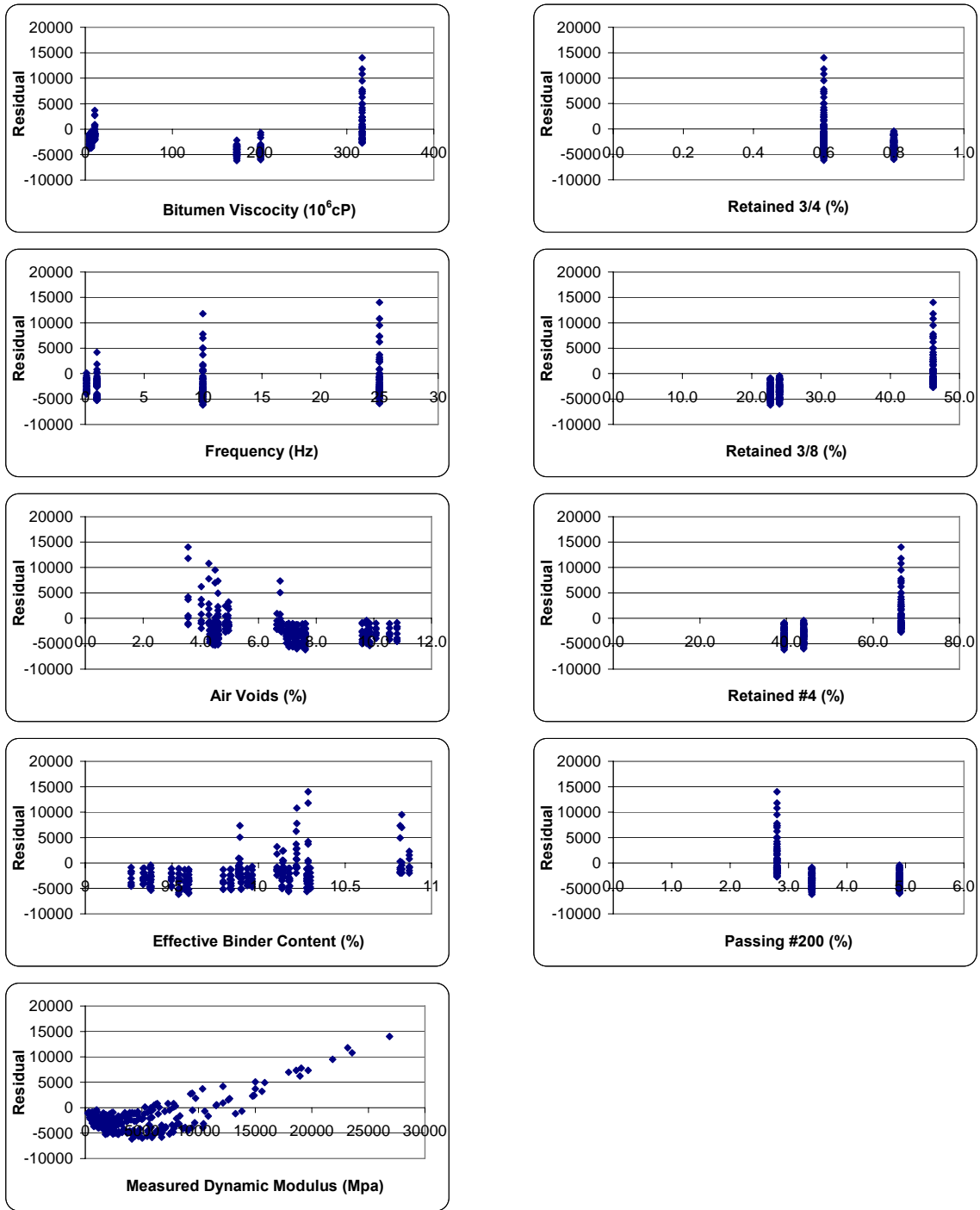
Witczak Predictive Equation Residual Plots

Recalibrated Witczak Predictive Equation Residual Plots